UNIVERSIDADE D
COIMBRA

João Soares de Albergaria Cabral Barata

ANÁLISE MULTI-ESCALA DE HETEROGENEIDADE EM UNIDADES CARBONATADAS DE MEIOS POUCO PROFUNDOS: CASOS DE ESTUDO EM AFLORAMENTOS DO JURÁSSICO NA BACIA LUSITÂNICA (PORTUGAL) E RESERVATÓRIO DO CRETÁCICO DO GRUPO THAMAMA, BACIA DE RUB AL KHALI (E.A.U.)

Tese no âmbito do Doutoramento em Geologia, Processos Geológicos, orientada pelo Professor Doutor Luís Vítor da Fonseca Pinto Duarte, Professora Doutora Ana Cristina Costa Neves dos Santos Azerêdo e Professor Doutor Jorge Salgado Gomes e apresentada ao Departamento de Ciências da Terra da Faculdade de Ciências e Tecnologia da Universidade de Coimbra.

Abril de 2021

Faculdade de Ciências e Tecnologia
da Universidade de Coimbra

Análise multi-escala de heterogeneidade em unidades carbonatadas de meios pouco profundos: Casos de estudo em afloramentos do Jurássico na Bacia Lusitânica (Portugal) e reservatório do Cretácico do Grupo Thamama, Bacia de Rub Al Khali (E.A.U.).

Multiscale heterogeneity analysis of shallow-water carbonate units: Case studies in Jurassic outcrops of the Lusitanian Basin (*Portugal) and Cretaceous reservoir of the Thamama Group, Rub Al Khali Basin* (*U.A.E.).*

João Soares de Albergaria Cabral Barata

Tese no âmbito do Doutoramento em Geologia, Processos Geológicos, orientada pelo Professor Doutor Luís Vítor da Fonseca Pinto Duarte, Professora Doutora Ana Cristina Costa Neves dos Santos Azerêdo e Professor Doutor Jorge Salgado Gomes e apresentada ao Departamento de Ciências da Terra da Faculdade de Ciências e Tecnologia da Universidade de Coimbra.

Abril de 2021

1 2 9 0

UNIVERSIDADE D
COIMBRA

Acknowledgements

First and foremost, I acknowledge the invaluable guidance and contributions of my supervisors, Dr. Luís V. Duarte, Dr. Ana C. Azerêdo and Dr. Jorge S. Gomes, to this work and to the production of this final thesis. I am grateful for their guidance, for providing all the support in pursuing the opportunity to work on this project and for all their help throughout this period. Their drive and enthusiasm were fundamental over the course of this project, with many fruitful and interesting discussions, as was the fundamental assistance in overcoming the more difficult moments.

The support of Dr. Luís V. Duarte and Dr. Ana C. Azerêdo on the field work in Portugal, at Peniche and the Maciço Calcário Estremenho, was vital and strongly appreciated. For the various field trips to Peniche and discussions with Dr. Luís V. Duarte, I am highly thankful. I thank the University of Lisbon and Dr. Ana C. Azerêdo for the production of the thin section material for the Peniche samples. The Maciço Calcário Estremenho active quarries field trips guidance and valuable discussions with Dr. Ana C. Azerêdo were fundamental. The participation and support of Nuno Inês in facilitating these visits, as well as the participation of Paulo Bizarro were highly appreciated. I thank the following companies for permission to access the respective quarries, as well as for the on-site assistance: Filstone - Comércio de Rochas, S.A.; M. Anastácio, Lda.; Mármores Rosal, Lda. and Telmo Duarte - Comércio de Pedras Naturais, S.A. I am grateful to ENMC/UPEP (presently DGEG) and Dr. José Miguel Martins for the permission to access well reports and thin sections for the analysed wells in the Lusitanian Basin.

I am grateful for the efforts and the support of Dr. Jorge S. Gomes in promoting and assisting with my 1-month period working at Khalifa University (Abu Dhabi, U.A.E.) as a visiting PhD student and in acquiring the permission to access the required data through ADNOC, which was fundamental for the development and advancement of this study. For the many interesting and valuable discussions with Dr. Jorge S. Gomes, I am thankful. I thank ADNOC for providing the respective permissions regarding the data analysed. I would also like to thank Mr. Ali Nasser Almazrouei and the ADNOC core store staff for their assistance in laying out the core material. I am thankful for the support of Dr. Andrea Ceriani and for his assistance during my time at the laboratories of Khalifa University. I thank Dr. Sadoon Morad and Mr. Prasanth Thiyagarayan for the assistance with the Scanning Electron Microprobe facility. Special thanks go to Dr. Mohammad Al Suwaidi for his endless support.

As a final note, I am grateful for the support of my family and for the tranquillity of many family moments. A special final word of gratitude goes towards my wife and my daughter for their understanding and endless support throughout the duration of this period.

Resumo

As rochas carbonatadas são conhecidas pela forte heterogeneidade nos seus parâmetros petrográficos e petrofísicos. Em casos de subsuperfície, onde os dados são limitados a sondagens e onde existe uma grande complexidade no que respeita a modelação e gestão dos reservatórios, estudos multi-escala integrados incidindo sobre os controlos geológicos na variabilidade das propriedades da rocha são indispensáveis. Os casos de estudo em afloramentos oferecem informação importante no que respeita aos controlos deposicionais na variação de fácies e, potencialmente, das propriedades de reservatório. Neste sentido, três casos foram analisados neste projeto, dois incluindo afloramentos da Bacia Lusitânica (BL), Portugal, e um na subsuperfície da Bacia de Rub Al Khali, E.A.U.: a sucessão carbonatada-siliciclástica do Membro CC5 da Formação de Cabo Carvoeiro do Toarciano-Aaleniano(?) em Peniche (BL ocidental); a Formação de Santo António-Candeeiros do Batoniano-Caloviano na região do Maciço Calcário Estremenho (MCE) (BL central), Portugal; e o Membro Upper Kharaib (UKM) do Barremiano na subsuperfície de Abu Dhabi (E.A.U.).

Em termos gerais, este estudo tem como objetivo principal oferecer um melhor entendimento dos controlos na heterogeneidade de fácies e de propriedades petrofísicas, assim como da variação de geometrias deposicionais. Para atingir estes objetivos, foram efetuadas uma análise multi-escala de afloramentos e uma análise petrográfica semi-quantitativa, incluindo análise digital de imagem (DIA) utilizando *machine learning* para a quantificação de tipos de porosidade no caso de Abu Dhabi. Foram analisadas 312 laminas delgadas dos afloramentos de Peniche, 2 sondagens no *offshore* próximas de Peniche e 4 sondagens no *onshore* de Abu Dhabi.

A Formação de Cabo Carvoeiro observa-se exclusivamente em Peniche. O intervalo do topo caracteriza-se por uma sucessão de 160 m composta por *grainstones* oolíticos-intraclásticos com grãos de quartzo, em contraste com a sucessão de sedimentos hemipelágicos da Formação de São Gião na generalidade do *onshore* da BL. Um esquema de classificação de fácies detalhado mostrou-se indispensável ao revelar variações subtis e ciclicidade de fácies, permitindo a proposta de três novas subdivisões do Membro CC5. Duas sondagens no *offshore* foram analisadas (40-45 Km a sul e 15-20 Km a norte de Peniche) de modo a verificar a extensão regional das fácies *grainstone* observadas em Peniche. Esta sucessão foi interpretada neste estudo de acordo com um modelo de *infralittoral prograding wedges* e as fácies observadas não têm expressão significativa nas duas sondagens analisadas. As variações laterais de fácies através de biselamento, interdigitação ou gradação representam potenciais armadilhas estratigráficas que poderão promover a acumulação de hidrocarbonetos, considerando que existem rochas potencialmente geradoras do Sinemuriano-Pliensbaquiano que terão gerado estes fluidos e unidades com potencial selante na região. Sucessões

estratigráficas semelhantes à de Peniche poderão ocorrer em contextos análogos, nas bacias Lusitânica e de Peniche, oferecendo oportunidades na exploração de hidrocarbonetos na região.

A Formação de Santo António-Candeeiros foi analisada ao longo de frentes recentes em pedreiras na região do MCE, permitindo a observação e interpretação de características e geometrias deposicionais a um nível de detalhe que não é possível em afloramentos deteriorados. No Codaçal, a sucessão aflorante do Membro do Codaçal evolui de um intervalo basal caracterizado por geometrias tabulares e em cunha a grande escala com estratificação cruzada, para um intervalo de corpos lenticulares oo-bioclásticos e, para o topo, biostromas isolados ricos em corais, que passam lateralmente a intercalações decimétricas de *grainstones* e *rudstones*. A grande escala, observa-se a continuidade lateral de pacotes deposicionais nos membros de Codaçal e Pé da Pedreira. No entanto, a pequena escala, verifica-se uma variabilidade forte de fácies e geometrias deposicionais. Esta forte continuidade de corpos a grande escala e a variabilidade a pequena escala observadas em afloramentos oferecem informação importante na interpretação do caso de estudo de Abu Dhabi, visto existir alguma semelhança entre estes dois casos.

No UKM, a variação vertical de fácies e de permeabilidade é bem conhecida, em contraste com a porosidade total, que mostra baixa variabilidade. Contudo, os fatores que controlam a heterogeneidade petrofísica a pequena escala não são entendidos na sua totalidade. Nas sondagens estudadas, intervalos pouco espessos, delimitados por superfícies de descontinuidade e granulodecrescentes para o topo ocorrem na parte superior do UKM. Esta variação rítmica varia nas sondagens analisadas, indicando geometrias deposicionais complexas e uma extensão lateral limitada de corpos. A porosidade do reservatório caracteriza-se por um sistema de macro e microporosidade, onde esta última constitui a fração dominante da porosidade total. Esta heterogeneidade tem um forte impacto no comportamento do reservatório. A análise petrográfica e a quantificação dos tipos de porosidade através de DIA revelaram que os intervalos de alta permeabilidade correspondem a *grainstones* bem calibrados, com macroporosidade intergranular alta e fraca cimentação do espaço poroso. As observações e interpretações adquiridas mostram a importância em desenvolver estudos semi-quantitativos integrados, com foco na variabilidade de fácies e geometrias deposicionais a pequena escala, visto oferecerem informação indispensável para obter um melhor entendimento da heterogeneidade em carbonatos. Tal permitirá o desenvolvimento de modelos de reservatório com maior precisão e incluindo informação geológica de maior detalhe.

Palavras chave: carbonatos de meios pouco profundos; análise de afloramento e de subsuperfície; heterogeneidade de reservatórios carbonatados; análise digital de imagem; Mesozóico; Portugal; U.A.E.

Abstract

Carbonate successions are known to show great heterogeneity in facies and rock properties. In subsurface cases, where data is limited to well locations and the complexity in petroleum reservoir modelling and management is relatively high, multi-scale integrated studies addressing the geological controls on rock property variability are indispensable and greatly beneficial. The analysis of outcrop case studies offers valuable insights into depositional controls on facies variability and, potentially, reservoir properties heterogeneity. In this context, three case studies are addressed in this work, two including outcrops from the Lusitanian Basin (LB), Portugal and one focusing on subsurface data from the Rub Al Khali Basin, U.A.E.: the Toarcian-Aalenian(?) carbonate-siliciclastic mixed succession of the CC5 Member of the upper Cabo Carvoeiro Formation (CC Fm.) in Peniche (western LB); the Bathonian-Callovian Santo António-Candeeiros Formation in the Maciço Calcário Estremenho (MCE) region (central LB), Portugal; and the Barremian Upper Kharaib Member (UKM) in the Abu Dhabi subsurface (U.A.E.). In general terms, the present study aims to offer further insight into the controls on facies and petrophysical properties heterogeneity, as well as the variability in depositional geometries. To achieve these objectives, multi-scale outcrop analysis was carried out, as well as semi-quantitative petrography and digital image analysis (DIA), including machine learning methods for pore type quantification in the subsurface case. A total of 312 thin sections were analysed from the Peniche outcrops, 2 offshore wells near Peniche and 4 onshore wells in Abu Dhabi.

The topmost interval of the CC Fm. cropping out exclusively in Peniche, is characterized by a 160 m succession of oolitic-intraclastic grainstones with quartz, contrasting with the hemipelagic sediments of the coeval S. Gião Fm. in the LB onshore. A detailed facies classification scheme proved indispensable to reveal the subtle facies heterogeneity and cyclicity, allowing for 3 new sub-divisions to be proposed for the CC5 Member. Two nearby offshore wells were analysed (40-45 km to the south and 15-20 km to the north) to address the regional extension of this grainstone interval, interpreted in this study to have been deposited in infralittoral prograding wedges, which have very little expression at the well locations. Lateral facies variations through pinching-out, interfingering or gradation represent potential stratigraphic traps for hydrocarbons accumulations, considering the presence of Sinemurian-Pliensbachian mature source rocks and of potential seals. This Peniche succession might potentially be replicated in analogous settings in the Lusitanian and Peniche basins, offering opportunities for hydrocarbon exploration in the region.

The Santo António-Candeeiros Fm. was analysed along freshly-cut quarry fronts at the MCE, allowing for the analysis of depositional features and geometries at levels of detail which are not possible in weathered outcrops. At Codaçal, the exposed Codaçal Member succession evolves from a basal interval characterized by tabular and large-scale wedge-like geometries

with cross-bedding, through a section containing oo-bioclastic lenticular bodies, and into a top interval with isolated coral-rich biostrome mounds, laterally transitioning into decimetric grainstone-rudstones layers over short distances. Moderate to strong continuity of depositional packages is observed over large distances for the Codaçal and Pé da Pedreira members, but stronger lateral variability occurs at smaller centimetre/metre scale, especially observed in the Codaçal Member. The continuity of large-scale geobodies at greater observation scales and the strong small-scale variability provides further insight into the depositional controls on facies heterogeneity in this case and in the Abu Dhabi subsurface case, as there is moderate similarity between both cases.

The UKM shows well-known vertical heterogeneity in facies and permeability, in contrast to total porosity, which show little variability. However, the controls on small-scale facies and petrographic heterogeneity are not fully understood. In the studied wells, small-scale, discontinuity-bounded fining-upwards intervals occur in the upper half of the UKM, to some extent controlling pore type distribution. These rhythmic intervals vary from well to well, indicating complex depositional geometry patterns and limited lateral extension of geobodies. The porous network is characterized by a dual-porosity system containing micro and macro-pores, where microporosity is the dominant fraction by volume. Such heterogeneity will have a strong impact on reservoir performance. Petrographic analysis and the quantification of pore types through DIA revealed that high permeability intervals correspond to well-sorted grainstones with higher interparticle macroporosity and very low to no interparticle cementation in the studied wells. The acquired observations and interpretations show the importance of performing an integrated semi-quantitative analysis, with attention given to small-scale variability in facies and geometries, as they provide valuable information to better understand the controls on carbonate heterogeneity. An improved understanding of these control factors will allow for the creation of more reliable reservoir models based on sound geological concepts.

Keywords: shallow-water carbonates, outcrop and subsurface analysis, carbonate reservoir heterogeneity, digital image analysis, Mesozoic, Portugal, U.A.E.

Contents

List of Figures

List of Tables

Chapter I. General introduction

I.1. Introduction

Carbonate rocks are known to show strong spatial variability in facies and petrophysical properties, which is an issue of great relevance in exploration and development projects in the oil and gas industry, strongly influencing the outcome of reservoir characterization and management efforts, as well as field development plans, as has been expressed in various published studies (e.g. Weber, 1986; Wardlaw, 1996; Dabbouk et al., 2002; Gomes et al., 2008; Din et al., 2010; Hollis et al., 2010; Serag El Din et al., 2010; Fitch et al., 2015; Wei et al., 2015; Shekhar et al., 2017; Ehrenberg et al., 2018; Nazemi et al., 2018; Edwards et al., 2019; Nazari et al., 2019; Tavakoli, 2020). Hydrocarbon reservoirs in carbonate rocks hold more than half of the world's conventional petroleum reserves. However, the primary recovery factors from these reservoirs are low, to a large extent due to their heterogeneous nature, and less than half of the hydrocarbon volume is normally recovered from these reservoirs (e.g. Roehl and Choquette, 1985; Lucia et al., 2003; Burchette, 2012, 2019; Garland et al., 2012). As such, it is vital to obtain an improved understanding of the controls on rock property heterogeneity at different scales, in order to develop improved reservoir models with increased accuracy and geological significance (e.g. Gomes et al., 2008; Burchette, 2012; Gomes and Alves, 2013; Chandra et al., 2015).

The primary controls on carbonate heterogeneity are depositional in nature, as driven by the depositional system itself, and affected by biological production, palaeoenvironmental factors such as hydrodynamics, current activity or topography, which will influence facies distribution, carbonate productivity and variations in particle size, sorting and other petrographic parameters (e.g. Folk, 1962; Flügel, 2004; McNeill et al., 2004; Lucia, 2007; Pomar and Kendall, 2008; Reeder and Rankey, 2008; Zeller et al., 2015; Chiarella et al., 2017). Carbonate sediments are also highly susceptible to diagenetic alteration starting from very early stages, during deposition, and continuing throughout burial and periods of uplift, leading to further transformation of the original rock properties through processes such as compaction, dissolution, cementation or recrystallization, amongst others, which might either deteriorate or enhance porosity, as well as permeability to fluid flow (e.g. Moore, 1981; Schmoker, 1984; Tucker and Wright, 1990; Oswald et al., 1995; Flügel, 2004; Ehrenberg, 2006; Lucia, 2007; Cox et al., 2010). This adds to the high complexity in modelling rock property variability in carbonate systems. The resulting, usually highly heterogeneous, complex carbonate pore networks will strongly affect fluid flow through the rock volume. Higher permeability intervals will behave as preferred fluid flow paths, leading to issues such as early water breakthrough during production, namely in the cases of waterflood field development projects, while significant volumes of bypassed oil might remain in place, within the less permeable or

microporous geobodies (in most cases associated with factors relevant to fluid behaviour, such as variable capillary pressure, relative permeability or wettability within the heterogeneous pore network), strongly impacting reservoir performance and reducing oil recovery efficiency (e.g. Weber, 1986; Namba and Hiraoka, 1995; Chilingarian et al., 1992; Wardlaw, 1996; Cunningham and Chaliha, 2002; Dabbouk et al., 2002; Masalmeh, 2002; Masalmeh et al., 2003; Carvalho et al., 2011). It is, therefore, highly relevant to pursue an improved understanding of the geological factors controlling such heterogeneities.

However, carbonate studies in the subsurface are based on well data, which provide limited control points, leaving inter-well areas to be populated by models, in most cases assisted by seismic data. In these cases, the limited resolution of seismic data and the uncertainty associated with reservoir models will impact the understanding of small-scale lateral heterogeneities (e.g. Mellvile et al., 2004; Yose et al., 2006; Lucia, 2007; Gomes et al., 2008; Carvalho et al., 2011; Burchette, 2012; Alnazghah et al., 2013). To this extent, outcrop studies are of great value in improving this understanding of carbonate systems, as they allow for detailed, laterally continuous observations on depositional geometries and spatial facies variability at different scales, which are not achievable in the subsurface (e.g. Weber, 1986; Borgomano et al., 2002; Van Buchem et al., 2002; Grammer et al., 2004; Strohmenger et al., 2006; Zeller et al., 2011; Jung and Aigner, 2012; Palermo et al., 2012; Fitch et al., 2015; Adam et al., 2018; Azerêdo et al., 2020; Petrovic, 2020).

In this context, two outcrop case studies in the Lusitanian Basin, Portugal, and one subsurface case in the Rub Al Khali Basin, U.A.E., were addressed in the present study (Figure I.1), with all three case studies representing carbonate successions originating in relatively shallow-water depositional environments. Although there are differences between the palaeoenvironment and depositional setting of these three cases, primary factors and depositional controls such as hydrodynamics and current activity are systematically present in shallow-water carbonate systems, affecting sedimentation and depositional patterns to a different extent in each different case (e.g. Braithwaite, 1973; Borgomano et al., 2002; Schlager, 2005; Ruberti et al., 2006; Pomar and Kendall, 2008; Reeder and Rankey, 2008; Alsharhan and Kendall, 2010; Alnazghah et al., 2013; Hönig and John, 2015). The age, as well as the depositional and stratigraphic settings are distinct between the three cases, as mentioned above, and will be described in further detail in each corresponding chapter. The analysed outcrops include the Lower Jurassic, Toarcian-Aalenian(?) upper Cabo Carvoeiro Formation in Peniche, Portugal, as well as the Middle Jurassic Bathonian-Callovian Santo António-Candeeiros Formation exposed in freshly-cut quarry fronts of the Maciço Calcário Estremenho (MCE), Portugal, which provide excellent opportunities to acquire further insights on facies heterogeneity and variations in depositional geometries at different observation scales. The lithostratigraphy and sedimentary features of these intervals are well studied in Peniche (e.g. Wright and Wilson, 1984; Duarte, 1995, 1997; Duarte and Soares, 2002) and in the MCE (e.g. Azerêdo, 1993, 1998, 2007; Azerêdo et al.,

2020). The subsurface case study of the U.A.E. is the main hydrocarbon reservoir unit in Abu Dhabi, represented by the Lower Cretaceous Barremian Upper Kharaib Member of the Kharaib Formation. It offers an excellent opportunity to further analyse carbonate heterogeneity in a subsurface case, given the vast availability of supporting data and the number of published studies addressing different subjects of the reservoir in different oil fields (e.g. Harris et al., 1968; Alsharhan, 1990, 1993; Lijmbach et al., 1992; Oswald et al., 1995; Taher, 1996; Alsharhan and Nairn, 1997; Van Buchem et al., 2002, 2010; Strohmenger et al., 2006; Cox et al., 2010; El Wazir et al., 2015; Morad et al., 2016; Ehrenberg et al., 2016, 2018; Morad et al., 2019). This stratigraphic unit has received continued attention over the years directed to its well-known variability in facies and to the issue of petrophysical properties variations (e.g. Grötsch et al., 1998; Melville et al., 2004; Strohmenger et al., 2006; Jeong et al., 2017; Ehrenberg et al., 2018), although relative uncertainty still remains regarding small-scale heterogeneity (Ehrenberg, 2019; Ehrenberg et al., 2020a, 2020b).

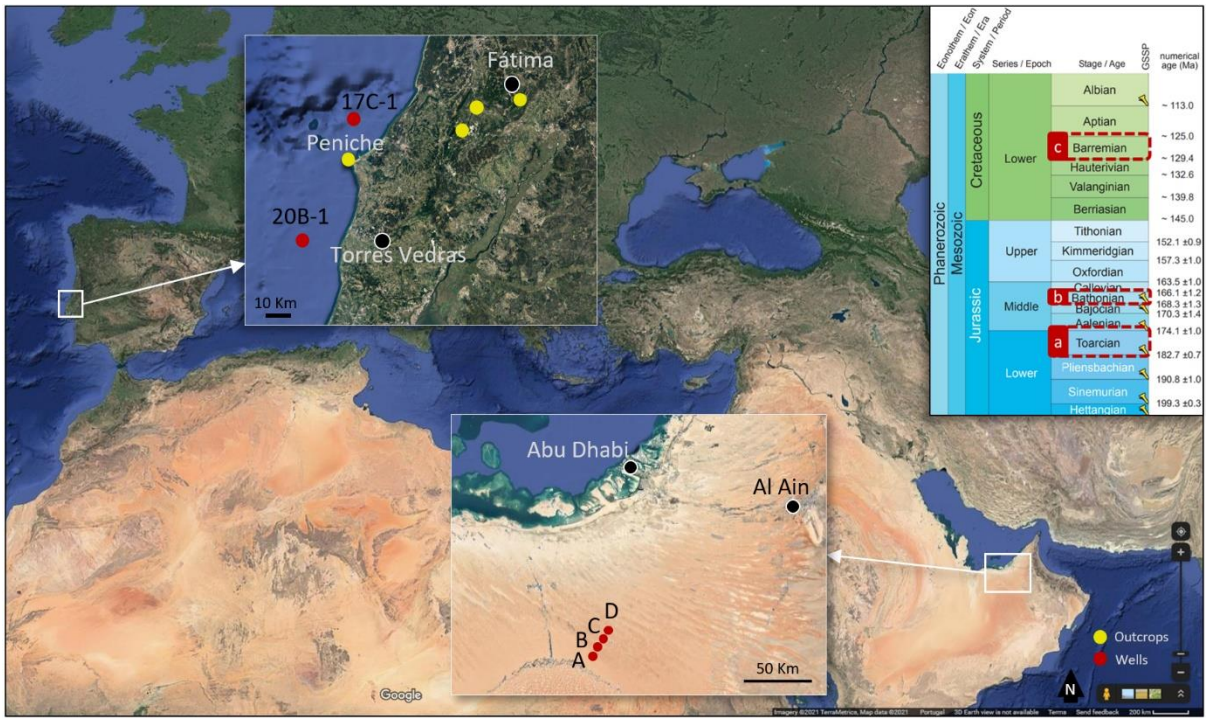

Figure I.1. Case studies overview, showing locations of studied outcrops in Portugal (yellow circles) and wells, both in Portugal and the U.A.E. (red circles). Satellite image of Central/Southern Europe, North Africa and Middle East, as well as the zoomed-in regions of Western Central Portugal and Abu Dhabi, U.A.E are represented here (Google, 2020a, b, c). The chronostratigraphic intervals for each case study are indicated in the inserted table (Cohen et al., 2013). a: Cabo Carvoeiro Formation, Peniche, Portugal; b: Santo António-Candeeiros Formation, MCE, Portugal; c: Kharaib Formation, Abu Dhabi, U.A.E.

I.2. Objectives

In general terms, the main objective of this study is to offer further insights into the factors controlling facies and petrophysical heterogeneity, as well as variations in depositional geometries, through the analysis of the mentioned case studies.

The objectives for the Peniche outcrop case study are to: (a) Provide a better understanding on the depositional factors controlling the cyclicity and spatial variability in the subtle petrographic characteristics of the rock; (b) Create a detailed facies classification scheme for the upper CC5 Member, using visual estimations and digital image analysis in a semi-quantitative approach, in order to capture subtle facies variability in an interval generally characterized by more than 120 m of grainstone facies; (c) Identify and interpret multi-scale depositional trends and geometric relationships between geobodies based on outcrop observations; (d) Address the hydrocarbon reservoir potential of the studied interval by integrating outcrop observations with subsurface data from nearby wells; (e) Identify and address the potential occurrence of different petroleum system elements.

The objectives of the MCE outcrop case study are to: (a) Define and interpret vertical and lateral geometric relationships between depositional bodies, by analysing depositional geometries at different scales; (b) Compare the outcrop architecture and geometric relationships with data from the Abu Dhabi subsurface case study, in order to provide further insight into the issues of lateral continuity of geobodies in inter-well space.

The objectives of the Abu Dhabi subsurface case study are to: (a) Provide further insight into small-scale vertical and lateral facies variability; (b) Quantify macroporosity through digital image analysis methodologies (visual estimation, colour selection and machine learning); (c) Address the vertical distribution of pore types, as well as the correlation with permeability variations; (d) Acquire an improved understanding of the controls on petrophysical properties variability and on the occurrence of high permeability layers, through the integration of semi-quantitative petrographic data and petrophysical data.

The direct observations on the two outcrop case studies allow for interpretations on spatial continuity of facies and depositional geometries at different scales, as previously mentioned. Undertaking a multi-scale outcrop analysis of freshly-cut quarry fronts at the MCE will help in interpreting the variability in depositional geometries at a level of detail which would not be possible in other outcrops affected by weathering or in the subsurface. In this study, different fit-for-purpose facies classification schemes are applied, based on the objectives, aiming to capture subtle facies variations in the Peniche outcrop case, as well as to provide an improved understanding of the relationship between depositional facies and petrophysical variability in the Abu Dhabi subsurface case.

An important objective of this study is the acquisition of semi-quantitative data to describe petrographic parameters, such as grain sorting, grain size and pore types, including data generated through digital image analysis, as this will provide valuable information (e.g. James, 1995; Tovey and Wang, 1997; Anselmetti et al., 1998; Nabawy, 2014; Fullmer et al., 2014; Buckman et al, 2017; Chandra et al., 2019; Nanjo and Tanaka, 2019; Pal et al., 2019; Al Khalifa et al., 2020). While a vast number of sedimentological and petrographic studies mostly present qualitative results, a quantitative approach is preferred, when possible, as it provides valuable numerical data that can be objectively compared and utilized in models, allowing to reduce the uncertainty of reservoir models and improving the predictability of reservoir properties in inter-well areas (e.g., Parker and Bruce, 1994; Flügel, 2004; Grammer et al., 2004; Lucia, 2007; Gomes et al., 2008; Nader et al., 2013; Inês et al., 2015; Nader, 2017).

I.3. Thesis outline

An overview of the organization of this thesis is here presented. As exposed in the sections above, the present chapter offers a general introduction and the overall context for the carbonate heterogeneity issues driving this study (Section I.1), as well as the main objectives defined to address this problematic in the different case studies (Section I.2). In this chapter, a brief overview of the three case studies (Section I.4) and of the methodologies applied (Section I.5), which will be further detailed in the respective chapters, are also presented. Following this introductory chapter, this thesis is separated into three main chapters, each depicting the different case studies, with the first two being subdivided into two sub-chapters. Each of these chapters/sub-chapters is written in the form of a scientific paper, with the perspective of publishing in international journals. The final chapter presents the summary and final considerations resulting from a global and integrated appreciation of this study. The main points of interest going forward are also briefly presented.

In Chapter II.1, the upper part of the CC5 Member of the Cabo Carvoeiro Formation is analysed at different observation scales and a detailed facies classification scheme is developed, in order to offer a better understanding of the palaeoenvironment and the factors controlling spatial variability in facies and geometric features. This chapter has resulted in an article published in the Journal of Iberian Geology (https://doi.org/10.1007/s41513-021-00163-2).

Chapter II.2 addresses the upper Cabo Carvoeiro Formation grainstone succession as a potential hydrocarbon reservoir unit. Thin sections from the coeval intervals of two nearby offshore wells were analysed to better understand the lateral extension of the overall grainstone facies observed on the Peniche outcrops. The potential petroleum system elements are addressed, taking into consideration the hypothetical development of favourable conditions for hydrocarbon accumulations in analogous locations of the Lusitanian and Peniche basin.

Chapter III.1 presents the outcome of the application of digital image analysis methods (visual estimation, non-contiguous colour selection and trained machine learning) to macroporosity quantification in the Abu Dhabi case study (Upper Kharaib Member of the Kharaib Formation). The results are compared in order to define the most objective method, considered to offer lower uncertainty levels.

Chapter III.2 discusses the controls on reservoir heterogeneity in the Abu Dhabi case study by integrating the results from macroporosity quantification through digital image analysis with petrographic and petrophysical data. A multi-scale analysis of vertical facies variability is presented based on core and thin section interpretations to provide further insights into paleoenvironmental controls on lateral facies variability.

The manuscripts for Chapters III.1 and III.2 were prepared for submission to international journals, pending permission to publish due to confidentiality issues, at the time of submission of this thesis.

Chapter IV presents the multi-scale outcrop analysis of depositional geometries done at different locations of the MCE for the Santo António-Candeeiros Formation (Codaçal and Pé da Pedreira members). Observations acquired from this case study provide further insight into reservoir heterogeneity driven by depositional factors and influenced by the architecture of deposition. A comparison with subsurface data from the Abu Dhabi case study is presented, to complement the observations and conceptual interpretations presented in the previous chapter. The resulting manuscript has been submitted to a specialized international journal for publication, at the time of submission of this thesis.

I.4. Geological framework and overview

An overview of the three case studies addressed in this project is presented in this section, as the geological background for each case study is described in further detail in each corresponding chapter. As previously mentioned, the two outcrop cases are located in the Lusitanian Basin, Portugal, while the subsurface case is located in the Rub Al Khali Basin, U.A.E.

I.4.1. The Lusitanian Basin, Portugal

This basin, extending along central western Portugal, is delimited to the east by the exposed Hercynian basement and to the west by a marginal system of uplifted blocks, part of a regional horst-graben system, separating it from the deeper offshore Peniche Basin and today only exposed in the form of the Berlengas archipelago (Figure I.2) (e.g. Vanney and Mougenot

1981; Wilson et al., 1989; Pinheiro et al., 1996; Alves et al., 2002, 2003a). The LB developed in an extensional regime associated with the Atlantic opening, under the influence of strong tectonic activity influencing sedimentation and structuration, including different rifting phases, leading to the creation of the above-mentioned horst-graben structures, as well as complex fault patterns and halokinetic structures (e.g. Wilson, 1975; Mougenot et al., 1979; Boillot et al, 1979; Vanney and Mougenot, 1981; Wright and Wilson, 1984; Wilson et al., 1989; Hiscott et al., 1990; Pinheiro et al., 1996; Rasmussen et al., 1998; Alves et al., 2002, 2003a, 2006; Kullberg et al., 2013). Deposition of the Mesozoic sediments and infill of the LB, depositional geometries and facies distribution were strongly influenced by this activity, through the creation of an irregular topography and localized depocenters in fault-bounded half-grabens for example, in addition to the underlying constraints of the depositional system itself (e.g. Mougenot et al., 1979; Wilson et al., 1989; Hiscott et al., 1990; Rasmussen et al., 1998; Alves et al., 2002, 2006; Kullberg et al., 2013). Parts of the Mesozoic succession are exposed at different locations across western central Portugal (Figure I.2).

The LB has received moderate attention regarding hydrocarbon exploration, with modern hydrocarbon exploration having started in 1938 (Gomes, 1981). A total of 175 wells targeting structural traps have been drilled in the LB, with 117 of these wells showing oil or gas shows but no relevant accumulations. The Peniche Basin further offshore, on the other hand, has not been drilled and is expected to contain the same petroleum system elements as the LB (ENMC/UPEP, 2016).

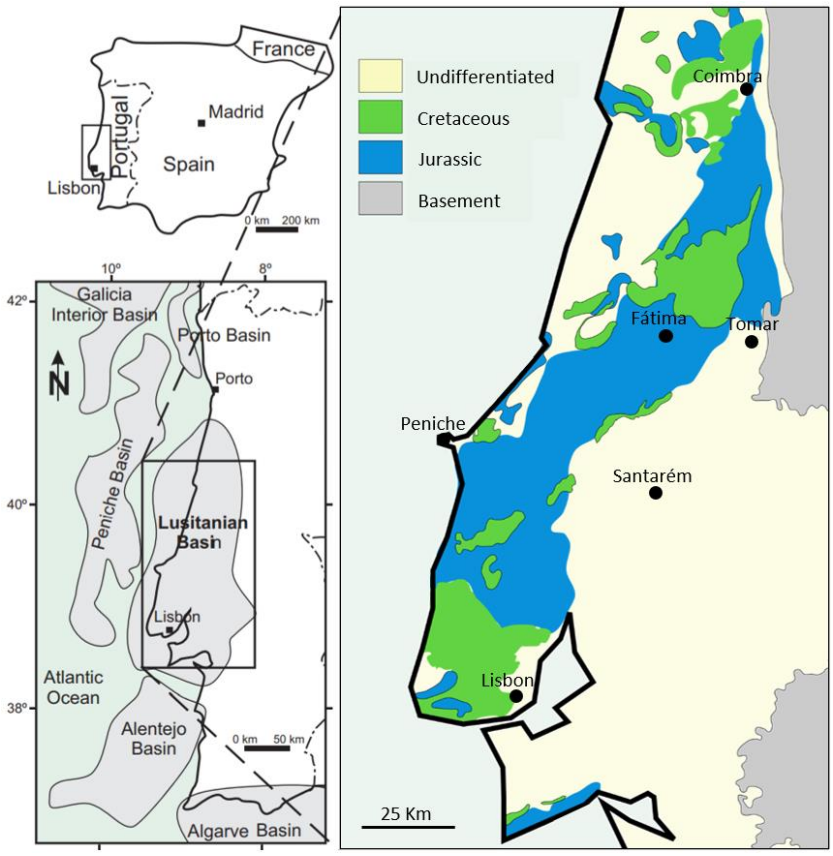

Figure I.2. Maps of the Iberian Peninsula and Portugal, indicating the location of major sedimentary basins (in Duarte et al., 2012). Simplified geological map of western central Portugal showing major areas where Mesozoic sediments are exposed (based on LNEG, 2010).

I.4.1.1. Stratigraphic context

The sedimentary infill of the LB, from Triassic to Cretaceous, initiates with a thick siliciclastic and evaporitic succession, and is characterized by deposition in an extensional regime, which led to the development of fault-block structures, as indicated by regional variations in sediment thickness, as mentioned above (e.g. Vanney and Mougenot, 1981; Montenat et al., 1988; Wilson et al., 1989; Soares et al., 1993). The Upper Triassic in the LB is characterized by the deposition of continental fluvial siliciclastics (Silves Group), as well as evaporites and dolomites of the Dagorda Formation and its lateral equivalent Hettangian Pereiros Formation (detrital limestones and dolomites) to the east (Figure I.3) (e.g. Palain, 1976; Azerêdo et al., 2003; Soares et al., 2012). This sedimentation of evaporitic and dolomitic nature continues into the Early Jurassic Hettangian-Sinemurian and reflects the beginning of a gradual transition into open marine settings, which prevail during the Early and Middle Jurassic, when a westward dipping homoclinal carbonate ramp is developed (e.g. Azerêdo, 1988, 1998; Soares et al., 1993; Duarte 1997, 2007; Duarte et al., 2001, 2010; Silva et al., 2015). An increasingly marked differentiation in sedimentation and depositional conditions is observed in the Middle Jurassic in the LB, with deeper water sediments dominating the western/northwestern region and shallower water facies progressively dominating the eastern/southeastern region (e.g. Azerêdo, 1988, 1993, 1998, 2007; Soares et al., 1993).

The basal Sinemurian succession of dolomitic sediments grading into limestones and marly limestones (Coimbra Formation), reflect the progressive establishment of marine conditions in the basin. In the upper Sinemurian, and into the Pliensbachian, the marly limestones of the Água de Madeiros Formation are deposited, followed by the outer ramp marly limestones of Vale das Fontes Formation, both of these considerably rich in organic matter, and the marly limestones and calcareous marls of the Lemede Formation (Figure I.3) (e.g. Soares et al., 1993; Duarte and Soares, 2002; Oliveira et al., 2006; Duarte et al., 2010, 2012; Silva et al., 2011, 2015; Coimbra and Duarte, 2020). The Toarcian is characterized by deposition of the hemipelagic marly limestones of the S. Gião in the generality of the basin, which are laterally equivalent to the bioclastic limestones of the Prado Formation in Tomar and the Cabo Carvoeiro Formation at Peniche (Duarte, 1997; Duarte et al., 2001, 2004; Duarte and Soares, 2002; Figure I.3), defined by intercalations of marls and fine-grained marly limestone in the base and intercalations of marls and intraclastic, siliciclastic and ooidal grainstones towards the top, with grainstones dominating the topmost interval (e.g. Wright and Wilson, 1984; Duarte, 1997).

In the Middle Jurassic, the western region is characterized by the deeper-water marls and marly limestones of the Cabo Mondego Formation (*sensu* Azerêdo et al., 2003), while in the eastern region, shallow water sediments are progressively dominant (e.g. Azerêdo, 1988, 1993, 1998, 2007; Soares et al., 1993; Azerêdo et al., 2003). The Middle Jurassic succession is particularly well studied in the MCE area, where the succession is characterized by the marls and marly limestones of the Aalenian-Bajocian Barranco do Zambujal Formation; marly limestones, dolomitized limestones and dolomites of the Upper Bajocian Chão das Pias Formation; the Bathonian-Callovian shallow water limestones of the Santo António-Candeeiros Formation and the laterally equivalent limestones and dolomitized micritic limestones of the Serra de Aire Formation (Figure I.3) (e.g. Azerêdo, 2007)

The Upper Jurassic is characterized by limestone sediments in the Oxfordian (Cabaços and Montejunto formations) (e.g. Wilson, 1979; Leinfleder, 1993; Azerêdo, 1998; Leinfelder and Wilson, 1998; Azerêdo et al., 2002) transitioning vertically into siliciclastic-dominated sedimentation (e.g. Wilson et al., 1989; Leinfleder, 1993; Leinfelder and Wilson, 1998), which continues into the Cretaceous, although depositional settings of increased marine influence occur towards the southern region of the LB during the Early Cretaceous (e.g. Dinis et al., 2008; Rey et al., 2006). Throughout the remainder of the Cretaceous, deposition of siliciclastics is dominant in the northern region of the LB (e.g. Cunha and Pena dos Reis, 1995; Rey et al., 2006).

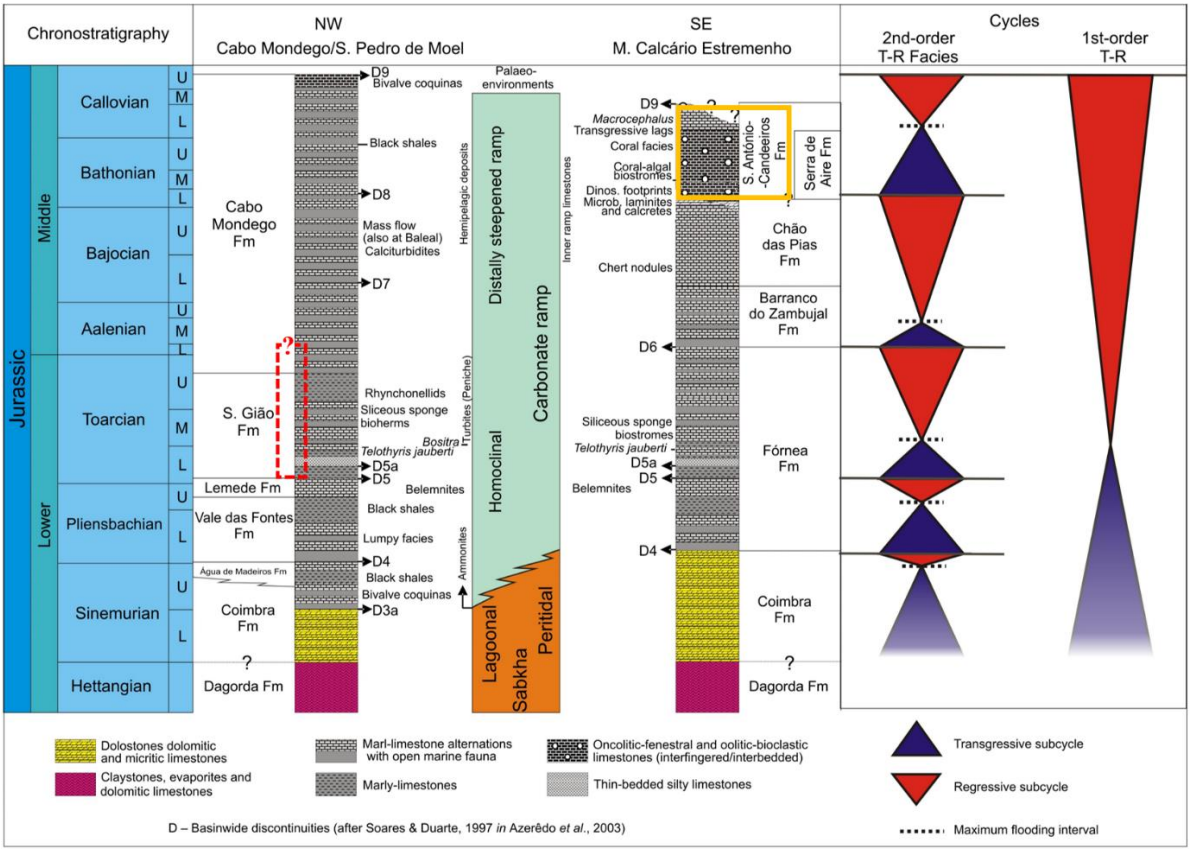

Figure I.3. Synthetic chart for the Lower and Middle Jurassic of the LB showing the chronostratigraphy, lithostratigraphy, and transgressive-regressive facies cycles (in Azerêdo et al., 2015). The singular Lower Jurassic Peniche succession addressed in this study is not represented in this table. However, its projected stratigraphic position and lateral equivalents are indicated (red rectangle). The analysed Santo António-Candeeiros Formation at the MCE is indicated (yellow rectangle).

I.4.1.2. The Cabo Carvoeiro Formation

The mixed carbonate-siliciclastic Toarcian-Aalenian(?) Cabo Carvoeiro Formation is divided into five members (CC1 to CC5) (Duarte and Soares, 2002) and crops out exclusively in the Peniche area, representing an evolution from hemipelagic to shallow-water sediments deposited under the influence of the progressive tectonic uplift of the Berlengas basement block (e.g. Wilson et al., 1989; Wright and Wilson, 1984; Duarte, 1995, 1997; Duarte and Soares, 2002). The upper part of the CC5 Member, which has been interpreted as originating from point-source sedimentation in a mid-fan environment or, alternatively as line-source sedimentation over a geographically limited area (Wright and Wilson, 1984; see also Barata et al., 2021), is the focus of this study. This interval is almost exclusively characterized by grainstones with intraclasts, ooids, skeletal grains and quartz grains, with the occurrence of beds with abundant crinoids and quartz-rich channel structures (e.g. Wright and Wilson, 1984; Duarte and Soares, 2002). These facies types are contrasting with the generally marly sediments of the S. Gião Formation (Figure I.3) deposited in the wider LB onshore region, which further details the singularity of this Peniche succession (e.g. Duarte, 1995, 1997; Duarte and Soares, 2002).

I.4.1.3. The Santo António-Candeeiros Formation

The Bathonian to Callovian Santo António-Candeeiros Formation (Figure I.3) was deposited in inner ramp and high energy barrier island depositional environments, is divided into the Codaçal, Pé da Pedreira and Moleanos members, varies in thickness from 350 m to more than 400 m, and is truncated at the top by a major discontinuity (e.g. Azerêdo, 1993, 1998, 2007; Azerêdo et al., 2002). The studied outcrops, exposing the analysed Codaçal and Pé da Pedreira members, are located in the Maciço Calcário Estremenho hills, in quarry fronts at different locations (Codaçal/Cabeço Vedeiro, Cabeça Veada and Casal Farto). This succession shows moderate facies variability, in general terms varying between bioclastic and oobioclastic grainstones, oobiosparite grainstones-rudstones with intraclasts, peloids and oncoids, with layers of coral and algal biostromes occurring in the Codaçal Member (Azerêdo, 2007); grainstones to rudstones containing ooids, peloids, skeletal grains and intraclasts, with frequent coarse-grained bioclastic layers, sometimes defining tempestites, as well as biostromes in the Pé da Pedreira Member (Azerêdo, 2007); rudstones, grainstones and packstones containing ooids, biolcasts, oncolites and lithoclasts intercalating with fossiliferous carbonate layers

described as coral/algal biostromes and bioturbated pelmicritic carbonates in the Moleanos Member (Azerêdo, 2007).

I.4.2. The Rub Al Khali Basin, U.A.E.

The studied UKM of the Lower Cretaceous Kharaib Formation was deposited in the Rub Al Khali Basin, which is a prolific hydrocarbon producing basin, holding all major reservoirs and fields in the U.A.E. and covering areas of Saudi Arabia, U.A.E. and Oman (Figure I.4) (e.g. Lijmbach et al., 1992; Alsharhan, 1989, 1993; Taher, 1996; Alsharhan and Nairn, 1997).

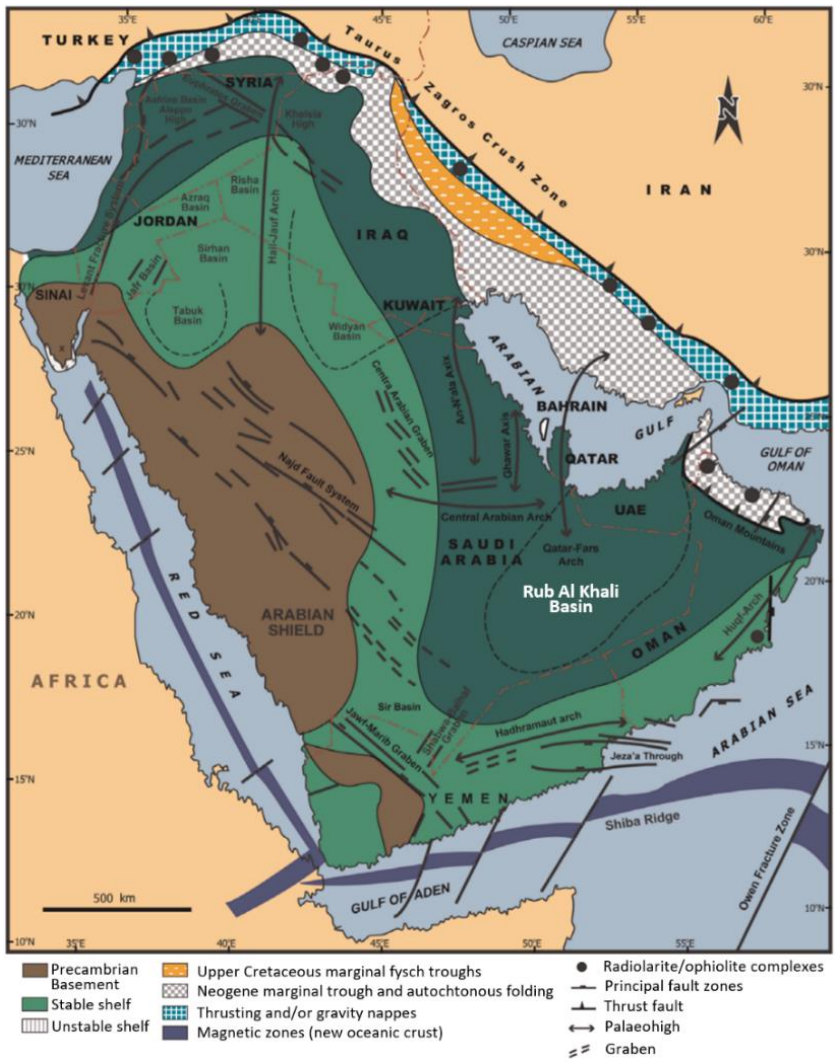

Figure I.4. Map of the Arabian Peninsula showing the location of the Rub Al Khali Basin. Main tectonic elements and structural trends are indicated (Alsharhan, 2014 and references therein).

This basin is located in the southeastern region of the Arabian Peninsula, extending into the Arabian Gulf. It is bounded to the north/northeast by the Zagros mountains, to the east-southeast by the Oman mountains, to the west/northwest by the Central Arabian Arch, Qatar Arch and Arabian Shield, and to the south by the Hadhramout Arch (Figure I.4) (e.g. Powers et al., 1966; Murris, 1980; Soliman and Al Shamlan, 1982; Alsharhan and Nairn, 1997). While the Early Cretaceous is characterized as a time of relative tectonic quiescence, from the Late Cretaceous onwards, the area is subjected to different compressional tectonic events which led to deformation of the strata and the creation of the present-day structural configuration of the Abu Dhabi subsurface strata, promoting the accumulation of large hydrocarbon volumes (e.g. Searle, 1988; Oswald et al., 1995; Loosveld et al., 1996; Alsharhan and Nairn, 1997; Johnson et al., 2005; Glennie et al., 2010; Searle et al., 2014; Stewart, 2016; Richard et al., 2017). The presence of thicker Cambrian Hormuz salt deposits in the Abu Dhabi offshore has also had a strong influence on structuration in this area (e.g. Alsharhan, 1990; Glennie, 2010; Thomas et al., 2015; Richard et al., 2017).

I.4.2.1. Stratigraphic context

Following the evaporitic sedimentation of the late Precambrian to early Cambrian, siliciclastic sedimentation is dominant through most of the Paleozoic. The late Carboniferous to the early Triassic in the U.A.E is generally characterized by a succession of fluvial siliciclastics, followed by carbonate deposition in a widespread carbonate platform characterized by the limestones and dolomites with anhydrite of the Late Permian-Early Triassic(?) Khuff Formation (Figure I.5) (e.g. Murris, 1980; Alsharhan and Nairn, 1997). Most of the Triassic is defined by sedimentation in a carbonate, evaporitic platform (limestones, argillaceous limestones, dolomites and thin anhydritic beds of the Early Triassic Sudair Formation and Middle Triassic Jilh/Gulailah Formation), although higher influx of continental siliciclastic sediments occurred in the Late Triassic, in response to a decrease in relative sea level (Minjur Formation) (e.g. Murris, 1980; Alsharhan and Nairn, 1997; Sharland et al., 2001).

During the Early Jurassic, widespread carbonate deposition gradually increases in a vast carbonate-evaporite platform in the region. A major inundation of the platform occurs in the Late Jurassic, leading to deposition of the organic-rich carbonate Diyab Formation (Figure I.5), which is a major source rock in the region (e.g. Lijmbach et al., 1992; de Matos and Hulstrand, 1995; Whittle and Alsharhan, 1996; Alsharhan and Nairn, 1997; Al Suwaidi et al., 2000; Sharland et al., 2001). Extensive sedimentation of evaporites occurs in the Tithonian driven by increased arid conditions, before the return to the predominant carbonate deposition in a wide-spread ramp setting. This setting prevails during the Early Cretaceous, with deposition of the Thamama Group succession, which is characterized by discontinuity-bounded intervals with major porous carbonate reservoir zones interlayered with argillaceous limestones, showing

lateral continuity over large distances and reflecting deposition in this relatively stable widespread epeiric carbonate platform (e.g. Harris et al., 1968; Murris, 1980; Alsharhan, 1989; Alsharhan and Nairn, 1997; Van Buchem et al., 2002, 2010; Davies et al., 2002; Strohmenger et al., 2006). As relative sea-level gradually increases, a basin wide inundation event is registered in the Aptian, with an intrashelf basin developing at this time (Bab Member, Shuaiba Formation; Figure I.5) (e.g. Murris, 1980; Alsharhan and Kendall, 1991; Azer and Toland, 1993; Van Buchem et al., 2002, 2010). A subsequent regression phase and major relative sea-level fall occurs, with deposition of the argillaceous limestones, siltstones and minor limestones of the Albian Nahr Umr Formation in shallow marine settings, which is a major sealing unit in Abu Dhabi (e.g. Murris, 1980; Alsharhan, 1991; Alsharhan and Kendall, 1991). This is followed by a period of overall mixed carbonate-siliciclastic sedimentation and general rise in relative sea-level, with an intrashelf basin developing in the late Albian-Cenomanian (Shilaif Formation) (e.g. Murris, 1980; Alsharhan and Kendall, 1991; Burchette, 1993; Alsharhan and Nairn, 1997). Above, siliciclastic influx and argillaceous limestones reflect sedimentation of increased continental influence, as relative sea-level decreases and a major discontinuity is registered in the wider region (e.g. Murris, 1980; Alsharhan and Kendall, 1991). At this time, and in the post-Turonian period, deep shelf, open-marine settings are generally established, mostly characterized by deposition of marls and marly limestones and influenced by the combined effects of relative sea-level changes and tectonics. During the late Maastrichtian, with a moderate decrease in tectonic activity, limestones and dolomitic limestones of the Simsima Formation (Figure I.5) are deposited in semi-restricted, shallow-water marine setting (e.g. Murris, 1980; Alsharhan and Kendall, 1991; Alsharhan, 1995; Alsharhan and Nairn, 1997).

During the Palaeogene-Neogene, the open marine basin gradually reduces in size due to progradation of the carbonate platform from the west and to the rise of the Zagros orogeny in the northeast (from Eocene until early Miocene). Sedimentation is generally characterized by anhydritic and argillaceous limestones, dolomitic limestones and limestones in shallow marine environments. In the Miocene, marls, thin beds of lacustrine limestone, sandstone, as well as anhydritic beds are deposited, reflecting the increasing influence of non-marine to marginal-marine settings (e.g. Murris, 1980; Alsharhan and Nairn, 1997).

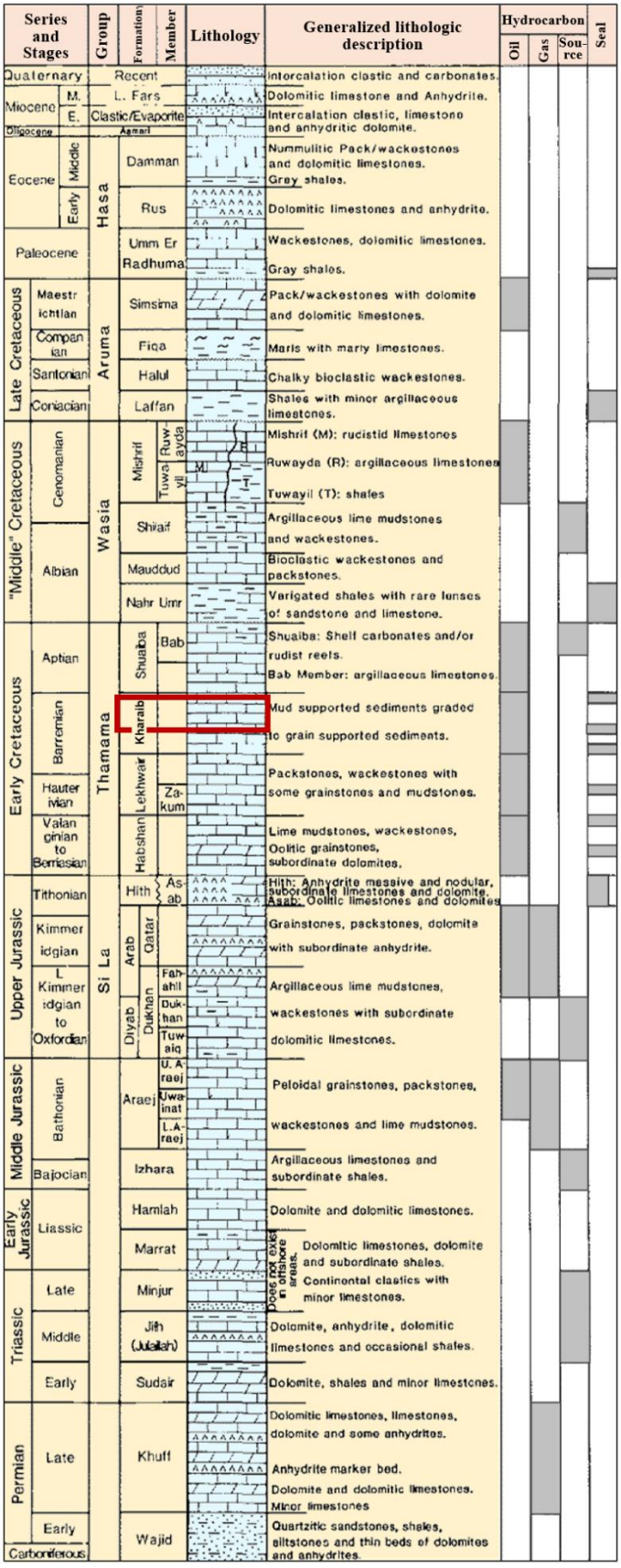

Figure I.5. General lithostratigraphy of Abu Dhabi and main petroleum systems elements (Alsharhan, 1993). The studied Barremian interval is indicated (red rectangle).

I.4.2.2. The Kharaib Formation

This unit is part of the Lower Cretaceous Thamama group and includes the Barremian UKM (Figure I.6), which is the most important reservoir in Abu Dhabi (e.g. Lijmbach et al., 1992; Alsharhan, 1989, 1993; Taher, 1996; Alsharhan and Nairn, 1997). Different informal terminologies are used to define this stratigraphic interval by the oil companies in Abu Dhabi, as well as by different authors in the region, as exemplified by Van Buchem et al. (2010) or Metwalli and Khouri (2016), for example. These nomenclatures include 'Thamama Zone B' (e.g. Harris, 1968; Alsharhan, 1993), 'Thamama Zone II', in the offshore (e.g. Alsharhan, 1990), 'Upper Kharaib Reservoir Unit' (Strohmenger et al., 2006) or the 'Upper Kharaib Member' (e.g. Pittet et al., 2002; Van Buchem et al., 2002, 2010). The latter is adopted in this work, as is the 'Kharaib Formation' terminology (e.g. Hassan et al., 1975; Alsharhan and Nairn, 1997).

The UKM reflects deposition in a widespread epeiric carbonate platform under the influence of minor or null tectonic activity, as previously mentioned (e.g. Harris et al., 1968; Murris, 1980; Alsharhan, 1989; Azer and Toland, 1993; Alsharhan and Nairn, 1997; Davies et al., 2002; Van Buchem et al., 2002). This stratigraphic interval shows an overall shallowing-upwards trend, developing from low-energy, deep-water (open marine/open platform conditions) skeletal wackestones with orbitolinids into high-energy, shallow-water inner ramp packstones, bioclastic-intraclastic grainstones and rudstone-grainstones with rudists, ending in a strong discontinuity surface (e.g. Alsharhan, 1989; Alsharhan and Nairn, 1997; Van Buchem et al., 2002, 2010; Strohmenger et al., 2006). This interval shows considerable heterogeneity at different scales, with well-known vertical variability in facies and permeability, in contrast to total porosity, which shows no clear vertical variability trends for a given well (Figure I.6) (e.g. Harris et al., 1968; Alsharhan, 1993; Alsharhan and Nairn, 1997; Grötsch et al., 1998; Van Buchem et al., 2002; Melville et al., 2004; Strohmenger et al., 2006; El Wazir et al., 2015; Ehrenberg, 2019; Jeong et al., 2017). Its porosity network is characterized by a dual porosity system containing micro and macro-pores, where microporosity is the dominant fraction by volume (e.g. Harris et al., 1968; Oswald et al., 1995; Budd, 1995; Morad et al., 2016; Ehrenberg et al., 2018; Ehrenberg, 2019), increasing the complexity in reservoir characterization and management efforts.

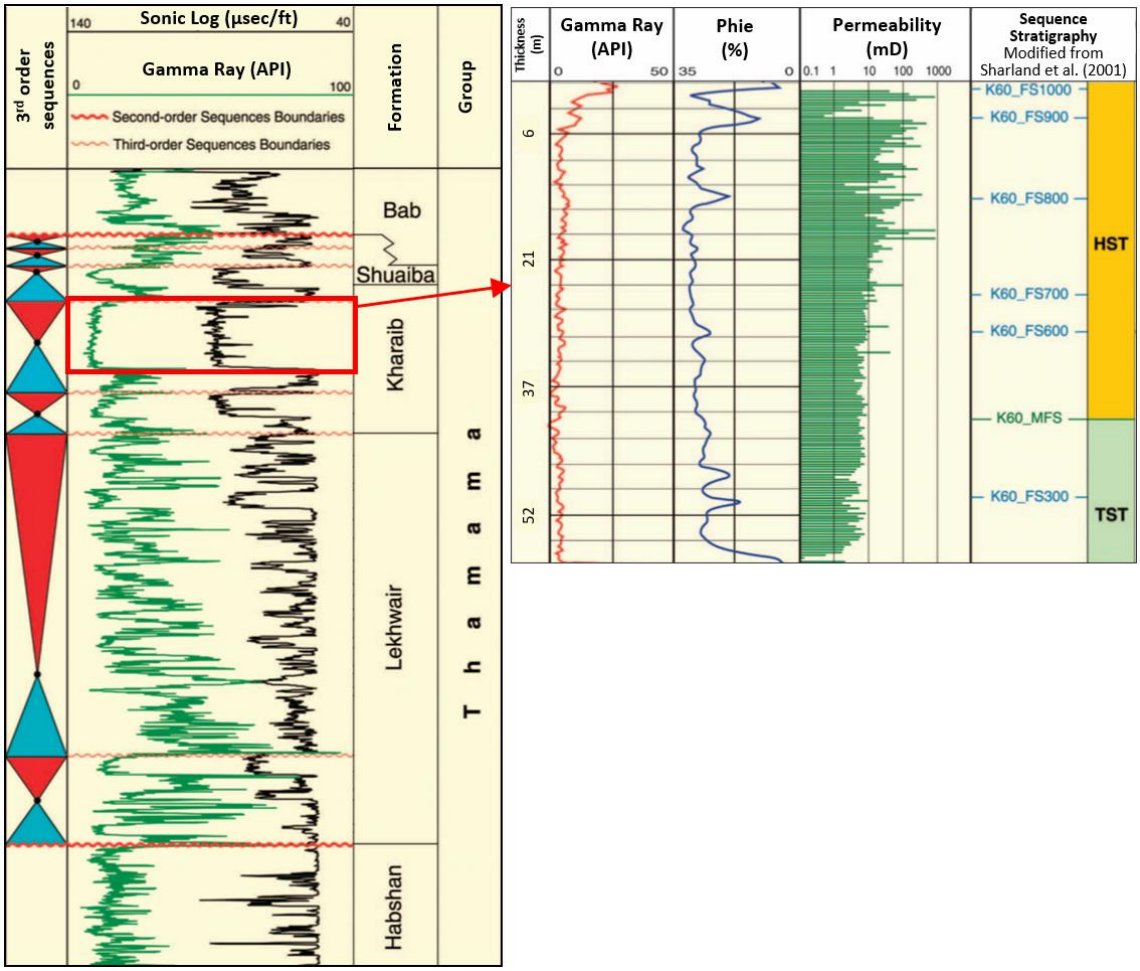

Figure I.6. **Left**: 3rd order sequences, lithostratigraphic context and typical gamma ray and sonic logs for the Lower Cretaceous Thamama Group in Abu Dhabi. **Right**: Typical gamma ray, porosity and permeability logs, as well as sequence stratigraphy for the UKM, highlighted by red box on the left-side panel (adapted from Strohmenger et al, 2006).

I.5. Materials and methods

A summary of the materials and applied methodologies is here presented, as this will be described in more detail in the following chapters, for each case study.

To help achieve the objectives defined for this study, outcrop sections were analysed along approximately 4 Km of the Peniche Peninsula and at different quarry fronts at three locations of the MCE (Codaçal/Cabeço Vedeiro, Cabeça Veada and Casal Farto). Data from 6 wells (2 in the LB offshore and 4 in the Abu Dhabi onshore) were analysed (Figure I.1), including well reports, wireline logs and conventional core analysis data. A total of 312 thin sections were analysed. Different methodologies were applied, including outcrop analysis, core analysis,

petrographic analysis including semi-quantitative visual estimations, as well as digital image analysis through non-contiguous colour selection and trained machine learning (Table I.1).

I.5.1. Outcrop analysis

Features observed on outcrop, such as discontinuity surfaces, lithology, thicknesses and sedimentary features were recorded for the CC5 Member of the CC Fm. along the western to southern margins of the Peniche Peninsula. The analysis was done along cliff-tops, as well as at eight selected locations of the southern Peniche Peninsula coastline where the descent along cliff-face is possible. Vertical profiles were here created to assist in the interpretation on spatial facies variability.

At the studied MCE quarry fronts, where the Santo António-Candeeiros Formation is exposed, the general characteristics of geobodies, depositional features and spatial geometric variability/relationships were analysed at different observation scales. These outcrops allowed for clear detailed observations and interpretations of the depositional architecture. Different fronts were analysed at different quarries, including a section of approximately 35 to 40 m in height and 40 to 60 m in length, which was further analysed in comparison with the depositional architecture of the Abu Dhabi subsurface case study.

I.5.2. Core analysis

In the Abu Dhabi subsurface case study, cores from 4 wells in the studied field were analysed, with attention given to the identification of discontinuity surfaces and small-scale variability in facies, as well as visible macroporosity. A continuous stratigraphic profile was created for each well, also allowing for interpretations on the lateral heterogeneity in the UKM. Core data provides valuable, vertically continuous information for an otherwise inaccessible source of geological data, facilitating the multi-scale analysis of vertical facies variability and depositional patterns.

I.5.3. Petrography

A semi-quantitative analysis of the relative abundance of each sample constituent and grain sorting was done based on visual estimations, using visual comparison charts (e.g. Longiaru, 1987; Flügel, 2004). These estimations were done on 107 thin sections from different outcrop locations along the western to southern margins of the Peniche peninsula and 142 thin sections

from the 4 Abu Dhabi wells in the studied field. In addition, 63 thin sections from cuttings available from the two offshore wells close to Peniche (17C-1 and 20B-1) were analysed.

In the Peniche case study, a detailed facies scheme for the top interval of CC5 member was developed, allowing for a detailed interpretation of cyclicity and spatial facies variability. Grain size was measured on the Peniche set of thin sections using the ribbon-counting method applied to the acquired thin section photos (Flügel, 2004). In the Abu Dhabi case study, a simplified facies classification scheme was applied, in an attempt to emphasize the textural elements linked to petrophysical properties. The generated petrographic data for the Abu Dhabi wells were analysed in integration with petrophysical data available from conventional core analysis. Elements from the classification schemes by Dunham (1962) and Folk (1959, 1962) were applied on facies description for all thin sections, using modifying terms to differentiate samples with similar facies but compositional differences of significance (e.g Lokier and Junaibi, 2016), while the grain sorting terminology is based on Folk (1966). A Scanning Electron Microprobe (SEM) was utilized in order to acquire a visual representation of the microporosity network on 5 core chips from an Abu Dhabi well.

I.5.4. Digital image analysis

In order to quantify macroporosity in the analysed thin sections of the UKM (Abu Dhabi), digital image analysis through non-contiguous colour selection and trained machine learning was carried out, in addition to visual estimations. These methods were applied to a total of 285 images captured from the 142 thin sections of the 4 Abu Dhabi wells, with more heterogeneous thin sections represented by more than one image. These methodologies are described in further detail in Chapter III.1.

Table I.1. Summary of the main methodologies applied and available materials for each case study (further details are presented in each chapter). The MCE case study is based on outcrop analysis, as previously mentioned, although part of the subsurface Abu Dhabi data is integrated in Chapter IV, when comparing both cases.

			Peniche (Chapter II)	Abu Dhabi (Chapter III)	MCE vs. Abu Dhabi (Chapter IV)
Methodologies	Outcrop analysis		■		■
	Core analysis/description			■	
	Petrographic analysis/interpretation		■	■	
	Semi-quantitative analysis (visual estimations)		■	■	
	Scanning Electron Microscope (SEM)			■	
	DIA	Digital grain size measurement (manual)	■		
		Digital quantification of macroporosity and pore sizes (non-contiguous colour selection and trained machine learning)		■	
Materials	Outcrop sections		■		■
	Wells (reports, logs)		2	4	
	Cores			■	
	Thin sections		170	142	
	Conventional Core Analysis Data (porosity-permeability)			■	

Chapter II. The Cabo Carvoeiro Formation, Lusitanian Basin, Portugal

II.1. Facies types and depositional cyclicity of a Toarcian-Aalenian(?) carbonate-siliciclastic mixed succession of the Cabo Carvoeiro Formation

(Published on the 27th of February, 2021, as: Barata, J., Duarte, L.V. and Azerêdo, A.C. (2021). Facies types and depositional cyclicity of a Toarcian–Aalenian(?) carbonate-siliciclastic mixed succession (Cabo Carvoeiro Formation) in the Lusitanian Basin, Portugal. *Journal of Iberian Geology*. https://doi.org/10.1007/s41513-021-00163-2.)

II.1.1. Abstract

The Toarcian-Aalenian(?) Cabo Carvoeiro Formation in the Lusitanian Basin (LB), Portugal, is characterized by a succession of mixed carbonate-siliciclastic sediments deposited under the influence of an active horst-graben system caused by the progressive tectonic uplift of the Berlengas basement block. Towards the top of the succession, this formation is characterized exclusively by grainstone facies (CC5 member), in contrast with the overall marly hemipelagic sediments of the coeval São Gião and Póvoa da Lomba Formations in the onshore LB region. A new subdivision of the CC5 member is here proposed based on outcrop observations and petrographic analysis, with three new subdivisions being identified, in addition to two pre-existing ones, and leading to the definition of the CC5a to CC5e sub-units. These are generally characterized by grainstone facies containing varying quantities of intraclasts, ooids, skeletal grains and quartz extraclasts. A detailed facies scheme was developed to allow for an interpretation of spatial facies variability and facies cyclicity inserted in a sequence stratigraphy framework. The CC5c to CC5e sub-units are interpreted to mark a departure from point-source deposition in a submarine fan-like setting to line-source deposition closer to the Berlengas platform edge, with the development of infralittoral prograding wedges. Deposition of these sub-units occurs during the late stages of a 2nd order regression phase, which culminates in a regionally recognizable discontinuity. Minor tectonic pulses accompanying the gradual decrease in relative sea-level influence the accommodation space variability, which is infilled by high sediment production/influx from the nearby high energy depositional settings of the Berlengas platform margin.

II.1.2. Introduction

The majority of the sedimentological studies focus either on carbonate or on siliciclastic systems. However, considerable attention has also been directed into mixed carbonate-siliciclastic systems (e.g. Doyle and Roberts, 1988; Dolan, 1989; Davies et al., 2002; Tucker, 2003; Zeller et al., 2015; Chiarella et al., 2017). Most mixed carbonate-siliciclastic systems are described as depositional sequences of alternating discrete bodies of siliciclastic and carbonate sediments, referred to as the reciprocal sedimentation model, where eustasy is seen as the main control (e.g. Van Siclen, 1958; Wilson, 1967; Dolan, 1989; Davies et al., 2002; McNeill et al., 2004; Bourillot et al., 2010). Different types of models are reported in published papers such as calcareous sediments accumulating between river source points or alluvial fans (e.g. Pilkey et al., 1988; Roberts and Murray, 1988) or mixed carbonate-siliciclastic cycles developing in a back-arc setting or under tectonic influence (e.g. Wright and Wilson, 1984; Zeller et al., 2015). Hydrodynamics and current activity will have a strong influence in the mixing of siliciclastic-carbonate facies and in sediment distribution in these systems (e.g. Flood and Orme, 1988; Spalletti et al., 2000; McNeill et al., 2004; Chiarella et al., 2017). Different types of carbonate-siliciclastic mixing can be observed at different scales leading to pronounced lateral and vertical facies variations through interfingering or through sharp transitions, creating considerable lateral and vertical heterogeneity (e.g. Roberts and Murray, 1988; Spalletti et al., 2000; Chiarella et al., 2017).

The present work offers a detailed look at a singular mixed carbonate-siliciclastic succession of the Lower-Middle Jurassic transition observed in the westernmost part of the Lusitanian Basin (LB), Portugal (Figure II.1.1). The studied stratigraphic interval corresponds to the upper part of CC5 member of the Cabo Carvoeiro (CC) Formation, as described by Duarte and Soares (2002), equivalent to unit 7 of Wright and Wilson (1984) (Figure II.1.2). This succession is composed of limestones with variable amounts of intraclasts, ooids, skeletal grains and quartz grains. It contains no marly limestone beds, in contrast with the underlying units and is found exclusively in the Peniche area, in contrast with the overall marly hemipelagic sediments of the coeval S. Gião and Póvoa da Lomba formations in the LB onshore region to the east/northeast (e.g. Duarte, 1997; Duarte et al., 2001; Duarte and Soares, 2002).

In a succession which is apparently homogeneous in terms of the depositional texture of the rock, a detailed facies classification scheme was developed in order to provide further insight into spatial variability and facies cyclicity. The results will help to develop a conceptual model to better understand the main controls on the peculiar sedimentary evolution in Peniche during this time (Toarcian-Aalenian(?)). Such detailed approaches to facies typing and facies cyclicity interpretations might prove to be useful tools to better understand subsurface heterogeneous carbonate rocks case studies.

The main objective of this study is to analyse the spatial facies variability in the upper part of CC5 Member corresponding to Unit 7 of Wright and Wilson (1984), although general observations are done on the full CC5 member interval, as well as on the transition from the CC4 Member. One additional objective is to achieve an interpretation of depositional cyclicity based on the identification of discontinuity-bounded facies/subfacies successions, comparing it to the sequence stratigraphy framework of the Lower Jurassic in the LB (Soares et al., 1993; Duarte, 1997, 2007) and to the framework defined for the wider European region (De Graciansky et al., 1998; Hardenbol et al., 1998; Haq, 2018).

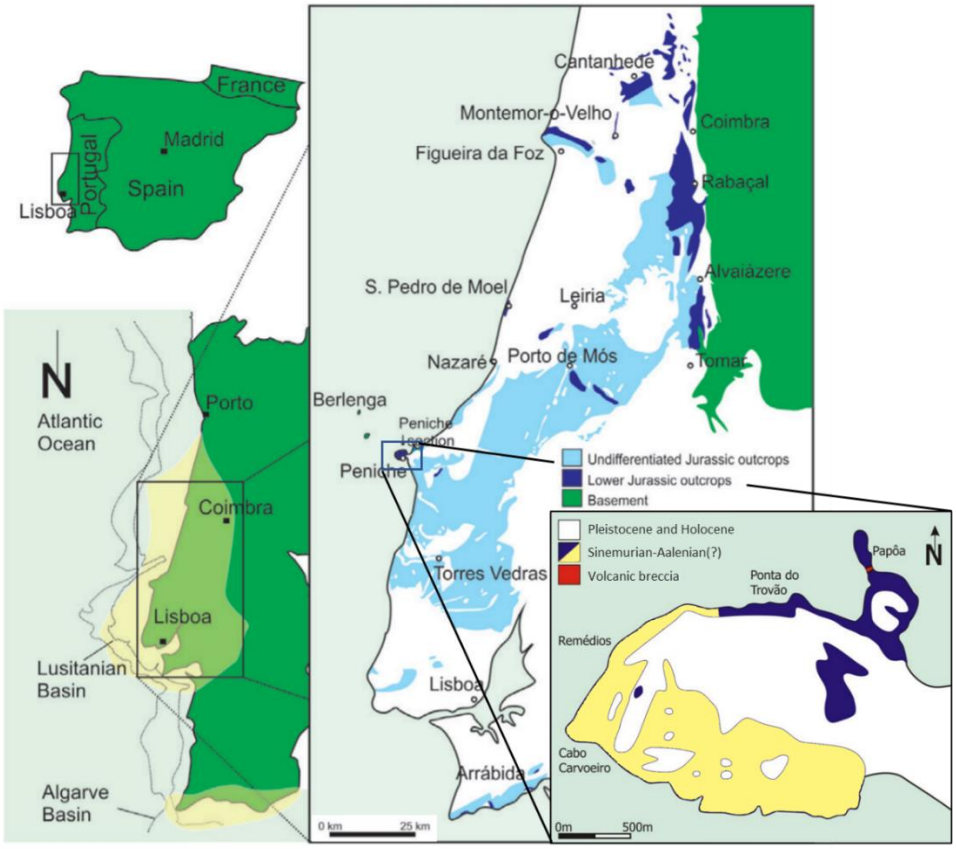

Figure II.1.1. Simplified geological map showing location of the LB and analysed Peniche outcrop locations along the western/southern margins of the Peniche peninsula. Blue: Sinemurian-Middle Toarcian; Yellow: Upper Toarcian-Aalenian(?) (based on Camarate França et al., 1960; Duarte et al., 2010, 2017).

II.1.3. Geological background

II.1.3.1. Structural context

The LB covers an area of approximately 23,000 Km^2 and extends over more than 250 km in a north-south direction. Its eastern limit is represented by the exposed Hercynian basement and

the western limit by an association of ridges and uplifted blocks represented today by the Berlengas archipelago (e.g. Wilson et al., 1989; Pinheiro et al., 1996; Alves et al., 2002, 2003a).

The Mesozoic sediments of the LB were deposited under the influence of different rifting stages marking the opening of the Atlantic Ocean and leading to the creation of complex fault patterns and horst-graben structures developed in association with extension and halokinesis. Such features have a strong effect on controlling sedimentation and depositional geometries through the creation of an irregular topography and localized depocenters in fault-bounded half-grabens (Figure II.1.2) (Mougenot et al., 1979; Wilson et al., 1989; Hiscott et al., 1990; Rasmussen et al., 1998; Alves et al., 2002, 2006; Kullberg et al., 2013).

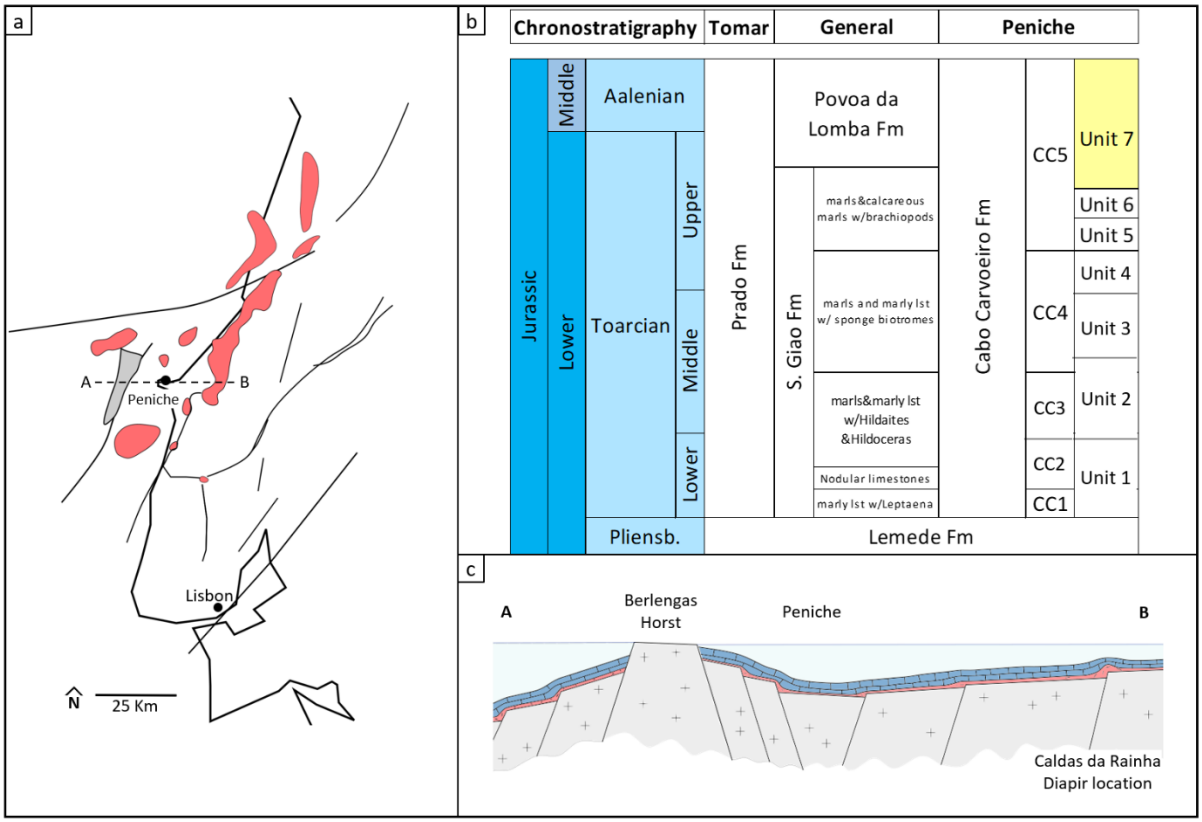

Figure II.1.2. **a**: Simplified structural map of the Peniche area, with main fault trends and halokinetic structures. *Black lines = main fault trends; Grey = Berlengas Horst; Red = Diapirs and halokinetic structures* (based on Wilson et al., 1989; Rasmussen et al., 1998; Alves et al., 2002). **b**: Overview of the LB Toarcian lithostratigraphy, including the Cabo Carvoeiro Formation CC1 to CC5 members (based on Duarte and Soares, 2002) and equivalent Units 1 to 7 (Wright and Wilson, 1984). Unit 7 marked in yellow is the interval of interest for this study. **c**: Simplified structural configuration for the Lower to Middle Jurassic. West-east cross section across Berlengas-Peniche-Caldas da Rainha Diapir, indicated by the A-B dashed line on map. The Caldas da Rainha diapir would be at an early stage of development (modified from and based on Vanney and Mougenot 1981; Wilson et al., 1989; Kullberg et al., 2013).

As part of the ongoing Atlantic opening, an active horst system related to a relatively small-scale rifting phase is recorded initiating in the Sinemurian, in between major Late Triassic and Late Jurassic phases, and is influencing sedimentation during the Early Jurassic in the Peniche region of the LB (Wilson, 1975; Boillot et al., 1979; Vanney and Mougenot, 1981; Wright and Wilson, 1984; Wilson et al., 1989; Alves et al., 2002, 2003a). Regional thickness and facies variations are reported, with higher amounts of siliciclastic content in the western region of the LB during the Early Jurassic (Wright and Wilson, 1984; Guéry et al., 1986; Wilson et al., 1989; Duarte, 1997). In the Peniche Basin, further offshore, the thickness of the Lower Jurassic succession increases, as a consequence of stronger subsidence in this more distal region (Walker et al., 2021). In the Peniche area, the particular succession of turbidites and mixed carbonate-siliciclastic deposits of the Cabo Carvoeiro Formation (Duarte and Soares, 2002) is indicative of deposition in a submarine fan setting under the influence of an active horst system, leading to the progressive tectonic uplift of the Berlengas basement block (Wright and Wilson, 1984; Guéry et al., 1986; Wilson et al., 1989; Duarte, 1997). This uplifted block is represented by the presently exposed Berlengas archipelago, located approximately 10 to 12 Km west of Peniche, where the largest island (the Berlengas island) has a maximum length of 1.6 Km, an average elevation of 85 m and its lithology is characterized as Hercynian granites (Vanney and Mougenot, 1981).

II.1.3.2. Overall sedimentary succession and stratigraphy

The Lower Jurassic in the LB develops within a major transgressive-regressive (T-R) cycle spanning from the Late Triassic to the end of the Middle Jurassic (Wilson et al., 1989; Soares et al., 1993; Duarte, 2007; Azerêdo et al., 2014). A 2nd order T-R facies cycle defines the Toarcian and lowermost Aalenian in the LB (Duarte, 2007; Duarte et al., 2001; Azerêdo et al., 2014), which is equivalent to the Toarcian-Aalenian T-R cycle recorded in other European basins defined by the Tethyan stratigraphic cycles (De Graciansky et al., 1998; Hardenbol et al., 1998).

The beginning of the Lower Jurassic (Hettangian) is characterized by the predominantly evaporitic sediments of the Dagorda Formation and their lateral equivalent in the Pereiros Formation (detrital limestones and dolomites) to the east, reflecting the initial stages of a gradual transition into a marine depositional environment (Soares et al., 1993). During the Sinemurian, the Coimbra Formation, with dolomitic deposits at the base gradually transitioning into limestones, reflects the progressive establishment of marine conditions (Soares et al., 1993). The upper Sinemurian is marked by the deposition of the organic-rich marly limestones of the Água de Madeiros Formation (Duarte et al., 2010, 2012) reflecting open marine settings which prevail during the Early and Middle Jurassic with the development of a westward dipping homoclinal carbonate ramp (e.g. Azerêdo, 1988, 1998; Duarte, 1997, 2007; Silva et al., 2015).

The Pliensbachian deposits are characterized by outer ramp marly limestones of Vale das Fontes Formation, particularly enriched in organic matter (Duarte and Soares, 2002; Silva et al., 2011, 2015; Coimbra and Duarte, 2020) transitioning into the alternations of marly and micritc limestones with calcareous marls of the younger Lemede Formation (Duarte and Soares, 2002). At Peniche, the uppermost part of this unit includes the Global Boundary Stratotype Section and Point (GSSP) that defines the base of the Toarcian Stage (Rocha et al., 2016; Duarte et al., 2017).

The Toarcian-Aalenian(?) Cabo Carvoeiro Formation is time-equivalent to the predominantly hemipelagic marly limestone units of the S. Gião and Póvoa da Lomba formations found generally in the basin and the bioclastic carbonates of the Prado Formation in the Tomar area (see Figure II.1.1) (Duarte, 1997; Duarte and Soares, 2002). It was deposited within the 2nd order T-R cycle starting around the Pliensbachian-Toarcian transition, and having its regressive phase extending from the middle Toarcian into the lower Aalenian, ending with a regionally recognizable discontinuity (Duarte, 1997, 2007; Duarte et al., 2001, 2004; Azerêdo et al., 2014). In the southern LB Arrábida area, the coeval succession is marked by an important hiatus, involving great part of the Toarcian. In this area, the lower Toarcian deposits are composed of mudstones and bioclastic wackestones with pebble conglomerates, followed by intercalated marly limestones and bioclastic wackestones overlaid by dolomitic limestones (Kullberg et al., 2001). The underlying Pliensbachian sediments are characterized by dolomitic marls and marly limestones, which represent the shallowest marine facies in the LB during this stage (Manuppella and Azerêdo, 1996; Azerêdo et al., 2003).

II.1.3.3. The Cabo Carvoeiro Formation

The Cabo Carvoeiro Formation, subdivided into 5 members (CC1 to CC5), is described as having a minimum thickness of approximately 210 m (Duarte and Soares, 2002), possibly greater than 350 m (Wright and Wilson, 1984). The top of the Peniche succession is not exposed, preventing interpretation on the transition into overlying units. The formation evolves gradually from intercalations of marls and fine-grained marly limestone beds in CC1 member to intercalations of marls and intraclastic, siliciclastic and ooidal grainstones in the CC4 and base of CC5 members (Wright and Wilson, 1984; Duarte, 1997; Duarte and Soares, 2002). The marly intervals become absent in the upper part of CC5 member, equivalent to units 6 and 7 of Wright and Wilson (1984). The grainstone beds in CC5 are described as having been deposited in an outer fan and braided mid-fan setting, as channel-fill sequences (Wright and Wilson, 1984) and in a littoral environment based on its palaeontologic content (benthonic fauna such as corals, crinoids, echinoids, large bivalves and gastropods) (Duarte and Soares, 2002). Unit 7, the main target of this study, is characterized by medium- to thick-bedded coarse-grained to pebbly sand grade limestones with large channels such as showed by Wright and Wilson (1984).

II.1.4. Materials and methods

To achieve the objectives of this study, outcrop sections were analysed along the cliff-tops of the northwestern, western and southern coast of the Peniche peninsula (Figure II.1.3). A number of locations where the descent along cliff-faces is possible were defined for the creation of vertical stratigraphic profiles to assist in the evaluation of lateral facies variability, with macro and microfacies interpretation being done on the collected hand specimen and thin sections. A previously existing dataset by Duarte (1995), including thin sections and an unpublished stratigraphic profile, was integrated into the present study, providing information covering the transition between CC4 and CC5 members and extending up to the lowermost Unit 7. A semi-quantitative analysis was done on thin sections, which included visual estimation of sample constituents and grain-size measurement through digital image analysis.

II.1.4.1. Outcrop analysis

Outcrops were analysed along an approximately 4 Km long sector exposing units 5, 6 and 7 of Wright and Wilson (1984). This sector extends from the northern/northwestern cliffs close to the Frei Rodrigo (FR) location (near the transition between CC4-CC5 members) until the locations close to the Portinho da Areia Sul beach (PAS), in the southern Peniche peninsula coast (Figure II.1.3). Discontinuity surfaces, bed thickness, lithology and sedimentary features were recorded along cliff-tops, as well as cliff-faces, where accessible. In Unit 7, the following locations were selected to develop eight vertical stratigraphic profiles along a 1 Km sector of the peninsula coast: Nau dos Corvos (NC), Lage dos Pargos (LP), Ponta das Gaivotas (PG), Furna que Sopra (FS), Poita Alta (PA), Cova de Dominique (D), Furninha (F) and Paços de D. Leonor (L) (Figures II.1.3, II.1.4).

The effects of weathering and karstification create some difficulties in outcrop observation, while faulting and fault zones in the analysed area lead to uncertainty regarding the thickness of certain intervals, as well as on the continuity of the facies succession.

II.1.4.2. Outcrop sampling

Sampling was carried out on the eight vertical profiles, with at least one oriented sample taken from each interpreted facies type in each bed. A number of thicker beds were sampled at more than one place. A total of 75 hand-specimens were collected and were saw-cut for macrofacies interpretations on the freshly cut rock face. Sample labelling on the vertical profiles between NC and L follows location names (Figure II.1.3) and sampling sequence for each profile.

Figure II.1.3. Peniche Peninsula satellite photo (Google, 2020) indicating approximate locations where limits between Cabo Carvoeiro Formation members/units are identifiable (dashed yellow lines). Yellow circles indicate sampling locations and yellow triangles indicate reference locations. FR = Frei Rodrigo; RM = Cruz dos Remédios; NC = Nau dos Corvos; LP = Lage dos Pargos; PG = Ponta das Gaivotas; FS = Furna que Sopra; PA = Poita Alta; D = Cova de Dominique; F = Furninha; L = Paços de D. Leonor; CJ = Carreiro de Joannes; PAS = Portinho da Areia Sul beach. P & A, 3000 and 2500 are samples locations.

II.1.4.3. Thin sections

A total of 107 thin sections were analysed under a polarized light microscope (Nikon Eclipse Ci Pol) coupled with a Nikon digital microscope camera. This dataset consists of 57 existing thin sections covering the CC4 to CC5 members (associated with the unpublished stratigraphic profile from Duarte, 1995) and 50 thin sections from strategic locations along cliff-tops and vertical outcrop profiles of Unit 7. The thin sections were studied using a semi-quantitative approach to assist in interpreting vertical variability in petrographic properties starting at the top of CC4 member and going through the CC5 member.

II.1.4.4. Semi-quantitative analysis

A semi-quantitative analysis of the relative abundance of each constituent, as well as estimations on grain sorting, was done on thin sections based on visual estimation using visual comparators (e.g. Longiaru, 1987; Flügel, 2004). While this methodology might be associated

with some level of subjectivity and uncertainty, its most important aspect is to identify trends and variability between relative values and not the absolute value for a given parameter.

Grain size was measured on the full set of thin sections through digital image analysis, using the ribbon-counting method (Flügel, 2004). The largest dimension of each grain was measured in pixels and converted into μm using a conversion factor based on the reference scale in each image. Both carbonate particles and quartz grains were measured and an average grain size value calculated. This method accounts for the measurements of smaller-sized grains, which might be missed by the point-count method (Flügel, 2004). The obtained results are approximations and might deviate from actual grain sizes due to the random direction of the cross-section plane along the cut surface of the grain.

II.1.4.5. Facies classification

A detailed facies classification scheme was developed where subfacies types were defined based on variations in relative amounts of constituents and grain sorting. This will improve interpretations and allow for a detailed representation of spatial variability of facies types on outcrop, in integration with hand specimens observations. The terminologies of Dunham (1962) and Folk (1959, 1962) were applied on sample description, using modifying terms to differentiate samples with similar facies but compositional differences of significance (e.g Lokier and Junaibi, 2016). Grain sorting terminology is based on Folk (1966).

II.1.4.6. Composite stratigraphic profile and correlation panel

A detailed overall composite stratigraphic profile based on the localized vertical profiles was built for Unit 7 of Wright and Wilson (1984), to offer further insight on the vertical stratigraphic evolution and facies cyclicity through this interval.

A correlation panel was created for the sector between NC and L (Figure II.1.3), integrating outcrop, hand-specimen and thin section facies observations to assist in visualizing and interpreting vertical and lateral facies variability. The identification of discontinuities and facies variability are integrated using a sequence stratigraphy approach.

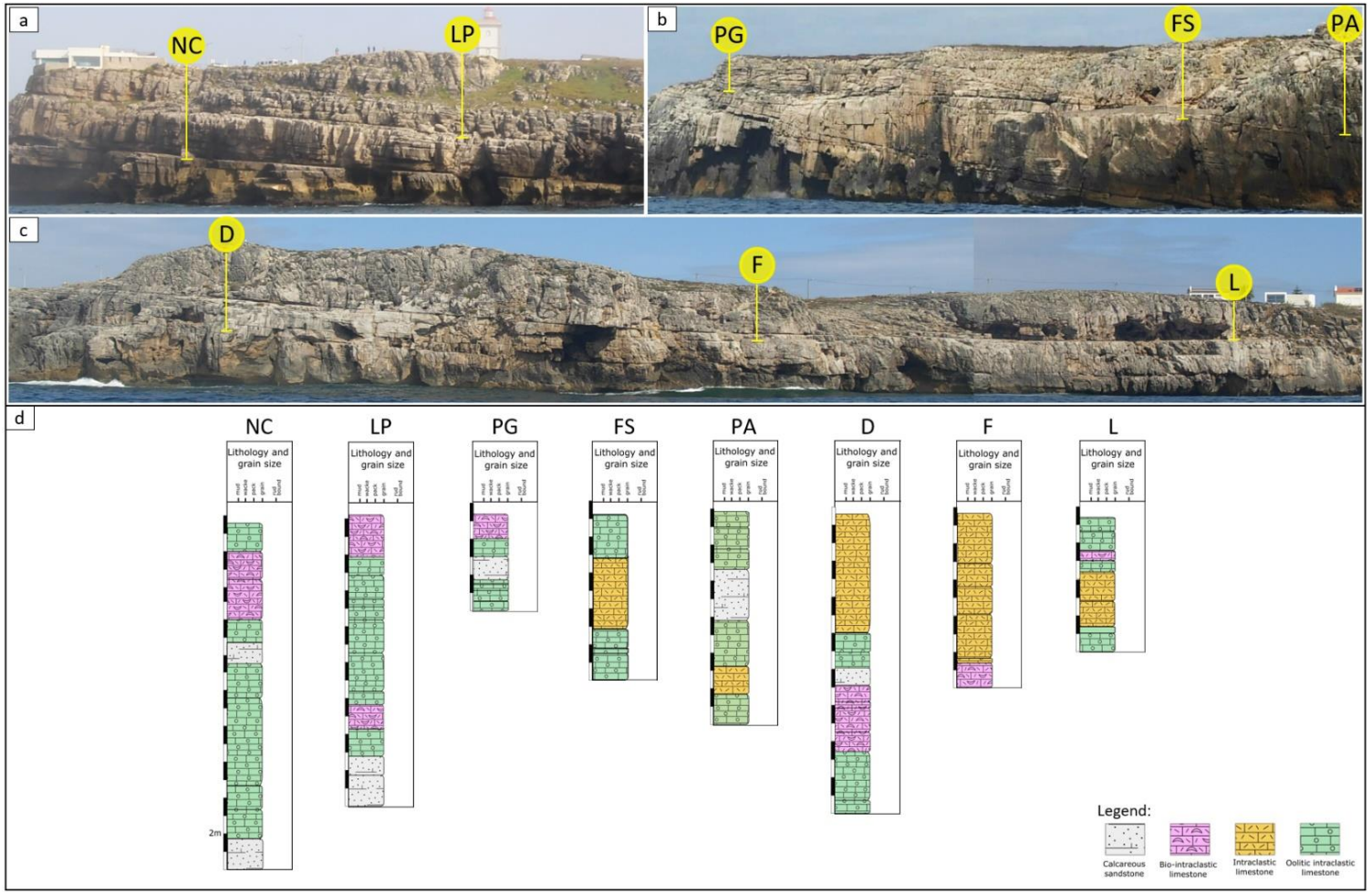

Figure II.1.4. Outcrop views of the southern margins of the Peniche peninsula, where vertical profiles were analysed (indicated by yellow circles). Photographed outcrop sectors **a**, **b** and **c** are indicated by the green arrows on Figure II.1.3. **d**: sedimentary logs for the indicated sections in a, b and c.

II.1.5. Results

II.1.5.1. Lithostratigraphy redefinition

The analysed outcrop sectors show important discontinuities which can be followed laterally along the western and southern Peniche peninsula (see Figure II.1.5 for outcrop mapping). Unit 7 was subdivided into three new proposed sub-units (Figure II.1.6), based on the presence of these major discontinuities, on stratonomy and on the observed petrographic variations. These three sub-units have a total measured minimum thickness of 120 m. A variation on the terminology of Duarte and Soares (2002) is used on the proposed subdivisions of CC5 member. The CC5a and CC5b sub-units are equivalent to Unit 5 and Unit 6 of Wright and Wilson (1984), respectively, and the CC5c to CC5e sub-units are equivalent to Unit 7 of Wright and Wilson (1984).

II.1.5.1.1. CC4 member

The CC4 member is generally described as intercalations of marly levels with ooidal and peloidal limestones (Duarte and Soares, 2002). The succession shows a marly basal interval and is thickening and coarsening upwards, with crinoids in some limestone layers (Duarte and Soares, 2002). This member has an approximate thickness of 45 m (Duarte and Soares, 2002) and, according to Wright and Wilson (1984), reflects deposition under the influence of turbidity currents. This interval ends on a major discontinuity marking a break in the succession. An abrupt transition from a thickest calcareous succession of the top of CC4 member into the lowermost marly interval of CC5 member is observed (Figure II.1.7a, b).

II.1.5.1.2. CC5a sub-unit

This sub-unit corresponds to Unit 5 of Wright and Wilson (1984) and to the basal succession of CC5 member of Duarte and Soares (2002). It is exposed around the FR location, has an estimated thickness of 43 m and is characterized by a basal interval of higher marly content, followed by intercalations of centimetric to decimetric layers of marls/marly limestones and limestones (Figure II.1.7a, b). Crinoid segments have been identified in some layers higher in this sub-unit. At the top, immediately underlying a major discontinuity surface, beds are strongly bioturbated and trace fossils are clearly visible, such as *Skolithos* sp. (Wright and Wilson, 1984; Duarte and Soares, 2002) (Figure II.1.7d, e).

II.1.5.1.3. CC5b sub-unit

This sub-unit is exposed between the FR and RM locations (Figure II.1.3) and is strongly karstified, creating strong limitations on outcrop observations and leading to uncertainty

regarding the continuity of the vertical succession along the exposed cliff-tops. This interval corresponds to Unit 6 described by Wright and Wilson (1984) and has an estimated thickness of 40 m (Wright and Wilson, 1984). The CC5b sub-unit lacks marly intervals and is generally characterized by coarser-grained limestone beds with internal planar stratification and sharp bedding planes. Cross-stratification and thickness variations are observed in places, indicating probable channel-like features, also identified by Wright and Wilson (1984).

II.1.5.1.4. CC5c sub-unit

This sub-unit is characterized in its entirety by coarse-grained detrital limestone beds with varying amounts of carbonate and siliciclastic material, including beds with the highest abundance of crinoid fragments in the whole succession (*Pentacrinus penichensis* (De Loriol, 1891)). Most beds show centimetric to decimetric planar stratification but cross-stratified intervals are also observed, having a stronger expression in the basal part of this sub-unit. Lateral thickness variations are also observed. Beds immediately overlying important discontinuities show planar stratification and generally higher content in quartz grains. Apparent sedimentary patterns, such as coarsening or fining upwards trends, are identified in some intervals of the profile although they are, most of the time, not clear. This sub-unit has an estimated thickness of between 35 and 40 m and beds are apparently dipping to the east/southeast with a very low angle (5^o or less). The estimation of total thickness for this sub-unit is affected by the presence of a probable large fault zone.

II.1.5.1.5. CC5d sub-unit

This sub-unit contains coarse-grained detrital limestone beds with variable thicknesses and is characterized by the occurrence of quartz-rich channel structures. Planar stratified, quartz-rich beds overlay discontinuities, as in CC5c. In similarity with the underlying sub-unit, most beds show centimetric to decimetric planar stratification, although lateral thickness variations seem to be more prominent. The amount of crinoid fragments identifiable on outcrop is lower than in the CC5c sub-unit, although they are still present in some layers. Channel-like bodies show an abundance of coarse sand-grade quartz grains and sharp lateral and vertical facies transitions onto the adjacent carbonate beds. In spite of the strong weathering effects, apparent truncation of carbonate layers by the quartz-rich geobodies is observed. Some of these channel structures are identified on outcrop but are not intersected by the vertical stratigraphic profiles developed at the selected locations, due to the limited lateral extension of these structures, the overall depositional architecture and the present-day dipping of the strata. This sub-unit has an approximate thickness of 45 m and layers are apparently dipping in the same direction as the CC5c sub-unit between locations PG and F, becoming closer to horizontal around the L location.

II.1.5.1.6. CC5e sub-unit

CC5e has virtually no cliff-face accessibility and the transition into the overlying units is not exposed. The vertical succession can be followed along cliff-top exposures, as beds are dipping with a low angle to the east/southeast, in similarity to sub-unit CC5c. Karstification and weathering have strongly altered the exposed rocks.

The base of the CC5e sub-unit is characterized by a sandstone layer containing limestone pebbles/boulders and abundant quartz grains (Figure II.1.7g). This bed is followed by sediments with high volumes of quartz grains, gradually decreasing upwards. Karstification prevents clear observations and interpretations on geometries of the depositional beds. Cross-stratification is, however, observed in some beds between the CJ and P&A locations (Figure II.1.3). This sub-unit has an estimated minimum thickness of between 40 and 45 m, although this estimation is conditioned by the erosional nature of the top limit.

II.1.5.1.7. Discontinuities

Several important discontinuities are observed which can be followed laterally over considerable distances along the outcrop. They define breaks in the succession reflecting changes in the overall nature of the sedimentary features (see Figure II.1.7a, c, f) and are generally overlain by planar-stratified quartz-rich beds. These major sedimentary breaks in CC5 member help define the proposed sub-units and are here referred to as D1 to D5 (Figures II.1.5, II.1.6), with D1 corresponding to the transition between CC4 and CC5 members.

The transition between CC5a and CC5b sub-units (discontinuity D2) reflects a change from interbedded limestones and very thin marl layers at the top of CC5a into more massive, planar and cross stratified limestones with no marly intervals in CC5b. Abundant bioturbation is visible on the bedding surfaces immediately underlying this major discontinuity (Figure II.1.7d, e).

An important discontinuity surface is identified within the interval corresponding to the present-day relative sea-level at RM. This surface is interpreted to mark the transition between CC5b and CC5c (discontinuity D3), in line with the observations of Wright and Wilson (1984). These authors have identified the limit between their Units 6 and 7 at approximately this location. Its exact stratigraphic position cannot be clearly defined due to karstification and associated terrain constraints. At approximately this stratigraphic position, beds start to become generally thicker and apparently coarser-grained, with larger channel structures observed on outcrop.

The discontinuity between the CC5c and CC5d sub-units (discontinuity D4) shows an abrupt change from crinoid-rich facies into quartz-rich beds, while the CC5d to CC5e transition (D5) is marked by a strong irregular erosive palaeosurface draped by a conglomeratic limestone containing limestone pebbles/boulders and abundant quartz grains (Figure II.1.7f, g).

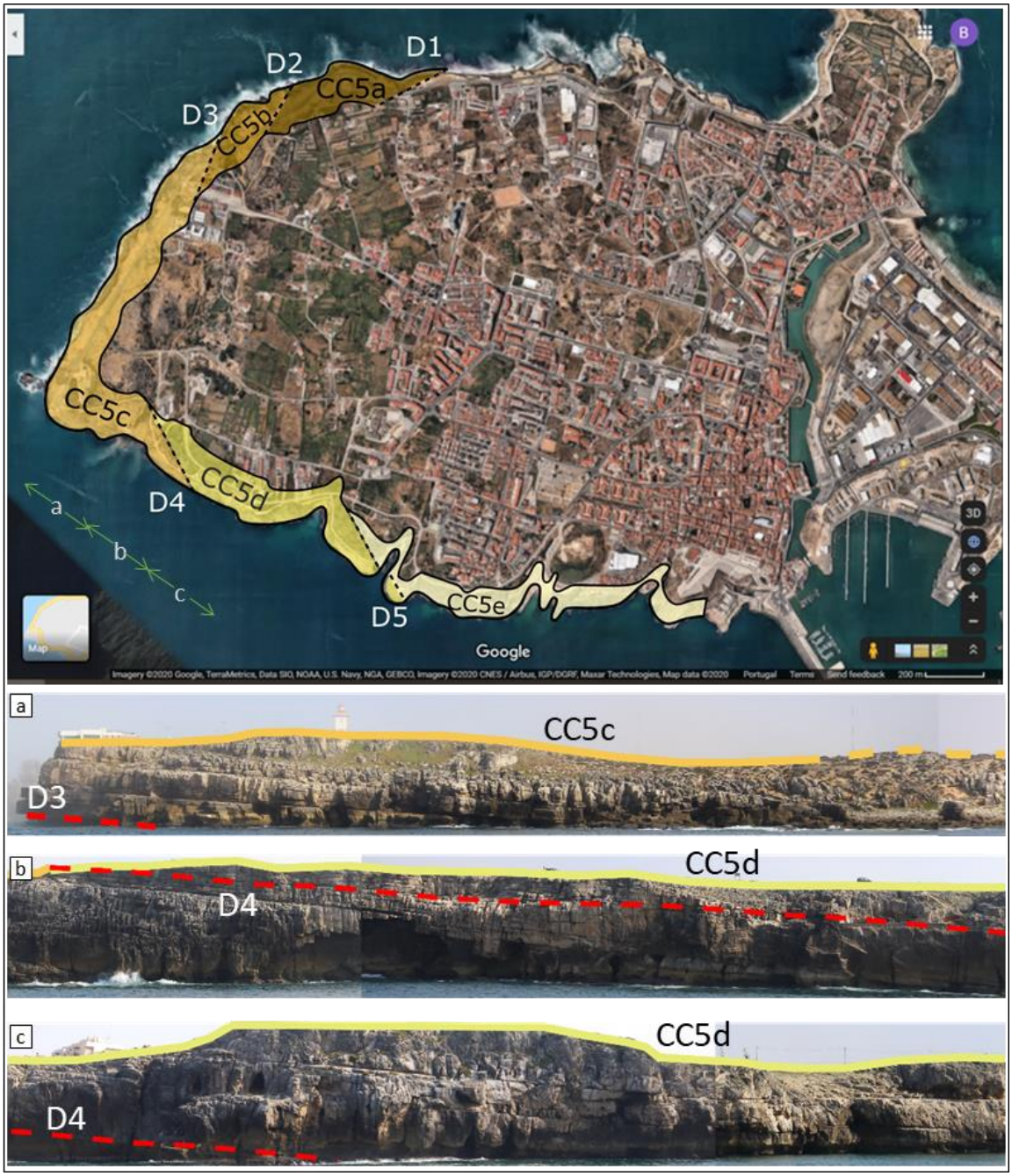

Figure II.1.5. Peniche Peninsula satellite photo (Google, 2020) showing schematic representation of approximate locations for identified discontinuities and sub-units exposed at cliff-tops. Bedding planes and discontinuity surfaces are pending with slightly different angles and, as such, dashed lines are a simplified representation on this map view. The location of outcrop photos **a**, **b** and **c** are indicated on the satellite map by the green arrows. Part of CC5c and CC5d, as well as discontinuity D3 and D4 (dashed red lines) are represented. Bedding planes have an approximate east/southeast dipping direction (variable low angle). Bed exposure is, therefore, limited by erosion at cliff-tops and submersion below present-day sea level.

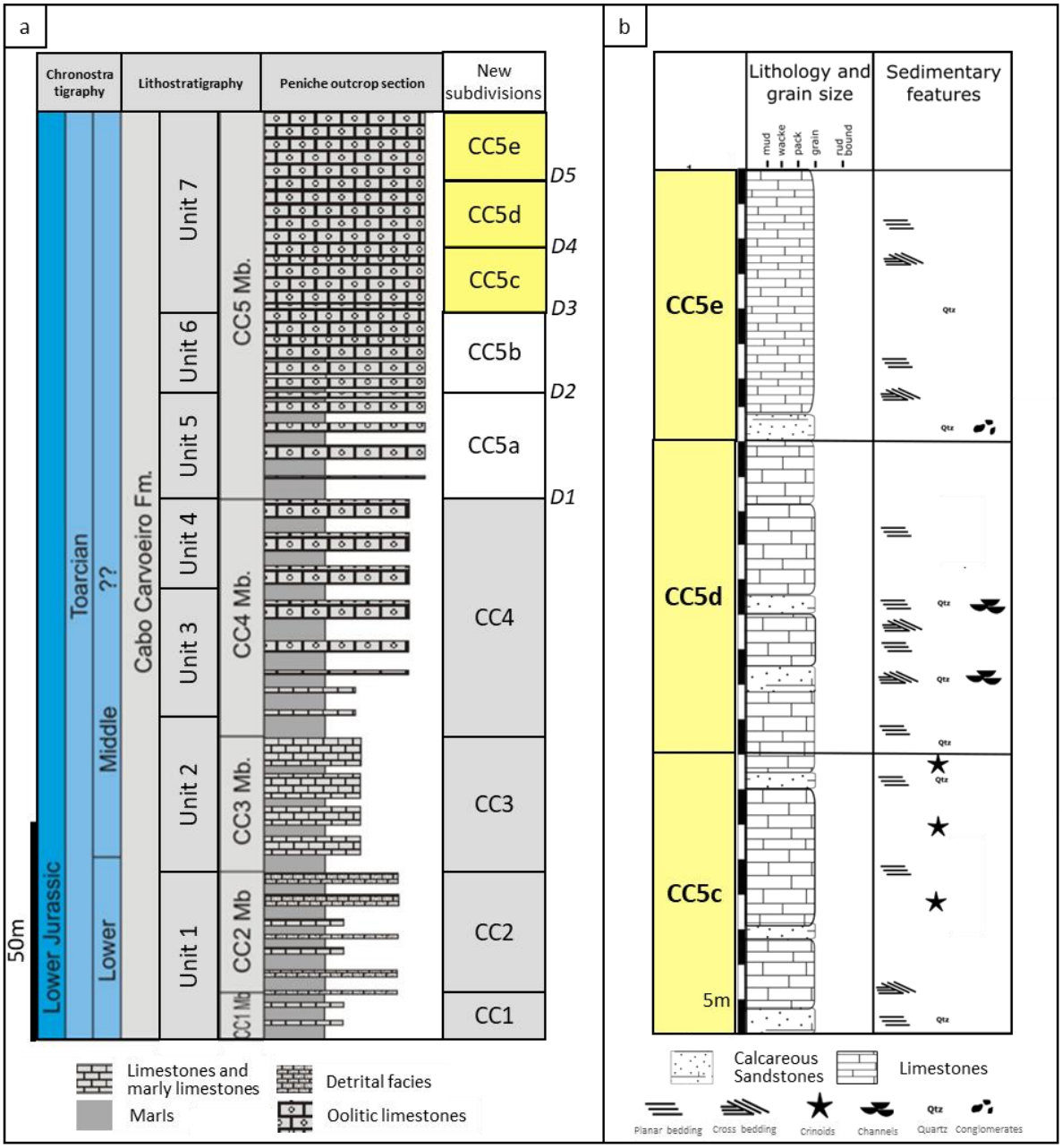

Figure II.1.6. **a**: Lithostratigraphic column for Cabo Carvoeiro Formation, containing subdivisions Unit 1 to Unit 7 (Wright and Wilson, 1984), CC1 to CC5 members (Duarte and Soares, 2002) and the nomenclature applied in this work for the subdivisions of CC5 member (marked in white and in yellow - CC5a to CC5e) and for the major discontinuities (D1 to D5). Yellow colour represents the new subdivisions as defined on this study. **b**: Simplified stratigraphic column focusing on members CC5c to CC5e. General lithology and facies are represented, as well as main sedimentary features. These indicate beds with the highest abundance of crinoids, channel figures and beds with strong planar or cross-stratification. Sub-unit thicknesses: CC5a = 43 m, CC5b = 40 m (Wright and Wilson, 1984); CC5c = 40 m, CC5d = 45 m, CC5e = 40 m (present study).

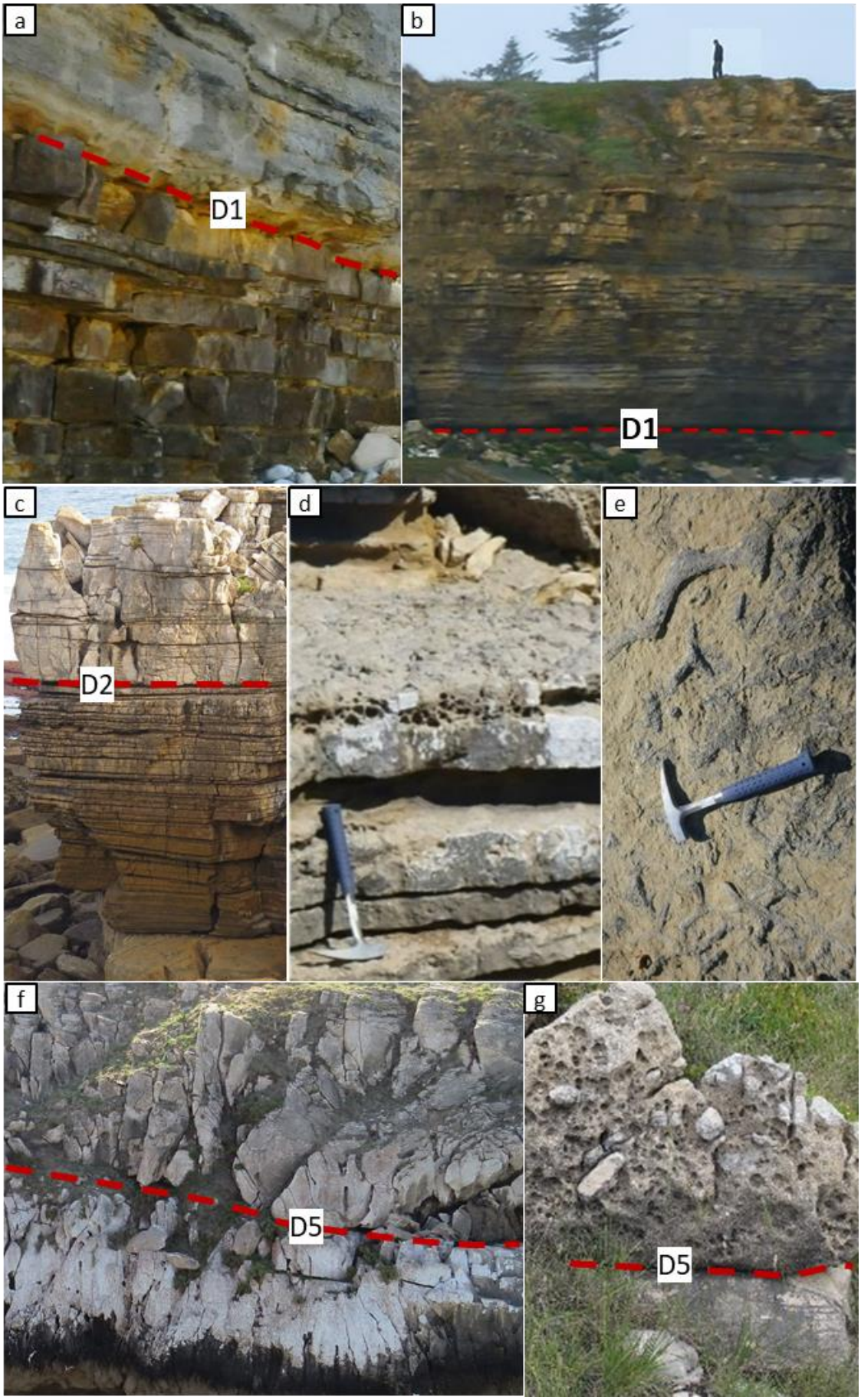
a
D1
b
D1
c
D2
d
e
f
D5
g
D5

Figure II.1.7. **a**: Detail photo of CC4-CC5 transition (discontinuity D1): limestones transitioning into the basal marly interval of CC5a. **b**: Lowermost CC5a. Limestone intervals are increasing in frequency and thickening upwards. Discontinuity D1 is visible at the bottom of the photo (strongest discontinuity surface). **c**: Transition from CC5a to CC5b (discontinuity D2), between FR and RM, with massive and stratified limestone beds and no marly intervals above strongest discontinuity. **d**: Heavily bioturbated layers at CC5a-CC5b transition (close to discontinuity D2). **e**: Trace fossils on a surface within the stratigraphic interval close to discontinuity D2. **f**: CC5d to CC5e transition (discontinuity D5) at the CJ location. **g**: detail of D5 discontinuity (western clifftop at CJ). Sharp transition between contrasting lithologies with abundance of quartz grains and carbonate pebbles/boulders above.

II.1.5.2. Petrographic analysis

II.1.5.2.1. Main features

The analysed samples in CC4 and CC5 members contain intraclasts (reworked/redeposited fragments of lithified carbonate sediments), coated grains, ooids, skeletal grains and extraclasts (quartz grains), with varying relative amounts of each constituent throughout the succession. Intraclasts are mostly micritic in nature but contain genetically varied elements such as ooids and skeletal grains, or different calcite cement phases (Figures II.1.8, II.1.9). Intraclasts containing degraded Porostromata (algae/cyanobacteria?) have been identified in the CC5c sub-unit and towards top of the CC5d sub-unit (Figure II.1.8). These components vary in size from fine to very coarse sand-grade, with an average value of 166 μm. The variation in average particle size through the succession is presented in Figure II.1.10. Ooids are present in varying amounts throughout the succession, mostly containing micritic or quartz nuclei and being fine to medium sand-grade in size. The structures surrounding the nucleus of ooids are mostly micritic, but radial-type ooids are also found (Figure II.1.8). The skeletal grains have undergone micritization or recrystallization and are identified as echinoderm fragments and spicules, bivalves, gastropods and foraminifera. There is no apparent clear abundance of a given type in a specific depositional facies type, apart from the crinoid-rich facies. Quartz grains vary in size, from fine to very coarse sand-grade grains, and are generally well-rounded, with some grains showing a thin layer of micritic coating (Figure II.1.8).

Significant early stage fibrous or bladed (sometimes difficult to distinguish) calcite cement rims are observed surrounding particles in all samples. Due to the effects of this earliest cementation stage, most particles are not in direct contact, but are contacting within the cement rim phases. This creates an apparent point contact to no contact between grains in most of the samples (Figure II.1.9). However, less significant early cementation is also observed in some samples, leading to different types of contacts between grains, such as long, concave-convex and sutured contacts, as the effects of compaction are expressed to different extents. Fracturing, displacement of grain rims and pressure dissolution along stylolites are also observed (Figure II.1.11c, d).

Earlier circumgranular rim cements are distinguishable from later pore-filling cements under normal light petrography (Figure II.1.9). These later cements are characterized by microcrystalline, granular equant or blocky spar or drusy mosaic types in different samples. Crystallization fabrics could be generally described as inequigranular xenotopic (Figure II.1.9c) and sometimes poikilotopic. These later cement phases completely occlude the remaining original pore space. Syntaxial cement overgrowths are observed on echinoderm fragments (Figure II.1.9). Circumgranular isopachous fibrous cements are typical of marine phreatic environments, normally shallow marine (e.g. Flügel, 2004). Anisopachous bladed calcite cement might, however, indicate different origins. The subsequent cement phases might represent early or late burial environments. Additional data would be required to further clarify the exact origins for these different cement phases. There is some variability in the amount of interparticle calcite cements between samples and an apparent relationship with facies types. Samples which are more poorly sorted, containing a coarser sand-grade fraction, with lower quartz volumes (also with less ooids and more intraclasts) show higher interparticle cement volumes. Samples with increasingly better sorting show lower estimated cement volumes. Quartz-rich samples show low to very-low cement volumes. Bioclastic and crinoid-rich samples show some variability in cement volumes but no clear relationship.

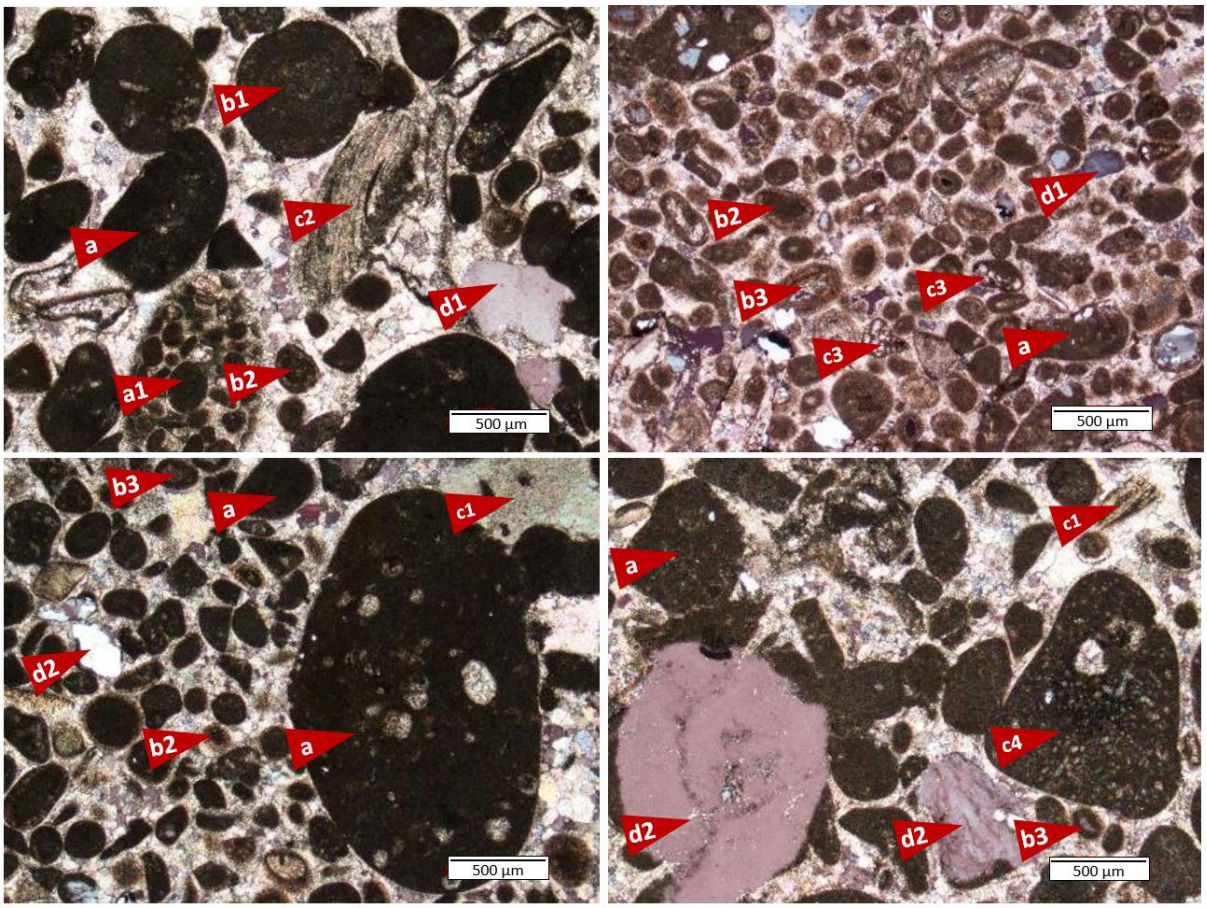

Figure II.1.8. Some petrographic aspects occurring in CC4 and CC5 members of Cabo Carvoeiro Formation. a: micritic intraclasts with different internal components; a1: intraclast/lithoclast representing a reworked fragment of an oolitic limestone; b1: micritized ooids; b2: radial ooids with apparent micritic nucleus; b3: apparent radial ooids with quartz grain nucleus; c1: echinoderm fragments with syntaxial calcite cement overgrowths; c2: bivalve fragments; c3: foraminifera with calcite cement-filled intratest porosity; c4: intraclast including a Porostromata fragment; d1: rounded to well-rounded quartz grains; d2: rounded to well-rounded quartz grains with a micritic coating.

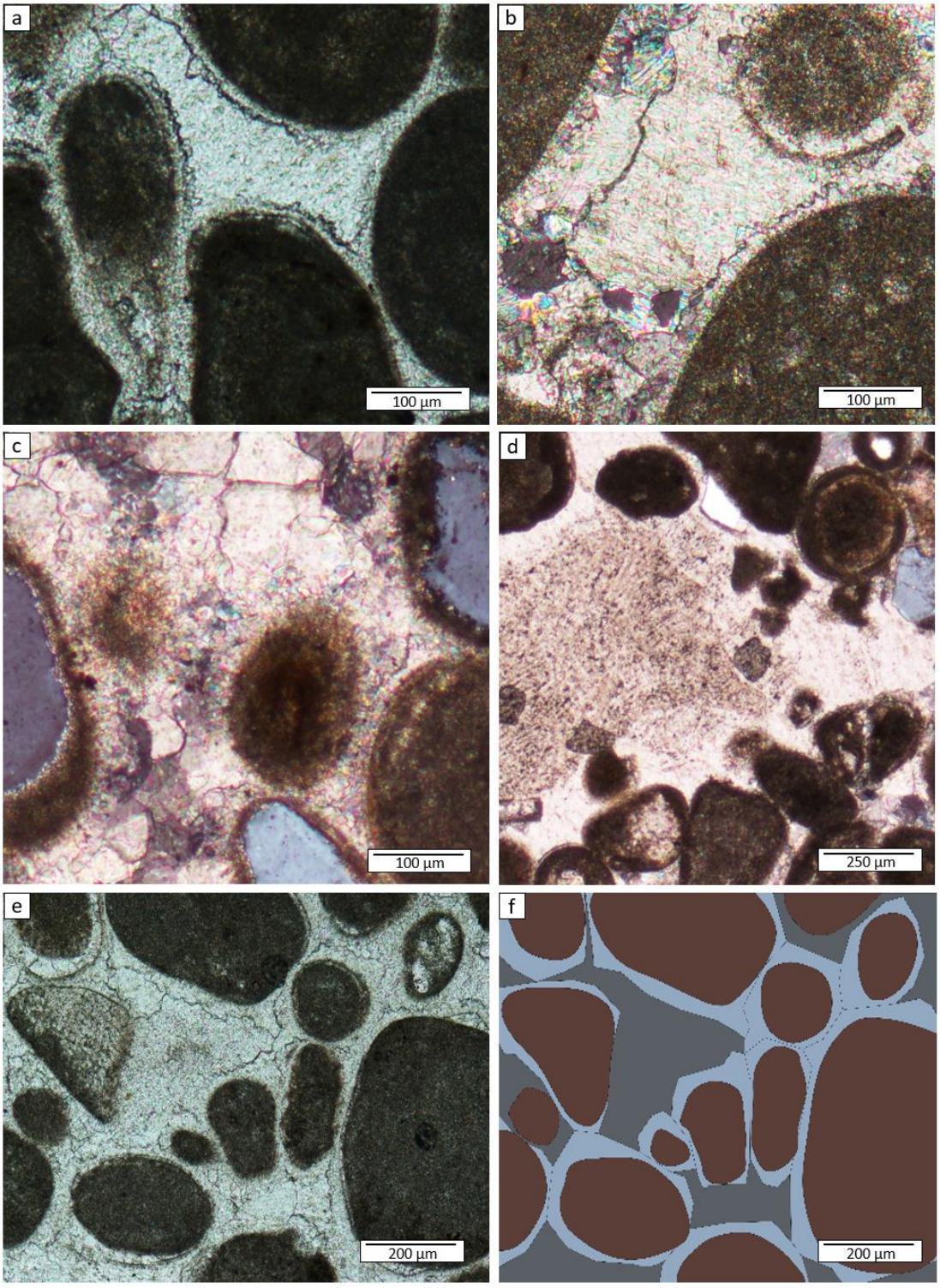

Figure II.1.9. **a**: Detail of apparently fibrous circumgranular rim cement phase (sample D3). **b**: Detail on fibrous circumgranular rim cement phase (sample F5). **c**: Interparticle calcite crystals with inequigranular xenotopic fabric (sample LP15). **d**: Syntaxial cement overgrowths on echinoderm fragment (sample LP15). **e**: original photomicrograph of sample F2 showing distinguishable cement phases. **f**: digitally altered photomicrograph of sample F2 for relative volumes estimation of different constituents through pixel counting.

II.1.5.2.2. Semi-quantitative analysis

The results of a detailed semi-quantitative analysis show vertical trends and considerable variability in relative volumes of each sample constituent from CC4 member through CC5 member (Figure II.1.10).

Higher volumes of ooids are observed from the top of CC4 to the base of the CC5d sub-unit, with a general decrease in CC5d and CC5e. Intraclast volumes are generally lower in CC5a, CC5b and CC5c, with an overall increase in the upper half of CC5d and in CC5e. High peaks in volumes of quartz grains are observed with more prominence in CC5a, CC5c and CC5e. These sharp increases in quartz grain volumes are accompanied by a decrease in volume of carbonate allochems. Skeletal grains content is slightly higher close to the CC5c-CC5d transition and in CC5e.

Grain size is generally increasing from around 100-150 μm in CC4, reaching a peak of around 650 μm close to the top of CC5d, before it starts decreasing throughout the CC5e sub-unit. A few isolated high peaks are seen throughout the studied interval, driven by the presence of coarse particles of different types (intraclasts, ooids, skeletal grains or quartz grains). The grain size peaks for each individual particle type are generally coinciding, although the actual values may vary. Intraclasts show the highest values for measured grain size, with an average value of 166 μm, ranging between 16 μm and 1910 μm. Of the total number of measured intraclasts, only 10 % are below 63 μm and less than 1 % are below 32 μm.

A comparison is made between visual estimations and quantitative measurements through digital image analysis for one sample (Figure II.1.9e, f), showing that there is some variation in the results, with no largely significant differences in estimated particles area and total cement area, but considerable variations between early and late cement areas (measured particles area = 61%; total cement area = 39%; early cement area = 20%; late cement area = 19%; as compared to visual estimations: Particles area = 60%; total cement area = 40%; early cement area = 10%; late cement area = 30%).

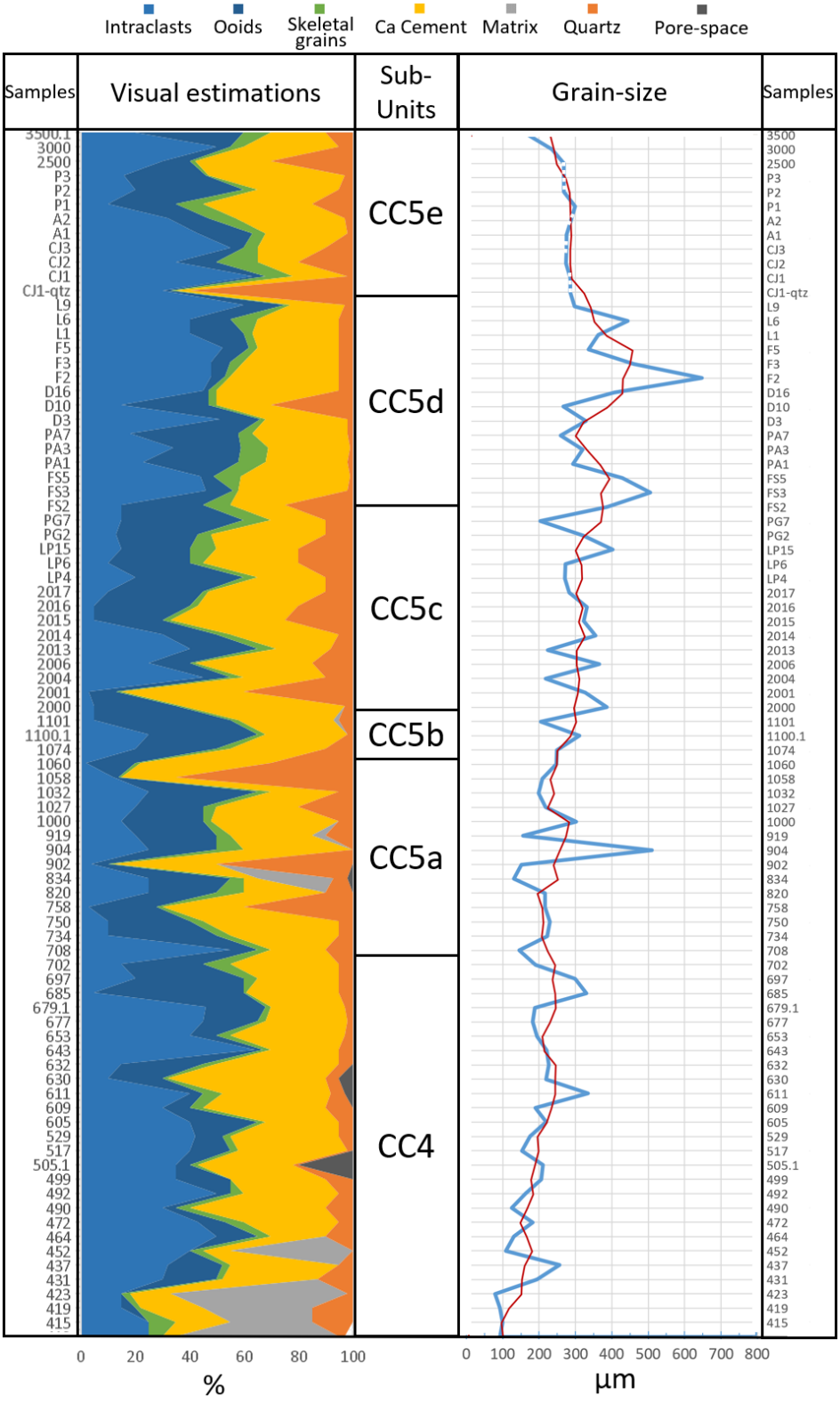

Figure II.1.10. Semi-quantitative analysis of samples in CC4 and CC5 members. **Left**: Percentage of each sample constituent based on visual estimations. **Right**: Digitally measured average grain size for the different types of particles combined (including quartz extraclasts); red curve represents a five-point moving average. Vertical axis represents sample reference, not height/thickness.

Based on the semi-quantitative analysis done through visual estimation, correlation factors between each estimated parameter were calculated (Table II.1.1). No clear correlation is observed between skeletal grains and other constituents apart from moderate inverse correlations with late calcite cements and total interparticle calcite cement (coefficients of -0.41 and -0.31 respectively). Ooid and intraclastic content shows a strong inverse correlation (coefficient of -0.64), while the ooid content and grain sorting show a moderate direct correlation (coefficient of 0.47). Quartz-rich intervals have lower amounts of carbonate particles, which is reflected by the correlation coefficients of -0.65. This relationship is also strongly reflected on the separate visual estimations done on the 75 hand specimens (showing a correlation coefficient of -0.9).

Table II.1.1. Correlation factors between volume of each constituent, sorting factor and estimated calcite cement volumes (based on thin sections data from sub-units CC5c to CC5e; from RM to PAS locations).

	Grain Sorting	Total allochems	Intraclasts	Ooids	Skeletal grains	Quartz grains	Early cements	Late cements	total cements
Grain Sorting	1.00								
Total allochems	*0.33*	1.00							
Intraclasts	*-0.08*	0.69	1.00						
Ooids	**0.47**	*0.12*	**-0.64**	1.00					
Skeletal grains	*0.07*	*0.02*	*-0.03*	*0.06*	1.00				
Quartz grains	*-0.10*	**-0.65**	**-0.47**	*-0.04*	*-0.09*	1.00			
Early cements	*-0.13*	**-0.49**	*0.00*	*-0.34*	*0.13*	*-0.06*	1.00		
Late cements	*-0.30*	*0.03*	*0.29*	*-0.34*	**-0.41**	**-0.47**	*-0.21*	1.00	
Total cements	*-0.37*	**-0.48**	*-0.32*	*-0.07*	*-0.31*	*-0.23*	**0.59**	**0.67**	1.00

II.1.5.3. Facies types

The samples in the CC5c to CC5e sub-units are generally similar in composition and in texture, and are generally characterized by grainstones with micritic intraclasts, ooids, skeletal grains and quartz extraclasts, as previously mentioned. As such, subfacies types were defined to capture higher detail in variability of the relative abundance of different particle types, as well as grain sorting. Three main facies types (FT1 to FT3) were defined reflecting variations in the relative volume of carbonate allochems and extraclasts, as well as crinoids, as the fossil component with greatest significance in the CC5 member. Subfacies types (SFT) are

summarized in Table II.1.2 and described in more detail in the text below. Facies type 1 (FT1) is defined as calcareous sandstone and contains quartz grain volumes higher than 45 %. Samples defined by facies type 2 (FT2) have an abundance of crinoid fragments, while showing variations especially in grain sorting, but also in allochems and quartz grain volumes. Subfacies types SFT2.1 to 2.3 attempt to capture this variability. Samples classified as facies type 3 (FT3) are dominated by allochems, showing variability in quartz grains and allochems volumes, as well as in grain sorting. This is reflected in the definition of SFT 3.1 to 3.7 (see Table II.1.2).

Table II.1.2. Summary of facies and subfacies types, with major differentiating factors. The column for carbonate particle size shows the average size and the range.

Facies		Major constituents	Grain Sorting	Quartz content	Carbonate particles sand-grade size
FT1	Calcareous sandstone	High content in quartz	Poor	Very High	Medium (Fine to coarse)
FT2	Intraclastic-crinoidal grainstone with quartz extraclasts	High content in crinoids	--	--	--
SFT2.1	Intraclastic-crinoidal grainstone with quartz extraclasts	Intraclasts, quartz crinoids	Poor	Medium	Medium (Medium to very coarse)
SFT2.2	Intraclastic-crinoidal grainstone with quartz extraclasts	Intraclasts, quartz crinoids	Moderate	Medium	Fine (Fine to coarse)
SFT2.3	Oo-intraclastic-crinoidal grainstone with a few quartz	Intraclasts, ooids crinoids, quartz	Good	Low to medium	Fine (Fine to coarse)
FT3	Oo-intraclastic grainstone with quartz extraclasts	Higher content in carbonate particles	--	--	--
SFT3.1	Quartz-rich oo-intraclastic grainstone	Intraclasts, quartz ooids	Good (to moderate)	High	Fine (Fine to medium)
SFT3.2	Intraclastic-oolitic grainstone with quartz extraclasts	Ooids, intraclasts quartz	Good (to moderate)	Medium	Medium (Fine to coarse)
SFT3.3	Oo-intraclastic grainstone with quartz extraclasts	Intraclasts, ooids quartz	Moderate	Medium	Medium (Fine to coarse)
SFT3.4	Oo-intraclastic grainstone with quartz extraclasts	intraclasts, ooids quartz	Poor (to moderate)	Medium	Medium (Fine to very coarse)
SFT3.5	Oo-intraclastic grainstone	Ooids, intraclasts	Poor (to moderate)	Very low	Medium (Medium to coarse)
SFT3.6	Intraclastic grainstone	Intraclasts, ooids	Poor	Low (to very low	Medium (Medium to very coarse)
SFT3.7	Intraclastic grainstone	Intraclasts, ooids	Very poor	Low (to very low	Coarse (Medium to very coarse)

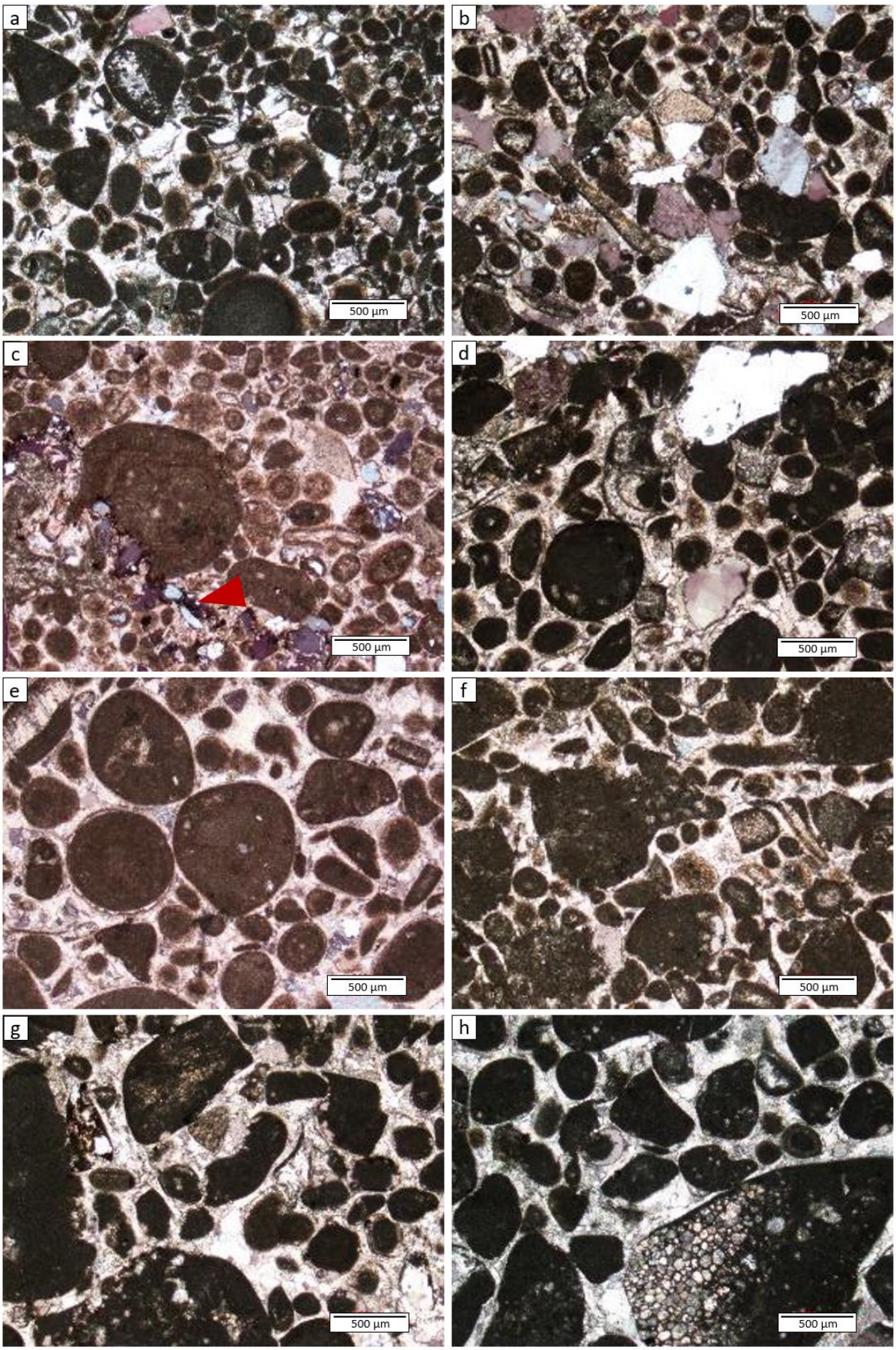
a
500 µm
b
500 µm
c
500 µm
d
500 µm
e
500 µm
f
500 µm
g
500 µm
h
500 µm

Figure II.1.11. Different facies types, with thin section examples. **a**: Sample LP15 (SFT2.3). **b**: Sample D10 (SFT3.1). **c**: Sample LP4 (SFT3.2). Red arrow indicates stylolite. **d**: Sample L1 (SFT3.3). **e**: Sample PG2 (SFT3.4). **f**: Sample PA3 (SFT3.5). **g**: Sample FS5 (SFT3.6). **h**: Sample FS3 (SFT3.7).

The quality and nature of the saw-cut hand specimens (Figure II.1.12) allow for visual estimations of grain sorting and relative abundance of crinoids, carbonate particles and quartz grains. These constituents are clearly identifiable, although uncertainty remains regarding the nature of carbonate particles, which might represent either ooids or intraclasts, as internal structures of these particles are not visible on hand specimens but only in thin section. The macroscopic analysis was used to define major facies types and is complemented by thin section analysis, used to further clarify facies and subfacies types (Figure II.1.11). The results of this facies classification scheme are applied to a correlation panel integrating lithology logs, major sedimentary features and discontinuity surfaces observed on outcrop (Figure II.1.13).

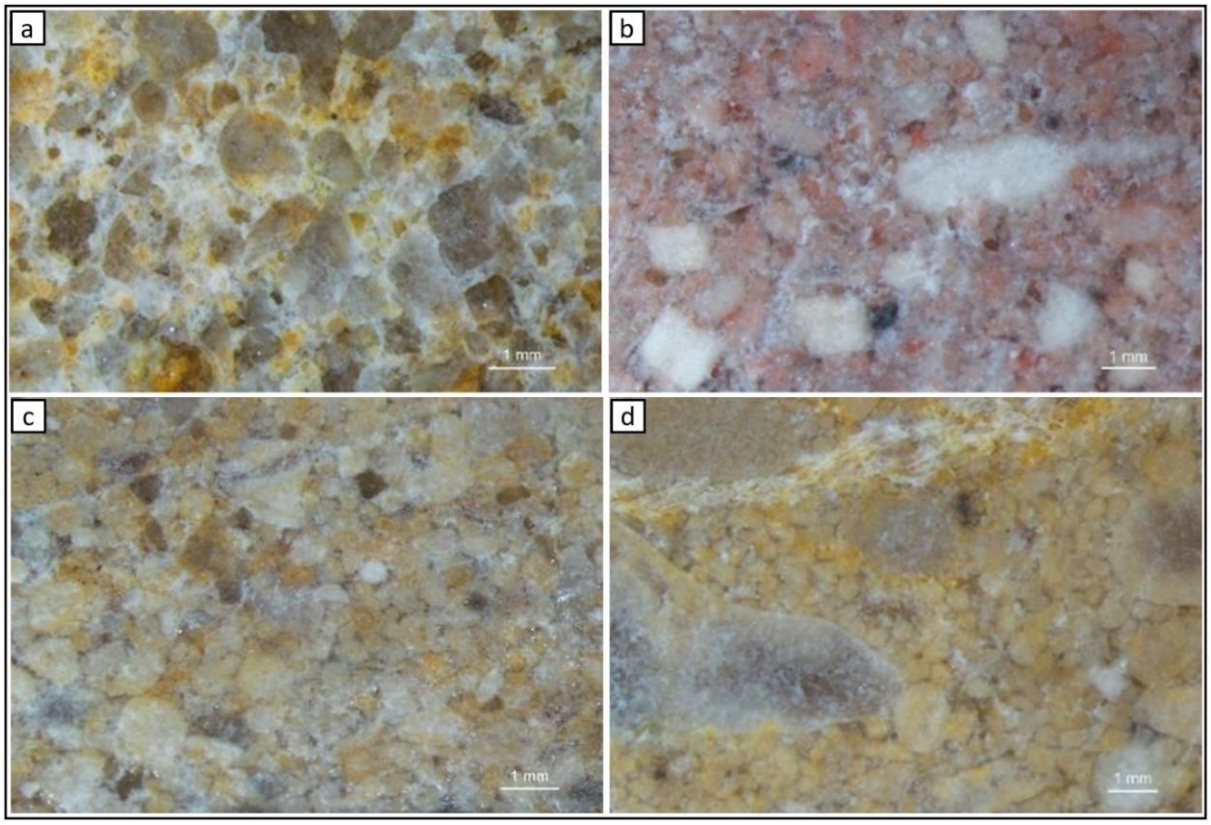

Figure II.1.12. Selected examples of hand specimen photos to show differences between main facies types. **a**: abundance of quartz grains (FT1, sample LP1). **b**: abundance of crinoid fragments (FT2, sample L7). **c** and **d**: dominated by allochems, with varying abundance of each constituent, varying grain size and varying grain sorting. Calcite cement volume is visible. **c**: Moderately (to poorly) sorted (FT3.3, sample PA6). **d**: Very poorly sorted (FT3.7, sample PA2).

Facies type 1 (FT1): Calcareous sandstone (based on hand specimen only). Shows an abundance of poorly sorted fine to very coarse quartz grains, between 45 and 65 % (containing a small fraction of quartz grains larger than 2mm). Contains fine to coarse allochems and the interparticle calcite cements are not as clearly visible on hand specimens as in other FT (Figure II.1.12a).

Facies type 2 (FT2): Intraclastic-crinoidal grainstone with quartz extraclasts. Characterized by the presence of crinoid fragments in moderate to high volumes. Contains fine to very coarse sand-grade intraclasts and ooids, as well as variable extraclast content in the form of moderately rounded quartz grains, which vary in grain size from fine to very coarse sand-grade. Subfacies are defined by grain sorting and variations in relative amounts of moderately rounded quartz grains and allochems.

- **Subfacies type 2.1** (SFT2.1): Intraclastic-crinoidal grainstone with quartz extraclasts. Poorly sorted. Medium to very coarse allochems (based on hand specimen only) and moderate (to high) volumes of quartz extraclasts (20 – 40 %), varying in size from medium to very coarse. Low to moderate volumes of visible calcite cement.
- **Subfacies type 2.2** (SFT2.2): Intraclastic-crinoidal grainstone with quartz extraclasts. Moderately sorted. Fine to coarse allochems (based on hand specimen only) and moderate volumes of fine to very coarse quartz extraclasts. Contains lower volume of very coarse quartz extraclasts than SFT2.1, estimated between 20 and 35 %. Low volumes of visible calcite cement.
- **Subfacies type 2.3** (SFT2.3): Oo-intraclastic-crinoidal grainstone with a few quartz grains. Well sorted. Intraclasts and ooids varying from fine to coarse sized, and low to medium volumes of quartz grains (5 – 15 %), varying in size from fine to coarse. Some quartz grains show a micritic coating. Moderate to high volumes of visible calcite cement (Figure II.1.11a).

Facies type 3 (FT3): Oo-intraclastic grainstone with quartz extraclasts. Contains varying fine to very coarse sand-grade intraclasts and ooids and fine to very coarse quartz grains. Subfacies reflect the variations in relative amounts of each component, as well as variations in grain sorting. Samples which are more poorly sorted contain coarser intraclasts. Samples generally contain poor to moderate volumes of visible calcite cement fully occluding interparticle space. skeletal grains are present in variable but relatively low volumes, generally in the form of fragments of bivalves and echinoderms, and microfossils (mainly foraminifera). Degraded Porostromata are observed on SFT3.4 to 3.7.

- **Subfacies type 3.1** (SFT3.1): Quartz-rich oo-intraclastic grainstone. Well sorted, with varying fine to medium sized intraclasts and ooids. Ooid content is estimated to be between 30 and 35 %. High volumes of fine to coarse quartz grains (25 to 35 %) and generally low estimated volumes of calcite cement are observed (Figure II.1.11b).

- **Subfacies type 3.2** (SFT3.2): Intraclastic-oolitic grainstone with quartz extraclasts. Well sorted, with varying fine to coarse sized intraclasts and moderate to high volumes of ooids (at an estimated 40 % on thin section). Coated grains are observed. Moderate volumes of fine to coarse sized quartz grains (between 10 and 15 %) and generally low estimated volumes of calcite cement (Figure II.1.11c).
- **Subfacies type 3.3** (SFT3.3): Oo-intraclastic grainstone with quartz extraclasts. Moderately sorted, with varying fine to coarse sized intraclasts and ooids. Volume of ooids is lower than in SFT3.2 (15 to 20 % on thin section). Moderate volumes of fine to coarse quartz grains (10 to 15 %). Moderate amount of calcite cement (Figure II.1.11d).
- **Subfacies type 3.4** (SFT3.4): Oo-intraclastic grainstone with quartz extraclasts. Poorly sorted. Varying fine to very coarse sized intraclasts and ooids (10 to 20 %). Moderate volumes of fine to very coarse quartz grains (5 to 25 %). A relatively small fraction of the quartz extraclasts show sizes close to the upper limit for very coarse particles. Moderate volumes of calcite cement are observed (Figure II.1.11e).
- **Subfacies type 3.5** (SFT3.5): Oo-intraclastic grainstone. Poorly sorted. Very low content in medium sized quartz grains (5 – 10 %). Varying medium to coarse sized intraclasts and ooids (15 – 40 %). This subfacies characterizes some samples with intraclasts containing degraded "Porostromata". Moderate volumes of calcite cement (Figure II.1.11f).
- **Subfacies type 3.6** (SFT3.6): Intraclastic grainstone. Poorly sorted. Varying medium to very coarse sized intraclasts and low volume of ooids (lower than in SFT3.5: 2 – 15 %). Very low to null volume of medium to coarse quartz grains (2 – 10 %). Degraded "Porostromata" and possible degraded algae fragments (probable dasycladacea in sample FS5) were observed within some intraclasts of this subfacies. Moderate to relatively high estimated volumes of calcite cement (Figure II.1.11g).
- **Subfacies type 3.7** (SFT3.7): Intraclastic grainstone. Very poorly sorted. Varying medium to very coarse sized intraclasts, containing a small fraction of intraclast larger than 2 mm. Very low volumes of ooids (10 % on thin section) and very low to null volume of medium sized quartz grains (2 – 10 %). This subfacies characterizes some samples with intraclasts containing degraded "Porostromata". Moderate to relatively high estimated volumes of calcite cement (Figure II.1.11h).

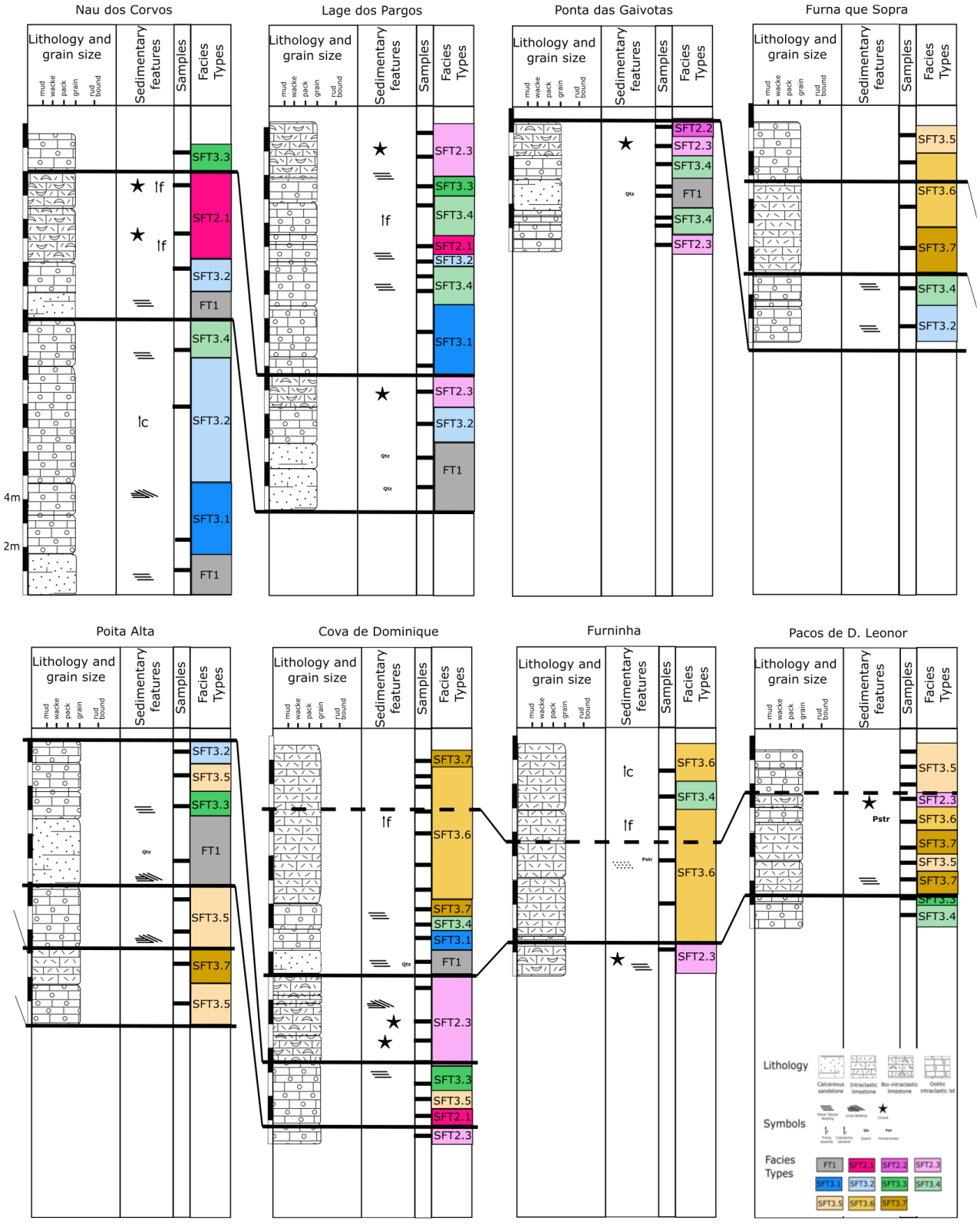

Figure II.1.13. Correlation panel showing lithology logs, major sedimentary features and subfacies types for each location and sample analysed. Correlation lines represent major discontinuity surfaces which can be followed laterally along the cliff face. This figure shows the great lateral variability in facies types in this CC5d sub-unit, which increases the difficulty in correlating lithologies.

II.1.6. Discussion

II.1.6.1. Paleoenvironmental interpretations

The CC5c to CC5e sub-units are characterized by the absence of fine carbonate particles or marly intervals and by the exclusive occurrence of grainstones with different content of oolitic, intraclastic, bioclastic and quartzy components, that were associated in the different facies scheme presented above (FT1 to FT3 and subsequent subfacies). These facies are typically representative of shallow-water depositional environments, controlled by different levels of energy which will affect particle transportation and distribution and will be reflected in parameters such as grain sorting and grain size (e.g. Folk, 1962; McNeill et al., 2004; Flügel, 2004; Reeder and Rankey, 2008). Subfacies types which are characterized by higher volumes of ooids and other coated grains generally show better grain sorting (SFT2.3 and SFT3.1 to SFT3.3), while samples characterized by lower content in ooids and higher intraclast volumes are generally more poorly-sorted (SFT2.1, 2.2 and SFT3.6, 3.7).

The different components in each facies type will have originated from different points of platform margin and platform interior settings and the relative proportion of each component will be related to variations in conditions of deposition and in relative sea-level as controlled by tectonic pulses and variations in accommodation space. The intervals which are characterized by quartz-rich mixed facies (such as FT1, SFT2.1 or SFT3.1) reflect periods of stronger influxes of siliciclastic material eroded and transported from the western granitic exposed platform (Berlenga Block), during which the carbonate factory will be less healthy. The intervals of predominantly carbonate content with moderate to minor quartz volumes (such as SFT2.2, SFT2.3 and SFT3.2 to 3.7) represent lower inputs from the exposed platform and healthier periods of the carbonate factory, with stronger influx of particles originating from different source points of the platform margin and inner platform. Wright and Wilson (1984) describe Unit 7 (corresponding to the CC5c to CC5e sub-units) as having similarities with large channel-fill sequences during the late stages of progradation of a submarine fan characterizing the younger units of the CC Formation. These authors do, however, also consider the possibility that Unit 7 develops through line-source deposition, with sediments originating from different source points, under the possible influence of tidal currents, as expressed by the presence of features such as bimodal cross-bedding, and as how we will see with the interpretations in the present study.

In this succession, the presence of high volumes of crinoids in the form of individual plates (or columnals) and column segments preserving their original pentagonal shapes (FT2) suggests relatively short to moderate transport distances. This would indicate deposition in relatively close proximity to the platform-margin shallow waters which are required for these rooted organism communities to thrive (e.g. Hess et al., 1999; Scholle and Ulmer-Scholle, 2003). The presence of corals in the CC5c sub-unit and of intraclasts containing degraded Porostromata

(suggesting the possible presence of algae too) in the CC5c and CC5d sub-units, are also indicative of close proximity to the platform-margin.

Brett (1999) describes a case study where crinoidal limestone layers are deposited in a high-energy shallow shelf environment close to normal wave-base. The author mentions that well-preserved crinoids are also found in deeper shelf beds (below normal storm wave base), and in the transition between shallow and deeper slope, while deeper basinal muds and grey shales show an absence of crinoids. The distribution of crinoids along a gently sloping ramp described by this author is interpreted to result from instability and sediment transportation caused by seismic disturbances. A study of outcrop sections in southern Poland, has also described crinoidal limestones as redeposited sediments originating from shallower positions in the basin, forming during shallowing of an uplifted tectonic block, and influenced by storm activity (Jach, 2005), which may lend some insight to the interpretations on the Peniche system. In a recent study, Krajewski et al. (2019) mention the occurrence of crinoids in biodetrital limestones with abundant oncoids and intraclasts preceding the deposition of marly sediments in central Poland. This sedimentary facies is considered to represent the result of transport and resedimentation of different types of particles originating in shallow-water environments, as might be the case with the interpreted crinoid-rich facies of the CC Formation.

Lower Jurassic crinoidal limestones in western Sicily have been characterized as localized and laterally discontinuous lenticular bodies deposited following the break-up of carbonate platform sediments, under the effects of tidal currents and, in some cases, related to storm events or tectonically-influenced activity, showing some similarities with the above-mentioned case studies (Jenkyns, 1971; Di Stefano et al., 2002). The crinoid facies in the Peniche outcrop are also limited in their lateral extent, which could be a result of similar types of depositional geometries being developed, although these are not clearly identifiable.

II.1.6.1.1. Lateral facies variability

Vertical facies variability is associated with relative sea-level variations and changes in accommodation space but will also be linked to lateral variations in depositional conditions through time. By defining subfacies types that take the relative amount of each constituent and grain sorting into account, subtle spatial variability in depositional facies becomes more apparent. An interpretative correlation of the facies and subfacies types was developed for the most continuous outcrop sector described by vertical profiles, to help better visualize spatial facies variability (Figure II.1.14).

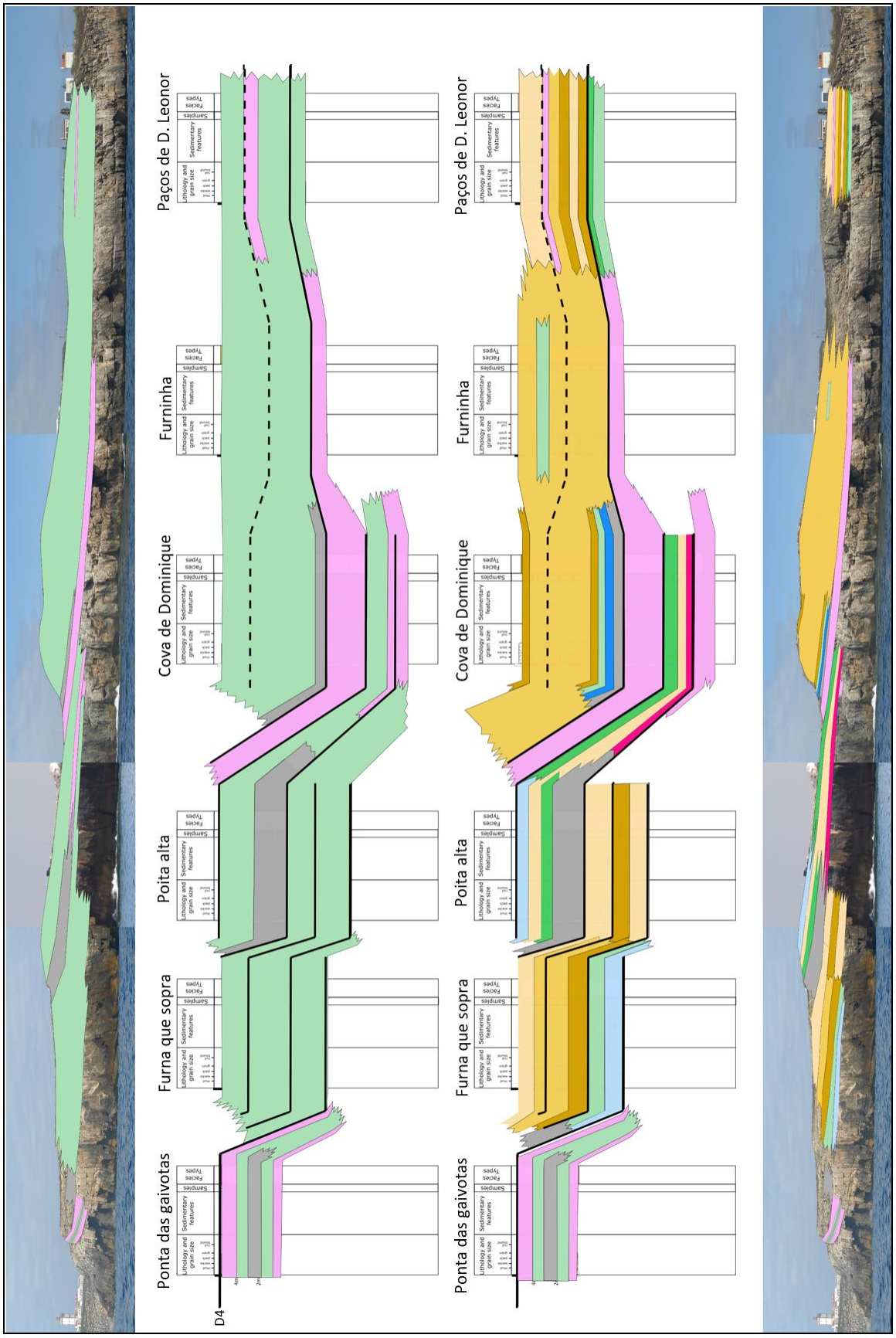

Figure II.1.14. Correlation panel covering most of the CC5d sub-unit, with facies and sub-facies types on stratigraphic profiles and on outcrop sector showing lateral variability. See Figure II.1.13 for colour code in lower panel. In upper panel, grey: FT1, Pink, FT2, Green: FT3.

In these sub-units, lateral facies variability is observed through abrupt to gradual lateral transitions, but is also related to pinching-out geometries between geobodies (Figure II.1.15a, b, d). These are sometimes difficult to assess due to the effects of outcrop degradation and weathering. Probable fault zones also add increased difficulties on outcrop observations between the LP and PG locations, as well as between F and L locations. Large quartz-rich channel structures are observed in the basal interval of the CC5d sub-unit, with abrupt lateral and vertical facies changes and truncation of older strata (Figure II.1.15e). The lateral thickness variations observed at different scales, the cross-bedding, truncation (Figure II.1.15c) and pinching-out geometries of depositional bodies are interpreted to result from relative lateral variations in depositional conditions, as promoted by currents and variable hydrodynamics. These complex variations have some control on the energy at the depositional interface and, consequently, on the sedimentation patterns (e.g. McNeill et al., 2004).

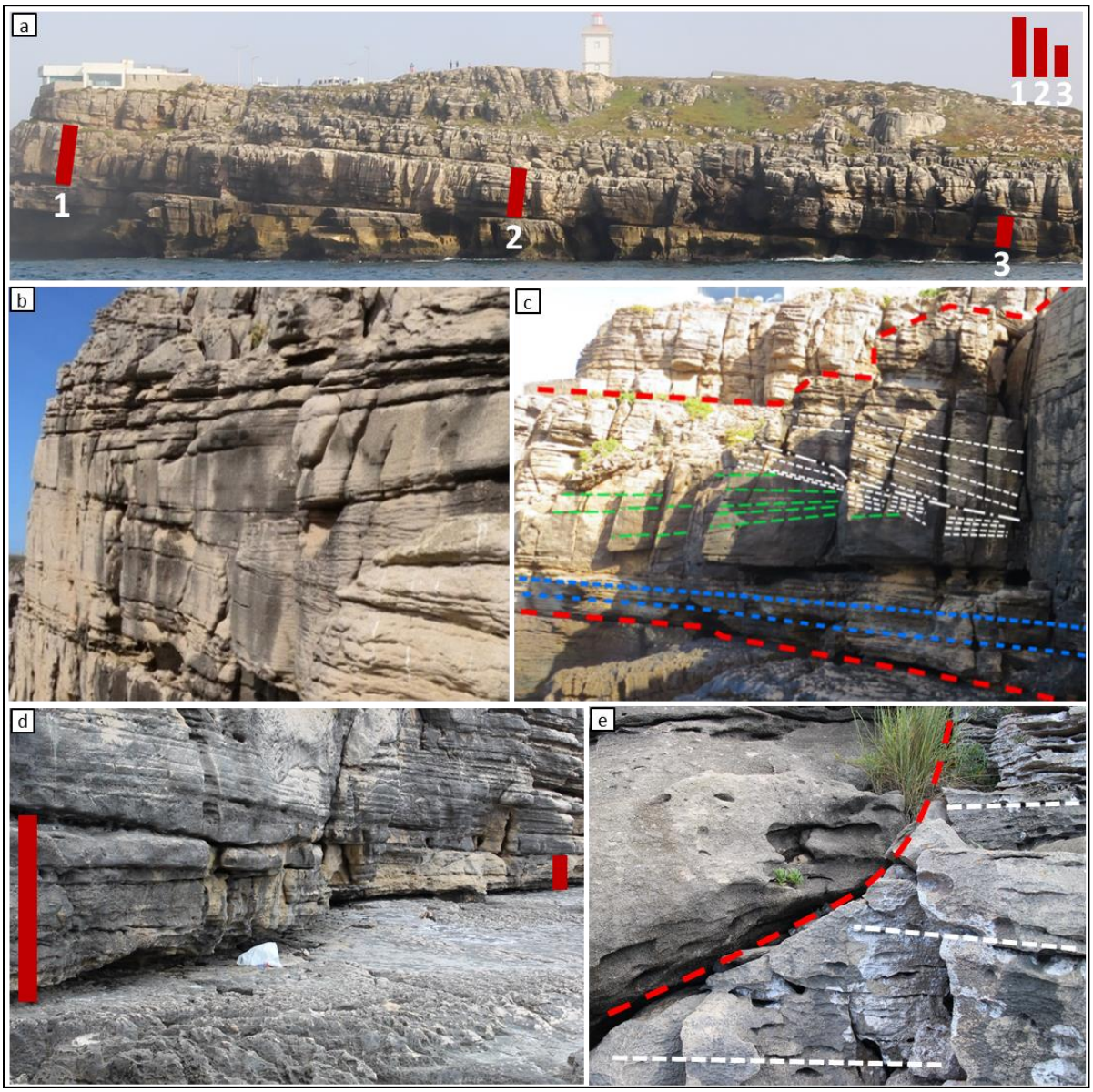

Figure II.1.15. **a**: CC5c sub-unit at locations NC and LP (see Figure II.1.3). Large scale thickness variation. Overlayed red boxes are shown side-to-side, in a schematic representation of this feature. **b**: CC5d sub-unit at FS location. Apparent lateral thickness variations, cross-stratification and moderate planar stratification. Horizontal distance along the photographed cliff-face is approximately 8 m. **c**: CC5c sub-unit at NC location. Strong discontinuities (red lines); quartz-rich interval with planar stratification (blue lines); truncation of depositional beds represented by bedding planes in green against younger beds represented by bedding planes with cross-stratification in white. Both sets of beds are characterized by planar-stratified quartz-oo-intraclastic grainstones. Horizontal distance along the photographed cliff-face is approximately 15 m. **d**: Bed thickness variation at the base of CC5c sub-unit at NC location (distance between red boxes is approximately 12 m). **e**: CC5d sub-unit at D location. Erosive surface with truncation of planar stratified quartz-oo-intraclastic grainstone (right – white lines) by calcareous sandstone (left). Sharp erosive surface and transition marked by dashed red line.

Facies variability, sediment distribution and grain sorting in present-day shallow-water environments characterized by the presence of ooids are strongly influenced by variable hydrodynamics and associated channel development and tidal activity, as expressed by the development of sand shoals and higher-energy channel pathways with poorly-sorted and coarser particles, such as in the Bahamas and Abu Dhabi (U.A.E.) (e.g. Reeder and Rankey, 2008; Alsharhan and Kendall, 2010). Although the sediments in the CC5 member in Peniche are also characterized by the presence of oolitic facies, the paleoenvironment and conditions of deposition will be different between the Peniche case and the two above-mentioned present-day cases. Sedimentation in the presently studied case is influenced by ongoing tectonic activity, translating into additional factors affecting deposition, which are not seen in the two above-mentioned cases. In addition, the Peniche succession is characterized by the presence of considerable volumes of siliciclastics, in contrast with these two cases.

II.1.6.1.2. The Peniche depositional system vs. mixed carbonate-siliciclastic models

The Peniche mixed depositional system is somewhat different from most documented mixed carbonate-siliciclastic systems, which are interpreted by the reciprocal sedimentation model, which describes the changes from highstand carbonate deposits to lowstand siliciclastic deposits as a response to short-term relative sea-level variations (e.g. Van Siclen, 1958; Wilson, 1967; Dolan, 1989; McNeill et al., 2004; Bourillot et al., 2010). This model has been described by different authors through different examples, such as continental siliciclastic deposits intercalating with carbonate shoals in shelf-edge barriers; siliciclastic sedimentation around river mouths intercalating with non-reefal carbonates or reefal bodies developing close to alluvial fan developments (e.g Flood and Orme, 1988; Pilkey and Rodriguez, 1988; Roberts and Murray, 1988; Tucker, 2003). While this model describes depositional sequences of alternating discrete bodies of terrigenous and carbonate sediments controlled by variations in relative sea level, the Peniche studied system is characterized by grainstone facies beds, composed by a mixture of high-energy carbonate particles and quartz grains.

The nature of the mixed facies types in Peniche implies a stable carbonate factory should be active along the platform-edge during the time of deposition of this succession (e.g. Spalletti et al., 2000; Zeller et al., 2015; Chiarella et al., 2017). While the carbonate factory keeps up with relative sea-level variations, both the siliciclastic material from the exposed platform and carbonate material from different points of the inner-platform to platform-edge setting are transported into proximal ramp positions, as previously mentioned, through gravity and current-driven flow (e.g. Pomar et al., 2015; Zeller et al., 2015; Chiarella et al., 2017). The mixing and cyclicity of relative carbonate-siliciclastic volumes can be analysed at different scales to help better understand vertical facies variability as controlled by variations in relative sea-level and accommodation space.

The Peniche depositional system shows similarities with the 'source mixing model' described by Mount (1984), which refers to systems with mixed deposits in flanks of carbonate shoal areas, resulting from the transportation of different material from an uplifted and eroded block containing siliciclastics, with deposition in relatively shallow shelf environments. Some characteristics of the CC5c to CC5e sub-units, such as the exclusive grainstone facies, as well as the observed geometries and large-scale lateral thickness variability, lends similarities to the 'infralittoral prograding wedge' model (e.g. Hernández-Molina et al., 2000; Pomar and Tropeano, 2001; Fernández-Salas et al., 2009; Pomar et al., 2015; Val et al., 2018). These large-scale wedges develop through line-source deposition below storm wave-base level between the onshore and offshore depositional environments and are composed of current-transported sediments from mixed shallow water environments, generally described as grainstones, which might be bioclastic or oo-intraclastic derived from coastal erosion (Pomar and Tropeano, 2001 and authors therein; Pomar et al., 2015).

The distinct grainstone facies of the CC5c to CC5e sub-units, with no fine carbonate fraction, contrasting with the predominantly marly limestones found not so far from Peniche, in the generality of the LB (e.g. Duarte, 1997; Duarte et al., 2001), as well as the complex geometries and thickness variations of the depositional bodies in Peniche, leads to the interpretation that deposition took place through the development of localized wedge-shaped geobodies. This interpretation, together with the previously discussed observations regarding facies types, would indicate the infralittoral wedge model as the best-fit model describing the depositional settings for these sub-units. Some uncertainty associated with this interpretation is related to the limited exposure of the Peniche outcrops.

II.1.6.2. Facies cyclicity

Although there is great similarity in facies between depositional beds, the detailed vertical association of facies and subfacies allowed to identify and define facies cycles at different observation scales. A multi-scale analysis provides valuable information on stratigraphic

cyclicity (e.g. Schlager, 2005; Catuneanu, 2006, 2019) and on the sedimentary facies distribution within the studied interval of the CC Formation, providing further insights on the controls on sedimentation. The hierarchy of this cyclicity will be further discussed in section II.1.6.3.

II.1.6.2.1. Higher frequency cycles

Throughout the vertical succession, the individual beds show very few clear internal sedimentary features. Some of the facies exhibit apparent fining upwards or coarsening upwards tendencies, although these patterns are not clear and are only seen at very few locations, which limits the possibility to establish detailed sedimentological cycles. The smallest identifiable facies cycles show an average thickness of 9 m (varying between 4 and 12 m). These cycles are bounded by discontinuities reflecting breaks in the sedimentary succession and are generally characterized by quartz-rich facies at the base (FT1, SFT3.1, SFT3.2), grading upwards into ooid-rich and crinoid-rich facies with varying volumes of intraclasts and decreasing volumes of quartz grains (FT2 and SFT3.3 to SFT3.6) (Figure II.1.16).This cyclicity is interpreted to result from the combined effects of tectonic pulses related to the Berlengas basement block uplift (e.g. Boillot et al., 1979; Vanney and Mougenot, 1981; Wright and Wilson, 1984), variations in accommodation space within the adjacent half-graben area and associated relative sea-level variations and variable sediment supply (e.g. Matenco and Haq, 2020).

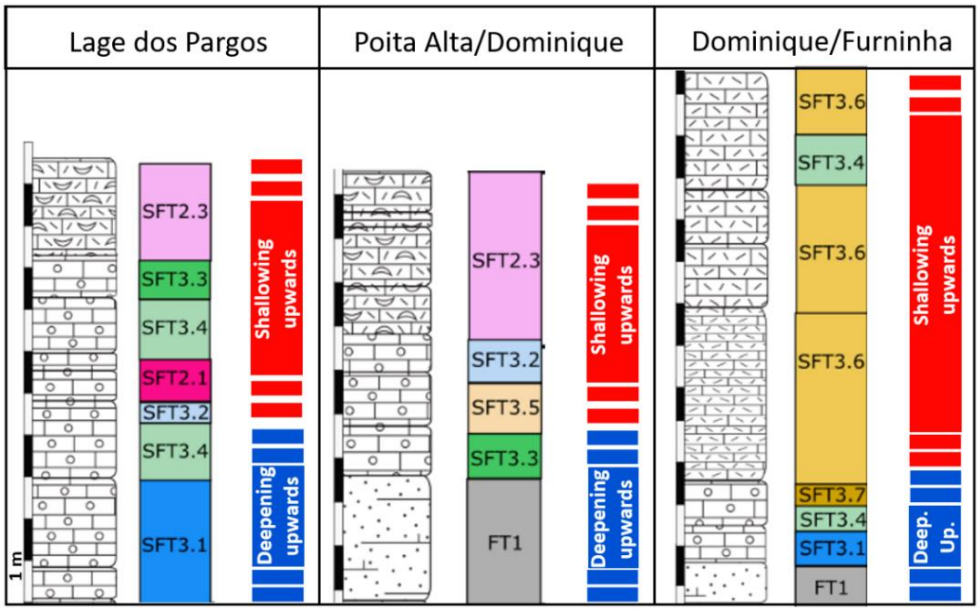

Figure II.1.16. Examples of facies cycles in CC5c and CC5d with interpreted deepening-upwards and shallowing-upwards trends at LP, PA/D and D/F locations. The deepening-upwards phase (blue) generally contains higher volumes of quartz grains, which decreases upwards into the shallowing-upwards phase (red). For each location, left column represents lithology, middle column represents facies types and right column represents the facies cycles trends (see Figure II.1.13 for facies code).

Because tectonic activity is seen as an important controlling factor on the observed facies successions, and not only eustasy, the sequence hemicycles will be referred to as deepening-upwards facies trends and shallowing-upwards facies trends (Figure II.1.16). Successive structural movements along the major fault plane will translate into moments of generalized uplift linked to shallowing-upwards facies trends and basinward shift of the shallowest facies, followed by moments of regional subsidence linked to deepening-upwards facies trends, sourceward movement of the shallowest facies and relative sea-level rise (e.g. Matenco and Haq, 2020). During a deepening-upwards phase, with higher accommodation space, an increase in siliciclastic input driven by current activity and hydrodynamics is observed. This will also reduce the influx of carbonate particles due to a decrease in carbonate factory productivity caused by the higher siliciclastic flux. A shallowing-upwards trend is defined by the overall relative increase in carbonate content, given the interpreted basinward shift of the shallowest facies; although siliciclastics influx is still ongoing due to exposure of the uplifted basement block, it would have a decreased influence versus the increasingly favourable conditions for higher carbonate rate production.

II.1.6.2.2. Lower frequency cycles

The CC5c, CC5d and CC5e sub-units are bounded by major discontinuities (D3 to D5) and have similar estimated thicknesses of 35-40 m, 45 m and 40-45 m, respectively. The basal intervals of the CC5c and CC5d sub-units typically show overall higher quartz volumes and are characterized by a stronger expression of sedimentary features such as cross bedding, pinching-out geometries and relatively large channel structures in the CC5d sub-unit, indicating the influence of current activity. The channel structures are characterized by quartz-rich calcareous sandstone facies (FT1), which would require strong-enough currents to enable the transport of coarser siliciclastic material to more basinward positions along preferred flow paths. Such features are interpreted to develop during deepening-upwards phases, when higher accommodation space develops (e.g. McNeill et al., 2004; Zeller et al., 2015; Chiarella et al., 2017). The transition into a shallowing-upwards phase, with decreasing accommodation space and relative sea-level then drives an overall decrease in siliciclastic influx and a progressive increase in transport and deposition of platform interior carbonate material, in similarity to the facies succession observed in the previously mentioned small-scale cycles.

The interpreted facies cyclicity is presented on the composite stratigraphic column describing the CC5c to CC5e sub-units (Figure II.1.17). The beds in the CC5e sub-unit do not present the same level of detail as the CC5c and CC5d sub-units, due to outcrop accessibility issues, as previously mentioned, and are generally described as intraclastic grainstones.

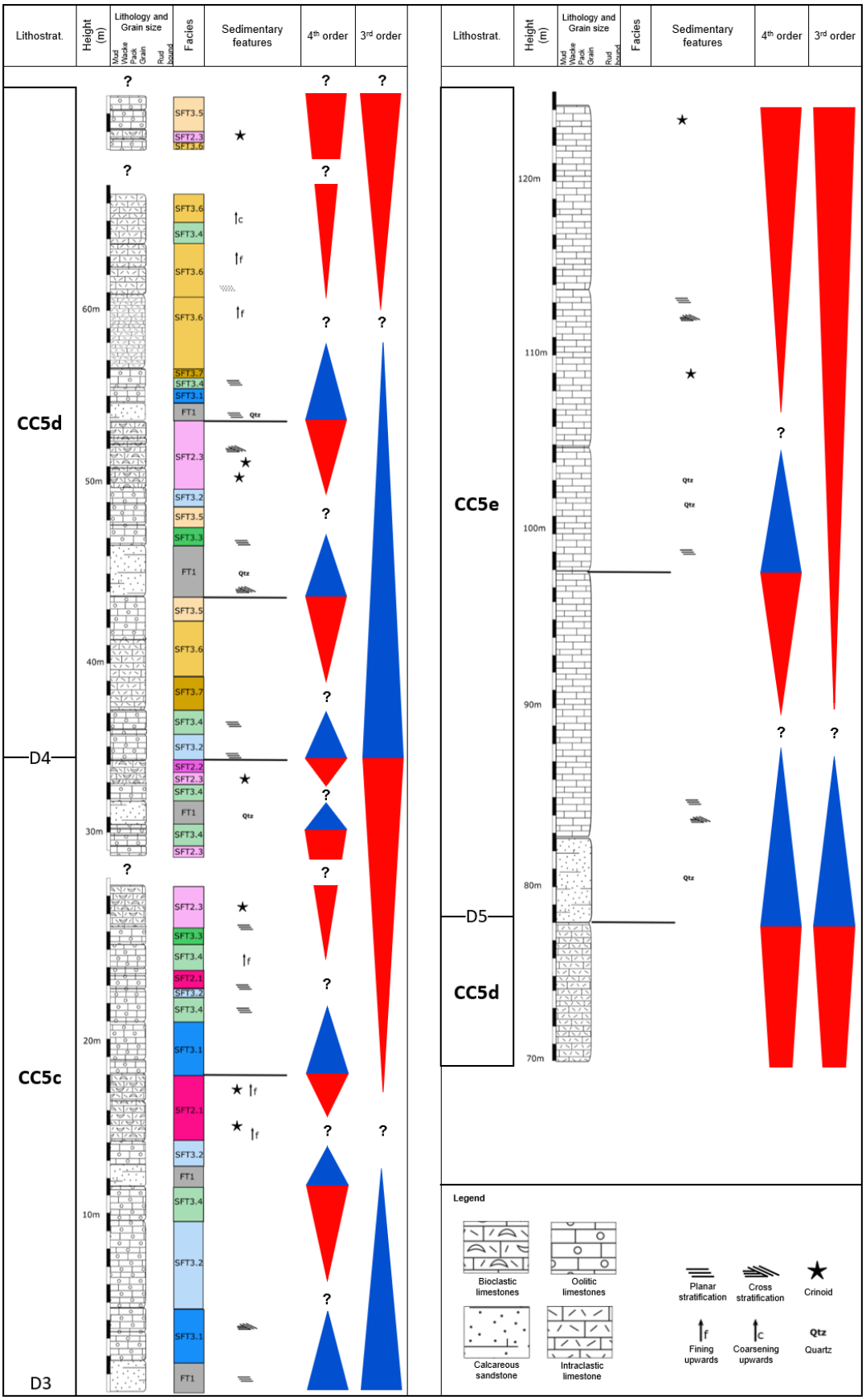
Lithostrat.
Height (m)
Lithology and Grain size
Mud Wacke Pack Grain Rud bound
Facies
Sedimentary features
4th order
3rd order
CC5d
CC5c
D4
D3
CC5e
D5
60m
50m
40m
30m
20m
10m
120m
110m
100m
90m
80m
70m
Qtz
Legend
Bioclastic limestones
Oolitic limestones
Calcareous sandstone
Intraclastic limestone
Planar stratification
Cross stratification
Crinoid
Fining upwards
Coarsening upwards
Quartz

Figure II.1.17. Facies cyclicity interpretation for the stratigraphic interval comprising the CC5c to CC5e sub-units (See Figure II.1.13 for facies colour code). Blue triangles represent deepening-upwards trends and red triangles represent shallowing-upwards trend.

The lithological parameter that stands out the most by offering a clear vertical trend throughout the succession is the average grain size of the combined carbonate and siliciclastic particles (Figure II.1.10), which is increasing from CC4 member to the CC5d sub-unit. This gradual increase in average grain size is seen as a reflection of an overall shallowing-upwards trend during an overall regressive phase, which is recognized in the generality of the LB (e.g. Duarte et al., 2001; Duarte, 1997, 2007; see also discussion below). The average grain size measurements in the CC5e sub-unit reflect a departure from this coarsening-upwards trend, showing a fining-upwards trend instead (Figure II.1.10). The significance of such a strong break in the succession remains uncertain and further studies would be required to translate this observation into a meaningful feature characterizing facies cyclicity within a sequence stratigraphy framework.

II.1.6.3. Sequence stratigraphic framework

Contrarily to the time equivalent uppermost S. Gião and Póvoa da Lomba formations, well dated by ammonites (Figure II.1.2b; Duarte and Soares, 2002), the studied succession of the uppermost CC Formation is limited in index fossils. The uppermost part of CC4 member is confirmed to represent the ammonite Bonarelli Zone (lowermost upper Toarcian; Figure II.1.2b), as expressed by the very rare occurrence of ammonites and the identification of *Nannirhyncia delgadoi* (Andrade, 2006). This species is also different from the species identified in the generality of the LB during the same time-frame (*Soaresirhynchia renzi*) (Andrade, 2006), providing further indication of a somewhat distinct depositional environment in Peniche. Uncertainty remains, however, regarding the age of the younger exposed sediments (CC5 member), due to the absence of index fossils in these shallow water carbonate facies (absence of ammonites and other possible fossil markers). The benthic foraminifer assemblage in this succession is poor and the species have a wide range, though in the LB they have been recognized only in the Middle Jurassic (Azerêdo, 1999 and personal commun.), thus making an Aalenian age plausible.

The outcrop exposure of the CC Formation is limited and localized, preventing observations at a larger scale. In the vicinity of Peniche, Toarcian-Aalenian(?) carbonate units are observed in areas of the Cesareda plateau only (approximately 11 to 15 Km to the east/southeast), although exposures of the succession are limited and non-continuous. The Middle to Late Jurassic succession is observed on outcrops of this plateau (e.g. Ruget-Perrot 1961; Manuppella et al., 1999; Azerêdo et al., 2003; Azerêdo, 2015). Close to the northwestern limit of the plateau, in

the area of Serra d'El Rei, partial exposures of the Toarcian-Aalenian(?) succession are observed at different locations, where middle to upper(?) Toarcian generally marly limestones are identified, but a biodetrital limestone interval with some oolitic content is also observed. This area shows clear indications of overall depositional instability caused by tectonic activity, increasing the difficulty in analysing a continuous succession (e.g. Guéry, 1984; Kullberg et al., 1997). Immediately north of Peniche, carbonate sediments (intercalated marls, marly limestones and limestones) of Bajocian-Bathonian age are exposed at Baleal (Azerêdo, 1988, 1998).

The analysis of cyclicity in the CC5 sub-units cropping out in Peniche in the context of a regional framework, coupled with observations on petrophysical parameters, might provide additional constraints that can help to further define the possible age of the CC5 sub-units. The observed facies cyclicity of the new proposed sub-units of the CC5 member were analysed according to the sequence stratigraphy concepts of Jacquin and De Graciansky (1998) and were then integrated with the existing sequence stratigraphy framework defined for the Toarcian (S. Gião and Póvoa da Lomba) in the LB (e.g. Duarte, 1997, 2007; Duarte et al., 2001).

The small-scale, high frequency facies cyclicity defined in section II.1.6.2.1, characterized by cycles with thickness between 4 and 12 m, is interpreted as equivalent to 4th order sequence cycles, based on the outcrop observations, on the physical amplitude defined for 3rd and 4th order sequences by Jacquin and De Graciansky (1998) (10s of meters) and considering the context of the studied basin. The cycles defined in section II.1.6.2.2, with estimated thicknesses of between 35 and 45 m, are interpreted to represent an increment of one order in this sequence stratigraphy hierarchy, and are therefore considered to be equivalent to 3rd order cycles. These interpreted cycles are part of the 2nd order sequence ST, which has been subdivided into four 3rd order sequences (St1 to St4) in the generality of the LB, as defined by Duarte et al. (2001) and Duarte (2007).

II.1.6.3.1. Comparing regional sequence stratigraphy frameworks

A brief comparison is here made between the new proposed 3rd order sequences in the Peniche succession and the coeval St4 sequence defined by Duarte (2007) for the generality of the LB.

The transgressive marly phase of St4a in Peniche, with a thickness of less than 10 m (Duarte, 1997) would be equivalent to the transgressive marly phase of St4 in the wider onshore area, although the latter shows considerable thickness increase towards the north/northwest, reflecting the variations in depositional settings depending on the paleogeographic location in the ramp profile (Duarte, 1997, 2007). The regressive phase of St4 in the wider LB area is characterized by intercalated marls and limestones showing considerable regional lateral heterogeneity (Duarte, 1997). This regressive phase would be equivalent to the Peniche interval

comprising the regressive phase of St4a and the full St4b to St4e cycles (Figure II.1.18), characterized by oo-intraclastic grainstone facies with quartz extraclasts and no marly content. The transition between St4a and St4b is marked by strongly bioturbated levels, which could possibly have some relation to the highly bioturbated basal interval of the Póvoa da Lomba Formation in the onshore LB area to the northeast of Peniche (Duarte, 1997, 2007; Duarte and Soares, 2002), although further studies would be required to confirm this.

In the onshore LB area northeast of Peniche, the total thickness of the deposits in the St4 sequence is increasing from south to north, from around 20 m to a minimum of 110 m (Duarte, 1997), while the exposed St4 sequence in Peniche has a minimum estimated thickness of approximately 200 m. The grainstone succession comprising sequences St4b to St4e has a minimum estimated thickness of 160 m and could be partly age-equivalent to the overall marly limestones of the Póvoa da Lomba Formation (Barbosa et al., 1988; Duarte, 1997, 2007; Duarte and Soares, 2002), which has a varying thickness of between 80 and 120 m towards the north, around the Cantanhede location, and is of upper Toarcian to lower Bajocian age (Barbosa et al., 1988; Azerêdo et al., 2003).

Such a thick succession in Peniche might result from the ongoing tectonic activity locally promoting the creation of relatively higher accommodation space in the area. This greater thickness of the Peniche succession and the possible partial correlation with the Póvoa da Lomba Formation, as mentioned above, might be an indication that this succession could include sediments of possibly younger ages (Aalenian).

The sequence boundary between St4d and St4e (discontinuity D5) marks a strong sedimentary break and a transition into the basal conglomeratic interval of CC5e, containing pebbles and boulder-sized clasts, as previously mentioned. This marks what appears to be the strongest discontinuity above D2 (CC5a to CC5b transition). Close to the D5 level, average grain-size starts decreasing upwards, marking a departure from the coarsening-upwards trend observed in the sections below (Figure II.1.10) and reflecting a strong sedimentary break, as previously mentioned. The possibility that D5 corresponds to the 3rd order sequence boundary DA1 (in Duarte et al., 2001; Duarte, 2007), also coinciding with the sequence boundary of the 2nd order sequence ST, which is a prominent discontinuity in the LB, as expressed by the sedimentary record and by carbon isotope data (e.g. Duarte, 1997, 2007), would place part of CC5d and the complete CC5e sub-unit in the Aalenian stage (Figure II.1.18). This analysis is associated with high levels of uncertainty, due to the absence of biostratigraphic data in the Peniche succession. The interpretations are therefore considered to be a working hypothesis that would require further testing.

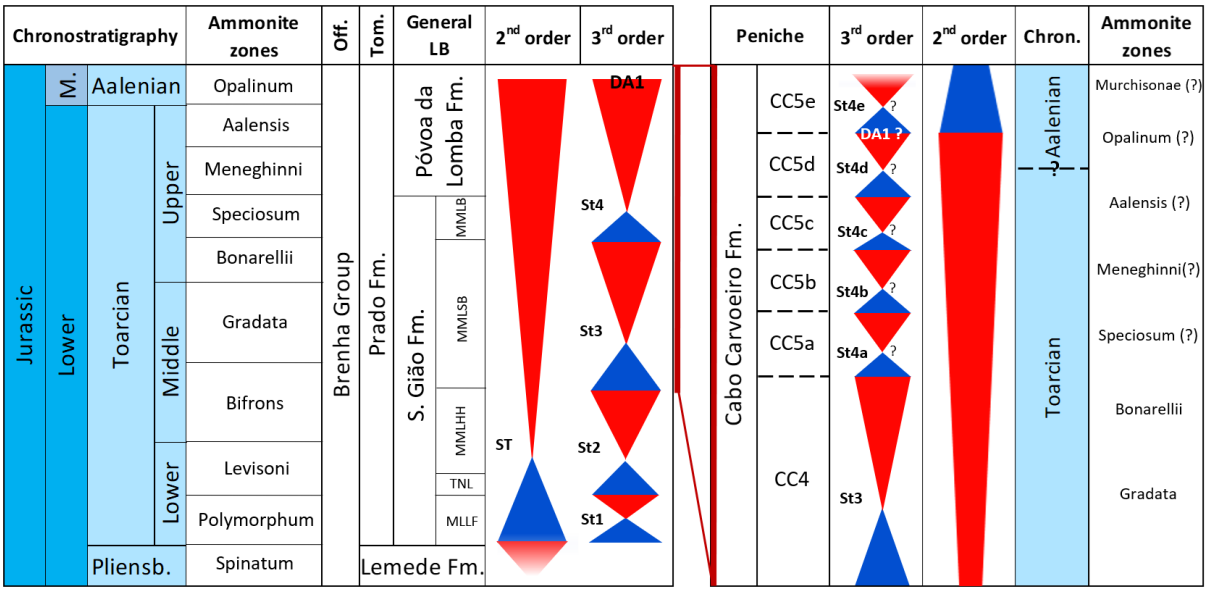

Figure II.1.18. Stratigraphy of the Toarcian interval for the offshore LB (Off.), the onshore Tomar region (Tom.) and Rabaçal area (General LB) east-northeast of Peniche (based on Duarte et al., 2001, 2004; Duarte and Soares, 2002; Duarte, 2007). The St3 to St4e 3rd order cycles for the Toarcian-Aalenian(?) in Peniche are represented on the right side. Uncertainty remains regarding the age of the CC5 sub-units and relation to the ammonite zones (see text also). (M. = Middle; Chron. = Chronostratigraphy).

The 2nd order sequence ST defined by Duarte (2007) is equivalent to the 2nd order 'Cycle 6' of the 1st order Ligurian cycle (De Graciansky et al., 1998; Hardenbol et al., 1998). This 2nd order cycle is subdivided into 3rd order sequences by Hardenbol et al. (1998) and Haq (2018), based on data from several European basins. Considering the new CC5 sub-units proposed in this work and their corresponding stratigraphic sequences (St4a to St4e), the Toarcian-Aalenian(?) CC Formation would represent eight 3rd order sequences (St1 to St4e in Figure II.1.18). A comparison is made with the regional datasets mentioned above (Figure II.1.19) but a direct correlation is not attempted, due to the uncertainty levels mentioned above and because the published frameworks are based on data from different locations and European basins, which are subjected to different controls on sedimentation, and a correlation with the Peniche area of the LB might lead to erroneous results (e.g. Posamentier and Allen, 1993).

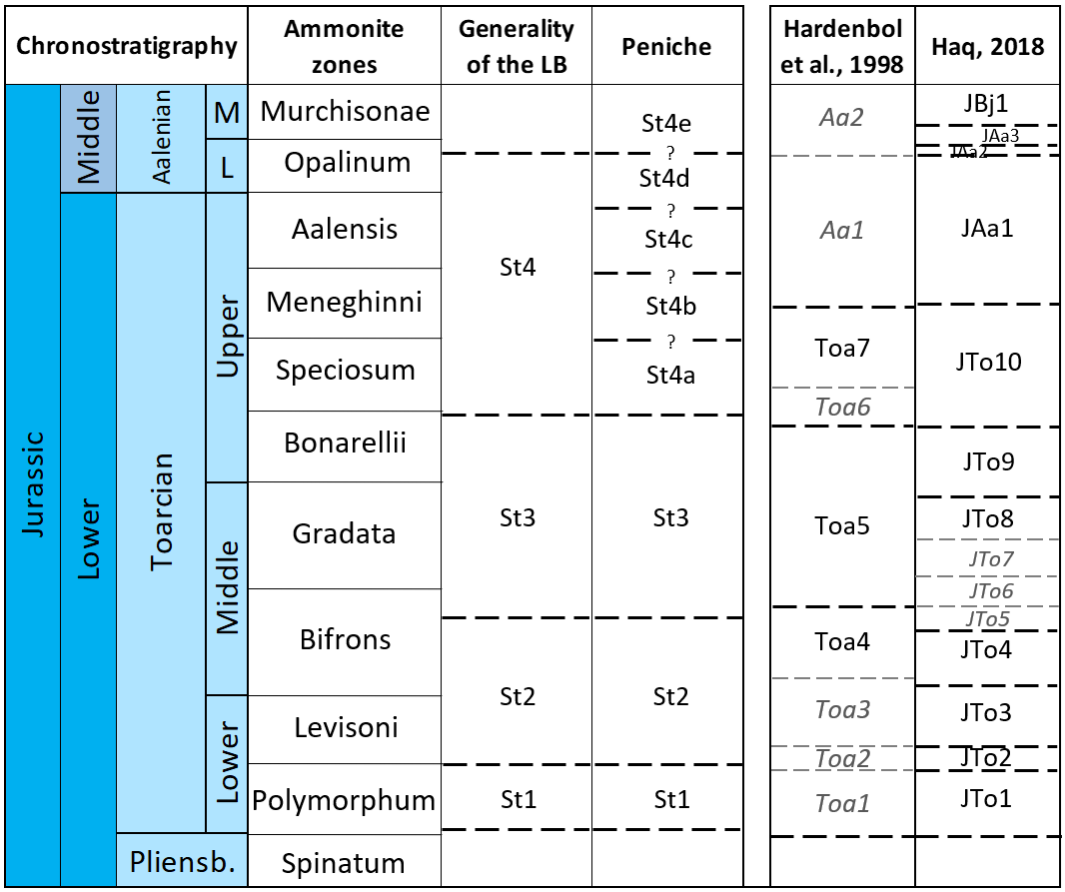

Figure II.1.19. Comparison between the 3rd order sequences proposed in this study, the sequences for the generality of the LB by Duarte et al. (2001, 2004) and Duarte (2007), and the regional sequence stratigraphy frameworks of Hardenbol et al. (1998) and Haq (2018). The ages of the St4a to St4e sequences are uncertain, as has been mentioned. Greyed-out sequences of Hardenbol et al. (1998) are only recognized in the Boreal/Subboreal realm, and not in the Tethyan realm. The three sequences JTo5–JTo7 of Haq (2018) are dependent on further confirmation, as indicated by the authors. (L = Lower; M = Middle).

II.1.7. Conceptual model

Tectonic activity, with the uplift of the Berlengas basement block and the creation of half-grabens in a rifting regime has led to the creation of steeply inclined slopes or submarine cliffs which promoted the development of a submarine fan during the Toarcian in the Peniche area (Wright and Wilson, 1984). With gradually decreasing tectonic influence (see also Kullberg et al., 2001), a period of relative tectonic quiescence was initiated (e.g. Wilson, 1975; Boillot et al., 1979) in association with the general decrease in relative sea-level during an overall regression phase which is capped by a basin-wide discontinuity (Duarte, 1997; Duarte et al., 2001; Azerêdo et al., 2003, 2014; Duarte, 2007). A gradual decrease in accommodation space,

as controlled by tectonics and by the continued sediment supply from the western Berlengas platform towards the east (present-day mainland), led to the infill of remaining available accommodation space, promoting the transition from deposition in steep slopes into deposition in less pronounced slopes (Figure II.1.20), interpreted to correspond to the time of deposition of the CC5b to CC5e sub-units (sequences ST4b to ST4e). Similar types of transitions have been described for extensional basins with infilled half-graben during periods of decreased tectonic activity (e.g. Ebdon et al., 1990; Burchette and Wright, 1992). An example of shelf to ramp evolution is also described by Read (1982), related to the infill of a back-arc basin, although the Peniche case might not represent such a pronounced transition.

Following this transition into less steep slopes, deposition would have most likely evolved from point-source deposition in fan-like settings to line-source deposition in wedge-shaped geobodies parallel to the coastline, in close proximity to a shoreface position, in similarity to the infralittoral prograding wedge model (e.g. Hernández-Molina et al., 2000; Pomar and Tropeano, 2001; Pomar et al., 2015; Val et al., 2018). The generalized sedimentation of intraclastic grainstones with ooids and quartz grains, with some facies containing corals or crinoid fragments showing low abrasion, further indicate particle transportation over relatively short distances and deposition in moderate to high energy environments, as mentioned in section II.1.6.1, and in agreement with the characteristics of the infralittoral prograding wedge model.

Outcrop features such as cross-bedding, lateral thickness variability (including apparent pinching-out geometries and strata truncation), as well as the presence of channel structures are also indicative of moderate to high energies of deposition, influenced by current activity and by hydrodynamics, which would vary laterally over moderate distances at a given point in time. Sediment transportation from different platform positions might have been controlled by this current activity and influenced by gravity flow, possibly also driven by tectonic instability or punctual storm events (e.g. McNeill et al., 2004; Lobo et al., 2005; Pomar et al., 2015; Zeller et al., 2015; Chiarella et al., 2017; Pomar et al., 2019). Lateral sediment distribution and particle sorting within the infralittoral prograding wedges, below the storm wave base, will have been affected in part by such activity, but possibly also by internal waves along a pycnocline breaking on the slope, in moderate similarity to the processes describing the deposition of oolitic-bioclastic grainstones in Lower Jurassic successions of Southern Spain (Pomar et al., 2019).

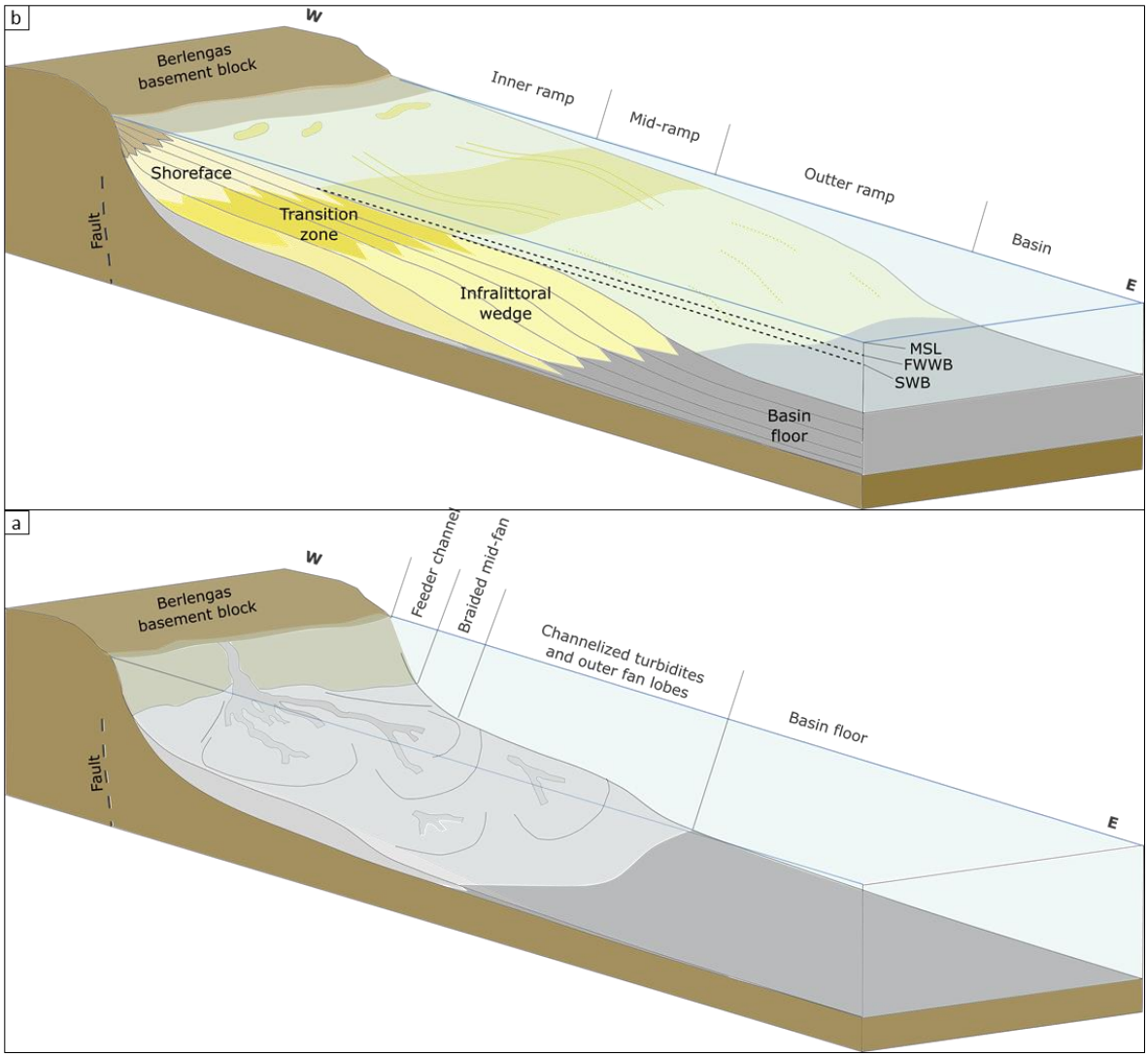

Figure II.1.20. Simplified conceptual block diagrams representing the depositional settings at the location between the Berlengas block and Peniche (west to east). Brown colour represents uplifted Berlengas block and undifferentiated sediments. Dark grey represents deeper water, finer sediments. **a:** Overall representation of the Peniche submarine fan system in the lower to middle Toarcian (based on Wright and Wilson, 1984). Feeder channel, braided mid-fan and turbidite channels are represented. Sediments are bypassing the margin and slope, being deposited in relatively deeper waters during the uplift of the Berlengas basement block. **b:** Rapid filling of available accommodation space with relatively high sediment production/influx during CC5 time of deposition (upper Toarcian-Aalenian(?)), as tectonic uplift becomes weaker during an overall regressive phase. Shades of yellow represent facies of inner to outer ramp settings, with development of infralittoral wedges (ILW). (MSL: mean sea level; FWWB: mean fair-weather wave base; SWB: mean storm wave base). The slope is interpreted to become progressively less pronounced upwards (from A to B) and deposition evolves gradually into higher-energy, shallower waters. Tectonic pulses would have influenced variations in the outer ramp slope, affecting depositional geometries and the development of sedimentary wedges. The Peniche grainstone succession correlates laterally to a marl-limestone succession on a wider, regional scale. This larger-scale factor is not represented on this diagram. Based on elements from Read (1982), Mount (1984), Ebdon et al. (1990), Burchette and Wright (1992), Hernandez-Molina et al. (2000), Pomar et al. (2015), Reijmer et al. (2015).

II.1.8. Conclusions

The CC5c to CC5e sub-units facies succession, generally characterized by oo-intraclastic grainstones with quartz extraclasts, is considerably different from the more marly sediments deposited in the generality of the LB during this time. This results from the development of distinct depositional conditions in the Peniche area, created as a consequence of tectonic activity and the Berlengas basement block uplift to the west. The mixed carbonate-siliciclastic grainstone facies of the CC5c to CC5e sub-units reflect line-source deposition, with current-transported particles originating from different positions of the high energy environment associated with this uplifted block, leading to deposition in geographically localized infralittoral wedge-like geobodies.

The developed facies and subfacies scheme revealed lateral variations in the relative volumes of different types of particles, as well as in grain sorting, considered to result from lateral variability in hydrodynamic conditions. This detailed classification scheme also provided useful information regarding vertical facies cycles, interpreted and organized according to a sequence stratigraphy hierarchy. The CC5a to CC5e sub-units are interpreted to represent five 3rd order sequences with siliciclastic-dominated deepening-upwards phases followed by carbonate-dominated shallowing-upwards phases. A direct correlation between these interpreted stratigraphic sequences and a regional sequence stratigraphy framework is not clear and the age of these sub-units is a major uncertainty, due to the absence of index fossils. However, taking into account the constraints and stratigraphic limitations discussed in this work, the interpretations of the obtained results allow for a working hypothesis to be presented, which proposes an Aalenian age for part of CC5d and the complete CC5e sub-unit.

The detailed facies classification scheme coupled with outcrop observations has offered useful insights into the factors controlling heterogeneity and cyclicity in the Peniche limestone succession, which is characterized almost exclusively by grainstone facies. Such detailed multi-scale approaches might prove useful in applications to different studies, such as hydrocarbon exploration and carbonate reservoir characterization studies, where rock heterogeneity is an important issue that will always benefit from added detailed information.

II.2. The carbonate-siliciclastic mixed deposits in the Lower to Middle Jurassic transition as potential hydrocarbon reservoir units.

II.2.1. Abstract

The Lower-Middle Jurassic transition in the westernmost Lusitanian Basin (Portugal) represents a particular hybrid facies association cropping out exclusively at Peniche, north of Lisbon. The studied succession has a minimum thickness of 160 m, it belongs to the Cabo Carvoeiro Formation (uppermost CC5 Member, assigned to the Toarcian-Aalenian?) and contrasts with the age-equivalent marls/marly limestones generally observed in the Lusitanian Basin. It is characterized by calcite-cemented quartz-oolitic-intraclastic grainstones deposited in infralittoral prograding wedges, with depositional conditions being influenced by the uplift and erosion of a marginal block which separates this basin from the deeper offshore Peniche Basin. These grainstone facies show good potential reservoir properties, with similarities to world class oolitic hydrocarbon reservoirs, although the original porosity has been fully occluded through diagenesis.

This study integrates onshore and offshore data, including 170 thin sections from outcrop and well cuttings. The grainstone facies on outcrop show an average cement volume of 31 %, potentially indicating moderate original porosity. The outcrop is strongly affected by two sets of fractures associated with strike-slip faults. The grainstone facies transition laterally through interfingering, gradation and pinching-out geometries into the coeval micritic mudstone-packstone observed in the southern 20B-1 and northern 17C-1 offshore wells, where grainstone intervals are limited. The infralittoral prograding wedges partially exposed at Peniche will not extend beyond the well locations, 40-45 km to the south and 15-20 km to the north. This grainstone interval overlies Sinemurian-Pliensbachian source rocks which have expelled hydrocarbons and there are strong indications for the potential presence of a potentially sealing unit, as well as structural/stratigraphic traps. This study provides valuable insights into the petroleum system associated with this Lower Jurassic case study and hypothetical analogue cases in the Lusitanian and Peniche basins.

II.2.2. Introduction

The petroleum systems of the Lusitanian Basin (LB) have received moderate attention in the past and have been the subject of a number of geological studies in a hydrocarbon exploration context (e.g. Rasmussen et al., 1998; Uphoff, 2005; Alves et al., 2006; Oliveira et al., 2006; Duarte et al., 2010, 2012; Spigolon et al., 2010; Silva et al., 2014; Pimentel and Pena dos Reis,

2016; Brito et al., 2017; Azerêdo et al., 2020). The first hydrocarbon exploration concessions in Portugal were awarded in 1901 in the Torres Vedras area (Figure II.2.1), although modern exploration based on geophysical data and on the application of petroleum geosciences concepts was only initiated in 1938 (Gomes, 1981). A total of 175 wells have since been drilled, most of them being shallow and targeting structural traps identified on seismic data, with oil or gas shows in 117 of these wells, but no relevant production (ENMC/UPEP, 2016). An assessment of undiscovered oil was done by the U.S. Geological Survey in 2016, reporting a mean risked volume of 55 MMBO of conventional oil resources (in addition to 66 MMBO of unconventional resources) for the LB Palaeozoic-Mesozoic total petroleum system (Schenk et al., 2016). The deep offshore Peniche Basin (see Figure II.2.1 for location) has not been drilled and is partially covered by 2D and 3D seismic data, which have provided indications of promising structural traps in the region. This basin is considered to be underevaluated and further studies in the region are fundamental to increase the understanding of potential petroleum systems (ENMC/UPEP, 2016).

The studied Toarcian-Aalenian(?) Cabo Carvoeiro (CC) Formation of the LB, cropping out exclusively at Peniche (Figure II.2.1), a coastline location ~80 km to the north of Lisbon, is divided into five members (CC1 to CC5) and contains a grainstone interval considered to represent depositional facies with strong hydrocarbon reservoir potential within the CC5 Member. This interval is defined by the informal CC5b to CC5e sub-units and is characterized as a thick succession (minimum of 160 m) of moderately to well sorted quartz-oolitic-intraclastic grainstones lacking marly intervals (Wright and Wilson, 1984; Duarte and Soares, 2002; Barata et al., 2021 – Chapter II.1). This succession is contrasting with the coeval succession of alternating marls and marly-limestones of the S. Gião and Póvoa da Lomba formations found generally in the basin (Duarte and Soares, 2002; Duarte et al., 2001). The CC Formation overlies source rock intervals of the Early Jurassic organic-rich Coimbra, Água de Madeiros and Vale das Fontes formations, which have generated and expelled hydrocarbons (e.g. Oliveira et al., 2006; Duarte et al., 2010, 2012, 2013; Silva et al., 2012; Poças Ribeiro et al., 2013; Silva and Duarte, 2015; Brito et al., 2017) and could have charged younger potential reservoir rocks, as indications of migrated hydrocarbons have been found in different Jurassic units (e.g. Gonçalves et al., 2014; Brito et al., 2017).

The main objective of this study is to address the depositional facies of the CC5b to CC5e sub-units as potential reservoirs and to investigate their regional extension, while also taking into consideration the potential deposition of similar facies in the western flanks of the Berlengas basement block, in the Peniche Basin. In addition, the re-interpretation of stratigraphic markers on the analysed wells and the facies classification of cuttings samples in thin sections from the two analysed offshore wells have been done. The added data from these wells provides valuable information to help better understand this system. The evaluation of the petroleum systems elements associated with the potential CC5 Member reservoir unit will be presented and

discussed in order to define the main uncertainties linked to hydrocarbon migration and entrapment in this hypothetical petroleum system and potential Lower Jurassic analogues of the LB.

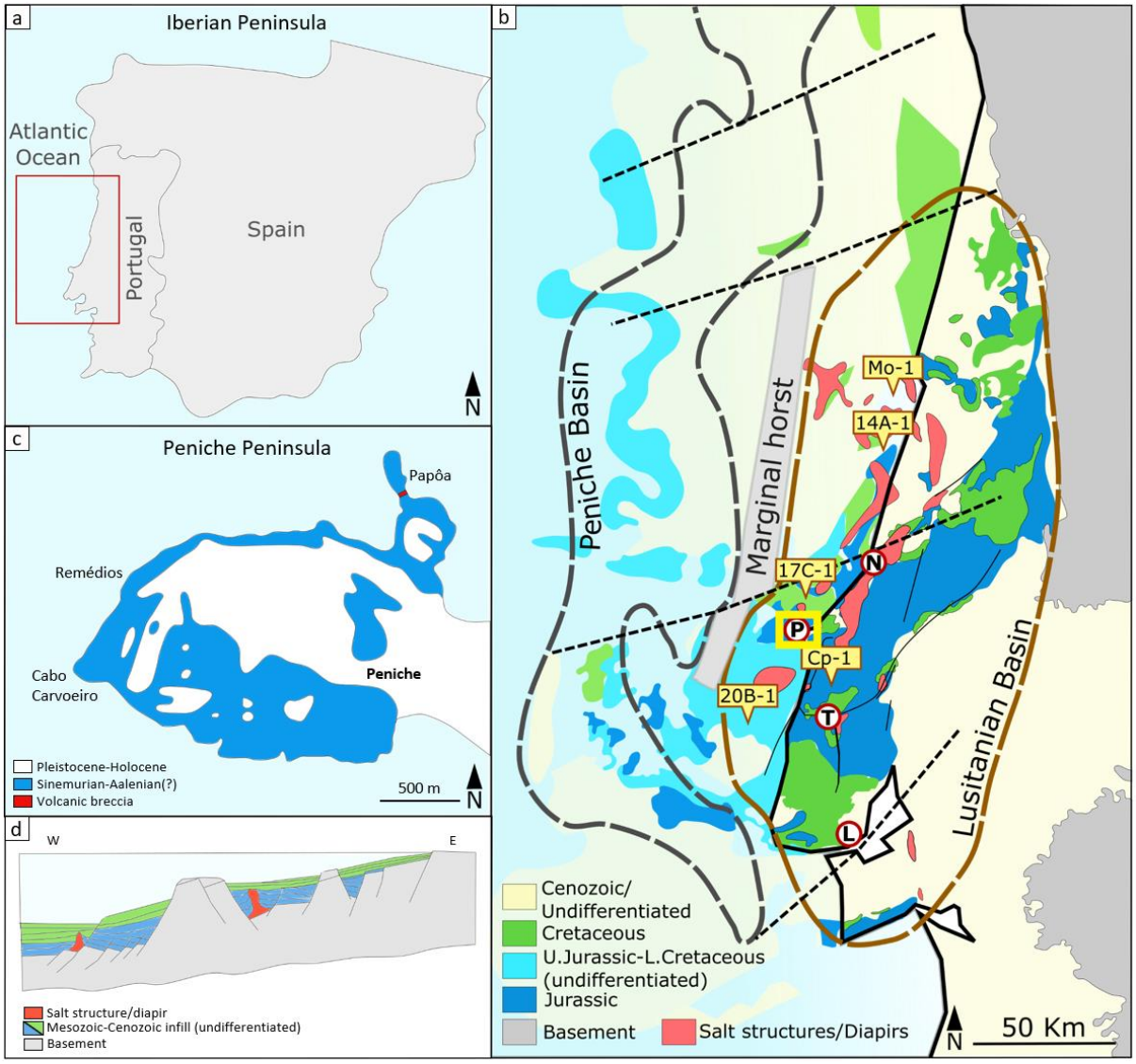

Figure II.2.1. **a**: Simplified map of the Iberian Peninsula; **b**: Simplified geological map of western central Portugal, showing locations of relevant wells, major salt structures, as well as location of the Lusitanian and Peniche basins and marginal horst in between both basins. L = Lisbon, T = Torres Vedras, P = Peniche, N = Nazaré. Dashed black lines represent major southwest-northeast transfer faults dividing the sectors of the basins (based on elements from Montenat et al., 1988; Wilson et al., 1989; Rasmussen et al., 1998; Alves et al., 2003b, 2006; LNEG, 2010); **c**: Simplified geological map of the Peniche Peninsula (based on Camarate França et al., 1960, Duarte et al., 2017); **d**: Simplified west-east geological cross section across the central Lusitanian Basin, marginal horst and into the Peniche Basin (based on, and modified from Vanney and Mougenot, 1981; Wilson et al., 1989).

II.2.3. Geological background

The Mesozoic LB extends along the present-day coastline of central to northern Portugal (Figure II.2.1) and its western limit is defined by a marginal horst structure, separating it from the deeper Peniche Basin, further offshore (Figure II.2.1b, d). These basins formed during the opening of the northern Atlantic Ocean, and were shaped by a succession of rifting phases and associated structural and halokinetic activity during the Mesozoic (e.g. Wilson et al., 1989; Pinheiro et al., 1996; Alves et al., 2002, 2003b, 2006; Kullberg et al., 2013). The number and timing of rifting episodes is debated among authors; according to Rasmussen et al. (1998) and Alves et al. (2002, 2006), four main rifting phases are identified in the Late Triassic, Sinemurian-Pliensbachian, Oxfordian and Late Jurassic to Early Cretaceous. This tectonic activity has had great control on subsidence patterns and depositional geometries, with deposition occurring in fault-bounded graben or half-graben during the Jurassic to early Cretaceous (e.g. Wilson et al., 1989; Hiscott et al., 1990; Pinheiro et al., 1996; Rasmussen et al., 1998; Alves et al., 2002, 2006; Kullberg et al., 2013).

Vertical salt migration occurs along major fault zones, in association with the tectonic activity and reactivation of basement faults (e.g. Wilson et al., 1989; Rasmussen et al., 1998; Alves et al., 2006; Walker et al., 2021). Halokinesis starts from the Early Jurassic onwards, increasing in intensity towards the Late Jurassic and into the Cretaceous, also leading to the development of salt anticlines and pillows (e.g. Montenat et al., 1988; Wilson et al., 1989; Alves et al., 2006). The combined effects of tectonics and associated halokinesis on subsidence and sedimentation leads to regional facies and thickness variations, and to the development of complex geometrical relationships between depositional bodies (e.g. Vanney and Mougenot, 1981; Montenat et al., 1988; Wilson et al., 1989; Rasmussen, 1998; Alves et al., 2002, 2006). Compartmentalization and the creation of sub-basins in the LB occurs as a result of this complex structural activity (e.g. Wilson et al., 1989; Alves et al., 2002, 2006). Later, mostly Cenozoic compressive movements related to the Alpine tectonism led to the reactivation of structural features, inversion and uplift, enhancing salt anticlines and further developing diapiric structures (e.g. Wilson et al., 1989; Rasmussen et al., 1998; Uphoff, 2005; Alves et al., 2003a, 2006).

The studied sub-units of the CC5 Member within the Toarcian-Aalenian(?) CC Formation (Figure II.2.2), were deposited during a 2nd order regressive phase ending in the lowermost Aalenian (Duarte, 2007; Duarte et al., 2001; Azerêdo et al., 2014), which is inserted in a Triassic-Middle Jurassic (Callovian) major cycle (see also Wilson et al., 1989; Soares et al., 1993). As mentioned in the introduction, these sub-units are characterized by grainstone facies (Wright and Wilson, 1984; Duarte and Soares, 2002; Barata et al., 2021), in contrast to the age-equivalent marls and marly-limestones of the S. Gião and Póvoa da Lomba formations generally found in the basin (Duarte et al., 2001; Duarte and Soares, 2002).

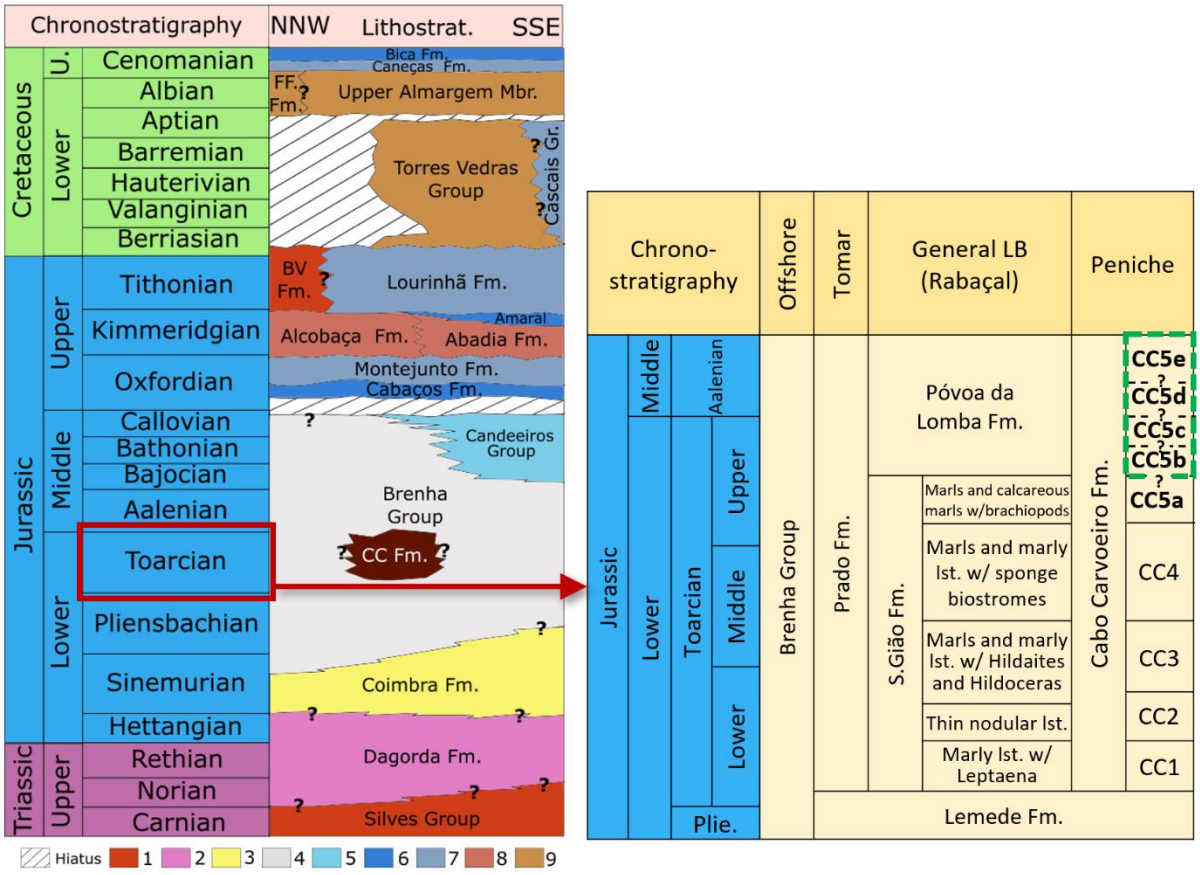

Figure II.2.2. **Left**: Simplified lithostratigraphy of the central onshore sector of the LB between the parallels of Torres Vedras and Nazaré, approximately (see Figure II.2.1 for locations). Only dominant lithologies and main units are shown (based on Wilson et al., 1989; Leinfelder, 1993; Azerêdo, 1998; Rey et al., 2006; Dinis et al., 2008; Kullberg et al., 2013; Duarte et al., 2014; Azerêdo et al., 2020), some of which are informal and generally used by the oil and gas companies (ENMC/UPEP, 2016). Only the Jurassic chronostratigraphy is to scale; the Triassic and Cretaceous intervals are condensed for visualization purpose. CC Fm. = Cabo Carvoeiro Formation; BV Fm. = Boa Viagem Formation; FF Fm. = Figueira da Foz Formation; U. = Upper; Lithostrat. = Lithostratigraphy. **Right**: Toarcian lithostratigraphy of the LB (based on Duarte and Soares, 2002), including the CC5 Member sub-units of uncertain age (dashed green rectangle), as discussed in Barata et al. (2021). Lithostratigraphy and dominating lithologies: 1: Redish siliciclastics; 2: Evaporites with dolostones and claystones; 3: limestones and dolostones; 4: Hemipelagic-open marine marls and limestones; 5: Oolitic-bioclastic and oncolitic limestones; 6: Lacustrine limestones (Cabaços Fm.), oolitic-biostromal limestones (Amaral Fm.), rudist limestones (Bica Fm./Cacém); 7: Open marine limestones (Montejunto Fm.), marls and marly limestones, with siliciclastics towards the top (Lourinhã Fm.); marls and limestones (Cascais Group, Caneças Fm.); 8: Marl-dominated with intercalated sandstones (Abadia Fm.), alternating marls, detrital limestones and sandstones (Alcobaça Fm.); 9: Estuarine and fluvial littoral sandstones.

The deposition of the CC Formation is related to the Berlengas basement block uplift and associated development of localized submarine fans and infralittoral prograding wedges in and around the Peniche area (e.g. Wright and Wilson, 1984; Barata et al., 2021). These Toarcian sediments overlie Sinemurian-Pliensbachian intervals characterized by the presence of potential source rock units rich in organic matter (see section 2.1.1 below), which were deposited in open marine settings (Duarte and Soares, 2002; Duarte et al., 2010, 2012; Silva et

al., 2011; Silva and Duarte, 2015; Coimbra and Duarte, 2020), giving way to the development of a homoclinal ramp dipping to the west-northwest during the Early and Middle Jurassic (e.g. Azerêdo, 1988, 1998; Duarte, 1997, 2007; Silva and Duarte, 2015).

The interval of interest for this study is part of the Brenha Group, a widely used informal nomenclature in the oil and gas industry (Figure II.2.2) (ENMC/UPEP, 2016; see also Wilson et al., 1989; Azerêdo, 1998; Azerêdo et al., 2020) referring to the predominantly open marine sediments of the Lower Jurassic-Middle Jurassic (e.g., Azerêdo, 1988, 1993, 2007; Soares et al., 1993; Duarte, 1997, 2007; Duarte and Soares, 2002; Azerêdo et al., 2003). This stratigraphic interval is well-studied in the onshore areas of the LB and is defined by a more detailed stratigraphic framework that includes the Toarcian-Aalenian(?) CC Formation and lateral equivalent São Gião Formation (Figure II.2.2) (e.g., Wright and Wilson, 1984; Duarte, 1997, 2007; Duarte and Soares, 2002; Barata et al., 2021). Deposition of increasingly shallower water carbonate sediments in the Middle Jurassic, informally referred to as the Candeeiros formation (Figure II.2.2) in the context of the oil and gas industry, is well studied in the onshore as well, and corresponds to a more detailed lithostratigraphy defined by different sedimentary packages. These include the Santo António-Candeeiros Formation, well studied in outcrops of the Maciço Calcário Estremenho region, in central Portugal, and its lateral equivalent Cabo Mondego Formation in the western, more offshore areas (e.g. Azerêdo, 1998, 2007; Azerêdo et al., 2003, 2020).

II.2.3.1. Overview of the LB petroleum systems

The Late Triassic to Early Jurassic evaporite-bearing Dagorda Formation has a highly variable thickness, from ~140 m up to around 2200 m (Uphoff, 2005; Davison and Barreto, 2020), partially resulting from thickening through tectonic activity and diapirism, and acts as a major regional sealing unit separating two stratigraphic intervals with very low to potentially null connectivity (e.g. Wilson et al., 1989; Uphoff, 2005; Davison and Barreto, 2020; Walker et al., 2021). It overlies the fluvial siliciclastic deposits of the late Triassic, consisting of massive halite intervals and transition zones of alternating anhydrites and dolomites, also containing intervals of dominant claystones and siltstones, and represents a gradual transition into a carbonate ramp setting prevailing during the Early and Middle Jurassic (e.g. Azerêdo, 1988, 1998; Soares et al., 1993; Duarte, 1997, 2007; Azerêdo et al., 2003; Duarte et al., 2010). Other marly or clay-rich units throughout the stratigraphic column have been identified as potential barriers or baffles to fluid flow, such as the marly or muddy limestone facies of the Middle Jurassic ramp system (e.g. Azerêdo et al., 2020), the clay-rich intervals of the Lourinhã Formation (upper Kimmeridgian-Tithonian) (Figure II.2.2) (e.g. Hill, 1989), or the Taveiro Formation deltaic clays (Maastrichtian) (e.g. Cunha and Pena dos Reis, 1995; Pimentel and Pena dos Reis, 2016). Potential source-reservoir rock pairs in the sections below and above the

Dagorda Formation will define distinct petroleum systems or combinations of systems. The evolution of these systems was affected by the strong tectonic activity in the basin, which has led to the creation of potential structural traps and to the development of abundant fractures and fault zones (e.g. Wilson et al., 1989; Rasmussen et al., 1998; Alves et al., 2002, 2006), which will have affected the effectiveness of sealing units and the potential migration and accumulation of hydrocarbons (e.g. Uphoff, 2005; Pimentel and Pena dos Reis, 2016).

The Jurassic sedimentary packages of the LB are considered to correlate with the sedimentary succession of the deeper offshore Peniche Basin, based on interpretations and correlation of seismic data (e.g. Alves et al., 2006; Walker et al., 2021). The petroleum systems identified in the LB are therefore expected to also be present in the deep offshore areas of the Peniche Basin, although the thicknesses of sedimentary packages are reported to increase considerably in the latter (Alves et al., 2006; Walker et al., 2021).

II.2.3.1.1. Source rocks

Potential source rock units have developed during the Early Jurassic, identified based on geochemical and petrographic analysis of onshore samples (e.g. Oliveira et al., 2006; Duarte et al., 2010, 2012, 2013; Silva et al., 2007, 2010; Silva et al., 2011, 2012; Poças Ribeiro et al., 2013; Brito et al., 2017). The quality of these source rocks is varying regionally, as controlled by the variability in redox conditions and of depositional environment conditions (e.g. Silva and Duarte, 2015; Ferreira et al., 2020). São Pedro de Moel outcrop samples of the upper Sinemurian to lowermost Pliensbachian Água de Madeiros Formation have a maximum TOC value of 22.5 wt.% and high values of Hydrogen Index (above 600 mg HC/g TOC), suggesting oil generation potential, although vitrinite reflectance data (0.43 % Ro and T_{max} between 410-437˚) indicate this source rock is immature at this location, as reported by the high-resolution study by Duarte et al. (2012). The marls-marly limestones of the Pliensbachian Vale das Fontes Formation, show maximum TOC values of ~ 15 wt.% measured on Peniche outcrop samples but are thermally immature at this location, with a T_{max} of around 430 ^{o}C presented in the high-resolution work of Oliveira et al. (2006). However, these source rocks are considered to have reached maturity at different locations, given the presence of migrated hydrocarbons in different units of the Lower-Middle Jurassic (e.g. Gonçalves et al., 2014; Brito et al., 2017).

Intervals of source rock potential have also been identified in the Middle and Upper Jurassic (e.g. Silva et al., 2014; Gonçalves et al., 2015). In the Upper Jurassic, the Oxfordian Cabaços Formation, of freshwater and brackish, lagoonal and restricted marine depositional environments (e.g. Leinfelder and Wilson, 1998; Azerêdo et al., 2002, 2003), has a maximum recorded TOC value of 30.6 wt.% measured on outcrop samples (Silva et al., 2014). Oxfordian subsurface samples from the Turcifal sub-basin have TOC values of up to 6 wt.% and vitrinite reflectance values indicating early oil window maturity (Uphoff et al., 2010). In addition,

different types of migrated bitumen were identified in outcrop at the Cesareda location (Azerêdo, 2015) and in subsurface samples from Middle and Upper Jurassic units, filling voids and fractures, but also scattered in the mineral matrix, where vitrinite reflectance was measured and varies between 1.13 and 1.48 % Ro (Gonçalves et al., 2014). Semi-quantitative TOC estimations based on the Passey method applied to data from the 14A-1 well (Figure II.2.1), indicate organic-rich intervals of the Coimbra, Água de Madeiros and Vale das Fontes formations as having good source rock potential in this offshore area (see Sêco et al., 2019).

II.2.3.1.2. Potential carbonate reservoir units

A few Jurassic carbonate units have been identified as having potential reservoir characteristics. The dolomites of the Lower Jurassic Hettangian Dagorda Formation have been reported to contain porosities of up to 20 % (Uphoff, 2005). Middle Jurassic Bathonian and Callovian shallow-water carbonates contain packstone, grainstone, dolostone and biostrome intervals described as potential reservoirs, with variable estimated porosities reaching up to 20 % (Azerêdo et al., 2020). Middle and earlymost Late Jurassic reefal and oolitic carbonates with oil shows have been identified in a well within the Arruda sub-basin, southeast of Peniche, showing porosities between 10 and 23 % (Uphoff et al., 2010), as well as in outcrop at the Cesareda location, to the southeast of Peniche (Azerêdo, 2015). In the Late Jurassic, potential reservoir units have also been identified in siliciclastic deposits of the Kimmeridgian-Tithonian, with up to 14 % porosity (Garcia et al., 2010). Additional potential reservoir units have been identified in siliciclastic deposits of the Lower Cretaceous, as well as in Upper Cretaceous (Cenomanian) shallow-marine deposits and carbonate reefs, although porosity has not been quantified in these units (Dinis et al., 2008, in Pimentel and Pena dos Reis, 2016). The CC5 sub-units addressed in this study, as well as a significant part of the Middle Jurassic (mostly Bathonian-Callovian) units of the LB, are considered to represent the carbonate intervals with best potential reservoir facies in this basin.

II.2.4. Materials and methods

The main objective of this study is to address the CC5b to CC5e sub-units of the CC Formation as potential hydrocarbon reservoirs, as well as to evaluate the potential associated petroleum system elements, as previously mentioned. In order to achieve these objectives, outcrop data was interpreted and analysed in integration with data from two offshore wells in the proximity of Peniche, in addition to a nearby onshore well.

II.2.4.1. Data from outcrop

Outcrop observations were carried out along an approximately 4 Km sector of the western-to-southern margins of the Peniche peninsula exposing the sub-units of the CC5 Member (Figure II.2.3). Depositional facies were defined based on a semi-quantitative analysis of 107 thin sections (Figure II.2.4), which are described in more detail in Barata et al. (2021). A basic description of fractures, as important structural features affecting elements of the petroleum system, is here presented, in order to define the main sets and strike directions.

Figure II.2.3. Satellite map of the Peniche peninsula (Google, 2020) with indication of sub-units cropping out along the peninsula margin. The cliffs along green arrows 1 and 2 are shown in Figure II.2.5. Images of location 3 in the southern margin, corresponding to the base of the CC5e sub-unit, are shown in Figure II.2.6. Faults and fractures strike directions were registered along the Peniche peninsula margins, with fractures at locations 'a' to 'e' represented in Figure II.2.7. A major fault zone is marked by the orange line, two fracture sets are marked by green and blue lines; calcite-filled fracture sets are marked in yellow. The strike directions of these fracture sets are represented on the bottom-right diagram.

II.2.4.2. Subsurface data

Well reports, wireline logs and cuttings from the 17C-1 and 20B-1 offshore wells were analysed and re-interpreted. In addition, well reports from the onshore Cp-1 well were analysed and relevant information was integrated in the interpretations and discussion (see Figure II.2.1

for locations). A total of 63 thin sections from cuttings in both offshore wells were analysed (Figure II.2.4) and facies were described following elements in the classification schemes of Folk (1959, 1962) and Dunham (1962), using modifying terms as required (e.g Lokier and Junaibi, 2016). The resulting facies information was integrated in a stratigraphic correlation panel, including outcrop data. Because cuttings are transported from the drill-bit depth to the surface by the mudstream during drilling, there is some uncertainty as to the exact depth of origin, due to the time lag between the breaking of the rock and the reaching of the surface (e.g. Maher, 1964; Garcia-Hernandez et al., 2007; Naganawa et al., 2018). The mixing of rock cuttings from different depths in the mudstream is therefore a possibility. In spite of this, cuttings provide indispensable information on the lithology and facies of the subsurface sections, which are otherwise non-appraisable, given the absence of core samples.

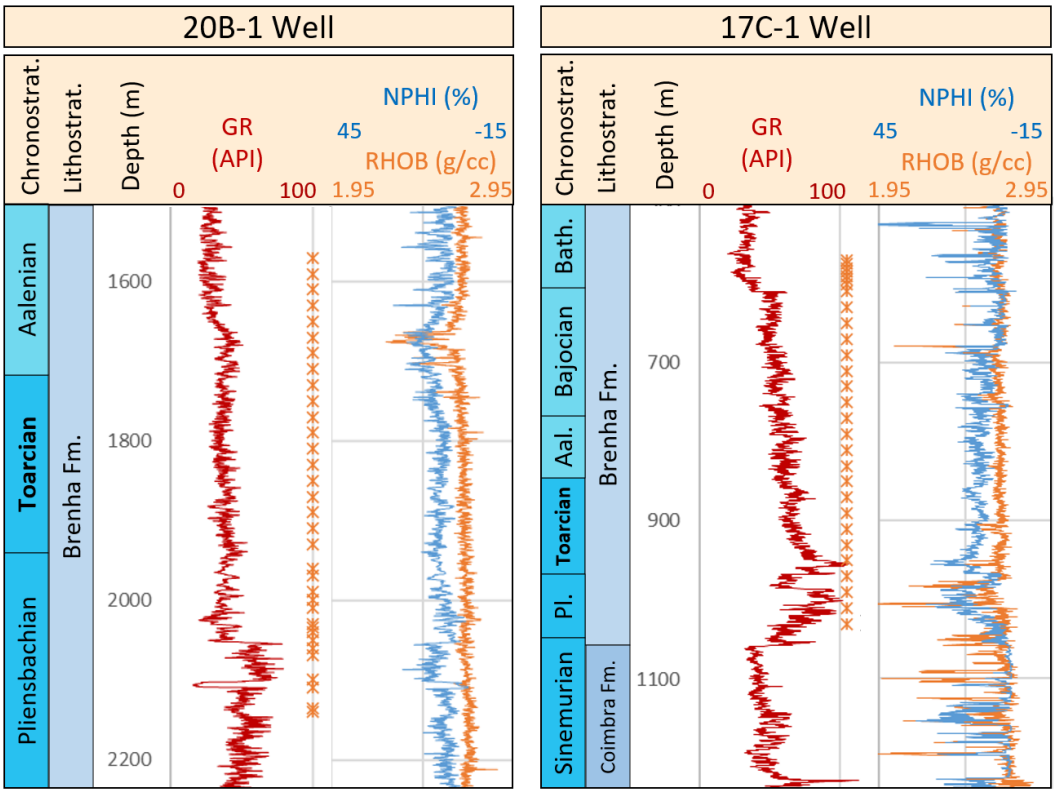

Figure II.2.4. Depth and stratigraphic location of analysed thin sections from cuttings (orange crosses), chronostratigraphy and lithostratigraphy, as indicated on well reports (ENMC/UPEP, 1976a, 1976b). Log data are also available from the same well reports. (GR = Gamma ray log; NPHI = Neutron porosity log; RHOB = Density log; Pl. = Pliensbachian; Aal. = Aalenian; Bath. = Bathonian).

II.2.4.3. Quantitative estimations

A semi-quantitative estimation of porosity through visual estimation was done on 41 samples from the CC5c to CC5e sub-units. Digital image analysis and pixel-counting was done on three selected control samples from the bottom, middle and top of the CC5d sub-unit, based on colour

selection of contiguous and non-contiguous areas using the different shades of colours representing micritic particles. The open-source *ImageJ* software was used for this procedure. Pixel counting through colour selection on the three selected samples is relatively straight forward, as the captured images contain no quartz grains. Samples which contain quartz grains will increase the complexity in digital image analysis due to the similarity between the colours in quartz grains and in different cement phases. Quantitative measurements through digital image analysis on samples containing quartz grains is not straight forward and considered to be unreliable. Visual estimation helps to avoid these limitations and provides comparable semi-quantitative results, although not as objective. In an effort to address uncertainty, different threshold levels for colour selection and pixel-counting were applied and an average value is calculated for the area occupied by calcite cement crystals.

II.2.5. Results

II.2.5.1. Outcrop observations

The CC5 Member interval showing good potential reservoir quality corresponds to the CC5b to CC5e sub-units and has a minimum thickness of 160 m, as previously mentioned. The outcrops of the CC5b to CC5e sub-units along the Peniche peninsula margins show marked structural features, relatively complex depositional geometries and are generally characterized by grainstones with ooids, skeletal grains, intraclasts and quartz grains. These sub-units are defined based on the occurrence of strong discontinuities, which can be followed laterally along the western and southern Peniche peninsula (Figure II.2.5), and on the observed facies variations and cyclicity throughout the succession (see Barata et al., 2021).

II.2.5.1.1. Depositional geometries and structures

Outcrops at Peniche are strongly degraded by the effects of weathering and karstification, in some cases preventing clear interpretations on features of sedimentary structures and depositional geometries. The development of fractures, including faults, in the area adds to the uncertainty in analysing structures and the continuity of the succession on outcrop. Internal sedimentary structures are not easily identifiable due to the strong effects of weathering, as mentioned above, although centimetric to decimetric planar stratification is regularly observed and small-scale cross-bedding is well defined at some locations (Figure II.2.6). Beds overlying major discontinuities generally show relatively stronger planar stratification, as well as higher volumes of quartz grains.

Figure II.2.5. Photos of the southern/southwestern margin outcrops of the Peniche peninsula along locations 1 and 2 in Figure II.2.3. **a**: Major discontinuities and large-scale moderate thickness variations of depositional bodies at the Nau dos Corvos/Lage dos Pargos locations; **b**: Marked bedding planes and strong thickness variations at the Ponta das Gaivotas/Furna que Sopra locations. Each coloured, dashed line represents a separate surface. Different surfaces at the top part of the cliff face are represented in red; where geometries are more complex, with the presence of cross-bedding and channel structures.

Figure II.2.6. Photos from outcrops to the E of Carreiro de Joannes, in the southern margin of the Peniche peninsula (location 3 in Figure II.2.3). Examples of cross-bedding in the CC5d sub-unit (b) and CC5e sub-unit (a and c). Yellow dashed lines indicate pseudo-horizontal bedding planes and red dashed lines represent oblique bedding planes and cross-bedding. Red vertical bars are approximately 20 cm.

At smaller observation scales (decimetre/metre), lateral thickness variations for most depositional packages are not clear and tabular geometries are perceived. The overall depositional architecture becomes clearer at larger observation scales (metre/decametre), with thickness variations, pinching-out and apparent wedge-like geometries (Figure II.2.5). However, the full extent of large-scale geometries is not appraisable, as these units are not exposed in their entirety. Beds are dipping with a low angle to the east/southeast (5º or less).

Channels with no clear internal structures are identified, showing high abundance of very coarse sand grade quartz grains and abrupt lateral facies transition into contacting geobodies, which are generally characterized by relatively finer grainstone facies and lower volumes of quartz grains.

II.2.5.1.2. Fractures

The Peniche outcrops show strong fracturation along different directions (Figure II.2.7). As important elements contributing to the possible creation of vertical fluid migration pathways, a qualitative analysis and basic observations have been done on the different sets of fractures (including faults). Two main sets of vertical fractures are identified in the Peniche peninsula outcrops (Figure II.2.7). One set has an approximate north-south strike direction (blue; ranging from N 10˚ E to N 20˚ W) and the other has an approximate northwest-southeast strike direction (green; ranging from N 50˚ W to N 70˚ W). The fractures in both sets are increasingly open towards the cliff-tops, due to the effects of weathering. These sets are oblique to almost perpendicular between them (30˚ to 80˚). A set of near-vertical fractures with different physical characteristics has also been identified (yellow, Figure II.2.3). They have an approximate northeast-southwest to east-west strike direction (N 75˚ E) and are calcite-filled. A fault zone with an approximate north-south strike direction and no apparent vertical throw is identified at the Lage dos Pargos location, extending in a northward direction and intersecting the peninsula margin at Miradouro dos Remédios (orange line in Figure II.2.3). The exposed cliffs at these locations are strongly deteriorated, preventing clear observations of this structural feature. Further studies would be required to properly characterize this fault zone.

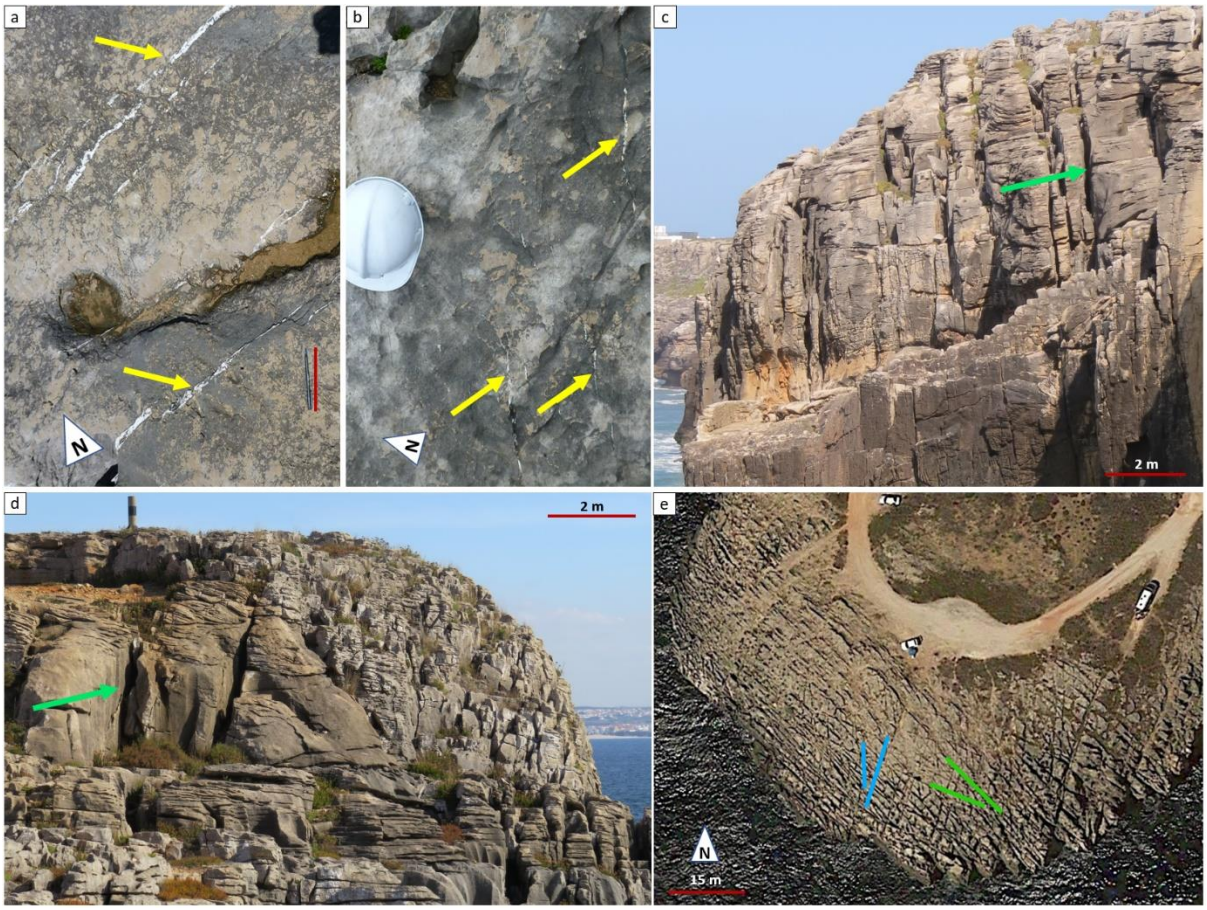

Figure II.2.7. **a** and **b**: Yellow arrows indicate set of cemented vertical fractures with an approximate northeast-southwest to east-west direction on a pseudo-horizontal erosion surface. Note red bar alongside pen, for scale in b; **c** and **d**: outcrop view of the N 50˚ W to N 70˚ W fracture set at the Poita Alta location (c) and Cova de Dominique location (d). Photo d shows how a channel-like structure seems to be less affected by fracturing (relatively darker facies indicated by green arrow in d). **e**: two main sets of vertical fractures with varying strike directions, just east of the Carreiro de Joannes location. A set of fractures with a roughly north-south direction (blue) and another set with a roughly northwest-southeast direction (green) are identified (satellite map from Google, 2020). Locations are marked on Figure II.2.3.

II.2.5.2. Offshore well data

Nearby wells 17C-1 and 20B-1 are the closest offshore wells to Peniche (Figure II.2.1). The analysis and re-interpretation of the stratigraphic framework in these wells, in integration with petrographic information, provided further insight on the lateral extension of the upper CC5 Member potential reservoir facies in the offshore area. Both wells were drilled in fault-related anticline structures (Figure II.2.8).

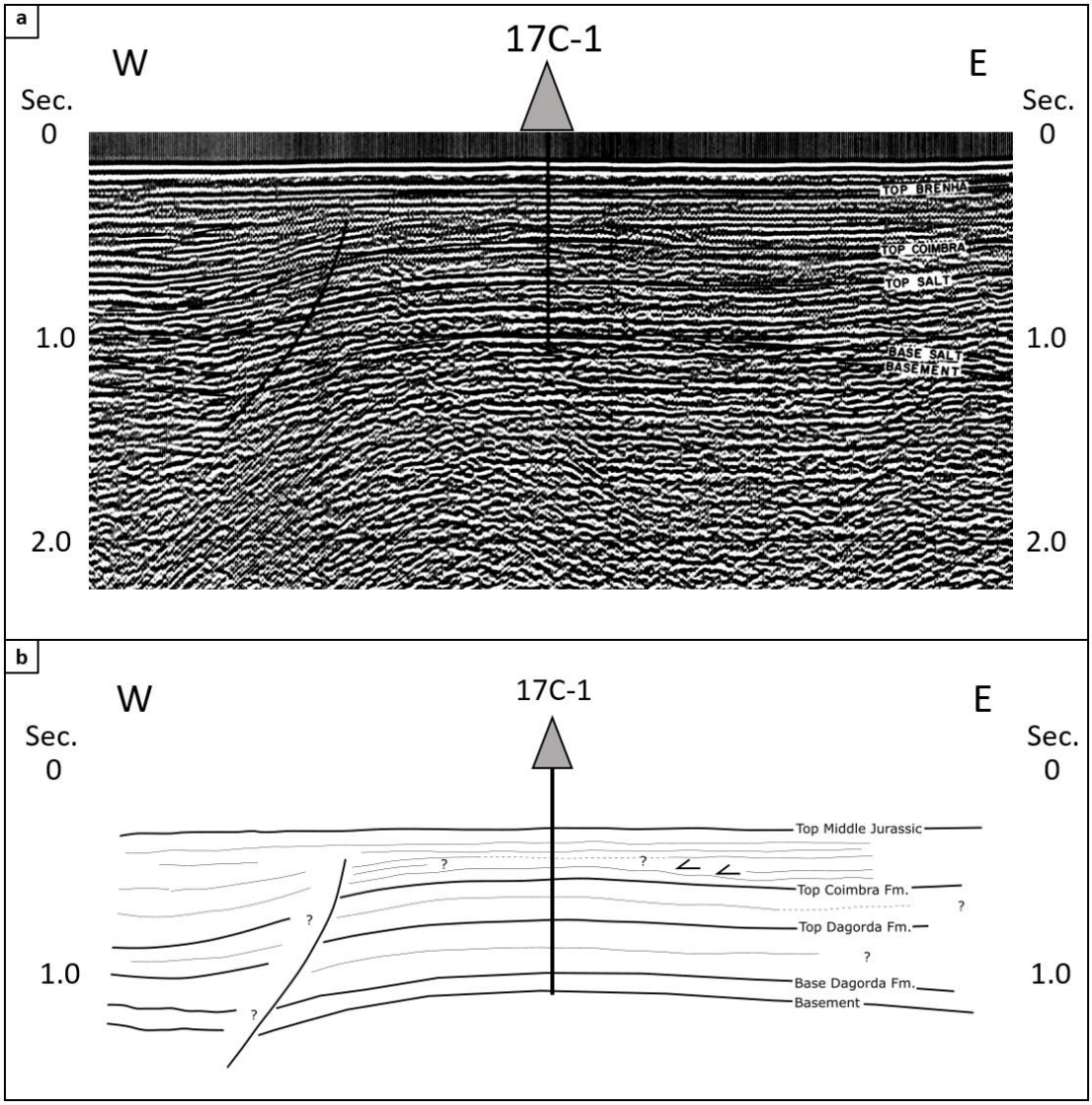

Figure II.2.8. **a**: Seismic cross-section across the gentle anticline structure targeted by well 17C-1, with indication of major stratigraphic levels. Top salt surface (Dagorda Formation), near top Hettangian; top Coimbra Formation surface, near top Sinemurian; top Brenha Group surface, close to the top of Middle Jurassic (ENMC/UPEP, 1976a); **b**: main surfaces picked on this seismic section (ENMC/UPEP, 1976a). Horizontal arrows indicate apparent onlap and thinning onto anticline structure, within the interval above the top of the Coimbra Formation. The structure targeted by the 20B-1 well is similar to the one here represented.

Well 20B-1 was drilled on the only identified fault-related anticline structure within its concession Block 20 and the adjacent Block 19 to the north, covering the area between this well and the Peniche location (ENMC/UPEP, 1976a, 1976b).

According to the well reports, no Upper Jurassic formations were intercepted in well 20B-1, which drills through Cretaceous sediments directly into Middle Jurassic Candeeiros Formation-like facies overlying Lower Jurassic deposits of the Brenha Group. No relevant porosity was found in the drilled Jurassic section. Well 17C-1 drilled through the complete Jurassic section, also finding very low porosities (between 1 and 7 %) and no hydrocarbon accumulations (ENMC/UPEP, 1976a, 1976b).

The stratigraphic framework for these two wells is defined in the corresponding well reports (Figure II.2.4), although a re-interpretation is presented in this study, as will be discussed in section II.2.6.2. The chronostratigraphic limits of late Sinemurian and Pliensbachian sections have been defined by Sêco et al. (2018) for well 17C-1, based on the correlation of GR log data and outcrop-measured GR. The basal Lower Jurassic lithostratigraphy applied to well 20B-1 follows the same terminology of Duarte and Soares (2002), and was defined based on well log correlation, using gamma ray (GR), density (RHOB) and neutron (NPHI) logs.

II.2.5.3. Petrography

II.2.5.3.1. Facies and petrographic features of outcrop rocks

The CC5b to CC5e sub-units are generally defined by coarse-grained limestone beds, with varying amounts of carbonate and siliciclastic material and abundant crinoid fragments in some levels. The depositional facies in the succession are mostly characterized by moderately to well sorted cemented grainstones containing intraclasts, ooids, skeletal grains and quartz grains (Figures II.2.9, II.2.10) with seemingly low heterogeneity. However, a more detailed sub-facies classification scheme has been developed, which allowed for an improved description and visualization of facies cyclicity, as well as of spatial variability in relative volumes of each constituent and grain sorting (Barata et al., 2021). Distinctly higher volumes of quartz grains are observed in channel structures, defining calcareous sandstone facies, and providing additional insight on the palaeoenvironmental conditions (Barata et al., 2021).

All analysed samples are fully cemented, showing two clearly distinguishable main carbonate cement phases. A calcite cement rim phase (bladed or fibrous) is observed in all samples (Figure II.2.9a), followed by microcrystalline, granular equant, blocky spar or drusy mosaic cement types in different samples (Figure II.2.9a, b, c). Syntaxial overgrowths are observed around echinoderm fragments. The original pore-space is fully occluded by the different calcite cement phases and no preserved porosity was identified in any of the samples. The effects of compaction are expressed to different extents by various features, such as long, concave-convex and sutured contacts, fracturing and displaced grain rims (Figure II.2.9c) or pressure dissolution along stylolites (Figure II.2.9d).

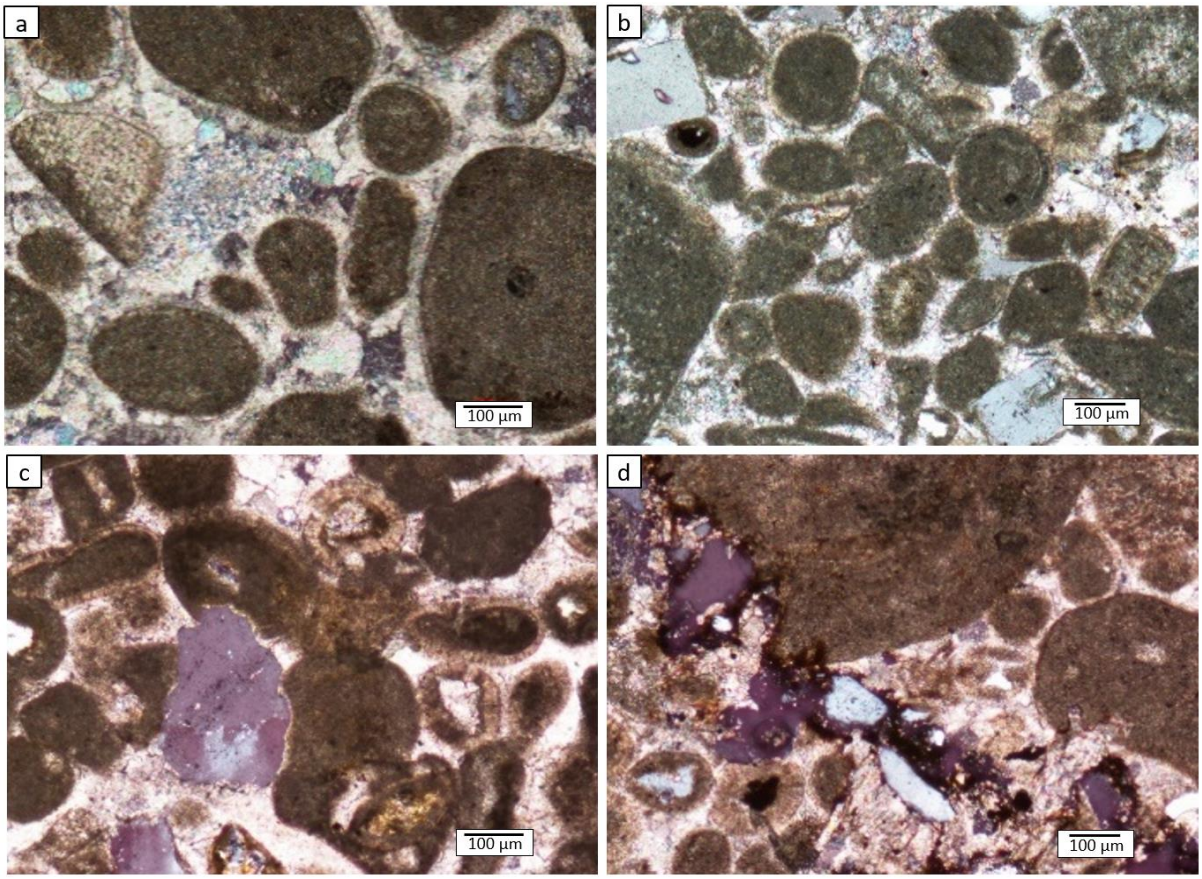

Figure II.2.9. Distinct compaction effects visualized on thin section under cross polarized light. **a**: Almost no contact between grains due to strong early circumgranular cementation. Circumgranular rim cement phase is clearly identifiable; interparticle calcite cement phase with xenotopic, poikilotopic inequigranular mosaic fabric fills interparticle space (middle part of CC5d sub-unit); **b**: Less extensive early cementation, grains are more closely-packed together, with point contact between grains (base of CC5d sub-unit); **c**: Strong compaction effects, with indentation and deformation of grains (top of the CC5c sub-unit); **d**: Stronger compaction effects, with development of stylolites through pressure solution (upper CC5c sub-unit).

The average estimated cement volume in the studied samples from the southern peninsula margin (CC5c to CC5e sub-units) is 31 %, varying between 5 % and 45 %, based on visual estimations. In selected control samples, cement areas as proxies for cement volumes were quantified through digital image analysis. Pixel counting through colour selection is associated with some uncertainty due to similarity in colour of different areas within particles and cement zones, as previously mentioned. Based on visual image inspection, tolerance levels of 50, 80, 110 and 130 were applied to colour selection of particle areas and a final average value for percentage of interparticle area was calculated based on the obtained results. The results are summarized in Table II.2.1.

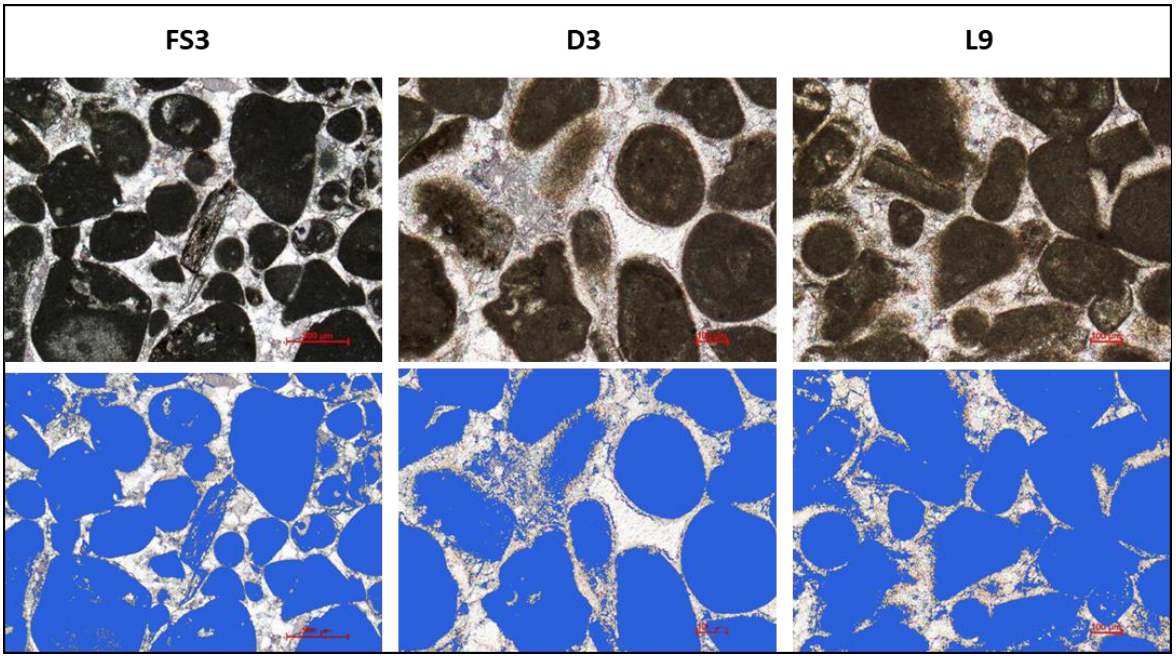

Figure II.2.10. Top row: original thin section images captured under cross polarized light. Bottom row: same images, after removing areas represented by shades of brown representing micritic particles, here represented in blue (threshold level = 80). Remaining area represents different phases of pore-filling calcite cements. FS3: base CC5d sub-unit; D3: middle CC5d sub-unit; L9: Top CC5d sub-unit.

Table II.2.1. Measured interparticle space using pixel-counting based on a range of different threshold levels for samples FS3, D3, and L9. Average percentage area is indicated for each sample.

	Interparticle space (%)		
Threshold level	**FS3**	**D3**	**L9**
50	38	43	35
80	32	32	26
110	25	27	18
130	21	22	16
Average (%)	**29**	**31**	**24**

II.2.5.3.2. Microfacies of subsurface samples

Petrographic analysis carried out on thin sections from cuttings from the 17C-1 and 20B-1 offshore wells allowed to identify the facies types, here described and summarized in the table below (Table II.2.2).

Facies type a (FTa): Laminated micritic mudstone. Overall micritic mudstone texture with very thin dark-coloured laminations. Scattered, unidentifiable, silt-sized (under 16 μm) skeletal grains and a few planktonic foraminifera are observed (Figures II.2.11a, II.2.12a).

Facies type b (FTb): Weakly laminated micritic mudstone. Lamination is not as clear as in FTa. Micritic mudstone texture, with relatively higher volume of unidentifiable, silt-sized skeletal grains than in FTa (coarser-sized also, at around 30 to 60 μm). Silt-grade coarse to sand-grade very fine quartz grains are observed (Figure II.2.11b).

Facies type c (FTc): Micritic mudstone. Mudstone texture with micritic matrix and scattered unidentifiable skeletal grains with variable size (silt-grade to sand-grade, up to around 100 μm). Calcite-filled fractures are observed. No clear sedimentary structures are identified (Figures II.2.11c, II.2.12b).

Facies type d (FTd): Micritic wackestone-packstone. Poorly to very poorly sorted quartz grains supported by a micritic matrix. No clear sedimentary structures are identified (Figures II.2.11d, II.2.12c).

Facies type e (FTe): Oo-intraclastic grainstone. Variable relative volumes of moderately sorted sand-grade fine to coarse-sized micritized intraclasts and radial ooids. Interparticle space is fully occluded by granular to blocky calcite cements with inequigranular xenotopic crystallization fabrics. These facies mostly show point-contact to no contact between micritized particles (Figures II.2.11e, II.2.12d, II.2.12e).

Facies type f (FTf): Calcareous sandstone. Abundance of poorly-rounded, poorly-sorted mostly fine (to medium) quartz grains. Contains a few identifiable micritic intraclasts and granular spar cement. No clear sedimentary structures are identified (Figure II.2.11f).

Samples from well 17C-1 are mostly micritic throughout the analysed interval, showing mudstone to wackestone textures (Figure II.2.11). The deepest analysed sample, at 1030 m, is shaley and thinly laminated (FTa, Figure II.2.11a) and is the only sample in the analysed set showing this type of facies. A few grainstone samples composed of ooids and micritized intraclasts, with interparticle space occluded by calcite cements (FTe, Figure II.2.11e), are observed at 830 m. The remaining samples are generally characterized by mudstone to wackestone facies with a micritic matrix supporting varying amounts of skeletal grains, intraclasts, peloids and quartz grains. In the interval between 790 and 690 m, a marked increase

in skeletal grains is observed. Samples with higher volumes of quartz grains are defined as calcareous sandstones (FTf, Figure II.2.11f).

Samples from well 20B-1 are also generally characterized by micritic mudstones to wackestones in the analysed interval, showing varying amounts of quartz grains, intraclasts and skeletal grains (Figure II.2.12). Thin sections at 2110 m and 1960 m contain fragments with ooids (FTe, Figure II.2.12e). At 1930 and 1970 m, cuttings showing grainstone facies with micritized intraclasts occur, where ooids are not clearly identifiable (FTe, Figure II.2.12d). From 1910 m upwards, the samples are mostly micritic, with mudstone to wackestone textures. At the depth of 1630, a fragment containing micritic intraclasts and showing grainstone facies (FTe) is observed. Cuttings characterized by grainstone facies are present in considerably lower quantities than the dominant rock-fragments with micritic mudstone-wackestone facies on each observed thin section.

The main facies types identified in the cuttings from both wells are presented in Appendix II.2.A (Tables II.2.3, II.2.4). The stratigraphic levels where oolitic and intraclastic grainstone facies with potential reservoir properties occur will be presented in section II.2.6.2.

Table II.2.2. Facies types defined based on interpretation of thin sections from cutting samples from the 17C-1 and 20B-1 wells.

Facies type	Facies and main features
FTa	Laminated micritic mudstone. Dark thin laminations, with scattered unidentifiable skeletal grains and a few planktonic foraminifera.
FTb	Weakly laminated micritic mudstone. Scattered unidentifiable skeletal grains and very fine sand-grade quartz grains.
FTc	Micritic mudstone. Micritic matrix with scattered unidentifiable skeletal grains.
FTd	Micritic wackestone-packstone with poorly sorted quartz grains.
FTe	Oo-intraclastic grainstone. Moderately sorted sand-grade fine to coarse-sized particles including radial ooids and calcite cement fully occluding interparticle space.
FTf	Calcareous sandstone. Poorly-rounded, poorly-sorted mostly fine (to medium) quartz grains, with a few micritic intraclasts and carbonate cement.

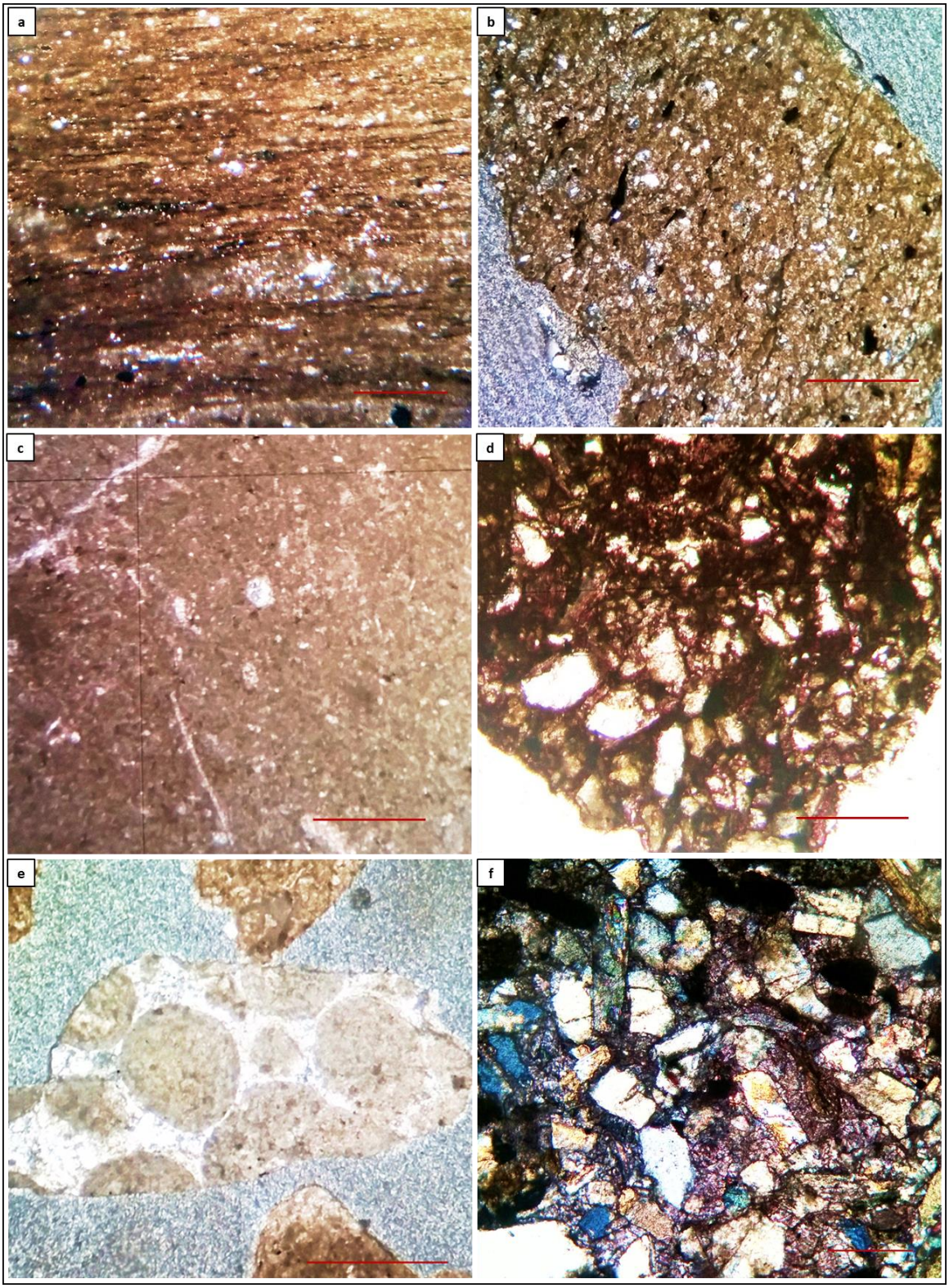

Figure II.2.11. Samples from the 17C-1 well, showing the recognized facies type. **a**: 1030 m. Laminated micritic mudstone (FTa); **b**: 950 m. Weakly laminated micritic mudstone (FTb); **c**: 930 m. Micritic mudstone (FTc); **d**: 990 m. Micritic wackestone-packstone with quartz (FTd); **e**: 830 m. Oo-intraclastic grainstone (FTe); **f**: 970 m. Calcareous sandstone (FTf). Red bars = 500 μm.

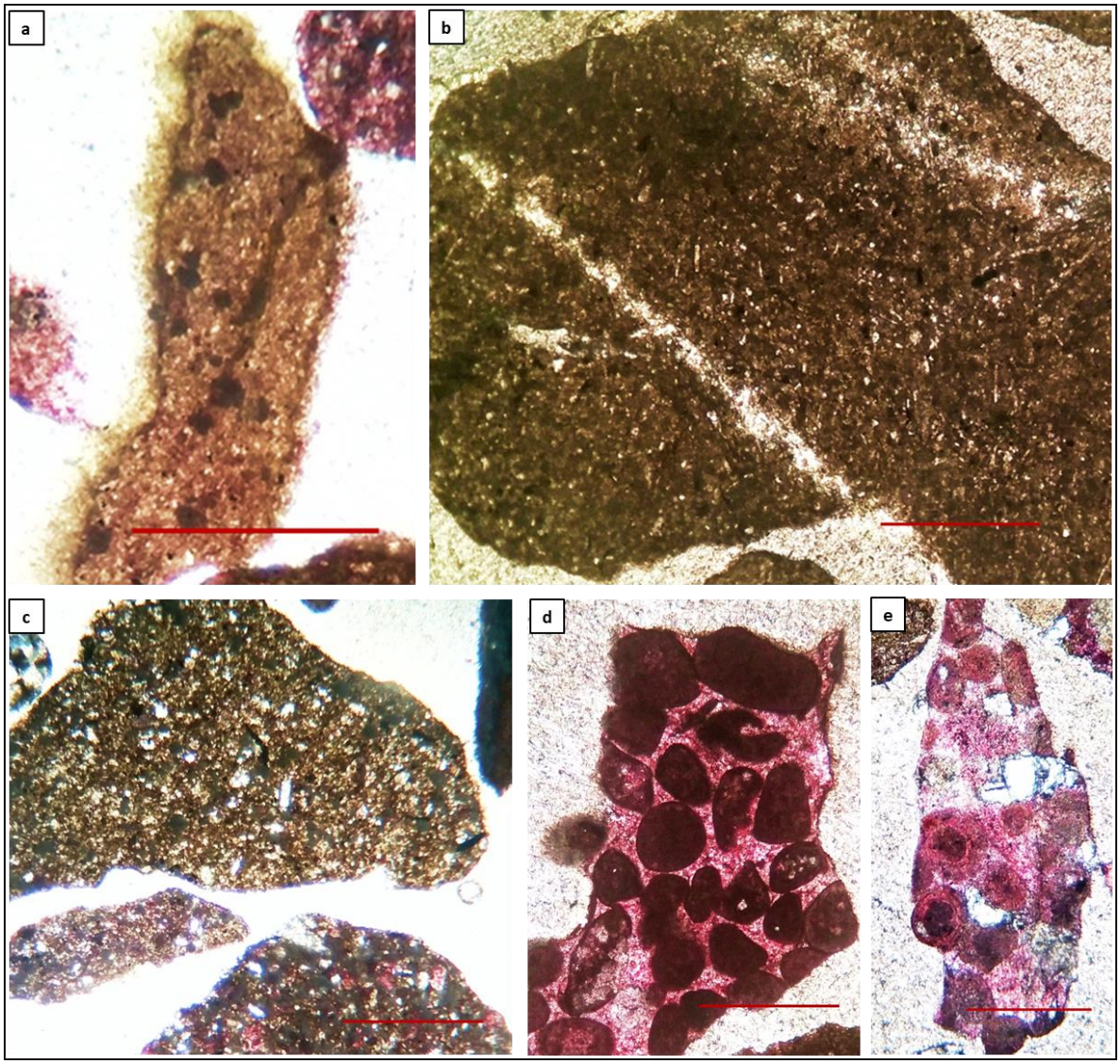

Figure II.2.12. Well 20B-1. **a**: 2030 m. Laminated micritic mudstone (FTa); **b**: 1910 m. Micritic mudstone (FTc); **c**: 2136 m. Micritic wackestone-packstone with quartz (FTd); **d** and **e**: 1930 m and 2110 m, respectively. Oo-intraclastic grainstone (FTe). Red bar = 500 μm.

II.2.6. Discussion

II.2.6.1. Potential reservoir properties and their degradation

As previously mentioned, the grainstone facies of the CC5b to CC5e sub-units cropping out in Peniche show good potential hydrocarbon reservoir properties. However, its petrophysical properties have been degraded through time, with the original porosity having been fully occluded by calcite cementation.

The circumgranular calcite cement phase observed in all samples, sometimes difficult to distinguish between a bladed or fibrous fabric, is indicative of precipitation in earlier diagenetic stages, during and soon after deposition. These earlier cement phases would have had an

important role in promoting the moderate preservation of some of the original rock porosity by strengthening the rock structure at a relatively early stage. However, subsequent phases of calcite cementation showing different types of fabrics have filled the remaining pore space throughout burial (see section II.2.5.3). In many cases, the contact between grains is seen to occur within these early calcite rims. In crinoid-rich levels, syntaxial overgrowths have an important role in the degradation of reservoir properties as well. This is of great relevance for this study, as very common beds with abundance of crinoids are identified in the CC5 sub-units, especially in CC5c. Compaction will have also had a strong impact in porosity degradation through the effects of overburden, amongst other associated factors. The effects of compaction are expressed to different extents, as previously mentioned, and are identifiable through different features, including sutured grain contacts or the development of stylolites through pressure dissolution, amongst others (Figure II.2.9). During uplift, in the Cenozoic, new phases of dissolution and consequent precipitation of calcite cements might have occurred, while the exposure of the rock to meteoric effects might have also led to additional alterations. The relative timing of precipitation of the different cement phases is uncertain and further studies would be required to clarify this.

The fractures observed on outcrop are important features, as they might create additional secondary porosity or enhance permeability, also leading to the development of vertical fluid flow paths. This would possibly promote vertical hydrocarbon migration, for as long as fractures remained open, before occlusion by the fracture-filling calcite observed in some cases on outcrop (Figure II.2.7). The different sets of fractures might represent a conjugate fracture system associated with the development of strike-slip vertical faults, which are interpreted to occur in this area, following the identification of a major fault zone showing no apparent vertical throw on outcrop. Another explanation would see the sets of fractures being created at different times, resulting from the rock being subjected to unrelated tension forces acting in different directions (e.g. Billings, 1946).

Considering the hypothetical scenario where occlusion of pore space by burial diagenesis had not occurred, the grainstones of the CC5b to CC5e sub-units, or hypothetical analogous coeval subsurface grainstones units, are considered to show potential moderate porosity. The average estimated volume of interparticle cement in the analysed samples is 31 %. This can be seen as an approximate indication of the hypothetical preserved porosity in these units at different subsurface locations, had a different diagenetic history occurred or hydrocarbon charge of the pore space taken place. It will not, however, be an exact representation due to uncertainties related to the effects of differential diagenesis and compaction throughout burial, amongst other factors, which are difficult to predict. These grainstone facies show moderate resemblance to oolitic facies of world-class hydrocarbon reservoirs (Figure II.2.13), such as the grainstone facies of the Khuff Formation (see Figure 9 in Ehrenberg et al., 2007), upper Arab D Member (see Figure 6 in Hollis et al., 2017) or the Upper Kharaib Member in the Middle East (e.g.

Alsharhan and Nairn, 1997; Van Buchem et al., 2002; Strohmenger et al., 2006; Ehrenberg et al., 2007; Alsharhan, 2014; Eltom et al., 2019), showing petrographic features that could have, therefore, hypothetically promoted its behaviour as a hydrocarbon reservoir.

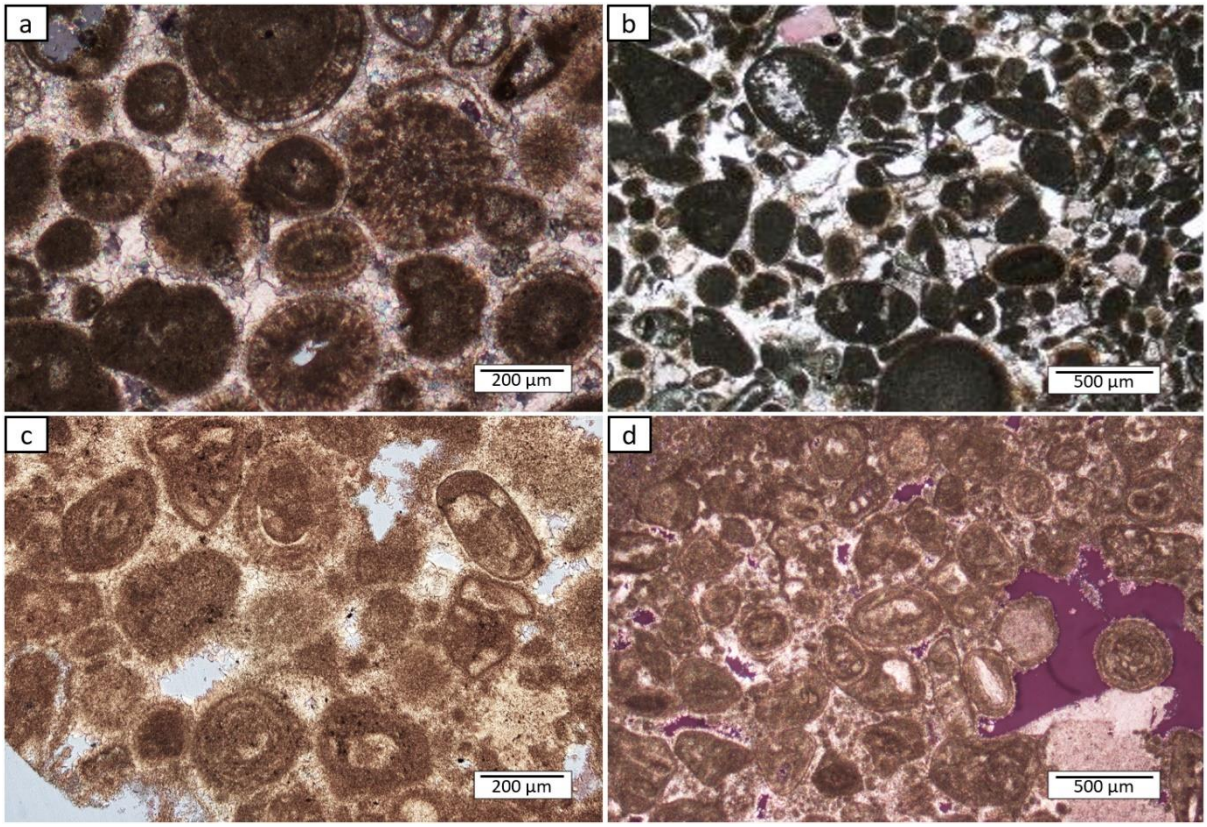

Figure II.2.13. Comparison between grainstone facies of the CC5 sub-units and Upper Kharaib Formation, in the U.A.E. **a**, **b**: Intraclastic-oolitic facies in samples of the CC5 Member, with calcite cements fully occluding the pore space. **c**, **d**: Intraclastic-oolitic facies of the Lower Cretaceous Upper Kharaib Formation, U.A.E, showing moderate porosity.

II.2.6.2. Outcrop to subsurface correlation

II.2.6.2.1. Facies variability

The quartz-oolitic-intraclastic grainstone facies of the CC5b to CC5e sub-units, together with the absence of fine-sized carbonate particles or carbonate mud, are an indication of high-energy conditions of deposition. The defined sub-facies scheme for the CC5 sub-units reveals relative spatial variability, which is driven by the dynamics and architecture of deposition, occurring through interfingering or gradation, but also driven by the creation of pinching-out geometries (Barata et al., 2021). In outcrops of the onshore LB areas to the north and northeast of Peniche, the stratigraphic intervals coeval to the CC5 Member are characterized by a succession dominated by marls and marly limestones, defining the hemipelagic deposits of the S. Gião and Póvoa da Lomba formations, in contrast to the high-energy deposits of the CC5 Member.

Further towards the east, in the Tomar region, relatively shallower-water carbonate deposits are identified, indicating a closer proximity to the eastern limit of the basin and to the continental margin (e.g. Duarte, 1997; Duarte and Soares, 2002; Duarte et al., 2004). High-energy facies similar to those observed at the Peniche outcrops have been identified in the subsurface, in the form of oolitic-intraclastic grainstones in the Toarcian interval of the onshore Cp-1 well, approximately 25 Km to the southeast of Peniche, based on the information from the well report (ENMC/UPEP, 1981) and on the observations of well samples reported by Wright and Wilson (1984). These authors have reported the presence of oolitic-intraclastic-peloidal grainstones in cutting samples from this well, mixed with mudstones containing skeletal grains, suggesting that the sediments in this area could have been deposited in a submarine fan setting, as is the case for the older members of the CC Formation in Peniche (Wright and Wilson, 1984). However, the genetic relationship of the successions at both these locations is, considered to remain an uncertainty and the grainstone facies in Cp-1 might be a result of deposition in shallow-water settings (for more details see Barata et al., 2021).

In the nearby 17C-1 and 20B-1 offshore wells, north and south of Peniche, respectively, the observed oo-intraclastic grainstone facies type FTe (see Table II.2.2) is similar to the high-energy facies type FT3 of Barata et al. (2021) (oo-intraclastic grainstone with quartz extraclasts) characterizing the Peniche outcrops. However, facies type FTe is observed in very limited intervals in these wells and is only identified in cuttings originating from certain stratigraphic levels (Figure II.2.14; see also section II.2.5.3.2). The majority of the interpreted Toarcian interval in both wells is generally characterized by micritic wackestone facies, with low to moderate presence of siliciclastic material.

The grainstone interval of the CC5 Member has an estimated minimum thickness of 160 m on outcrop. In the 17C-1 well, cuttings with grainstone facies are observed at a depth of 830 m, in between cutting samples composed of micritic mudstone-wackestone facies, from depths of 810 and 850 m. An exact thickness for a probable grainstone layer within this interval is therefore unknown, but it is interpreted to be considerably lower than 40 m, considering the much lower number of cuttings characterized by grainstone facies, compared to those defined by micritic wackestone facies. In the 20B-1 well, an oo-intraclastic grainstone interval with a thickness of approximately 5 to 7 m occurs at the depth of 2103 m, based on the observation of cutting samples, well report information and on log data. Samples with intraclastic grainstone facies and lower volume of ooids are observed between the depths of 1930 and 1970 m and at the depth of 1630 m, between micritic wackestone samples at depths of 1610 and 1650 m. These are associated with a much higher number of cuttings with micritic mudstone-wackestone facies. The thickness for eventual grainstone layers occurring within these intervals will therefore be less than 40 m as well, but is difficult to estimate, as thin section samples are not continuous. However, given the much higher percentage of fragments characterized by micritic wackestone facies, no thick layers are considered to occur and only thin streaks are

expected at the well locations. The lateral transition between the high energy grainstone facies observed on the Peniche outcrops and the generally micritic facies of the coeval intervals in the analysed wells is interpreted to be driven by pinching-out geometries over moderate distances, relating to the depositional architecture of the interpreted infralittoral prograding wedge setting (Barata et al., 2021), probably combined with interfingering or gradation between the different facies.

II.2.6.2.2. Stratigraphic correlation

The interpretations based on well log correlation show considerable thickness variations between the analysed locations. The interval including the Água de Madeiros, Vale das Fontes and Lemede formations in 17C-1 well is considerably thinner than the coeval interval towards the S, varying from 89 m in 17C-1 (Sêco et al., 2018) to 344 m in 20B-1. In this southernmost well, the Vale das Fontes Formation is marked by the occurrence of a grainstone interval of 5 m, at the depth of 2103 m, as mentioned above. In 17C-1, the deepest analysed sample, at 1030 m, is shaley and thinly laminated (FTa) in similarity to the facies typically observed in outcrops of the Vale das Fontes Formation (Duarte and Soares, 2002). The thickness variation for the interval equivalent to the São Gião Formation is not as expressive but is still high. It varies between approximately 130 m in well 17C-1 and around 320 m in well 20B-1, as compared to the minimum 319 m thickness estimated from Peniche outcrop measurements, although uncertainty remains regarding the age of the youngest sub-units of the CC Formation. The possibility exists that the youngest sub-units of CC5 Member (part of CC5d and CC5e) are of Aalenian age (Barata et al., 2021), as also hypothesized by some authors (e.g. Mouterde et al., 1979; Duarte, 1997; Andrade, 2006). If the top interval is indeed of Aalenian age, the CC Formation interval equivalent to the São Gião Formation would be at least 45 m thinner than the defined total CC Fm. thickness (Barata et al., 2021). Even though there is some uncertainty associated with the chronostratigraphic and lithostratigraphic interpretations, which translate into the thickness variations observed, these are clearly higher at the 20B-1 well location, towards the south. To the north of well 17C-1, the Lower Jurassic succession is also reported to increase in thickness (e.g. Wilson, 1975; Rasmussen et al., 1998; Sêco et al., 2018), with a depocenter being developed during the Sinemurian/Pliensbachian in the offshore area between the Nazaré and Figueira da Foz locations (e.g. Duarte et al., 2010; Sêco et al., 2018), where the Água de Madeiros, Vale das Fontes and Lemede formations interval reaches a thickness of 247 m in the 14A-1 well, offshore Figueira da Foz, (e.g. Sêco et al., 2018; see Figure II.2.1 for location). These observed regional thickness variations between the 20B-1, 17C-1 and 14A-1 well locations are a probable indication of considerable tectonic and structural influence on sedimentation in the region, in addition to the effects of relative sea-level changes and to the constraints associated with the ramp model of deposition itself.

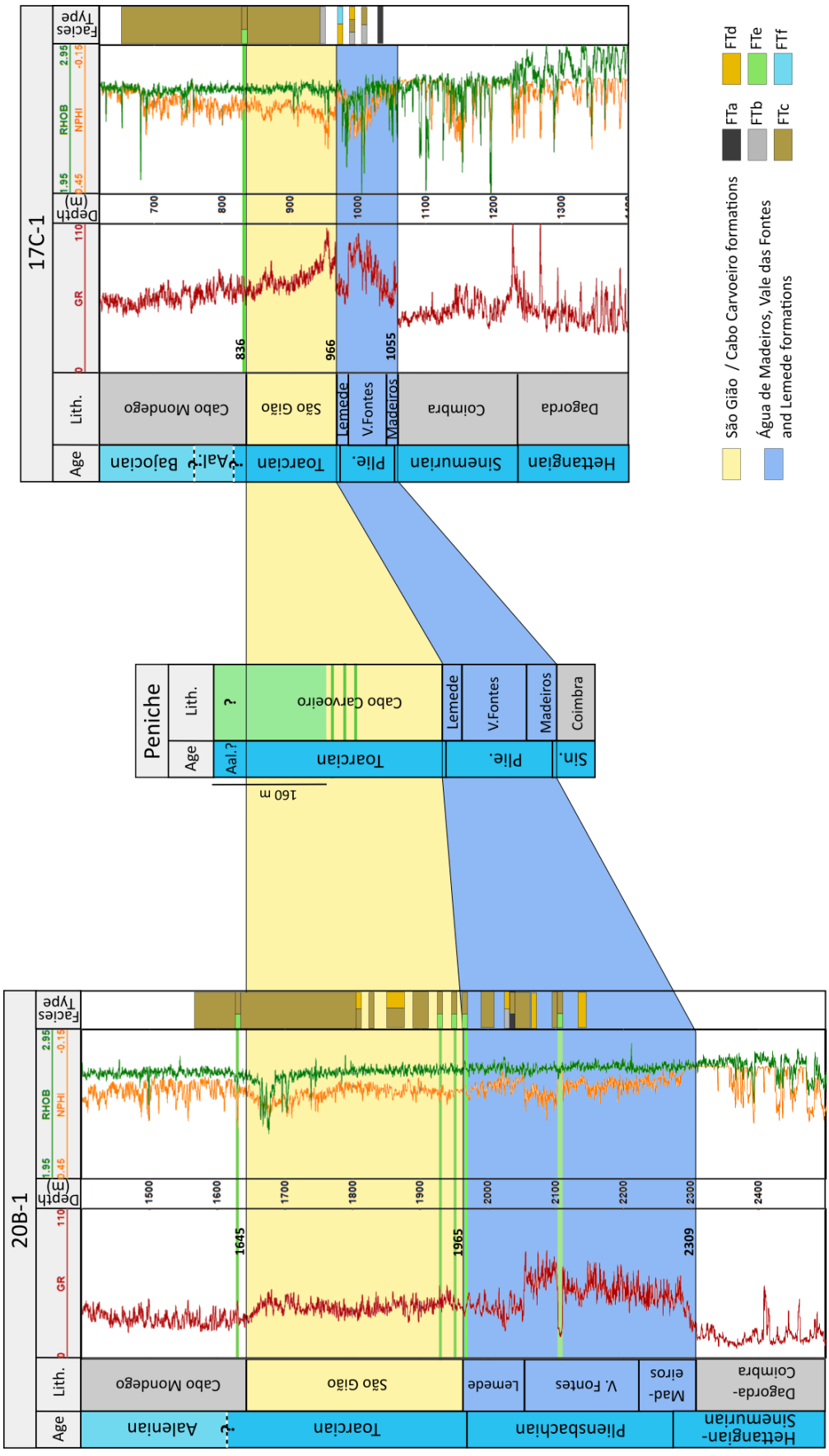
17C-1
20B-1
Peniche
Age
Lith.
Facies Type
Depth (m)
GR
RHOB
NPHI
Hettangian
Sinemurian
Coimbra
Dagorda
Pliensbachian
Toarcian
Aalenian
Bajocian
Cabo Mondego
São Gião
Cabo Carvoeiro
Lemede
V.Fontes
Madeiros
Plie.
Sin.
Aal.?
160 m
836
966
1055
1645
1965
2309
São Gião / Cabo Carvoeiro formations
Água de Madeiros, Vale das Fontes and Lemede formations
FTa
FTb
FTc
FTd
FTe
FTf

Figure II.2.14. Outcrop to subsurface correlation panel flattened to the top of São Gião Formation. Well log data and chronostratigraphy are interpreted based on the data from well reports ENMC/UPEP (1976a, 1976b). Lithostratigraphic nomenclature is based on Duarte and Soares (2002) and Azerêdo et al. (2003), the 17C-1 Sinemurian/Pliensbachian sub-divisions are from Sêco et al. (2018). The lithostratigraphic sub-divisions of the Pliensbachian in 20B-1 interpreted in this work are based on well logs correlation. Madeiros = Água de Madeiros Formation; V. Fontes = Vale das Fontes Formation; Sin. = Sinemurian; Plie. = Pliensbachian; Aal. = Aalenian; Lith. = Lithostratigraphy. See Figure II.2.1 for locations.

II.2.6.3. Tectonic and palaeotopographic controls on sedimentation

As mentioned above, sin-depositional tectonic, structural activity and associated halokinesis are interpreted to affect regional thickness and facies variations through the continued influence on accommodation space variability and on depositional settings. In addition, basin compartmentalization occurs during the Mesozoic, through the development of sub-basins, more expressive in some areas to the east-southeast of Peniche (Figure II.2.15), as well as to the north (e.g. Montenat et al., 1988; Wilson et al., 1989; Rasmussen et al., 1998; Alves et al., 2002, 2006; Kullberg et al., 2013). In the Peniche Basin, located immediately to the west/northwest of the Berlengas archipelago, such localized depression or sub-basins are also reported to influence deposition during the Mesozoic (e.g. Alves et al., 2006; Walker et al., 2021). Although this compartmentalization might still be weak during the earlymost Early Jurassic, deposition and sediment distribution would have still been affected by fault activity and the ongoing development of a sea-floor topography (e.g. Wilson et al., 1989; Rasmussen et al., 1998; Alves et al., 2002, 2006). Indications of thickness variability during the Early Jurassic are visible on the seismic section across the 17C-1 location, where the stratigraphic interval between the tops of the Coimbra Formation and of the Middle Jurassic, corresponding to the seismic sequence J20 (equivalent to the J2 megasequence) of Alves et al. (2002), seems to show onlap and thinning onto the anticline structure (Figure II.2.8). This same J2 unit is reported to show thickness variations and growth onto faults associated with graben/half-graben structures, both in the LB and the Peniche Basin (Alves et al., 2002, 2006).

The thickness of the intervals of interest is increasing to the north and to the south of the 17C-1 well location, as mentioned above, which is located close to the Nazaré transfer fault zone, implying an increase in accommodation space towards these areas. This southwest-northeast oriented major transfer fault is active through the Mesozoic-Cenozoic and is delimiting sectors of the LB with distinct structural evolutions and sedimentary patterns (e.g. Rocha and Soares, 1984; Wilson, 1975; Wilson et al., 1989; Rasmussen et al., 1998; Alves et al., 2006). During the Early Jurassic, stronger tectonic activity is reported to the south of this fault zone, as compared to the northern regions (e.g. Wilson et al., 1989; Rasmussen et al., 1998; Alves et al., 2002). This ongoing tectonic activity leads to regional variability in depositional conditions

and to differential subsidence rates across the region and, in addition to the effects of eustasy, is an important factor influencing sedimentation in the basin (e.g. Vanney and Mougenot, 1981; Wilson et al., 1989; Rasmussen et al., 1998; Alves et al., 2002, 2006).

The Toarcian-Aalenian(?) grainstone succession of the CC5c to CC5e sub-units in Peniche is seen as resulting from localized, line-source sedimentation closely related to the uplift of the Berlengas basement block (Barata et al., 2021). The effects of uplift are interpreted to be stronger in the area closer to the Nazaré transfer fault and in the vicinity of Peniche, as reflected by the increasing thickness of the Pliensbachian-Toarcian interval from the 17C-1 well location towards the location of 20B-1 well to the south, in response to the associated increase in accommodation space. The exposure and erosion of the Berlengas basement block would have been, in this case, stronger in the area closer to this transfer fault, resulting in the deposition of the eroded sediments in geographically localized fans and infralittoral prograding wedges in and around the Peniche area (e.g. Wright and Wilson, 1984; Barata et al., 2021).

As previously mentioned, the high energy facies deposited in these infralittoral prograding wedges are interpreted to transition laterally into the predominantly micritic wackestone facies observed in the coeval intervals of the 17C-1 and 20B-1 wells through probable interfingering or gradation, also being affected by the development of pinching-out geometries (Figure II.2.15). This interpretation assumes no compartmentalization and the absence of strong structural features between these locations at the time of deposition in the area, which could have led to abrupt breaks on depositional trends and sediment distribution. It takes into consideration an underlying control by gentle sea-floor topography, as well as the larger-scale tectonics and accommodation space variability. Additional data would, however, be required to confirm this hypothesis. Based on the above-discussed, the CC Formation infralittoral prograding wedges are interpreted to not extend beyond the areas surrounding the 20B-1 and 17C-1 wells, approximately 40-45 km to the south and 15-20 km to the north, respectively (Figure II.2.15).

The observed facies association and interpreted depositional settings at Peniche might be replicated in the western flank of the uplifted Berlengas basement block, within the Peniche Basin domain, where depositional features and structures comparable to the Peniche case might potentially occur. One of the main differences between the Lusitanian and Peniche basins during the Early Jurassic is the thickness of the seismic units, given the deeper settings of the Peniche Basin, as reflected in the reported 5 km of syn-rift subsidence during the Late Triassic-Early Jurassic extensional phase, contrasting with the registered 1 km for the LB (Walker et al., 2021).

In addition to influencing sedimentation in the region, the combined tectonic and associated halokinetic activity has led to the development of complex structural configurations in the

subsurface, having also had an important role in the hydrocarbon migration and entrapment history in the LB, as will be discussed in section II.2.6.4.

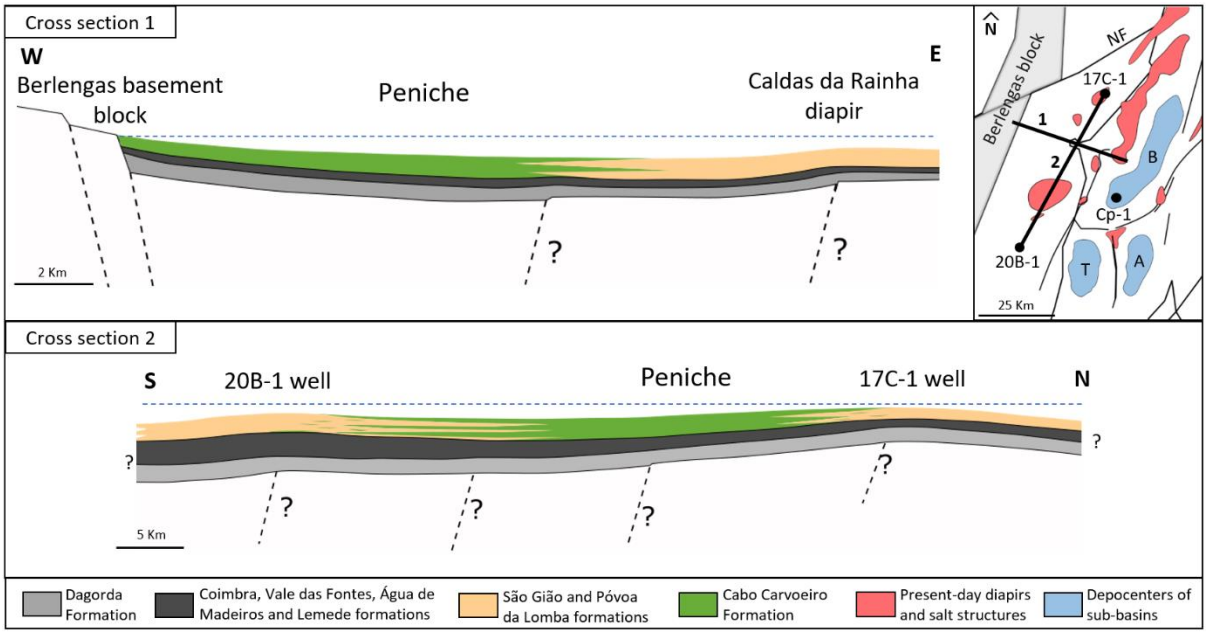

Figure II.2.15. Interpreted simplified cross-sections for lines 1 and 2 on insert map, at Toarcian time. Vertical scale is exaggerated approximately 3x for cross section 1 and 10x for cross section 2, as to facilitate perception of potential gentle topographic variations on sea floor caused by tectonics and halokinesis. Dashed horizontal blue line represents approximate relative sea level. Dashed black lines represent simplified representation of possible major fault zones. Based on elements from ENMC/UPEP (1976a, 1976b), Rasmussen et al. (1998), Alves et al. (2002). Insert map is a simplified structural map of the LB in the Peniche area. Intersection of lines 1 and 2 marks the Peniche location. NF: Nazaré fault; B: Bombarral-Alcobaça sub-basin; T: Turcifal sub-basin; A: Arruda sub-basin. Based on elements from Vanney and Mougenot (1981), Wilson et al. (1989), Leinfelder and Wilson (1998), Rasmussen et al. (1998) and Alves et al. (2002, 2006).

II.2.6.4. Petroleum system elements and hydrocarbon exploration potential

In order to provide a better understanding of the hypothetical Lower Jurassic petroleum system identified in this Peniche case study, in addition to the presence and quality of the CC Formation potential reservoir, the Sinemurian-Pliensbachian source rocks, migration pathways, sealing units and trapping mechanism elements are here addressed. The interpreted relative timing of the petroleum system events is also presented, in order to help further define the main uncertainties relating to this system.

II.2.6.4.1. Source rock maturation and hydrocarbon migration

The Early Jurassic source rocks have reached maturity and have generated and expelled hydrocarbons in the LB, as indicated by oil and gas shows that have been recorded in different

Jurassic intervals of different wells (e.g. Brito et al., 2017; Figure II.2.16). These source rocks of the Sinemurian/Pliensbachian (Coimbra, Água de Madeiros and Vale das Fontes formations) are generally of good quality (e.g., Oliveira et al., 2006; Duarte et al., 2010, 2012, 2013; Silva et al., 2012; Poças Ribeiro et al., 2013; Brito et al., 2017), although this quality will vary regionally in accordance with the variability in paleoenvironmental and bottom-water conditions of the LB at this time (e.g. Duarte et al., 2010; Silva and Duarte, 2005; Ferreira et al., 2020). The confirmed presence of this source rock interval in the LB is fundamental in the definition of this potential Lower Jurassic petroleum system. Although outcrop samples of Lower Jurassic source rocks show levels of immaturity (e.g. Oliveira et al., 2006; Duarte et al., 2012; Poças Ribeiro et al., 2013), different published burial models show maturity was reached in the subsurface, with source rocks entering the oil generation window during the Late Jurassic to Early Cretaceous (e.g. Uphoff, 2005; Cardoso et al., 2014), and possibly entering the gas generation window within localized depocenters of the Lusitanian and Peniche basins at a later time (Cardoso et al., 2014), although these models are associated with some uncertainty. The subsidence and thickness differences between the Lusitanian and Peniche basins reported by Walker et al. (2021) could hypothetically indicate the presence of thicker source rock, as well as reservoir intervals, in the Peniche Basin, although this can only be confirmed by drilling a well in the area.

Geochemical correlation of migrated oil and source rock extracts by Brito et al. (2017) has identified the presence of oil in the Sinemurian/Pliensbachian Água de Madeiros Formation originating from the Sinemurian Coimbra Formation, indicating its effectiveness in generating and expelling hydrocarbons. In the Moreia-1 and 14A-1 wells, penetrating Jurassic units offshore Figueira da Foz (see Figure II.2.1 for locations), oil shows were reported at various stratigraphic levels throughout the Jurassic (Figure II.2.16). As previously mentioned, migrated bitumen has also been identified in Middle and Upper Jurassic units of outcrop and subsurface samples to the southeast of Peniche (Gonçalves et al., 2014; Azerêdo, 2015), confirming the presence of effective migration pathways. The high number of faults identified on seismic in the region (e.g. Rasmussen et al., 1998; Alves et al., 2002), and the abundance of smaller-scale fractures, as observed on the CC Formation Peniche outcrop, might be an important contribution to vertical hydrocarbon migration, in addition to the potential lateral migration through carrier beds. The timing of calcite precipitation in open fractures could perhaps also be addressed in future studies, to understand if the different fracture sets were open or closed during the time of hydrocarbon migration, as they would have behaved as vertical fluid conduits, promoting hydrocarbon migration into shallower strata and to the surface. Considering the above-mentioned, it would be acceptable to propose that hydrocarbons originating in the Lower Jurassic source rocks could have migrated through, and hypothetically charged, potential reservoir units of Toarcian age in locations of the LB that are analogous to

the Peniche case, which might be characterized by depositional facies similar to the grainstones of the CC5 sub-units.

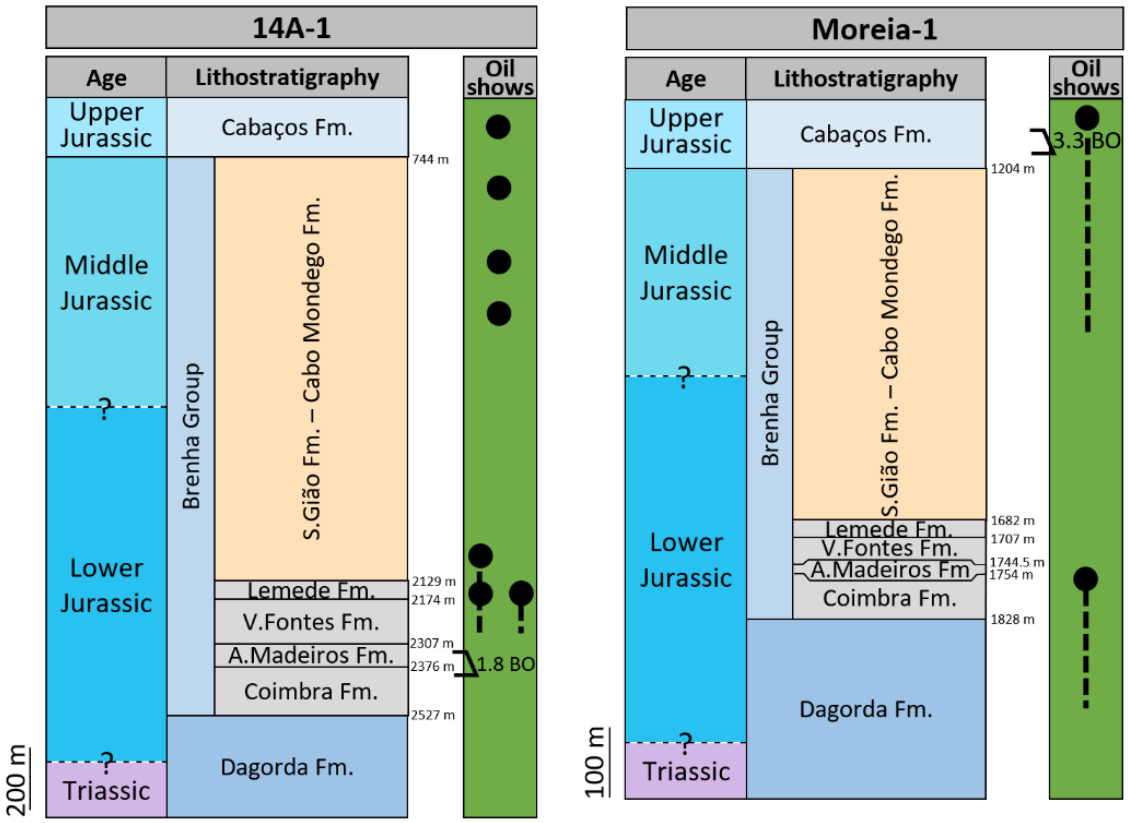

Figure II.2.16. Examples of two offshore wells with oil shows. Left: 14A-1 well with indication of oil and gas shows (black circles) throughout the Jurassic and oil recovery from drillstem test made in the Lower Jurassic (1.8 BO recovered). This well was drilled on interpreted thrust fault trap offshore Figueira da Foz (ENMC/UPEP, 2018). Right: Moreia-1 well with oil and gas shows in the Lower Jurassic (black circles) and oil recovery from drillstem test made in the Upper Jurassic (3.3 BO recovered). The well was drilled on an anticline offshore Figueira da Foz (ENMC/UPEP, 2018). A.Madeiros Fm. = Água de Madeiros Formation; V.Fontes Fm. = Vale das Fontes Formation; S.Gião Fm. = São Gião Formation. The lithostratigraphy sub-divisions here shown are based on Sêco et al. (2018) for the Lower Jurassic and on correlation with the interpretations of the 17C-1 and 20B-1 wells, based on the nomenclature in Azerêdo et al. (2003). The chrono- and lithostratigraphic limits within the uppermost Lower Jurassic and Middle Jurassic are uncertain. Depths of formations tops are indicated in metres.

II.2.6.4.2. Potential seals and trapping mechanisms

At Peniche, the section immediately overlying the CC5 grainstones is not observable on outcrop. As such, an appraisal of the possible presence of a sealing unit and its effectiveness is not possible. However, data from the Cp-1 well report (see Figure II.2.1 for location) indicates the presence of an interval of dark-coloured marly limestones which directly overlie the section considered to be the lateral equivalent of the oolitic units of the CC5 Member (ENMC/UPEP,

1981; Wright and Wilson, 1984). This marly interval, at the depths of between 2900 and 2950 m, is approximately 30 to 35 m thick and marks a moderate increase on the GR log, as well as a gentle to moderate increase on the acoustic log (ENMC/UPEP, 1981). This marked transition between two distinct depositional facies seems to be replicated in well 20B-1 at the depths of 1660 to 1700 m (ENMC/UPEP, 1976b) and could indicate a potential contrast in petrophysical properties between both units, which would suggest a potentially sealing behaviour of the overlying unit. Additional petrophysical data and further studies would be required to confirm this hypothesis. However, close to the top of this marly unit in Cp-1, gas accumulations are reported in large vugs (ENMC/UPEP, 1981), providing additional indications of a potential sealing behaviour of the encasing rock fabric. Such a stratigraphic configuration could hypothetically be replicated in coeval intervals of other sub-basins of the LB, with analogous depositional settings.

The complex structural history of the LB, with the development of tilted blocks, strong faulting and folding, has led to the creation of a large number of potential structural hydrocarbon traps in the LB and Peniche Basin (e.g. Rasmussen et al., 1998; Alves et al., 2002, 2003b, 2006; Uphoff, 2005). Potential trapping mechanisms created through combined vertical salt movement and faulting resulted in the anticline structures which have been regularly targeted in the LB, as is the case with the structures at the 17C-1 and 20B-1 well locations (Figure II.2.8), where no relevant hydrocarbon accumulations were reported. The truncation of reservoir units against fault planes is an additional trapping mechanism that might occur, in cases where the fault plane achieves sealing conditions (e.g. Biddle and Wielchowsky, 1994). Almost all wells in the LB have targeted structural traps, with no significant hydrocarbon accumulations having been found (ENMC/UPEP, 2016). The occurrence of moderate to abundant open faults and fractures, as observed at Peniche, or the absence of efficient seals, might be the main factors preventing potential hydrocarbon accumulations in these targeted anticline structures.

The mobilization of the Dagorda Formation salt in wrench zones has created complex structural episodes such as the formation of diapirs piercing the surface in some locations (e.g. Montenat et al., 1988; Wilson et al., 1989; Davison and Barreto, 2020; Walker et al., 2021). Hydrocarbon trapping might possibly occur in reservoir units laterally truncated against these rising diapirs in locations where sealing conditions might have been established. However, hydrocarbon surface seeps have been identified onshore the LB, such as around the Caldas da Rainha diapir area, east of Peniche, depicting the low efficiency of the associated potential traps (e.g. Pimentel and Pena dos Reis, 2016; Davison and Barreto, 2020).

Lateral facies variations through interfingering or pinching-out geometries, as observed on outcrop and interpreted to occur between the Peniche outcrop succession and the 17C-1 and 20B-1 well locations, might lead to the development of stratigraphic traps (e.g. Dobrin, 1977).

The grainstone facies characterizing the interpreted infralittoral prograding wedges of the CC5c to CC5e sub-units will transition laterally into the fine-grained micritic facies identified in wells 17C-1 and 20B-1, which would behave as baffles to fluid flow and promote the accumulation of hydrocarbons within the grainstone facies, in similarity to the scenario hypothesized for the inner ramp Middle Jurassic units towards the centre of the LB (Azerêdo et al., 2020). A top seal would, however, also be required to be in place for such a trap configuration to be effective.

II.2.6.4.3. Relative timing of petroleum system events

Based on the topics presented and discussed above, it is important to make a brief consideration on the relative timing of the petroleum system events relating to the hypothetical Lower Jurassic source-reservoir pair addressed in this study (Figure II.2.17). The relative timing for trap formation is controlled by the Mesozoic-Cenozoic continuous structural evolution of the LB, as previously mentioned. Structuration, faulting and diapirism associated with rifting during the Jurassic-Cretaceous represent the main processes in the creation of structural traps. By the end of the Jurassic, potential trapping mechanisms would have already been developed in the basin (e.g. Wilson et al., 1989; Alves et al., 2002, 2003b, 2006; Uphoff, 2005). However, the continued tectonic activity and the inversion during the Cenozoic would have had an important role in the reconfiguration of trapping structures, possibly leading to the remigration of hydrocarbons (e.g. Uphoff, 2005).

The timing for source rock maturation has been reported in published studies based on 1D models in the Aljubarrota-2 well, northeast of Peniche (Uphoff, 2005), in the Campelos-1 well (Teixeira et al., 2012) and in 10 onshore wells and 15 offshore pseudo-wells (Cardoso et al., 2014). Although there will be some uncertainty associated with these models, the results for the timing of this event are similar, with the Lower Jurassic source rocks reaching maturity and the oil generation window during the Late Jurassic to Early Cretaceous. The subsequent hydrocarbon expulsion and migration might have therefore occurred at a time when potential structural traps are in place, but are subsequently subjected to different phases of restructuration or deformation.

The main risks and uncertainties will be related to the presence and effectiveness of a sealing unit and trapping mechanisms, as previously discussed. Over 90 % of the wells drilled in the LB targeted structural traps identified on seismic, with no significant hydrocarbon accumulations (ENMC/UPEP, 2016). This provides further indications on the major risks associated with structural traps and on their low efficiency in holding hydrocarbons in place, most likely due to the development of fractures and faults and the breaching or absence of seals. Stratigraphic traps as mechanisms for potential hydrocarbon accumulations, such as the lateral facies transitions of CC5 Member of the CC Formation discussed for this Peniche case, are underevaluated and could be the focus of future exploration activities in the basin.

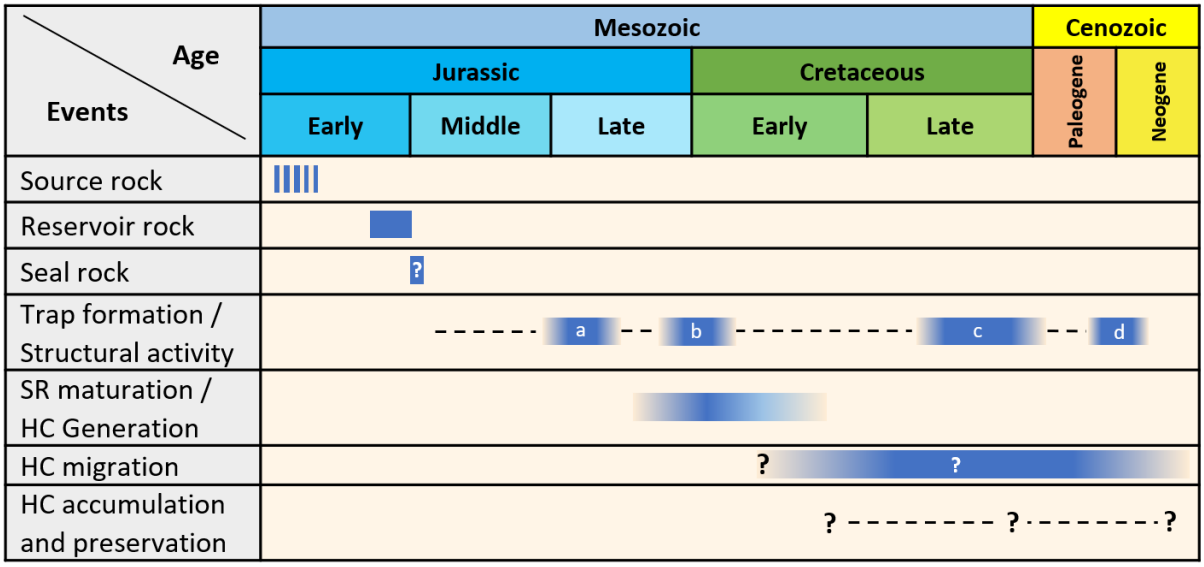

Figure II.2.17. Relative timing of events affecting the potential petroleum system of the Sinemurian-Pliensbachian source rocks and Toarcian-Aalenian(?) potential reservoir unit (CC5 Member). Considering the ongoing strong tectonic activity in the LB throughout the Mesozoic and Cenozoic, together with the associated halokinesis, different traps might form at different times. Ongoing structural activity is represented by dashed black line, following the deposition of the potential reservoir unit, and blue rectangles represent the most important periods. a: Oxfordian rifting phase; b: latest Late Jurassic to earliest Early Cretaceous rifting phase; c: relatively stronger halokinesis and salt tectonics; d: compressional phase, with structural inversion and uplift. Based on the above-discussed, and on elements from Wilson et al. (1989), Rasmussen et al. (1998), Alves et al. (2002, 2003a, 2003b, 2006), Uphoff (2005), Oliveira et al. (2006), Duarte et al. (2010, 2012), Teixeira et al. (2012), Cardoso et al. (2014), Brito et al. (2017) and authors therein.

II.2.7. Conclusions

The integration of regional geological information with outcrop and well data allowed the development of an improved conceptual model attempting to better describe facies variability in and around the Peniche area during the Early - Middle Jurassic transition and offered a better understanding of this hypothetical Lower Jurassic petroleum system and its elements.

The upper interval of the CC5 Member of the CC Formation (CC5b to CC5e sub-units), with an estimated minimum thickness of 160 m, is characterized in its entirety by quartz-oolitic-intraclastic grainstone facies with good potential hydrocarbon reservoir properties, contrasting with the alternating marls and marly-limestones of the S. Gião and Póvoa da Lomba formations found generally in the basin. The original petrophysical properties of this potential reservoir unit have, however, been altered by diagenesis and, specifically, by porosity-occluding calcite cementation, as observed on outcrop samples. The present-day interparticle cemented space

corresponds to an approximate average value of 31% of total space, indicating hypothetical moderate to good reservoir quality prior to porosity occlusion by cementation.

The re-interpretation of lithostratigraphic markers and the facies interpretations done on cuttings from the two analysed offshore wells allowed us to further define the regional extent of these grainstone facies. The lateral transition into the predominantly micritic wackestones observed at well locations is considered to occur through interfingering, gradation or in association with the probable pinching-out geometries associated with the depositional architecture of an infralittoral prograding wedge setting. The well data also provided relevant information regarding the regional thickness variability of the analysed interval, which is increasing towards the S, and the possible presence of a sealing unit overlying the potential reservoir interval. Stratigraphic and sedimentary configurations analogous to the Peniche succession might be present in other sub-basins of the LB, as well as in the western flank of the Berlengas block in the Peniche Basin domain, where the potential development of similar depositional facies acting as hydrocarbon reservoirs associated with potential trapping mechanisms could represent good opportunities for the occurrence of hydrocarbon accumulations.

The relative timing of fluid migration events, diagenetic events and structural events has strong implications on the evolution and development of potential hydrocarbon accumulations. In the studied case, the major risks and uncertainties are related to the presence and effectiveness of sealing units and trapping mechanisms.

Further studies and additional data would be required to reduce these uncertainties and improve the understanding of the discussed concepts and factors contributing to potential accumulations of hydrocarbons in depositional settings analogous to the Peniche case study in the Lusitanian and Peniche basins.

Appendix II.2.A

Table II.2.3. Facies types and main features identified in cuttings from the 17C-1 well.

17C-1 Well	
Depth (m)	**Facies types**
570	FTc and FTe. Micritic mudstone with a micritic matrix containing scattered unidentifiable skeletal grains. Fragment with oo-intraclastic grainstone fabric, moderately sorted, with calcite cement fully occluding interparticle space.
575	FTc. Micritic mudstone with a micritic matrix containing scattered unidentifiable skeletal grains.
580	FTc. Micritic mudstone with a micritic matrix containing scattered unidentifiable skeletal grains.
585	FTc. Micritic mudstone with a micritic matrix containing scattered unidentifiable skeletal grains.
590	FTc. Micritic mudstone with a micritic matrix containing scattered unidentifiable skeletal grains.
595	FTc and FTe. Micritic mudstone with a micritic matrix containing scattered unidentifiable skeletal grains. Fragment with intraclastic grainstone fabric, moderately sorted, with calcite cement fully occluding interparticle space, and containing ooids/coated grains.
600	FTc and FTd. Micritic mudstone with a micritic matrix containing scattered unidentifiable skeletal grains. Fragments with micritic wackestone-packstone fabric, with poorly sorted quartz grains.
610	FTc. Micritic mudstone with a micritic matrix containing scattered unidentifiable skeletal grains.
630	FTc and FTe. Micritic mudstone with a micritic matrix containing scattered unidentifiable skeletal grains. Fragment with intraclastic grainstone fabric, moderately sorted, with calcite cement fully occluding interparticle space. Very well rounded micritized intraclasts but ooids are not clear.
650	FTc. Micritic mudstone with a micritic matrix containing scattered unidentifiable skeletal grains.
670	FTc. Micritic mudstone with a micritic matrix containing scattered unidentifiable skeletal grains.
690	FTc. Micritic mudstone with a micritic matrix containing scattered unidentifiable skeletal grains and bivalve fragments.
710	FTc. Micritic mudstone with a micritic matrix containing scattered unidentifiable skeletal grains and echinoderm fragments and bivalve fragments. Apparently finer matrix than 730, 750 and 770.
730	FTc. Micritic mudstone with a micritic matrix containing scattered unidentifiable skeletal grains.
750	FTc. Micritic mudstone with a micritic matrix containing scattered unidentifiable skeletal grains and echinoderm fragments.

Depth (m)	Facies types (continued)
770	FTc. Micritic mudstone with a micritic matrix containing scattered unidentifiable skeletal grains and echinoderm fragments.
790	FTc. Micritic mudstone with a micritic matrix containing scattered unidentifiable skeletal grains.
810	FTc. Micritic mudstone with a micritic matrix containing scattered unidentifiable skeletal grains and filaments.
830	FTc and FTe. Micritic mudstone with a micritic matrix containing scattered unidentifiable skeletal grains. Fragment with oo-intraclastic grainstone fabric, moderately sorted and including ooids. Calcite cement fully occludes the interparticle space.
850	FTc. Micritic mudstone with a micritic matrix containing scattered unidentifiable skeletal grains.
870	FTc. Micritic mudstone with a micritic matrix containing scattered unidentifiable skeletal grains.
890	FTc. Micritic mudstone with a micritic matrix containing bivalve fragments and scattered unidentifiable skeletal grains.
910	FTc. Micritic mudstone with a micritic matrix containing bivalve fragments and scattered unidentifiable skeletal grains.
930	FTc. Micritic mudstone with a micritic matrix containing bivalve fragments and scattered unidentifiable skeletal grains.
950	FTb. Weakly laminated micritic mudstone, with scattered unidentifiable skeletal grains and very fine sand-grade quartz grains.
970	FTd and FTf. Micritic wackestone-packstone with poorly sorted quartz grains. Calcareous sandstone fragments, with poorly-rounded, poorly-sorted mostly fine (to medium) quartz grains, with a few micritic intraclasts and carbonate cement.
990	FTb, FTc and FTd. Fragments showing weakly laminated micritic mudstone fabric, with scattered unidentifiable skeletal grains and very fine sand-grade quartz grains. Fragments with a micritic mudstone fabric, with a micritic matrix containing scattered unidentifiable skeletal grains. Fragments showing a micritic wackestone-packstone fabric with poorly sorted quartz grains.
1010	FTb and FTc. Weakly laminated micritic mudstone. Scattered unidentifiable skeletal grains and very fine sand-grade quartz grains. Micritic mudstone. Micritic matrix with scattered unidentifiable skeletal grains.
1030	FTa. Laminated micritic mudstone. Dark thin laminations, with scattered unidentifiable skeletal grains.

Table II.2.4. Facies types and main features identified in cuttings from the 20B-1 well.

20B-1 Well	
Depth (m)	**Facies types**
1570	FTc. Micritic mudstone. Micritic matrix with scattered unidentifiable skeletal grains.
1590	FTc. Micritic mudstone. Micritic matrix with scattered unidentifiable skeletal grains.
1610	FTc. Micritic mudstone. Micritic matrix with scattered unidentifiable skeletal grains.
1630	FTc and FTe. Micritic mudstone. Micritic matrix with scattered unidentifiable skeletal grains. Intraclastic grainstone, moderately sorted micritized intraclasts, with calcite cement fully occluding interparticle space. The presence of ooids is not clear.
1650	FTc. Micritic mudstone. Micritic matrix with scattered unidentifiable skeletal grains.
1670	FTc. Micritic mudstone. Micritic matrix with scattered unidentifiable skeletal grains.
1690	FTc. Micritic mudstone. Micritic matrix with scattered unidentifiable skeletal grains.
1710	FTc. Micritic mudstone. Micritic matrix with scattered unidentifiable skeletal grains.
1730	FTc. Micritic mudstone. Micritic matrix with scattered unidentifiable skeletal grains.
1750	FTc. Micritic mudstone. Micritic matrix with scattered unidentifiable skeletal grains.
1770	FTc. Micritic mudstone. Micritic matrix with scattered unidentifiable skeletal grains.
1790	FTc. Micritic mudstone. Micritic matrix with scattered unidentifiable skeletal grains.
1810	FTc and FTd. Micritic mudstone. Micritic matrix with scattered unidentifiable skeletal grains. Micritic wackestone-packstone with poorly sorted quartz grains.
1830	FTc. Micritic mudstone. Micritic matrix with scattered unidentifiable skeletal grains.
1850	FTc and FTd. Micritic mudstone. Micritic matrix with scattered unidentifiable skeletal grains. Micritic wackestone-packstone with poorly sorted quartz grains.
1870	FTc and FTd. Micritic mudstone. Micritic matrix with scattered unidentifiable skeletal grains. Micritic wackestone-packstone with poorly sorted quartz grains.
1890	FTc. Micritic mudstone. Micritic matrix with scattered unidentifiable skeletal grains.
1910	FTc. Micritic mudstone. Micritic matrix with scattered unidentifiable skeletal grains.
1930	FTc and FTe. Micritic mudstone. Micritic matrix with scattered unidentifiable skeletal grains. Oo-intraclastic grainstone. Moderately sorted micritized intraclasts including ooids, with calcite cement fully occluding interparticle space.

Depth (m)	Facies types (continued)
1960	FTc and FTe. Micritic mudstone. Micritic matrix with scattered unidentifiable skeletal grains. Oo-intraclastic grainstone. Moderately sorted micritized intraclasts including ooids, with calcite cement fully occluding interparticle space.
1970	FTc and FTe. Micritic mudstone. Micritic matrix with scattered unidentifiable skeletal grains. Oo-intraclastic grainstone. Moderately sorted micritized intraclasts including ooids, with calcite cement fully occluding interparticle space.
1990	FTc. Micritic mudstone. Micritic matrix with scattered unidentifiable skeletal grains. (radiolários).
2000	Ftd (and Fte?). Micritic wackestone-packstone with poorly sorted quartz grains. Intraclastic grainstone, moderately sorted micritized intraclasts, with calcite cement fully occluding interparticle space. The presence of ooids is not clear.
2010	FTc. Micritic mudstone. Micritic matrix with scattered unidentifiable skeletal grains.
2030	FTd and FTb. Micritic wackestone-packstone with poorly sorted quartz grains. Weakly laminated micritic mudstone, with scattered unidentifiable skeletal grains and very fine sand-grade quartz grains.
2034.5	FTa, FTc(?). Laminated(?) micritic mudstone. Dark thin laminations, with scattered unidentifiable skeletal grains and a few planktonic foraminifera. Lumpy?
2040	FTc. Micritic mudstone. Micritic matrix with scattered unidentifiable skeletal grains.
2050	FTc. Micritic mudstone. Micritic matrix with scattered unidentifiable skeletal grains.
2060	FTc (FTb and FTd?). Micritic mudstone. Micritic matrix with scattered unidentifiable skeletal grains, crinoids. Some micritic fragments show apparent weak lamination. Some micritic fragments show wackestone-packstone texture with poorly sorted quartz grains.
2070	FTd. Micritic wackestone-packstone with poorly sorted quartz grains.
2100	FTc. Micritic mudstone. Micritic matrix with scattered unidentifiable skeletal grains.
2110	FTc and FTe. Micritic mudstone. Micritic matrix with scattered unidentifiable skeletal grains. Oo-intraclastic grainstone. Micritized intraclasts, ooids and quartz grains. Calcite cement fully occluding interparticle space.
2136	FTd (and FTe(?)). Micritic wackestone-packstone with poorly sorted quartz grains. Contains very few ooids.
2140	FTd (and FTe(?)). Micritic wackestone-packstone with poorly sorted quartz grains. Contains an oo-intraclastic fragment with grainstone texture. Calcite cement fully occluding interparticle space.

Chapter III. The Kharaib Formation, Rub Al Khali Basin, U.A.E.

III.1. Carbonate pore type quantification through digital image analysis – the dual-porosity system of the Lower Cretaceous upper Kharaib Formation reservoir

III.1.1. Abstract

The Barremian Upper Kharaib Member of the Kharaib Formation is characterized by a dual macro and microporosity system. Reservoir performance is strongly affected by the nature of this porous network, with microporosity holding volumes of hydrocarbons in place and contributing very little to fluid flow. The lower half of this reservoir is defined by wackestone facies, while packstones, grainstones and rudstone-grainstones characterize the more heterogeneous upper half. Macroporosity was quantified through digital image analysis, using visual estimation, non-contiguous colour selection and trained machine learning. These semi-automated methodologies were applied to 285 images from 142 thin sections in 4 different wells. Images were segmented and pixels representing macroporosity were quantified as a proxy for macropore volume. Microporosity represents, on average, more than 60% of total porosity, reaching up to 100 % in the lower half of the studied interval. Total porosity variations show no clear vertical trends, contrasting with permeability, which reaches significantly higher values in the upper half of the succession. The latter shows higher macroporosity, reaching close to 50 % of total porosity in some grain-dominated intervals, where microporosity in micritized particles account for the remaining pore volume. Interparticle macroporosity shows moderate correlation with permeability, as opposed to total porosity, making it a better predictor for permeability. Trained machine learning is considered to offer more consistent results, when compared to the other methodologies, offering an objective, relatively quick and inexpensive methodology to complement petrography and core analysis. A better understanding of pore type distribution within the reservoir is indispensable for proper reservoir characterization and modelling, assisting in field development plans.

III.1.2. Introduction

The carbonate Upper Kharaib Member (UKM) of the Lower Cretaceous Kharaib Formation, a nomenclature widely used in the region (e.g. Pittet et al., 2002; Van Buchem et al., 2002, 2010; El Wazir et al., 2015) and adopted in this study, is the main hydrocarbon reservoir in Abu Dhabi (U.A.E.) (Lijmbach et al., 1992; Taher, 1996; Alsharhan and Nairn, 1997). Its pore network is characterized by a dual-porosity system containing micro and macro-pores, where microporosity is the dominant fraction by volume (e.g. Harris et al., 1968; Oswald et al., 1995; Budd, 1989; Morad et al., 2016; Ehrenberg et al., 2018; Ehrenberg, 2019). Total porosity in the UKM shows no clear vertical variability trends, as opposed to permeability, which reaches significantly higher values in the sediments of the regressive phase, in the upper half stratigraphic interval of this reservoir (e.g. Harris et al., 1968; Alsharhan, 1993; Strohmenger et al., 2006; Ehrenberg, 2019). While high permeability intervals might behave as important features leading to issues such as early water breakthrough in the cases of waterflood field development projects, having a strong impact on reservoir performance, microporosity will hold volumes of bypassed oil, strongly reducing the oil recovery efficiency (e.g. Weber, 1986; Namba and Hiraoka, 1995; Wardlaw, 1996; Cunningham and Chaliha, 2002; Dabbouk et al., 2002; Carvalho et al., 2011). It is, therefore, highly relevant to pursue an improved understanding of this heterogeneous system and of the pore type distribution in this reservoir.

Porosity obtained from conventional core analysis (CCA) provides total porosity values and makes no distinction between macro- and microporosity. Objective and semi-automated quantitative digital image analysis (DIA) methods have been used in many previous studies (e.g. James, 1995; Tovey and Wang, 1997; Anselmetti et al., 1998; Nabawy, 2014; Fullmer et al., 2014; Buckman et al., 2017; Chandra et al., 2019; Nanjo and Tanaka, 2019; Pal et al., 2019; Al Khalifa et al., 2020) and are useful tools to measure macroporosity and improve the understanding on the heterogeneous pore network of the UKM. Such added geological data allows for an improved characterization of the reservoir and for a better understanding of its pore system and the petrophysical properties variability.

In this context, the main objective of this study is to apply and compare different digital image analysis methodologies (visual estimation, non-contiguous colour selection and guided machine learning) to provide further insights into the macro- and microporous dual-porosity network characterizing the UKM, as well as into pore type distribution. A total of 142 thin sections from 4 crestal wells in a major onshore Abu Dhabi field were analysed.

III.1.3. Geological background and reservoir properties

The Barremian UKM shows a thickness of approximately 180 ft (55 m) in the crest of the studied field (e.g. Alsharhan, 1993; Grötsch et al., 1998; Strohmenger et al., 2006). It is part of the Lower Cretaceous Thamama Group and was deposited in a carbonate ramp setting within the Rub Al Khali Basin, in the eastern-southeastern Arabian platform (Figure III.1.1) (e.g. Harris et al., 1968; Murris, 1980; Alsharhan, 1993; Alsharhan and Nairn, 1997; Van Buchem et al., 2002, 2010; Strohmenger et al., 2006).

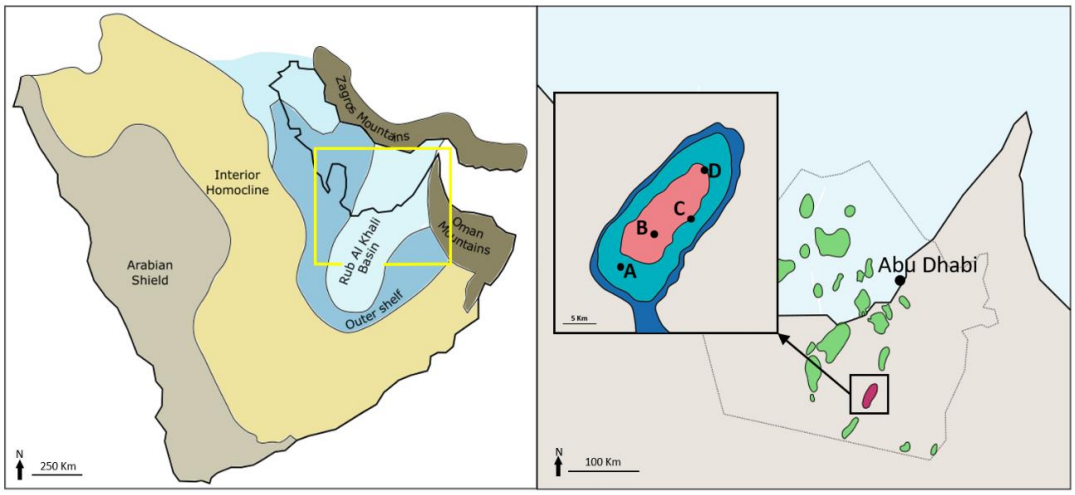

Figure III.1.1. **left**: Major structural provinces of the Arabian Peninsula (based on Powers et al., 1966; Schlumberger, 1981; Alsharhan and Nairn, 1997); **right**: U.A.E. map showing major producing fields in Abu Dhabi (green), with the studied field highlighted in red (based on Schlumberger, 1981; Alsharhan and Nairn, 1997; Strohmenger et al., 2006). Zoomed-in area shows simplified structural map of the studied field (red: shallower; dark blue: deeper) showing location of studied wells A to D (Melville et al., 2004).

This interval is composed of wackestones to packstones deposited during a transgressive phase, with bioclastic packstones, grainstones and rudstone-grainstones dominating the regressive phase interval (Figure III.1.2) (e.g. Harris et al., 1968; Alsharhan, 1993; Grötsch et al., 1998; Van Buchem et al., 2002, 2010; Strohmenger et al., 2006; El Wazir et al., 2015; Ehrenberg et al., 2018). The UKM is subdivided into 6 regionally correlatable reservoir subzones (SZ) (e.g Harris et al., 1968; El Wazir et al., 2015; Ehrenberg et al., 2018). The boundaries for these subzones are defined by the operating companies based on the occurrence of low porosity layers, which also correspond to intervals with subtle increases in alumina content, proportional to clay content, as reported by Ehrenberg et al. (2016, 2018). These intervals have also been reported to correspond to the boundaries of parasequence sets (Strohmenger et al., 2006; Ehrenberg et al., 2018). Although the limits for these subzones are not clearly represented in the GR or the facies log (Figure III.1.2), they are consistently defined across the Abu Dhabi fields based on the porosity log signature (e.g. Harris et al., 1968; Alsharhan, 1990, 1993; El

Wazir et al., 2015; Ehrenberg et al., 2018). This subzone classification scheme is widely used in the operating companies in Abu Dhabi and in published studies, and will be the terminology here applied, for practical reasons.

The reservoir has a heterogeneous porosity system with a dominant microporous fraction, which has previously been discussed by different authors in regards to its nature and origin (e.g. Budd, 1989; Moshier, 1989; Oswald et al., 1995; Vahrenkamp et al., 2014; Morad et al., 2016). The present-day dual-porosity network is a result of combined depositional and diagenetic effects, with calcite cementation and micritization having an important role (e.g. Ehrenberg et al., 2016, 2020a; Morad et al., 2016; Paganoni et al., 2016). The microporosity has been described as originating under the influence of marine pore waters, during early diagenesis (e.g. Budd, 1989; Moshier, 1989), but has also been proposed to originate during later burial stages in recent studies, related to the development of micro-rhombic calcite phase (e.g. Vahrenkamp et al., 2014; Morad et al., 2016). The wackestone facies of the lower half of the reservoir is almost fully microporous, while in the packstone, grainstone and rudstone-grainstone facies of the younger sections of the reservoir, a more heterogeneous pore system is observed, characterized by interparticle macroporosity but also microporosity within the micritized grains and micritic matrix, when present (e.g. Budd, 1989; Morad et al., 2016).

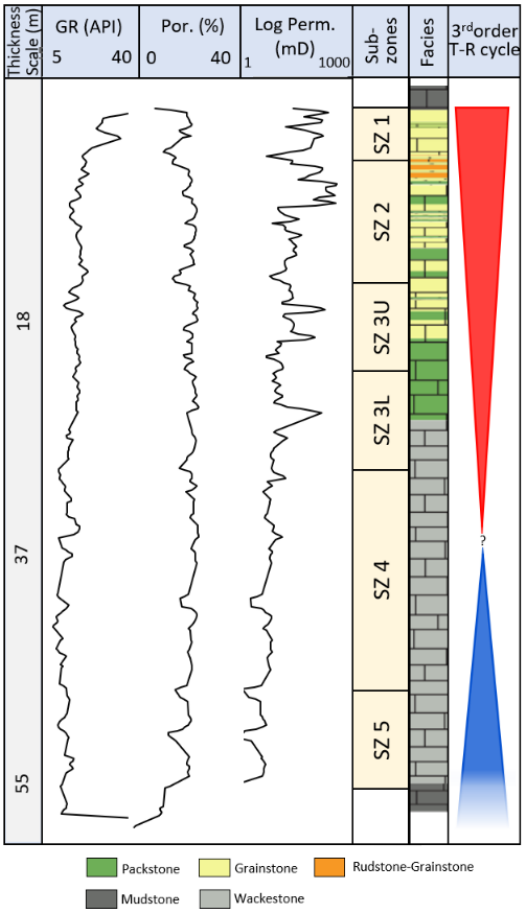

Figure III.1.2. Composite panel for the UKM interval in Well C, showing Gamma Ray log (GR), CCA porosity (Por.) and permeability (Log Perm.), with indication of reservoir subzones (based on Harris et al., 1968; Alsharhan, 1993; Ehrenberg et al., 2018) and simplified facies types. Sequence stratigraphy hemicycles of the 3rd order cycle are based on Strohmenger et al. (2006).

III.1.4. Materials and methods

To achieve the objectives of this study, a total of 285 images were used for DIA, captured from 142 thin sections from 4 wells along a southwest-northeast section across the field crest (Figures III.1.1, III.1.3). In more heterogeneous thin sections, up to five different images were captured and analysed. Wireline log data and porosity/permeability measurements from conventional core analysis were available from the 4 studied wells and integrated in this study. The southernmost well was used as reference well due to the higher sampling frequency. Some of the thin sections are impregnated with blue epoxy resin for porosity visualization and some are stained with Alizarin red S to differentiate calcite from dolomite. The ImageJ software and Weka plugin were used for DIA (Hall et al., 2009; Schindelin et al., 2012) on a computer with a dual-core 1.1-2.7 GHz processor and an installed memory (RAM) of 4.00 GB.

The different semi-automated, quantitative approaches of visual estimation, colour selection based on histogram analysis and guided machine learning were used to measure macroporosity on thin section images. The macroporosity areas measured on thin section images are seen as a proxy for macropore volume and microporosity is calculated by subtracting measured macroporosity from total plug-measured porosity. CCA data was used as reference for these measurements, with thin sections available from depths that are at most 0.2 ft (6 cm) away from the plug depth. Core depths were checked and shifted to log depth where necessary, based on the integrated analysis of cores, thin sections and wireline logs. The depths here depicted are masked and shifted to a reference level deeper than present-day sea level and do not represent true depth, for confidentiality reasons. For the purpose of this study, a simplified facies classification scheme was defined, describing the major textural properties by applying elements from the classification schemes by Dunham (1962) and Folk (1959, 1962). Scanning Electron Microprobe (SEM) images were acquired from 5 core chips from well A, with the purpose of capturing the finer details of microporosity.

Macroporosity in this study is defined as pores larger than the smallest pores that can be visually identified on thin section using a petrographic microscope at 2x and 4x magnification. All pores with diameters below 10 μm are not visually identifiable and are therefore considered as microporosity for the purpose of this study. Choquette and Pray (1970) define the upper limit for microporosity as 1/16mm (62.5 μm) and Pittman (1971) established a considerably lower limit, at 1 μm. Fullmer et al. (2014) define micropores as pores with diameters between 1 and 3 μm.

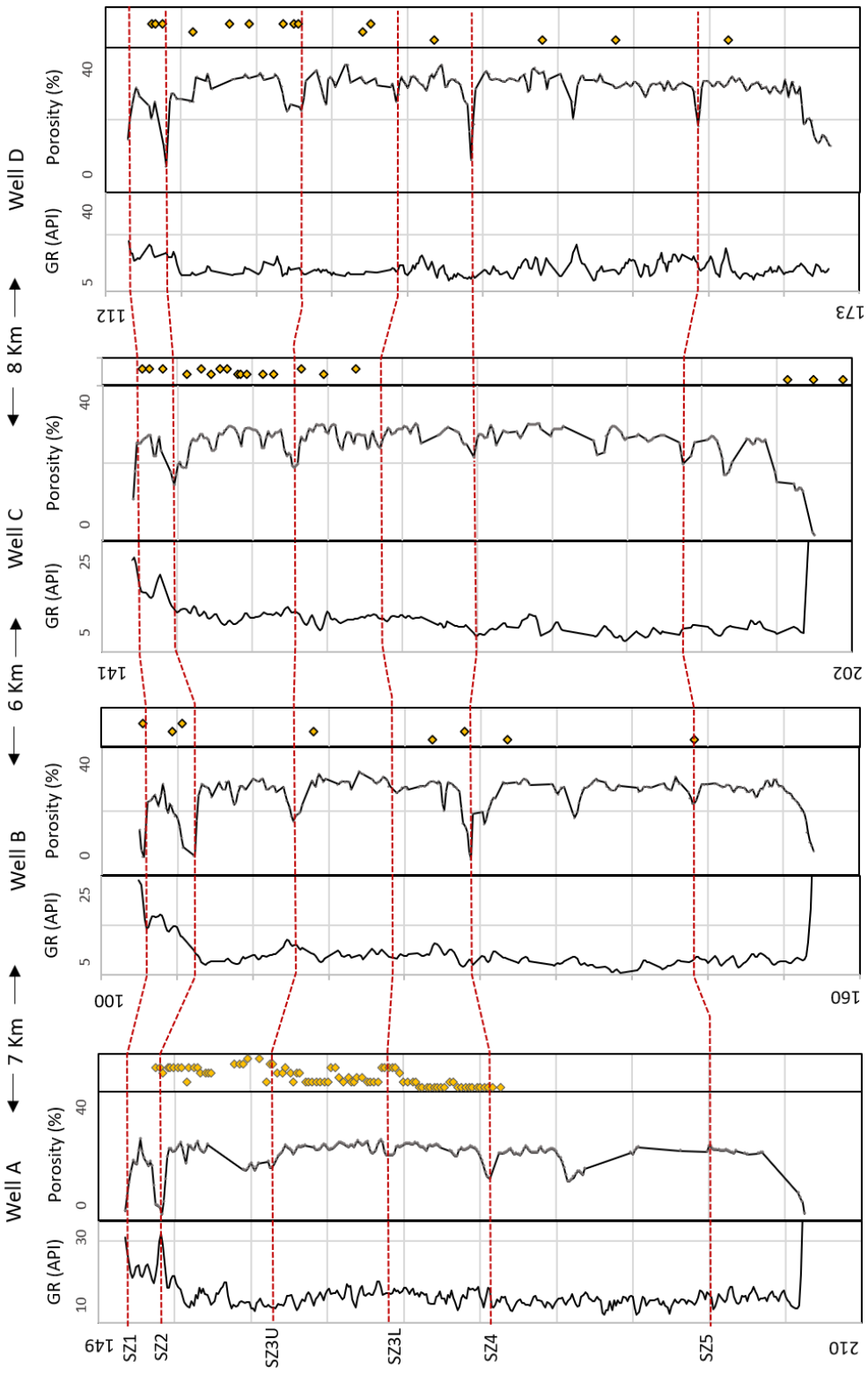

Figure III.1.3. Representation of the four analysed wells, including GR and core porosity logs. Thin section depths are represented by yellow circles on the third column for each well. Vertical axis represents shifted depths in metres. Approximate distance between wells is indicated. See Figure III.1.1 for well location.

III.1.4.1. Visual estimation

A semi-quantitative analysis of total macroporosity was done on the total set of thin sections through visual estimation using visual comparators (e.g. Longiaru, 1987). This methodology is associated with some level of subjectivity, but because it was carried out by the same operator, the results obtained for the different thin sections using this method are considered to be comparable. In addition to quantifying total macroporosity, interparticle and non-connected macroporosity (e.g. Choquette and Pray, 1970; Lucia, 1983, 2007) were differentiated and estimated, as this would be almost impossible using an automated approach. The latter might be represented by intraparticle, mouldic porosity (resulting from dissolution of skeletal grains, peloids or other particles), fenestral, shelter, vuggy or fracture porosity (e.g. Choquette and Pray, 1970).

III.1.4.2. Non-contiguous colour selection based on histogram data

Thin section photos were taken under cross polarized light, in order to acquire images where macroporosity is represented in black to facilitate identification during the DIA process. In thin sections that are impregnated with blue epoxy resin, some microporous areas will show a patchy blueish colour under normal light and would be accounted as macroporosity in a semi-automated pixel counting approach through colour selection, if blue colour was the selection criteria for identifying macroporosity. This would lead to an overestimation of macroporosity. Some elements of the methodology here applied are similar to those utilized in previously published studies (e.g. Ehrlich et al., 1984; Anselmetti et al., 1998; Grove and Jerram, 2011; Ghiasi-Freez et al., 2012). However, the colour selection methodology here applied is defined for this specific case study.

For a given image, the colour histogram for the area of a selected macropore considered to be representative was analysed to define a range of RGB values to apply in colour selection on the full image, and on batches of selected similar images. This range of values was defined based on the averages and standard deviation of the RGB values of the selected area. Each well is analysed separately and, for each well, different image batches were created as necessary. Three RGB values were defined for each batch and, in addition, three different tolerance values for colour selection were defined. The colour selection tool will therefore consider the area around selected pixels, limited by the defined tolerance value. A maximum tolerance value that captures an extreme measurement maximizing macroporosity selection was defined and was verified for its validity and significance after obtaining the first results.

Using the selected parameters, images were batch processed for the selection of non-contiguous macroporosity areas and quantification of pixels within these areas (Figure III.1.4). For each of the 285 images, 9 total macroporosity measurements were obtained, resulting in a total of 2565 measurements. The results were then verified using the thin section photos and manual

measurements, when further confirmation was necessary, and an average value was calculated for each image based on the verified measurements.

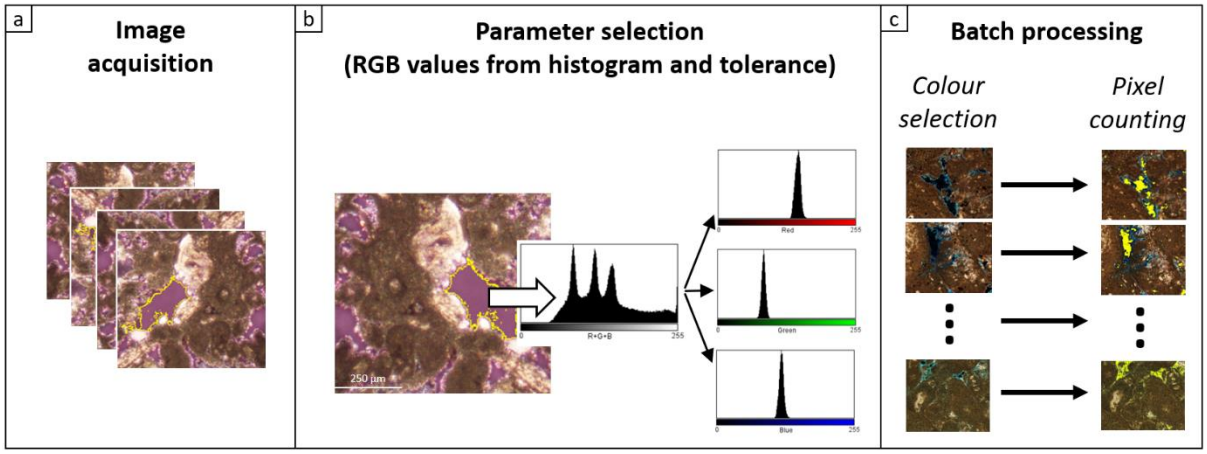

Figure III.1.4. Simplified workflow for pixel counting through colour selection based on histogram data from a selected reference pore area, as defined for this study.

III.1.4.3. Machine learning using training images

Image segmentation was done using the open-source software Trainable Weka Segmentation (TWS) which works as a plugin for image processing software ImageJ (Schindelin et al., 2012). It applies algorithms developed in the machine learning toolkit Waikato Environment for Knowledge Analysis (WEKA) (Hall et al., 2009). In this methodology, a user-controlled dataset is used to define the set of rules utilized for image segmentation, which is then applied to sets of unknown data/images using the resulting classification model, with no required supervision (Figure III.1.5).

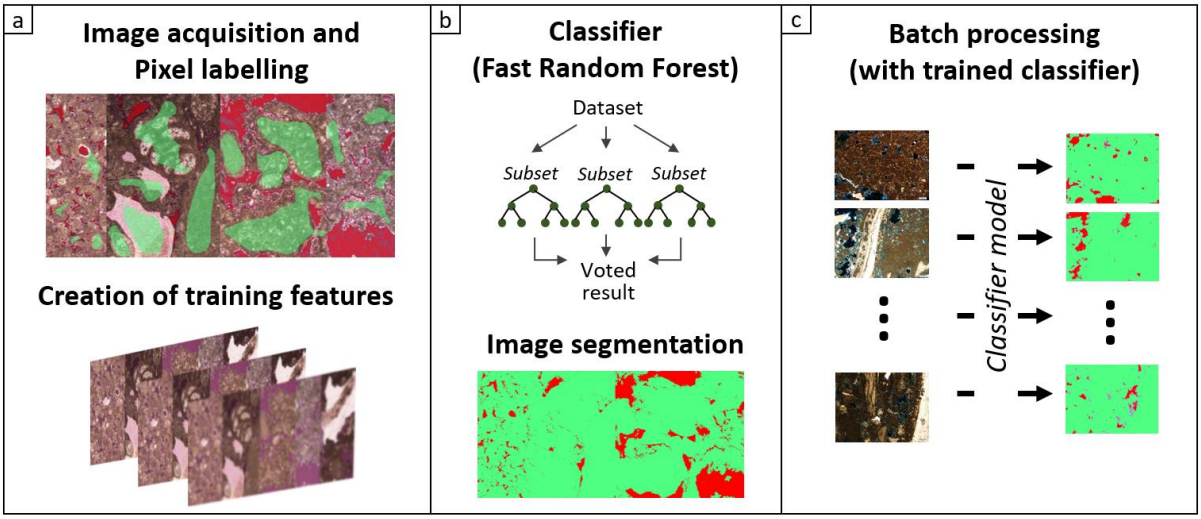

Figure III.1.5. Simplified workflow for the machine learning methodology (elements based on Arganda-Carreras et al., 2017; Breiman, 2001; Hall et al., 2009). **a**: Acquisition/selection of training images and pixel labelling. Creation of training features using gaussian blur techniques to reduce noise; **b**: Fast random forest algorithm is used to classify each pixel on the training image and create a segmented image of the training data; **c**: The trained classifier is applied to image batches for image segmentation and pixel-counting is done on the resulting segmented images through batch-processing.

After selecting the training images considered to be representative of the user-defined batches, different sets of pixels representing 2 major classes (porous and non-porous space) were manually selected and classified. These manually classified pixel sets were used by the classifier during the training process on the training images.

In cases where the transition between pore space and carbonate particles is marked by different phases of calcite cement rims, an area with varying shades of blue is observed. A third pixel class was created for better detection of these different phases. The selection of the training image depends on the nature of the images within the defined batches. When considerable variability in colour or contrast/brightness is observed between different images, a higher number of training images was used (Figure III.1.6).

A set of image features created using a gaussian blur filter was used as training input for the purpose of noise reduction and the classifier was trained on the original image and on the transformed versions of the original (Arganda-Carreras et al., 2017). The applied classifier was a version of random forest (Breiman, 2001) which utilizes 200 trees with 2 random features per node known as 'Fast Random Forest' developed for Weka (https://code.google.com/archive/p/fast-random-forest/) (Hall et al., 2009; Arganda-Carreras et al., 2017), which creates an average result of multiple decision trees, reducing variance (e.g. Breiman, 2001; Hastie et al., 2008). Once the classifier was trained, the classification model was exported and applied to batches of selected images (Figure III.1.5) (Arganda-Carreras et al., 2017). The resulting segmented images were then batch-processed for pixel-counting of areas corresponding to macroporosity.

To illustrate the time required to obtain macroporosity measurements from the guided machine learning methodology, the results from a batch of 60 images from well C are here presented. These details will be comparable to the remaining batches of images from the different wells. Training the classifier model with the user-defined classes on the training selected images took 372 seconds. Classifying the full training image using this trained model took 116 seconds, while the full batch of 60 selected images took 15850 seconds to classify. It should be noted that the processing time is closely related to the processing power of the computer used.

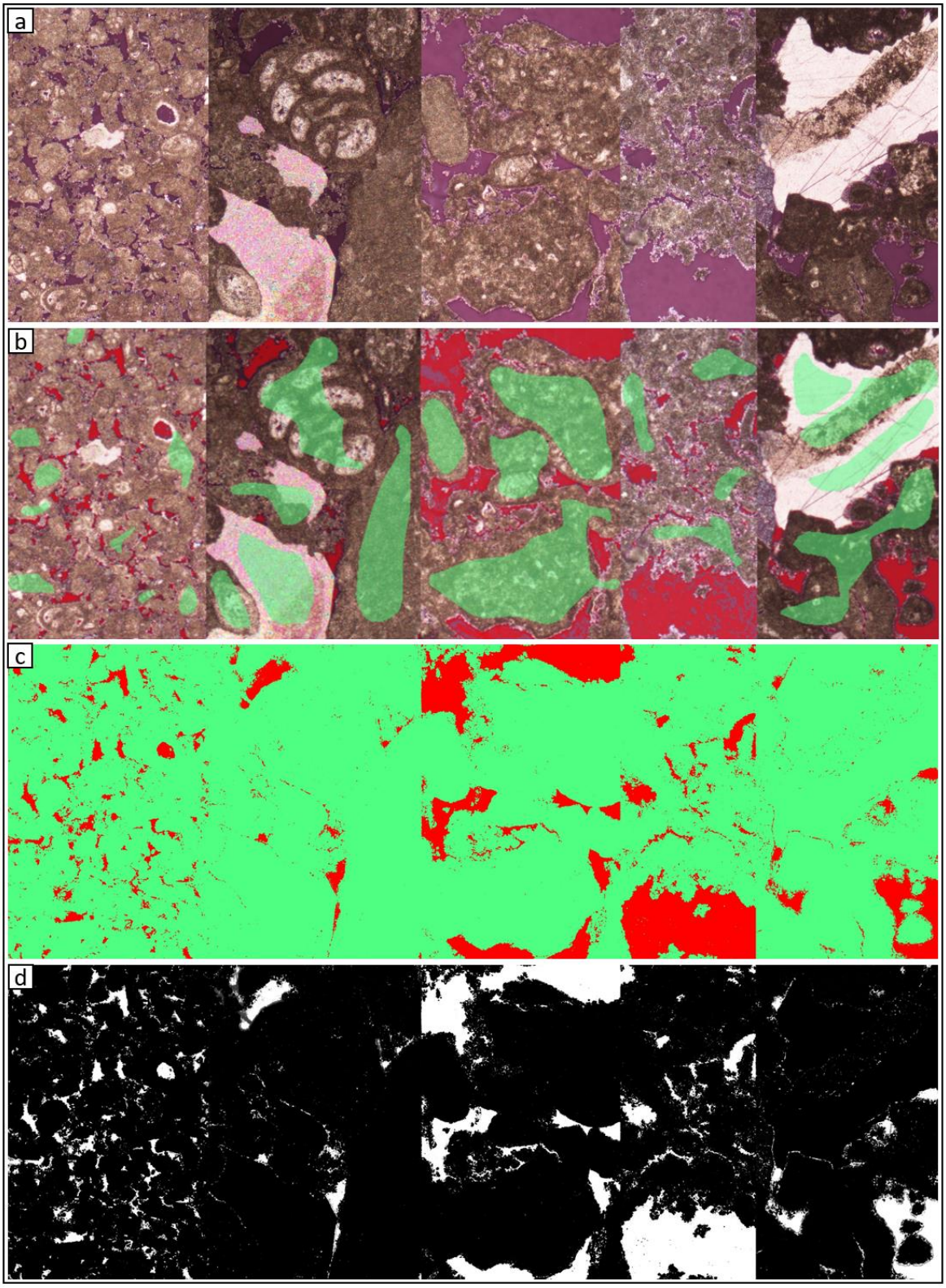

Figure III.1.6. Example of pixel classification and image segmentation through guided machine learning applied to images from the present study; **a**: Composite training image composed of 5 images from different thin sections. **b**: Manually selected areas for pixel classification; **c**: Segmented image produced as the outcome of the guided classifying process; **d**: Binary black and white image.

III.1.4.4. Pore size measurements

Using the segmented images obtained from the previously described methodologies, automatic thresholding was applied to create binary, black and white images. These are required as input for the particle analyser plugin in ImageJ, which was used to measure each pore area in different images. A low-end cut-off of 5 pixel^2 was applied, in order to reduce the amount of generated noise. The pore sizes and mean values were obtained, with the pore-size values in pixel^2 converted into μm^2 using a conversion factor based on the image scale of the acquired images. The output also provides a colourized image for easy visual analysis of different pore sizes in each sample (Figure III.1.7). Each measured pore is identified by its X/Y image coordinates in order to preserve information regarding the correspondence between the results and each measured pore.

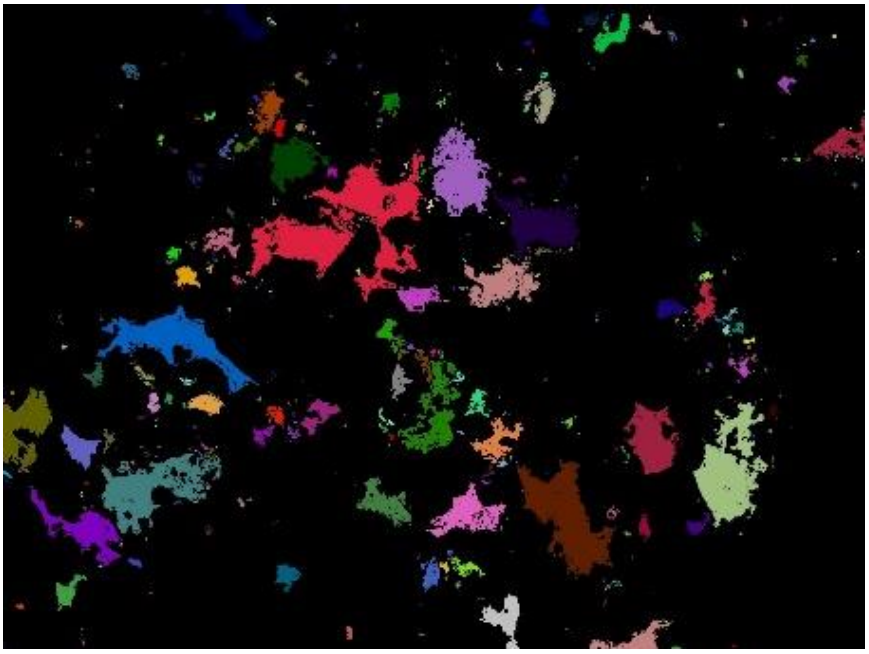

Figure III.1.7. Pore size measurements example result from well A. Each identified and measured pore is colourized for easier visualization and referenced through an X/Y coordinate.

III.1.5. Results

III.1.5.1. Petrographic observations

The applied facies classification scheme offers a basic description of the major depositional textures in this reservoir as a considerable simplification of the facies scheme developed by Strohmenger et al. (2006) for the UKM. The main depositional textures identified are wackestone, packstone, grainstone and rudstone-grainstone (Figure III.1.8). A more detailed description is presented in Chapter III.2.

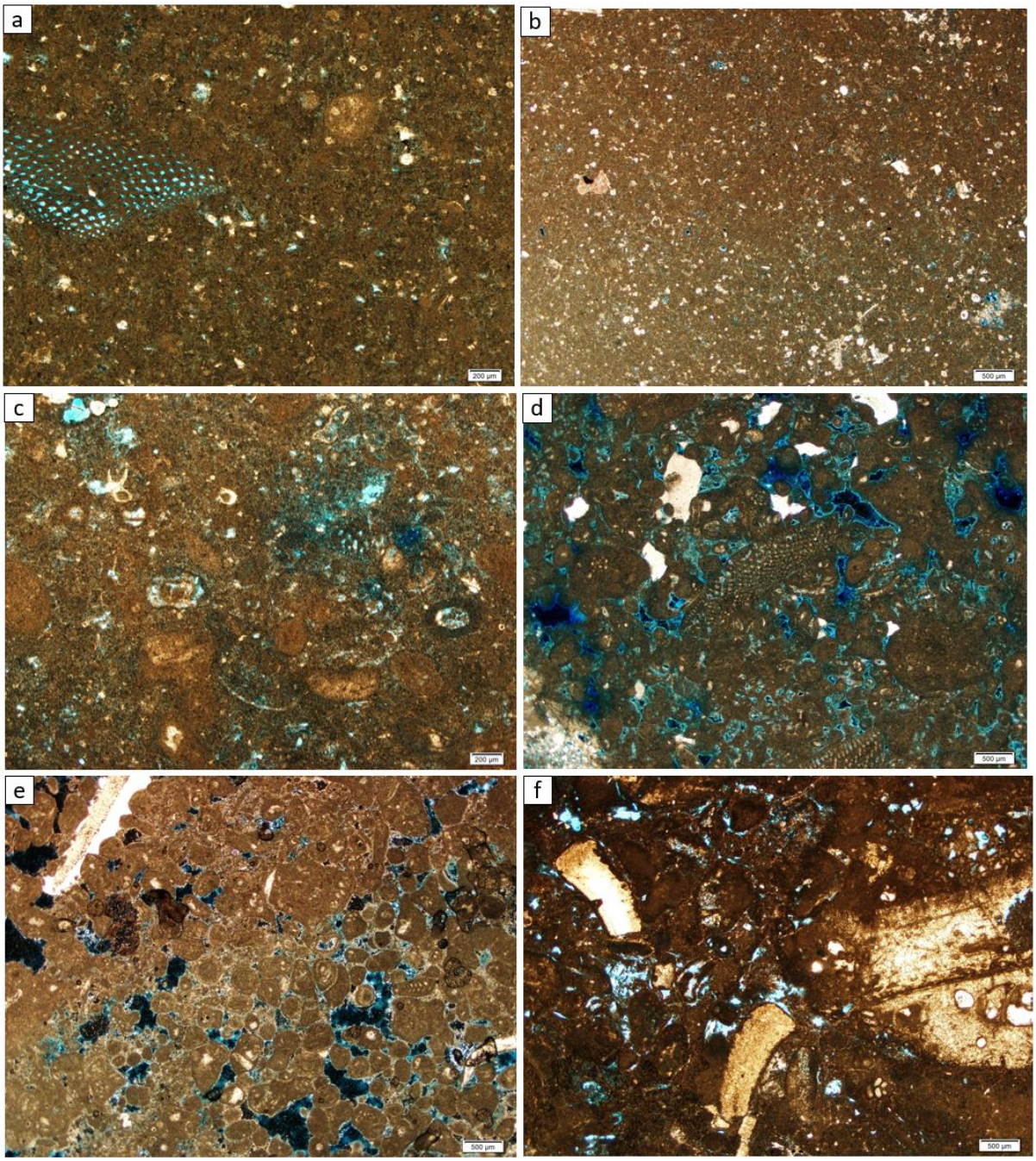

Figure III.1.8. Examples of major depositional facies of the UKM in well A. **a**: Biomicritic wackestone with orbitolinids and few scattered micritized intraclasts; **b**: Biomicritic wackestone with floating dolomite rhombs; **c**: Intrabioclastic packstone with micritized intraclasts and a micritic matrix; **d**: Poorly sorted intrabioclastic grainstone with micritized orbitolinids, intraclasts and skeletal grains, including echinoderm fragments with syntaxial cement overgrowths. Most of the interparticle space is open; **e**: Moderately to well sorted intrabioclastic oolitic grainstone with micritized intraclasts, as well as skeletal grains, including echinoderm fragments with syntaxial cement overgrowths; f: Very poorly sorted rudstone-grainstone with micritized intraclasts and skeletal grains, including rudist fragments.

The wackestone facies are generally characterized by a micritic matrix containing scattered skeletal grains, including foraminifera, echinoderm fragments and micritized orbitolinids in varying low abundance (Figure III.1.8a, b). Bioturbation occurs in wackestone intervals with variable intensity. Some layers are moderately dolomitized, showing floating microrhombic dolomite crystals. Wackestones are typically represented in SZ4 and SZ3L (Figure III.1.2). The observed packstone facies are generally characterized by the presence of a micritic matrix and micritized intraclasts, peloids and skeletal grains including foraminifera, bivalves, echinoderm fragments and orbitolinids (Figure III.1.8c). Packstone facies occur in SZ3, SZ2 and SZ1.Grainstone facies occur in SZ3U, SZ2 and SZ1, while rudstone-grainstone are typically observed in SZ2 (Figure III.1.2). They are characterized by grain-supported textures with different associations of intraclasts, peloids, coated grains (ooids, oncoids) and skeletal grains, including foraminifera, bivalves, echinoderms and rudists (Figure III.1.8d, e, f). Grainstones with higher amounts of coated grains (Figure III.1.8e) typically occur towards the top of SZ2 and in SZ1. Rudstone-grainstone facies showing a strong abundance of rudist shell fragments occur in SZ2 (Figure III.1.8f). Some intervals in SZ2 are characterized by packstone-grainstone facies where the interparticle space is partially occluded by a finer, micritic phase. Interparticle calcite cementation is minimal in the analysed thin sections (Figure III.1.8d, e, f).

III.1.5.2. Pore type variability

Grainstone and rudstone-grainstone intervals are characterized by the occurrence of higher macroporosity volumes (Figures III.1.8d, e, f, III.1.9a), although some of these intervals show a micritic fraction with a microporous texture in between the coarser particles, as mentioned above. Packstones are characterized by a dominant microporous micritic matrix with some samples showing low to moderate volumes of interparticle and mouldic macroporosity. The pore network in wackestones is mainly composed of microporosity with only minor to moderate volumes of mouldic macroporosity (Figure III.1.9b, c).

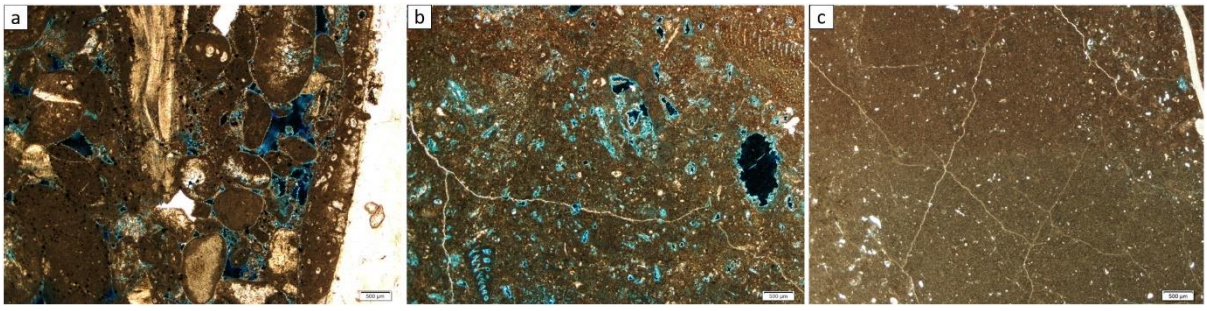

Figure III.1.9. **a**: Well A, SZ2. Intrabioclastic rudist rudstone-grainstone. Total porosity is 20.2 %, macroporosity is 2.9 % (fully interparticle); **b**: Well A, SZ3U. Micritic wackestone. Total porosity is 29.2 %, macroporosity is 1.8 % (mostly mouldic, but minor intraparticle macroporosity occurs within micritized particles); **c**: Well A, SZ4. Bio-micritic wackestone with floating microrhombic dolomite crystals. Total porosity is 27.2 %, average macroporosity is 0 %.

While microporosity clearly dominates in wackestones of the lower half of the reservoir (SZ 3L, 4 and 5), it also has a major role in the upper half, as previously mentioned, resulting from the micritization of allochems (e.g. Morad et al., 2016) and the presence of a micritic matrix (Figure III.1.10). Thin section photos and SEM images illustrate the relative proportions of microporosity in samples at different depths, from different subzones (Figures III.1.9, III.1.11). Microporosity comprises more than approximately 60 % of total porosity.

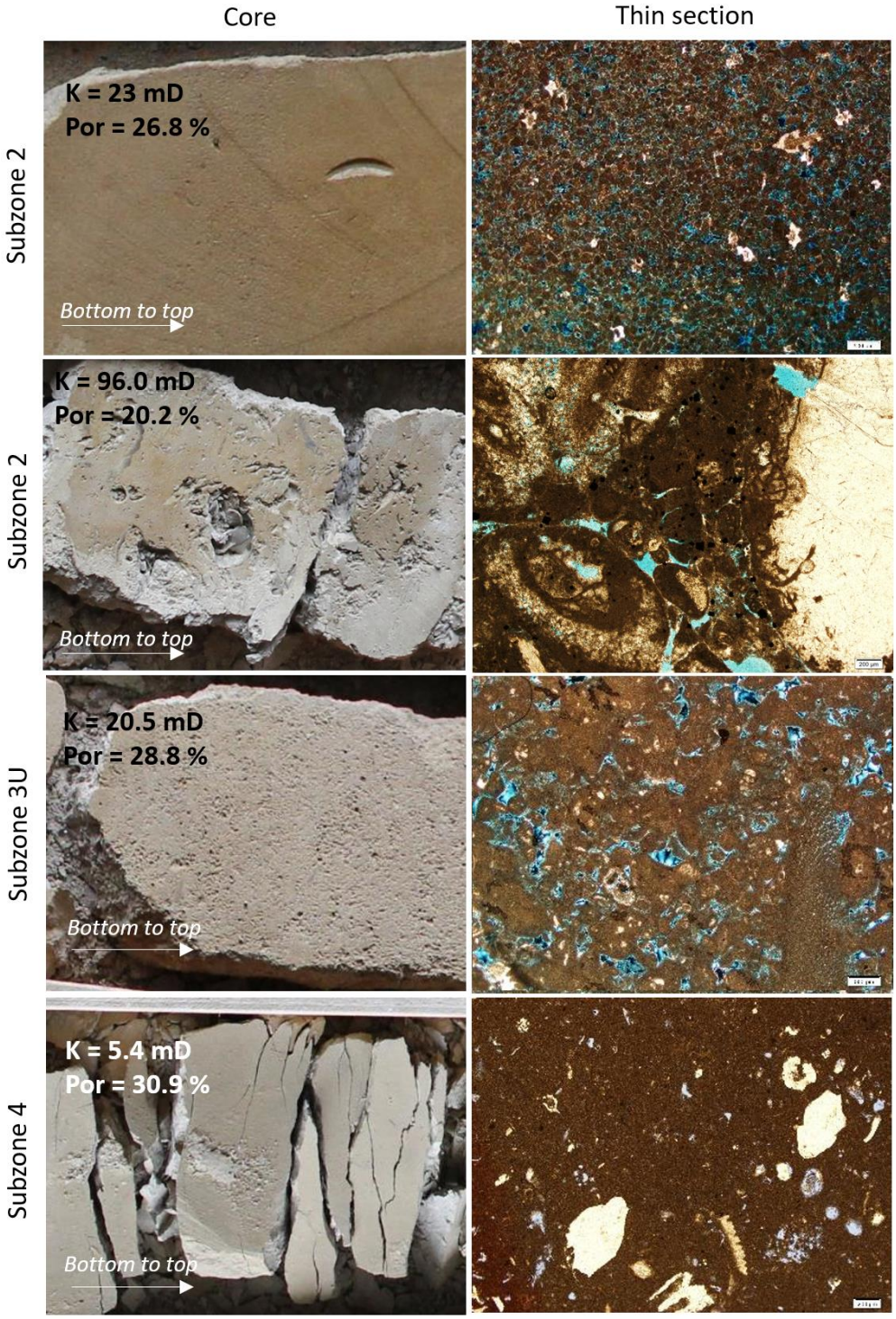

Figure III.1.10. The lower half of the UKM is characterized by wackestone facies and a microporous system (SZ4 core and thin section example represented in this figure). The upper half of the UKM is more heterogeneous, generally dominated by packstone, grainstone and rudstone-grainstone textures with a dual porosity system (SZ2, SZ3U core and thin section examples are presented in this figure).

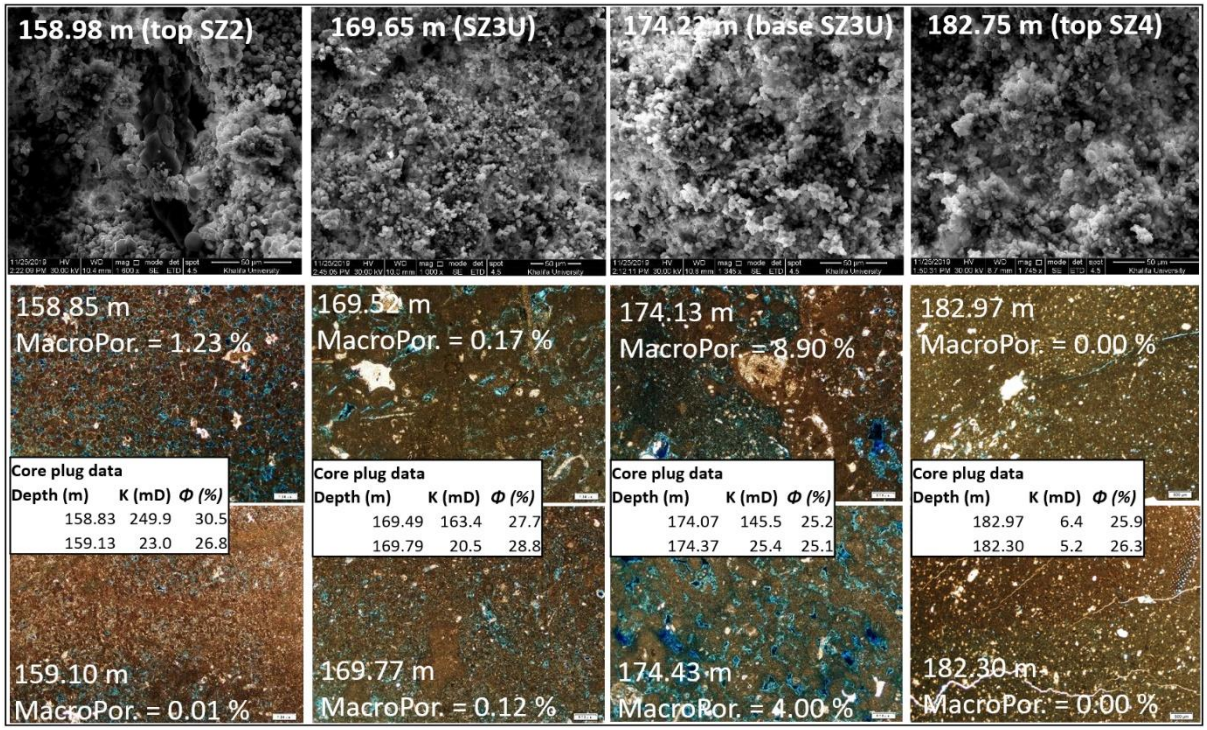

Figure III.1.11. SEM images (top row) and thin sections (mid and bottom row) from Well A, with indication of macroporosity from DIA (MacroPor.). Thin sections immediately adjacent to the SEM samples depth are shown. Total CCA porosity and permeability from adjacent core plugs are also indicated for comparison (white tables). SEM images show the dominant microporous texture, which is reflected in the difference between total porosity and macroporosity. Shifted depths in metres are indicated.

III.1.5.3. Non-contiguous colour selection

The results from this applied methodology show that the highest tolerance value defined to maximize macropores selection tends to overestimate total macroporosity in samples with a dual macro and microporosity network, as it will include pixels of darker micritic patches or image artifacts within portions of micritic particles or micritic matrix, when present (Figure III.1.12). Measurements using the maximum tolerance value were therefore not considered in the calculation of average macroporosity for these samples. In micritic samples with virtually no macroporosity, only the minimum tolerance was considered when applying the colour selection methodology, as the higher tolerance values were verified to consistently include darker patches within the micritic matrix, overestimating macroporosity, as well (Figure III.1.12).

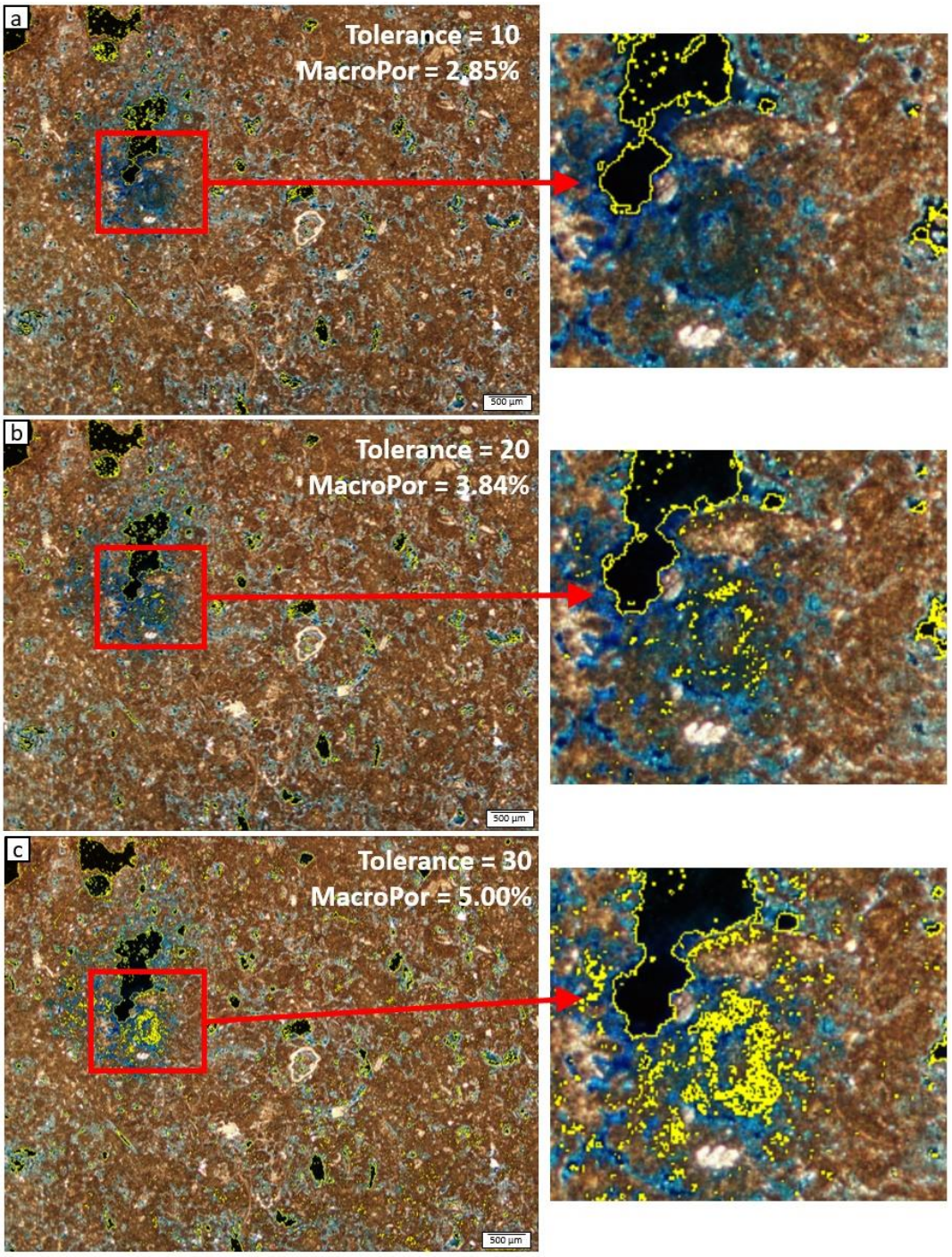

Figure III.1.12. The effects of applying different tolerance values for the same RGB parameters. Increasing tolerance values from (a) to (c) result in slightly higher macroporosity measured in (b) and in (c), but also leads to the selection of areas within the micritic matrix.

During the result verification process, a limited number of images showed erroneous macroporosity measurements which were related to variations in brightness and contrast of the acquired image or image artifacts, affecting the outcome of pixel counting through colour selection. The range of applied parameters was adapted and results were corrected for these

images. Such limitations expose the pitfalls and uncertainty levels associated with variable image properties/parameters when applying this methodology. The non-contiguous colour selection methodology offers a range of macroporosity values for each image analysed, with a final verified average value being calculated (Figure III.1.13).

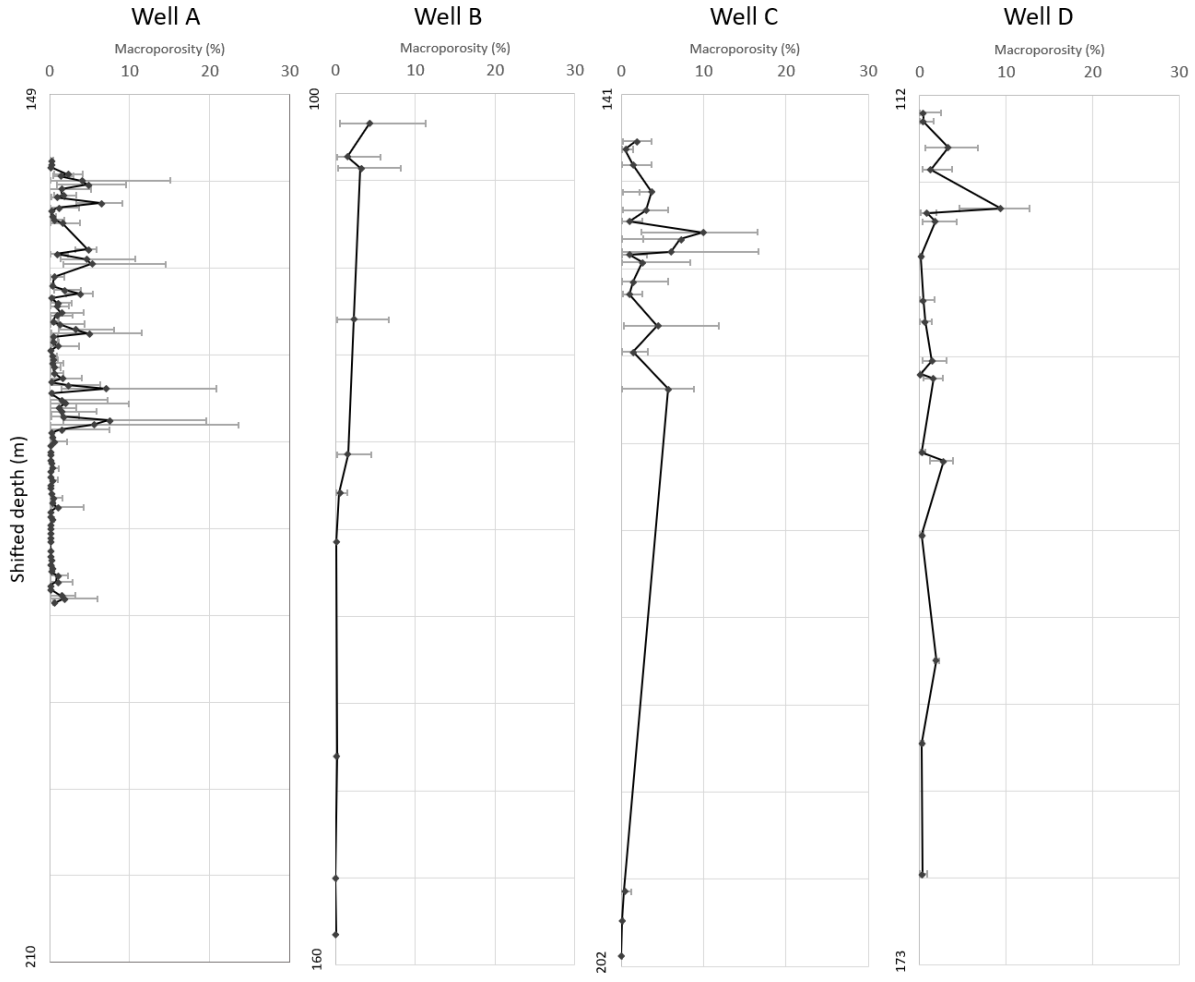

Figure III.1.13. Verified average macroporosity measurements from the colour selection methodology. Horizontal bars represent minimum and maximum measurements resulting from the range of RGB and tolerance values applied. Vertical axis represents shifted depth in metres. The full reservoir zone is represented.

III.1.5.4. Machine learning

The results obtained from guided machine learning are similar to the results from visual estimation and non-contiguous colour selection. The three data sets show similar trends and variability, although the absolute values are different (Figure III.1.14). Reference well A, with a higher density dataset, shows the marked transition from the more homogeneous microporous wackestone interval with extremely low or null macroporosity into the more heterogeneous upper half of the reservoir showing stronger variability in macroporosity and dominated by

dual macro/microporosity packstone, grainstone and rudstone-grainstone facies (Figures III.1.14, III.1.15). This transition occurs approximately at the top of SZ3L (Figures III.1.2, III.1.15).

Macroporosity trends are considerably different from total porosity trends (Figure III.1.15). There is a strong general decrease in macroporosity with depth, which is strongly related to facies variations, from rudstone-grainstones, grainstones and packstones in the upper half of the UKM, into wackestones in the lower half, reflecting the primary depositional controls on macroporosity variability. Grainstones generally show the highest macroporosity measurements (varying between 4 and 14 %), while packstone samples show only 2 measurements above 5 % and wackestones show macroporosity generally lower than 1 % (with most measurements below 0.1 %).

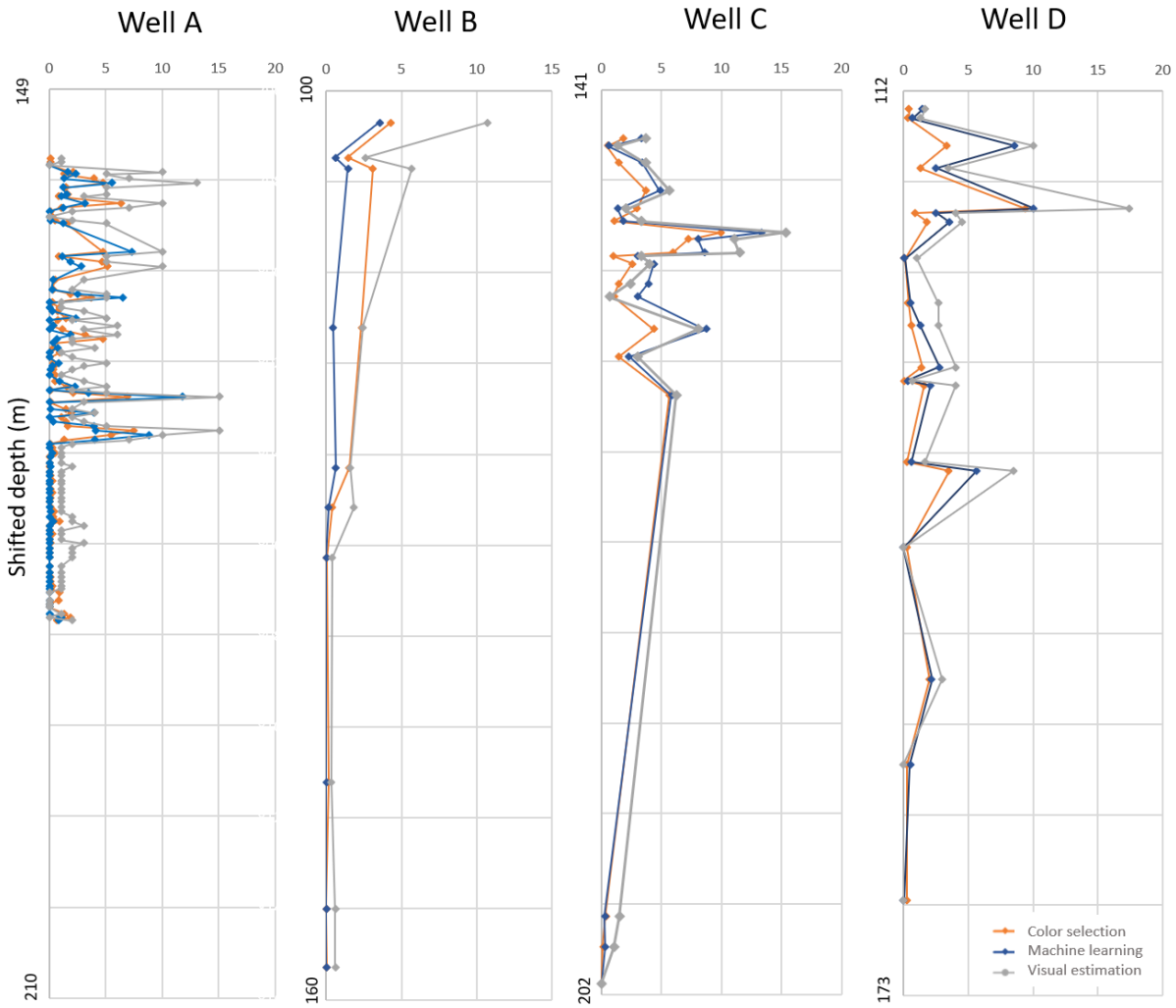

Figure III.1.14. Reviewed results for total macroporosity acquired from the different methodologies. Horizontal axis in the four plots represent the percentage of macroporosity. Vertical axis represents shifted depth in metres. The full reservoir zone is represented.

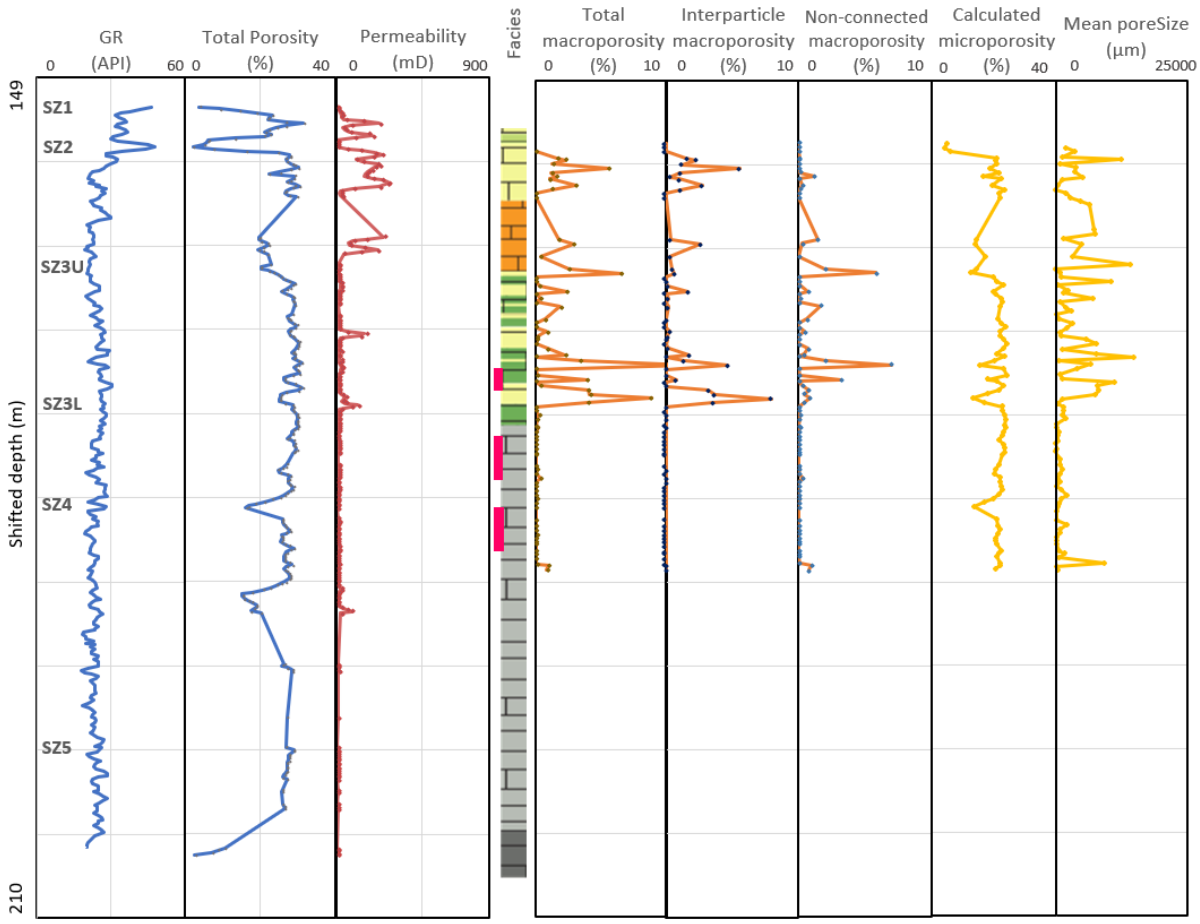

Figure III.1.15. Composite panel for reference well A, showing Gamma ray (GR), core porosity, core permeability, depositional facies (see Figure III.1.2 for colour code; identified dolomitized zones are in pink), measured porosity types and average pore size based on DIA (machine learning). SZ tops (SZ1 to SZ5) are indicated on the GR log. Vertical axis represents shifted depth in metres.

III.1.6. Discussion

III.1.6.1. Comparing the outcome of the different methodologies

While the overall variation trends in macroporosity measured using the different methodologies are identical, moderate disparity is observed between the resulting values, as previously mentioned. Overall, visual estimation methods tend to result in higher macroporosity values than the semi-automated methodologies (Figures III.1.14, III.1.16). The colour selection methodology provides relatively lower values generally in Well D, for packstone/grainstone facies of Well C and relatively higher values in the upper half of the reservoir in Well B (Figure III.1.14). When comparing the colour selection method with guided machine learning, the results are similar and correlatable for packstones, grainstones and rudstone-grainstones, although some differences occur (Figure III.1.16a). However, machine learning tends to capture higher detail and the stronger variability in images with macroporosity lower than 1 % and 0.1 % (Figure III.1.16a) in wackestones, which are almost fully characterized by

microporosity, with most of the macroporosity representing less than 1 %. This difference regarding the quantification of smaller macropores would be related to the uncertainty associated with the parameters defined for colour selection and with the minor colour variability occurring within each image.

Measurements through visual estimation result in thin sections with practically null macroporosity (but not 0 %) being reported as having a value of 1 %, due to user-related limitations and the difficulty in visually differentiating between macroporosity values below 1 %. This explains the lower-limit truncation observed on the cross-plots (Figure III.1.16b, c). Visual estimations are generally higher than results from both semi-automated DIA methodologies (Figure III.1.16b, c).

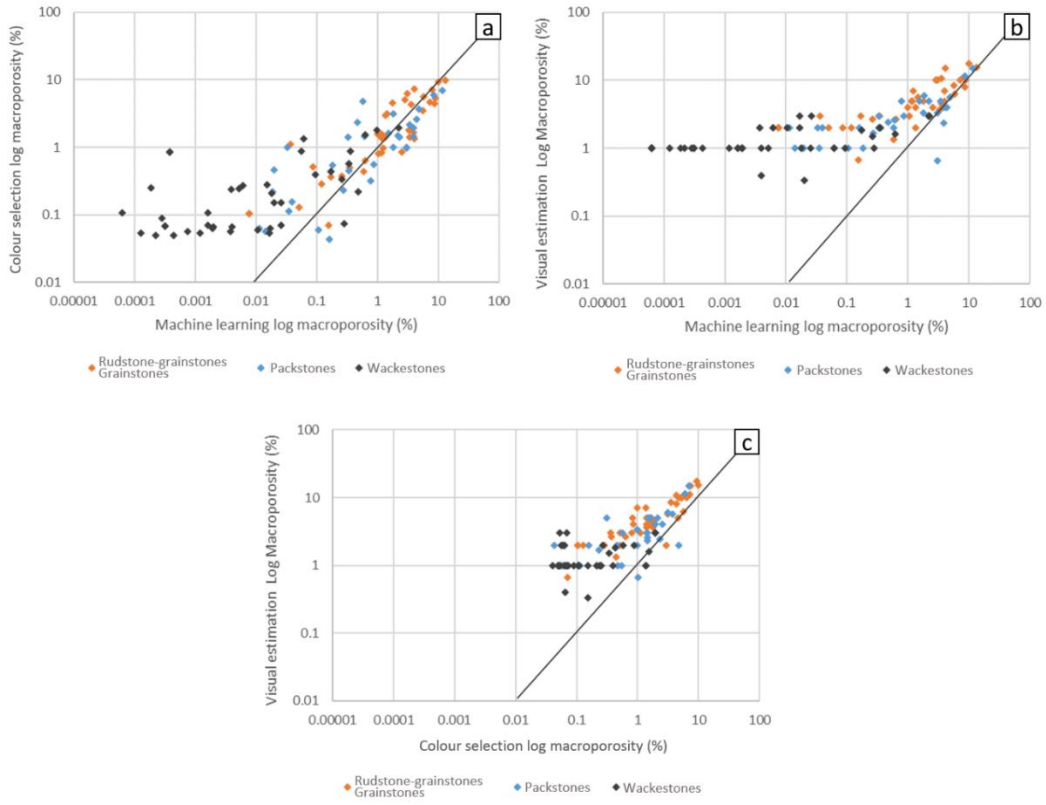

Figure III.1.16. Cross-plots comparing the three applied methodologies. a: correlation coefficient = 0.79; b: correl. coeff. = 0.86; c: correl. coeff. = 0.80. The black line in each plot represents a 1:1 relationship.

Six selected samples are here presented as examples to compare the results from the different methodologies with fully manual measurements done through colour selection and pixel counting (Table III.1.1). Using this manual approach, tolerance values are increased until the full macroporous area is included, in order to maximize the selection of macroporosity. The segmented image will show a certain amount of noise (Figure III.1.17), slightly overestimating

macroporosity. The machine learning methods will minimize the level of noise and artifact selection during segmentation, showing lower results than manual measurements (Table III.1.1, Figure III.1.17). Overall, and after the verification against manually measured macroporosity in selected control samples, colour selection and visual estimation methods are considered to offer less consistent results when compared to machine learning, offering results that are both higher and lower than the reference manual measurement, depending on the analysed image (Table III.1.1). This uncertainty will be closely related to user-dependent and image acquisition issues, as previously mentioned. In this case study, the machine learning methodology is seen as offering the most objective and consistent results and is therefore considered as the reference dataset for macroporosity estimation in the analysed wells. In addition, this methodology will capture higher details in microporosity-dominated intervals, as mentioned above.

Table III.1.1. Comparison between manually measured macroporosity values with visual estimation, semi-automated colour selection and machine learning for selected samples. The differences between the results from each method and manual measurements are shown, as well as the average value for absolute differences. Machine learning values are consistently lower, while visual estimation and colour selection result in both positive and negative differences (Diff.).

	Manual measurement	Visual estimation		Machine learning		Colour selection	
		Result	Diff.	Result	Diff.	Result	Diff.
Sample a	0.99	**1**	0.01	**0.06**	*-0.94*	**1.81**	*0.81*
Sample b	3.29	**2**	-1.29	**0.98**	*-2.31*	**2.46**	*-0.84*
Sample c	1.86	**2**	0.14	**0.19**	*-1.67*	**2.31**	*0.44*
Sample d	2.57	**2**	-0.57	**0.51**	*-2.06*	**1.66**	*-0.92*
Sample e	3.80	**2**	-1.81	**0.50**	*-3.31*	**3.74**	*-0.07*
Sample f	1.12	**5**	3.88	**0.51**	*-0.61*	**0.96**	*-0.16*
Averages of absolute diff. values			*1.28*		*1.82*		*0.54*

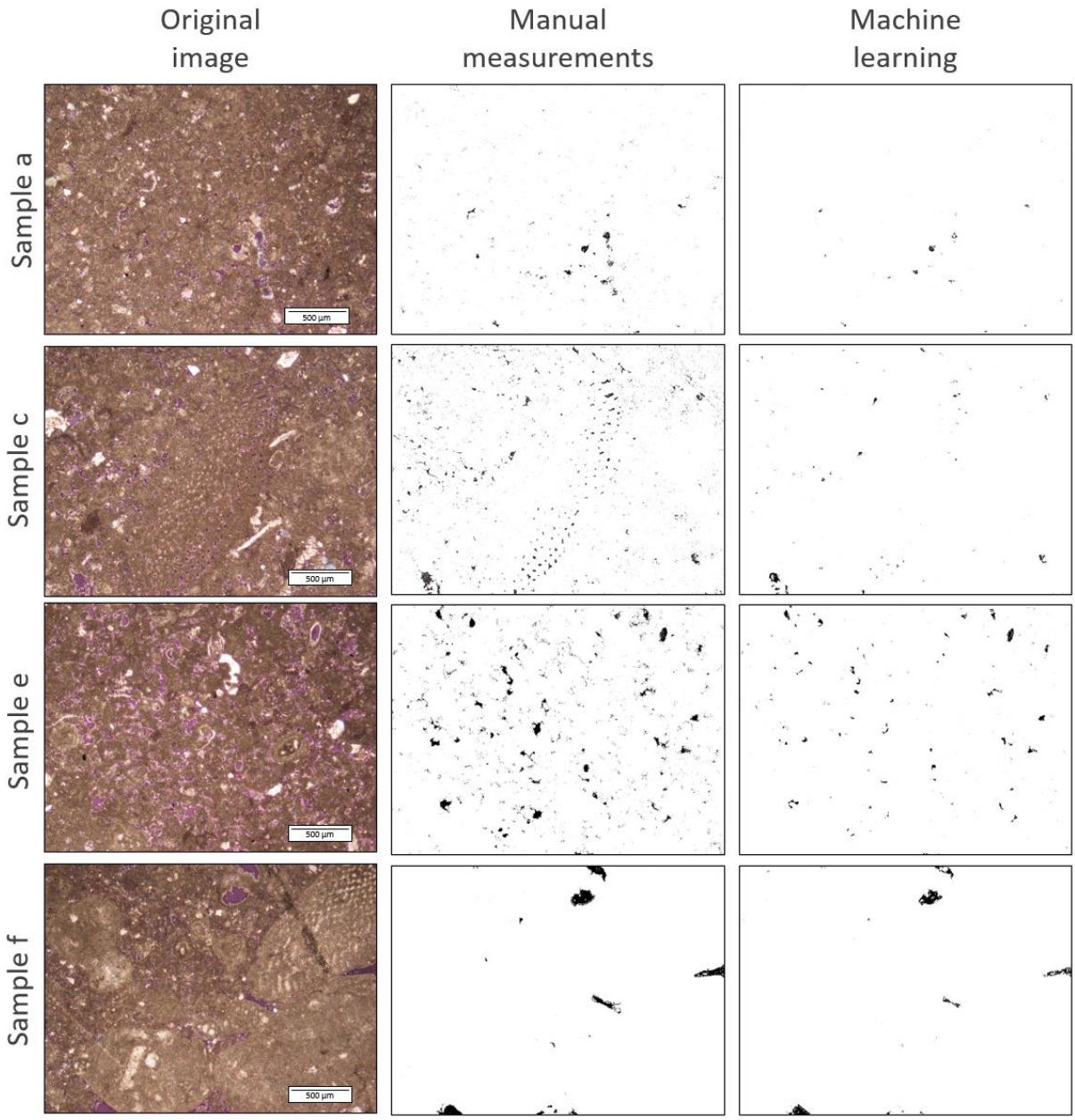

Figure III.1.17. Comparing original thin section photos with segmented images through manual measurements and through trained machine learning. Results from manual measurements show higher detail but also some amount of 'noise' generated, slightly overestimating macroporosity. In sample c, for example, intraparticle macroporosity within the micritized orbitolinid is more clearly visible on the result from manual colour selection, while in the machine learning result this macroporosity is only partially represented, although generated 'noise' is considerably lower in the latter. The values are presented in Table III.1.1 above.

III.1.6.2. Vertical variability in total porosity and macroporosity

As previously mentioned, total porosity in the UKM shows very weak vertical variability for each well (Figure III.1.3), in contrast with permeability, which is considerably higher in the upper half (Figures III.1.2, III.1.15), as generally observed and previously reported for the UKM in Abu Dhabi (e.g. Harris et al., 1968; Alsharhan, 1993; Alsharhan and Nairn, 1997; Grötsch et al., 1998; Van Buchem et al., 2002; Strohmenger et al., 2006; Ehrenberg et al., 2018, 2020a). On a larger scale, total porosity shows relatively stronger variability with depth, with shallower wells generally preserving slightly higher total porosity (Figure III.1.18). Such variability with depth has been reported for this interval in Abu Dhabi (e.g. Oswald et al., 1995; Melville et al., 2004; Ehrenberg et al., 2020a) and generally for Cretaceous reservoirs in the Arabian Platform (e.g. Ehrenberg et al., 2008). The more homogeneous wackestone intervals show values between approximately 25 and 30 % in the deeper wells and between 28 and 33 % in the shallower wells.

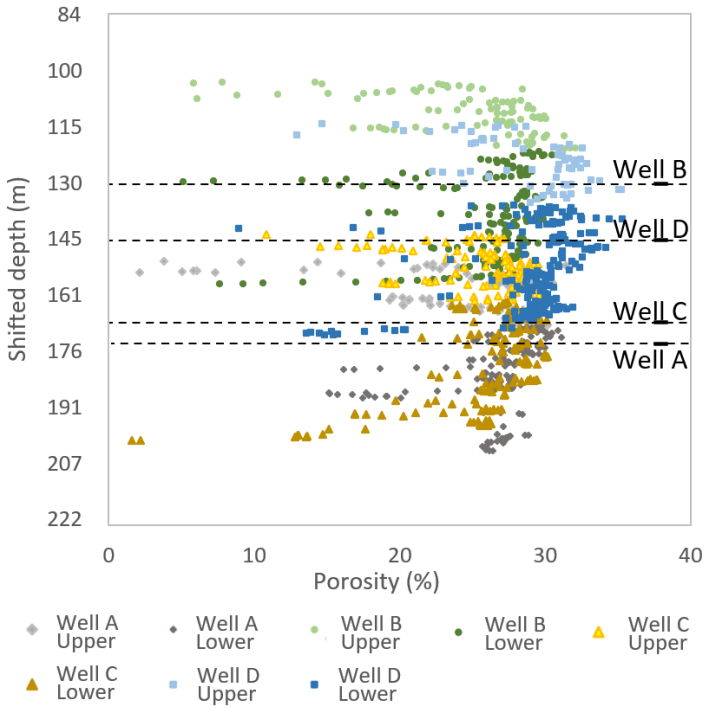

Figure III.1.18. Total porosity from the four different wells plotted against depth. The upper (more heterogeneous) and lower (more homogeneous) reservoir intervals are differentiated using different colours. Vertical axis represents shifted depth in metres.

As mentioned above, in addition to being influenced by the textural nature of the sample, macroporosity variability is also affected by diagenetic factors, such as compaction and calcite cementation, amongst other factors. This will be further discussed in Chapter III.2, as a

continuation of this study, in an attempt to integrate the results from this semi-quantitative pore type analysis with petrographic and petrophysical data.

In order to illustrate the vertical variability in macroporosity, data from the more densely-sampled reference well A is here discussed. Analysing a single well individually will also eliminate the potential influence of factors controlling lateral variability (see Chapter III.2). In well A, higher macroporosity is recorded in the basal part of SZ3U and top zone of SZ2, with a few high peaks in between (Figure III.1.15), corresponding to intervals with generally larger average pore size (Figure III.1.15). Samples with total porosity below approximately 20 % correspond to intervals that are close to the subzone boundaries, which are characterized by increased clay content (e.g. Ehrenberg et al., 2016, 2018). Stronger dissolution and cementation of original pore space is observed in the immediately adjacent layers (e.g. Davies et al., 2002; Paganoni et al., 2016; Ehrenberg, 2019).

The more heterogeneous SZ2 and SZ3U in well A show minimum and maximum total macroporosity values of 0 % and 11.68 %, averaging at 1.80 % (Table III.1.2). In these subzones, macroporosity accounts for up to 31.64 % of total porosity in the analysed images (4.16 % on average). Macroporosity is considerably lower than total measured porosity for grainstone and rudstone-grainstone textures, due to the relatively large volumes of microporosity developed in the micritized particles (Figure III.1.19; Morad et al., 2016). Total CCA porosity in this well has an average value of 26.5 %, considering all subzones, with microporosity representing between 62 and 100 % of total porosity in the analysed intervals. In the more homogeneous microporous basal section only (SZ4 and SZ3L), micropores represent between 95 and 100 % of total porosity. Macroporosity in this lower section is virtually non-existing and, when present, is represented by mouldic/vuggy porosity, as previously mentioned. Considering the full dataset in all wells, microporosity generally represents more than 62 % of total porosity, with only two samples below this value, at 51 % in well C and 58 % in well D (Figure III.1.19c, e).

Table III.1.2. Comparing porosity types between the studied intervals in subzones 2, 3U, 3L and 4 in reference well A.

		Total porosity	Total macro-porosity	Interparticle macro-porosity	Non-connected macro-porosity	Micro-porosity
Heterogeneous section (SZ2, 3U)	avg	26.69	1.80	1.12	0.69	24.89
	min	7.03	0.00	0.00	0.00	7.30
	max	31.12	11.68	7.98	7.01	30.33
Homogeneous section (SZ3L, 4)	avg	27.10	0.09	0.01	0.08	27.01
	min	16.89	0.00	0.00	0.00	16.87
	max	30.00	0.99	0.07	0.94	29.84

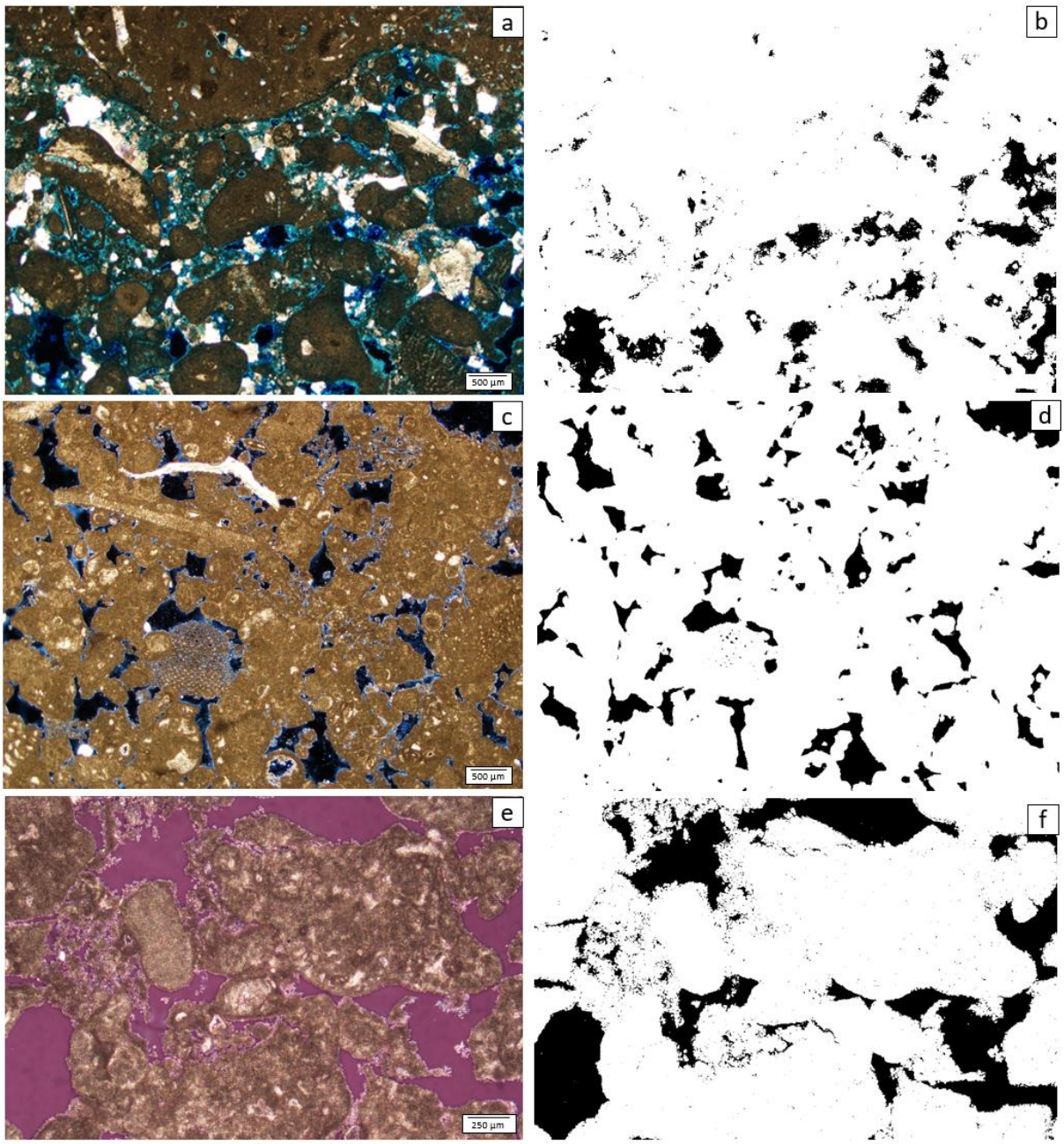

Figure III.1.19. Comparing total porosity and measured macroporosity in examples of grainstone facies from different wells. **a:** well A, SZ3U. Total porosity = 25.2 %; **b:** macroporosity in black = 8.9 %; **c:** well D, SZ1. Total porosity = 20.2 %; **d:** macroporosity in black = 8.6 %; **e:** well C, SZ2. Total porosity = 27.4 % **f:** macroporosity in black = 13.3 %.

III.1.6.3. Brief insight into factors controlling porosity/permeability variations

The correlation between permeability and total porosity is non-existing for the full dataset (correlation coefficient of -0.06), reflecting the difficulty in predicting permeability from total porosity. When differentiating between facies, this correlation is clearer for the more homogeneous, microporous wackestones but is increasingly weaker for facies with a more heterogeneous pore network (Figure III.1.20a), as has also been reported in previous studies

(e.g. Fullmer et al., 2014; Ehrenberg, 2019). Total macroporosity measured through DIA and guided machine learning offers a better predictor for permeability, as expressed by the higher correlation factor of 0.37 (Table III.1.3) and as visually expressed by the permeability-porosity cross plots (Figure III.1.20). The correlation coefficient between permeability and measured interparticle macroporosity is higher, at 0.45 (Table III.1.3), although this requires the integration of information acquired through visual estimation, in order to differentiate between types of macropores. At larger field and regional scales, when considering average permeability and porosity values for the full UKM stratigraphic interval per well, the correlation factor is improved (e.g. Alsharhan, 1990; Oswald et al., 1995; Ehrenberg et al., 2020b), although in these cases, small-scale details are filtered-out and lost in the process.

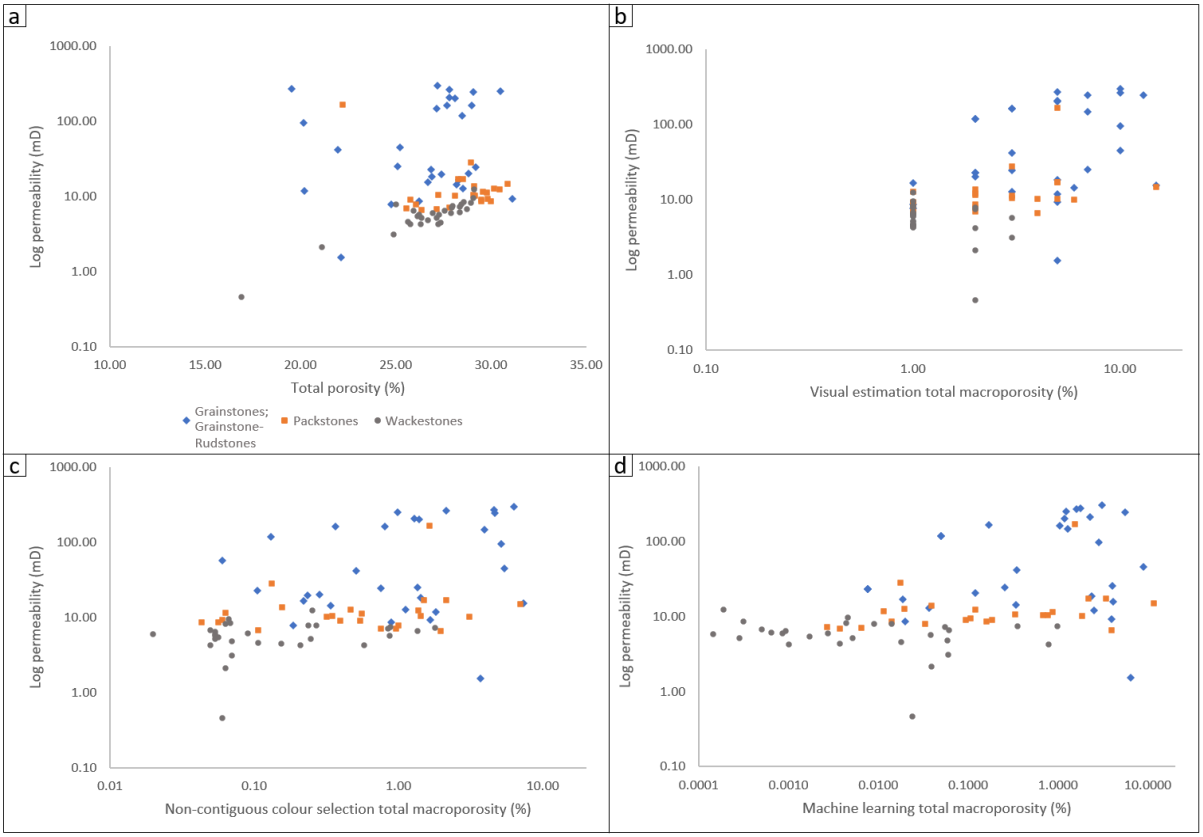

Figure III.1.20. Permeability-porosity cross plots. CCA permeability is plotted against total porosity from CCA (**a**), visually estimated total macroporosity (**b**), total macroporosity measured through non-contiguous colour selection (**c**) and total macroporosity measured through trained machine learning (**d**). A seemingly better correlation is obtained between permeability and machine learning macroporosity, in contrast to the correlation between permeability and total CCA porosity.

The variability in permeability is controlled by the variations in pore size and pore throat size, which in turn is associated with the variability in depositional facies and diagenetic factors (e.g. Lucia, 1983; Wardlaw, 1996; Ehrenberg et al., 2008; Ehrenberg, 2019; Swei and Tucker, 2012;

Hollis et al., 2017). In the studied wells, the depositional facies control on permeability and macroporosity variability is expressed by the moderate correlation coefficients of 0.44 and 0.40, respectively (Table III.1.3). Petrographic analysis shows that higher permeability values correspond to grainstone-dominated intervals of SZ2 and SZ3U, which show increased measured interparticle macroporosity, in moderate similarity to the observations reported for nearby fields (e.g. Alsharhan, 1990; Ehrenberg, 2019). Average pore size shows no clear correlation with other parameters, showing only poor correlation with permeability and facies (0.27 and 0.25, respectively). This might, in part, be explained by the utilized methodology, which measures all macropores without differentiating between interparticle and mouldic (or vuggy) macropores. The latter will most likely have very little or null contribution to fluid flow, or permeability.

With all correlation coefficients below 0.50, the results show there is no clear unique permeability predictor, but a probable combination of different depositional and diagenetic parameters and controlling factors. A more detailed analysis of these controlling factors will be discussed in Chapter III.2.

Table III.1.3. Correlation matrix between different parameters for the full dataset.

	Depth	CCA Permeability	CCA Porosity	Total macro-porosity	Interparticle macroporosity	Non-connected macroporosity	Calculated microporosity	Facies	Mean pore size
Depth	1.00								
CCA Permeability	-0.29	1.00							
CCA Porosity	-0.05	-0.06	1.00						
Total macro-porosity	-0.12	**0.37**	-0.02	1.00					
Interparticle macroporosity	-0.13	**0.45**	0.02	0.91	1.00				
Non-connected macroporosity	-0.03	-0.05	-0.09	0.52	0.12	1.00			
Calculated microporosity	0.02	-0.24	0.86	-0.53	-0.45	-0.34	1.00		
Facies	**-0.40**	**0.44**	-0.02	**0.40**	**0.38**	0.17	-0.22	1.00	
Mean pore size	-0.15	0.27	0.08	0.16	0.19	-0.01	-0.02	0.25	1.00

III.1.7. Conclusions and final remarks

Quantifying pore types and addressing pore type distribution within the reservoir zone(s) is vital for proper reservoir characterization, improved model construction, understand reservoir performance and, ultimately, assist in field development decisions. In the 4 studied wells, total porosity shows very little variation throughout the reservoir and shows a weak correlation with permeability. Separating porosity into its different types offers an improved understanding of the reservoir, as well as relatively better permeability predictability using interparticle macroporosity measurements. Interparticle macroporosity shows a stronger correlation with permeability (correlation coefficient of 0.45) when compared to the weak correlation between permeability and total porosity (correlation coefficient of -0.06). Microporosity represents the largest fraction of total porosity (generally more than 60 %), contributing very little to fluid flow and holding large amounts of hydrocarbons in place, affecting oil recovery efficiency. Macroporosity is generally low, reaching up to 13 % in the analysed samples of the upper half of the reservoir, and is virtually null in the lower half.

While the methodologies here utilized provide valuable quantitative data that can be used to improve the understanding on the controls on reservoir heterogeneity, they are still associated with some uncertainty. Visual estimation is a relatively quick method for obtaining the relative volumes of sample constituents, as well as macroporosity. While this method provides results that respect the true variability trends of each parameter analysed, the absolute values will deviate from reality. The more objective pixel counting approaches based on non-contiguous colour selection and trained machine learning methodologies reduce the amount of subjectivity associated with visual estimation methods, improving the consistency of the results. However, the DIA methods will also be associated with some uncertainty related to the overall image quality and consistency. Considerable amounts of user-end input is required when using these methodologies, regarding data preparation, quality control and result verification. The amount of training images applied to machine learning is defined by the user and will depend on the variability of the data to be analysed, with increasingly heterogeneous datasets requiring higher amounts of training images. For the present study, the selected trainings images were considered to be sufficient, with the total set of thin sections photos being divided into batches with comparable visual properties.

The trained machine learning methodology was considered to offer more consistent results, when compared to visual estimation and non-contiguous colour selection methodologies. The integrated analysis of these results with wireline logs and core data increases the efficiency and objectivity of petrographic interpretations, helping in obtaining a detailed view of the geological properties of the reservoir. These semi-automated, user-guided methodologies help to reduce the work load in petrographic analysis and to identify and measure macroporosity, although user-driven verification and quality control steps are still indispensable.

III.2. Heterogeneity and macroporosity distribution in the Lower Cretaceous upper Kharaib Formation

III.2.1. Abstract

The Barremian Upper Kharaib Member of the Kharaib Formation (Thamama Group, Abu Dhabi) was deposited in a carbonate ramp setting and shows moderate vertical facies variability, transitioning from a transgressive phase dominated by wackestone facies into a regressive phase with dominant packstone, grainstone and rudstone-grainstone facies towards the top. A dual-porosity system containing micro and macro-pores characterizes this reservoir, with microporosity as a dominating fraction of total porosity. While total porosity in the reservoir section shows no clear vertical trends, permeability is significantly higher in grainstone and rudstone-grainstone facies, affecting the reservoir performance and oil recovery efficiency. In order to acquire an improved understanding of the controls on rock properties variations, 4 wells in a giant onshore field in Abu Dhabi were analysed, by integrating petrographic data with quantitative data on pore types and pore type distribution obtained through digital image analysis.

Small-scale, discontinuity-bounded intervals generally showing fining-upwards facies trends were identified in the Upper Kharaib Member. These depositional trends indicate deposition under the influence of varying energy levels controlled by hydrodynamics, enhanced by storm events. This rhythmic facies variability is different from well to well, which indicates a complex depositional architecture and limited lateral extension of geobodies. This spatial variability in reservoir properties is difficult to predict in inter-well areas. However, the high-permeability intervals are mainly characterized by well-sorted porous grainstones in the studied wells, suggesting that strong permeability variations are, therefore, linked to depositional facies distribution and interparticle macroporosity variability in this field. Macroporosity distribution is, therefore, a useful parameter for better understanding reservoir heterogeneity, which can be obtained through the semi-automated digital analysis of thin section images.

Integrating semi-quantitative petrographic and petrophysical data with digital image analysis results provides further insights into the factors controlling heterogeneity in rock properties, offering invaluable information for the development of reservoir models with improved geological meaning, potentially offering higher degrees of predictability.

III.2.2. Introduction

The Barremian carbonate Upper Kharaib Member (UKM) of the Kharaib Formation in the Lower Cretaceous Thamama Group is the most important reservoir in Abu Dhabi (U.A.E.), holding large amounts of hydrocarbons in place (e.g. Lijmbach et al., 1992; Alsharhan, 1993; Taher, 1996; Alsharhan and Nairn, 1997).

This reservoir shows strong facies and permeability heterogeneity, with well-known vertical facies variability, as well as vertical variations in permeability; in contrast, total porosity is similar throughout and relative lateral homogeneity is observed at a larger scale (e.g. Harris et al., 1968; Alsharhan, 1993; Alsharhan and Nairn, 1997; Grötsch et al., 1998; Van Buchem et al., 2002; Strohmenger et al., 2006; El Wazir et al., 2015; Ehrenberg et al., 2016, 2018, 2020a, 2020b; Jeong et al., 2017). The reservoir rock is generally characterized by a dual-porosity macro and microporosity network, where microporosity is the dominant fraction by volume (e.g. Harris et al., 1968; Budd, 1989; Oswald et al., 1995; Morad et al., 2016; Ehrenberg, 2019). This microporous space holds volumes of hydrocarbon in place and contribute very little to fluid flow, while high permeability layers represent the main drivers for fluid flow, in some cases leading to early water breakthrough (e.g. Namba and Hiraoka, 1995; Wardlaw, 1996; Cunningham and Chaliha, 2002; Dabbouk et al., 2002; Carvalho et al., 2011). To obtain a better understanding of this dual porosity system and the controls on the distribution of pore types is of great importance and will improve reservoir modelling efforts.

The strong vertical variation in permeability through the reservoir has been discussed in published papers and is seen as a combined product of depositional and diagenetic controls (e.g. Harris et al., 1968; Oswald et al., 1995; El Wazir et al., 2015; Ehrenberg et al., 2016; Ehrenberg, 2019). Many sedimentological and diagenetic studies on this reservoir have been published, allowing for the comparison of different geological parameters and features between the studied field and other fields in Abu Dhabi (e.g. Alsharhan, 1990, 1993; Grötsch et al., 1998; Van Buchem et al., 2002; Strohmenger et al., 2006; Cox et al., 2010; El Wazir et al, 2015; Morad et al, 2016; Ehrenberg et al., 2016; Ehrenberg, 2019; Jeong et al., 2017), with a number of recent studies giving increased attention to the controls on small-scale cyclicity and petrophysical heterogeneity in Abu Dhabi reservoirs (e.g. Jeong et al., 2017; Shekhar et al., 2017; Ehrenberg et al., 2018, 2020b; Ehrenberg, 2019).

In order to obtain further insights into the controls on facies and reservoir properties heterogeneity, the present study analyses data from 4 crestal wells across the elongated axis of an onshore field in the southeast of Abu Dhabi, including cores and thin sections, with attention given to small-scale facies variability. Facies characterization was done in integration with petrophysical data available from core analysis and with quantitative data on pore type distribution obtained through digital image analysis (DIA). While plug-measured porosity obtained from conventional core analysis (CCA) provides total porosity values and makes no

distinction between macro- and microporosity, DIA provides objective and semi-automated quantitative macroporosity data. This information will help to better describe the pore system and pore type distribution, allowing for a better understanding of the controls on reservoir heterogeneity. The main objective of this study is to evaluate the links between facies variability and petrophysical heterogeneity for this reservoir in the studied field.

III.2.3. Geological Background

The Barremian UKM was deposited in the Rub Al Khali Basin, which represents an Arabian Plate depression created through tectonic differentiation (Figure III.2.1a) (e.g. Powers et al., 1966; Murris, 1980; Soliman and Al Shamlan, 1982; Alsharhan and Nairn, 1997). It is one of the most prolific hydrocarbons producing basins in the world, holding all major fields in the U.A.E and covering substantial areas of Saudi Arabia and Oman (e.g. Lijmbach et al., 1992; Alsharhan, 1993; Taher, 1996; Alsharhan and Nairn, 1997). This basin extends into the Arabian Gulf and is bounded to the north-northeast by the Zagros mountains, to the east-southeast by the Oman mountains, to the west-northwest by the Central Arabian and Qatar archs and Arabian shield, and to the south by the Hadhramout arch (Figure III.2.1) (e.g. Powers et al., 1966; Murris, 1980; Alsharhan and Nairn, 1997). In the Abu Dhabi area of the Rub Al Khali Basin, three intrashelf sub-basins have developed at different times (Late Jurassic, Early Cretaceous and Middle Cretaceous) covering approximately the same area (e.g. Murris, 1980; Vahrenkamp et al., 2015b).

During the Late Cretaceous (Campanian), the overthrust and emplacement of the Semail Ophiolites on the Cretaceous carbonate section eastwards of the Rub Al Khali Basin, led to the creation of the Oman mountains, with signs of plate convergence as early as the Cenomanian (e.g. Searle, 1988; Loosveld et al., 1996; Searle et al., 2014). This event caused deformation of the strata in Abu Dhabi, contributing to the creation of the north-south giant anticlines where the important oil fields and producing reservoirs of the Lower Cretaceous Thamama Group are found today (e.g. Oswald et al., 1995; Alsharhan and Nairn, 1997; Richard et al., 2017). These giant structures show trends similar to the deep basement fault lineaments and are reported to have been enhanced by the reactivation of these deep faults (e.g. Alsharhan, 1989; Alsharhan and Nairn, 1997; Johnson et al., 2005; Glennie, 2010; Stewart, 2016).

The obduction of the Masirah ophiolite to the east/southeast during the Palaeocene (e.g. Peters and Mercolli, 1997; Richard et al., 2017), with evidence for activity starting in the Late Cretaceous (e.g. Loosveld, 1996), followed by the Zagros collision to the north starting towards the Oligocene (e.g. Searle, 1988; Oswald et al., 1995; Agard et al., 2011; Searle et al., 2014) and continuing to the present day (e.g. Ellouz-Zimmermann et al., 2007; Blanc et al., 2003),

have led to further restructuration in Abu Dhabi, and tilting of the strata towards the north-northeast (Figure III.2.2).

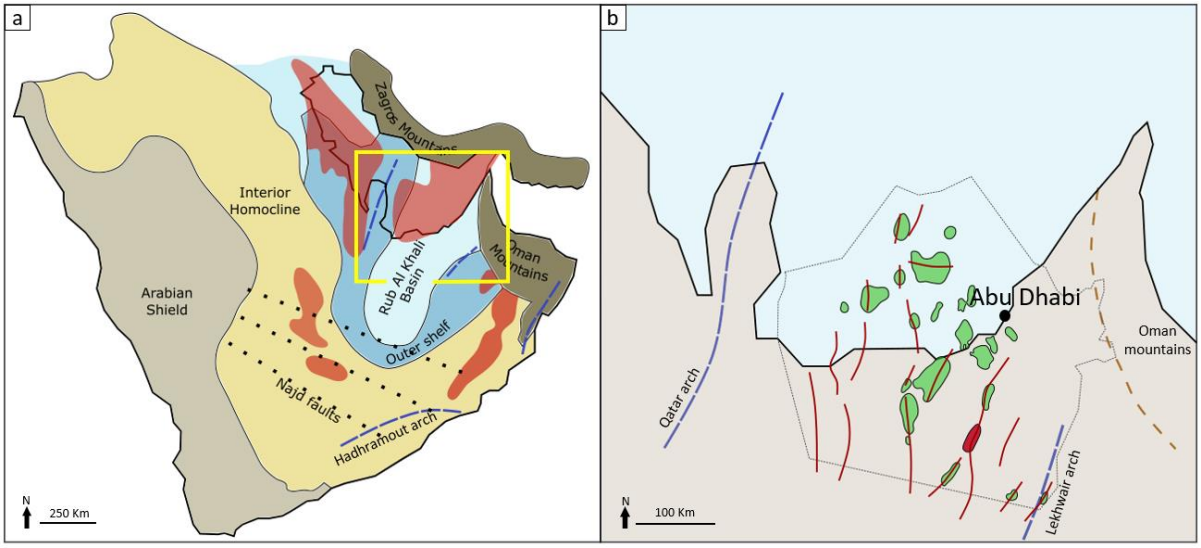

Figure III.2.1. **a**: Structural provinces and location of Rub Al Khali sub-basin in the Arabian Peninsula (based on Powers et al., 1966; Schlumberger, 1981; Alsharhan and Nairn, 1997; Pierson et al., 2010; Thomas et al., 2015; Stewart, 2016). Cambrian Hormuz salt basins are represented in red (based on Glennie, 2010; Thomas et al., 2015; Stern and Johnson, 2010); **b**: Map of Abu Dhabi with location of major fields and main structural trends in red (based on Schlumberger, 1981; Alsharhan and Nairn, 1997; Strohmenger et al., 2006).

III.2.3.1. Stratigraphic context

Following a Triassic evaporitic platform, the Early Jurassic in Abu Dhabi is characterized by a vast carbonate-evaporite platform with widespread carbonate deposition. The Jurassic, as well as the Cretaceous in Abu Dhabi are typified by shallow-water carbonates accumulating in shelf and inner platform environments. The end of the Jurassic is marked by extensive deposition of evaporites before a return to carbonate sedimentation and a ramp-type depositional environment in the Early Cretaceous (e.g. Murris, 1980; Alsharhan, 1989; Alsharhan and Nairn, 1997).

The UKM of the Kharaib Formation is part of the Thamama Group, which represents a Lower Cretaceous Berriasian to Aptian succession bounded by two major unconformities (Figure III.2.2) (e.g. Alsharhan, 1990; Alsharhan and Nairn, 1997; Van Buchem et al., 2002, 2010; Davies et al., 2002). This Group is described as having an overall ‘layer cake’ stratigraphy characterized by carbonate reservoir zones interlayered with argillaceous limestones, showing lateral continuity over large distances, reflecting deposition in a widespread epeiric carbonate platform under the influence of minor or null tectonic activity (e.g. Harris et al., 1968; Murris, 1980; Alsharhan, 1989; Azer and Toland, 1993; Alsharhan and Nairn, 1997).

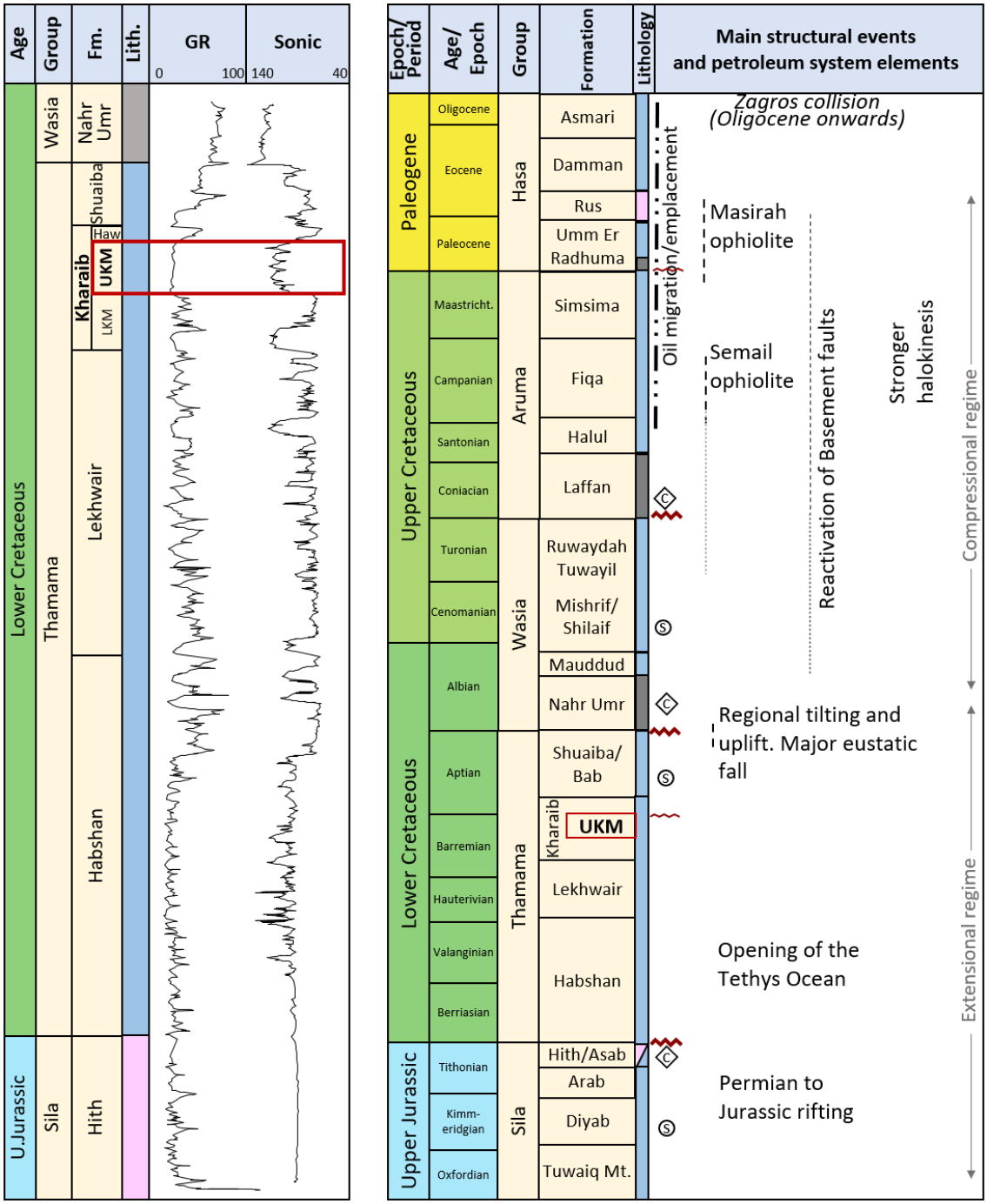

Figure III.2.2. **Left**: Typical GR, sonic log signature and general lithology for the Thamama Group. Pink: anhydrite; blue: limestone; grey: shale (Alsharhan and Kendall, 1991). Note the GR cyclicity from the upper Habshan Formation to the Kharaib Formation. Red box indicates the studied Upper Kharaib Member (e.g. Van Buchem et al., 2002, 2010). (LKM = Lower Kharaib Member, UKM = Upper Kharaib Member, Haw = Hawar Member) **Right**: Simplified stratigraphic succession of Abu Dhabi from Upper Jurassic to Cenozoic (blue: limestone dominated; grey: shales; pink: anhydrite). Studied UKM interval is indicated in red. Major source rock (s) and cap rock (c) intervals are indicated (based on Alsharhan, 1993; Alsharhan and Nairn, 1997; Alsharhan, 2014). Main unconformities are indicated (red wavy lines), as well as main tectonic events (based on Searle, 1988; Peters and Mercolli, 1997; Loosveld et al., 1996; Alsharhan and Nairn, 1997; Agard et al., 2011; Searle et al., 2014; Al Kindi and Richard, 2014; Vahrenkamp et al., 2015b; Richard et al., 2017; Bazalgette and Salem, 2018).

III.2.3.1.1. The Upper Kharaib Member

The UKM carbonate sediments were deposited in a stable carbonate platform connected with the Tethys ocean towards the east-northeast (e.g. Murris, 1980; Alsharhan, 1989; Alsharhan and Nairn, 1997; Van Buchem et al, 2002; Strohmenger et al, 2006), while to the west, in Saudi Arabia, the Barremian is characterized by the siliciclastic sediments of the Biyadh Formation deposited in closer proximity to the Arabian shield (e.g. Murris, 1980; Soliman and Al Shamlan, 1982; Alsharhan and Nairn, 1997; Davies et al., 2002).

The UKM, together with the underlying dense zone are defined by a 3rd order transgressive-regressive cycle (Figure III.2.3) (e.g. Azer and Toland, 1993; Van Buchem et al, 2002, 2010; Strohmenger et al, 2006). This interval shows an overall shallowing trend, generally developing from low-energy, deeper-water mudstones and wackestones into high-energy, shallow-water inner ramp and shoal grainstones and rudstones (e.g. Azer and Toland, 1993; Van Buchem et al., 2002; Strohmenger et al., 2006). During the transgressive phase of this 3rd order sequence, non-porous dense argillaceous limestones are deposited, followed by skeletal/bioclastic wackestones with orbitolinids, echinoderm fragments, bivalves and bioturbation horizons (burrowing), reflecting low energy, outer ramp conditions. Following the maximum flooding and during the regressive phase, sedimentation of intercalated intervals of bio-peloidal packstones, bio-intraclastic grainstones, coated grain grainstones and rudstone-grainstones with rudists, reflecting shallower water, moderate to high energy, middle ramp to inner ramp with shoals occurs (Figure III.2.3) (e.g. Schlumberger, 1981; Alsharhan, 1990; Alsharhan and Nairn, 1997; Van Buchem et al., 2002; Strohmenger et al., 2006; Ehrenberg et al., 2018). The transition into the overlying dense zone (Hawar Member) is marked by a strong discontinuity, namely a subaerial exposure, as rootlets have been identified on Abu Dhabi cores, as reported by Van Buchem et al. (2002).

The UKM in most fields is subdivided into 6 subzones (Figure III.2.3) (e.g Harris et al., 1968; El Wazir et al., 2015; Ehrenberg et al., 2018). The tops of these subzones are defined based on the occurrence of thin low porosity layers, which reflect an increase in clay content and higher stylolite development, correlatable within a given field and also between fields (e.g. Harris et al., 1968; Paganoni et al., 2016; Ehrenberg, 2019). These subdivisions are considered to correspond to parasequence sets (e.g. Strohmenger et al., 2006; Ehrenberg et al., 2018), but the more widely used ‘subzone’ terminology will be used in this study.

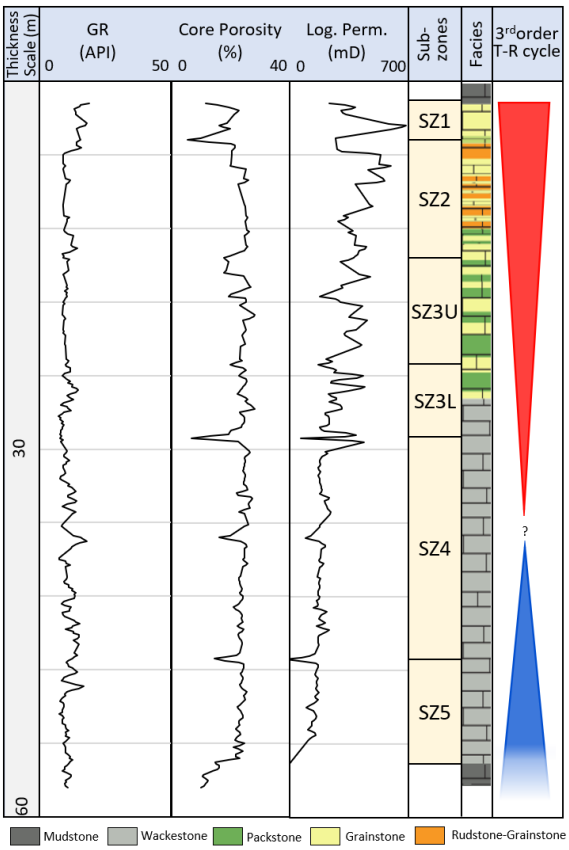

Figure III.2.3. Type logs for the UKM, with indication of subzones and facies, as defined for well D, analysed in this study. Reservoir zonation follows the established scheme (e.g. Harris et al., 1968; Alsharhan, 1990, 1993; Strohmenger et al., 2006; El Wazir et al., 2015). 3rd order cycle is based on previous publications (e.g. Van Buchem et al., 2002, 2010; Strohmenger et al., 2006).

III.2.3.2. Petroleum systems

The main source rock intervals in Abu Dhabi are found in the Upper Jurassic Diyab Formation (Figure III.2.2), also known as the Dukhan Formation, and equivalent to the Tuwaiq Mountain, Hanifa and Jubailah formations in the wider Arabian Peninsula region (e.g. Lijmbach et al., 1992; de Matos and Hulstrand, 1995; Whittle and Alsharhan, 1996; Alsharhan and Nairn, 1997; Al Suwaidi et al., 2000; Alsharhan and Scott, 2000; Vahrenkamp et al., 2015b), with maturation initiating in the Late Cretaceous (e.g. Lijmbach et al., 1992; Oswald et al., 1995). However, volumetric calculations suggest that additional sources are required to account for the total hydrocarbon found in the studied reservoir units (Taher, 1996). Dense limestones in the Thamama Group and the Aptian Bab Member of the Shuaiba Formation (Figure III.2.2) also contribute as source rocks for the UKM, having reportedly reached sufficient levels of maturity and contributing to the volumes of hydrocarbon found in the Mesozoic and, specifically, the Early Cretaceous Thamama Group reservoir rocks (e.g. Beydoun, 1991; Lijmbach et al., 1992; Azzam and Taher, 1995; Al Suwaidi et al., 2000). Hydrocarbon expulsion and migration started during the Santonian/Campanian and continued throughout the Cenozoic (e.g. Oswald et al., 1995; Taher, 1996; Van Laer et al., 2012). The main hydrocarbon migration pathways in Abu Dhabi are lateral, through reservoir units and carrier beds (e.g. Lijmbach et al., 1992; Taher, 1996), but also vertically as controlled by seal capillary entry pressure and by faults/fractures (e.g. Alsharhan, 1993; Whittle and Alsharhan, 1996; Van Laer et al., 2012). Accumulations

occur in various units, at various stratigraphic levels, but the UKM is the main producing interval in Abu Dhabi, as previously mentioned.

Structural traps are well developed in the region, in the form of extensive and gentle anticlines in the onshore and the presence of effective reservoir-seal pairs is well established. The Nahr Umr shale overlies the Thamama Group and is the most effective regional seal in Abu Dhabi (e.g. Harris et al., 1968; Taher, 1996). The thinner low-porosity and low-permeability dense mudstones of the Thamama Group also behave as seals for the adjacent reservoir units, such as the Hawar Member argillaceous limestones sealing the UKM (e.g. Alsharhan, 1989, 1993; Beydoun, 1991; Strohmenger et al., 2006; Van Buchem et al., 2010).

III.2.4. Materials and Methods

In order to analyse the rock properties heterogeneity of this dual-porosity reservoir, as well as to offer further insight into the controlling factors, an integrated study of core analysis, digital image analysis, petrographic and petrophysical data was conducted. Textural and microfacies interpretations on thin sections are used to complement core observations. The quantitative data on macroporosity and semi-quantitative data on the different types of porosity was acquired from thin sections through digital image analysis and is presented in higher detail in Chapter III.1. Heterogeneity is assessed at different observation scales, focusing on the upper half of the reservoir, which shows considerably higher facies and petrophysical variability, when compared to the lower half.

The cores of 4 wells along a southwest-northeast section across the crest of the reservoir structure were studied (Figure III.2.4), as well as a total of 142 thin sections for depositional facies interpretation and quantification of sample constituents and pore types through digital image analysis. Wireline logs were used in integration with core and thin section data to correlate subzones (e.g. Harris et al., 1968; Alsharhan, 1990, 1993; Strohmenger et al., 2006) between wells. Porosity and permeability laboratory measurements from core plugs were also integrated in this study. Core depths were shifted as required, to match log depth, in integration with wireline logs, core data and thin section data. The indicated depths are masked and shifted to a reference level below present-day sea level, and do not correspond to true depths, for confidentiality reasons. Macroporosity is defined as pores with diameters larger than 10-15 μm, which is approximately the smallest size identifiable on thin section using a petrographic microscope. Pores which have a diameter smaller than 10 μm are considered as microporosity. For comparison, the upper limit for diameter of micropores has been defined in published studies as 1/16 mm (or 62.5 μm) (Choquette and Pray, 1970), 1 μm (Pittman, 1971) or between 1 and 3 μm (Fullmer et al., 2014).

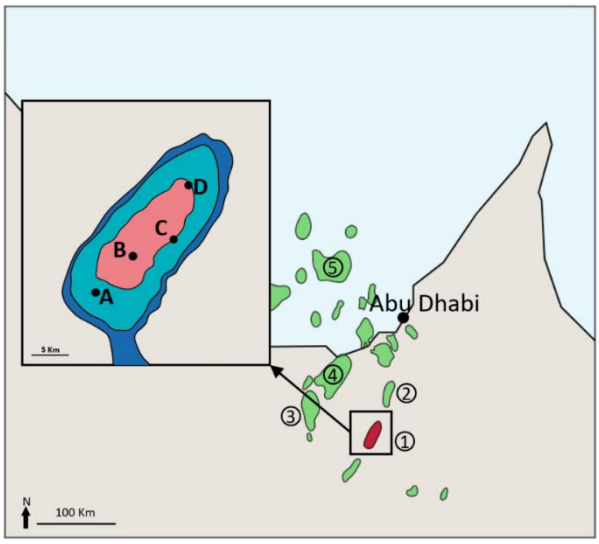

Figure III.2.4. Major field locations in Abu Dhabi (green) (based on Schlumberger, 1981; Alsharhan, 1993; Alsharhan and Nairn, 1997; Strohmenger et al., 2006). Fields which are referred to in the text (in Section III.2.6.4.4) are labelled 2 to 5. Simplified structure map of studied field 1 based on seismic data is represented (Melville et al., 2004) (red: shallower; dark blue: deeper). The locations of the studied wells A to D are indicated.

III.2.4.1. Core analysis

The core slabs from each of the four wells were analysed, with attention given to the identification of discontinuity surfaces, small-scale cyclicity and facies variability. The interpreted macrofacies were classified according to visually identifiable aspects and texture. However, some portions of the cores showed considerable degradation, affecting continuity of the observation.

III.2.4.2. Petrography

Thin sections were analysed using a transmitted light microscope and described following the textural classification schemes by Dunham (1962) and Folk (1959, 1962), using modifying terms to differentiate samples with similar facies but compositional differences of significance (e.g Lokier and Junaibi 2016). Facies types (or groups) are defined as to emphasize the textural elements controlling petrophysical properties, following the guidelines and classification scheme from Lucia (2007), in order to facilitate the interpretation and description of the relationship between rock fabric and petrophysical properties. The main facies and textural classes were divided into sub-groups, differentiating between grainstones/rudstones with and without a minor interparticle micrite volumes (or samples which are more condensed). Packstones were also subdivided into two sub-groups, according to the relative volume of allochems. The resulting facies type scheme is a simplification of the facies scheme defined by Strohmenger et al. (2006). Five core chips from well A were analysed using a scanning electron microprobe (SEM) and photomicrographs were taken, in representation of the microporous framework.

III.2.4.3. Semi-quantitative analysis

A semi-quantitative analysis of the relative abundance of each sample constituent was done on thin sections, based on visual estimation and on the use of visual comparators (e.g. Longiaru, 1987; Flügel, 2004), with estimations on grain sorting also done for grain-supported facies. While visual estimations might be associated with some level of subjectivity and uncertainty, the most important aspect of this analysis is to identify trends and variability between relative values and not the absolute value for a given parameter. An automated approach to classify the different sample components based on digital image analysis would be difficult to achieve, as most particles are micritized and exhibit highly similar visual properties. The quantification of macroporosity was done based on digital image analysis of thin section photos, through non-contiguous colour selection and guided machine learning using the open-source software Trainable Weka Segmentation (TWS) and the machine learning toolkit Waikato Environment for Knowledge Analysis (WEKA) (Hall et al., 2009), which function as plugins for the image processing software ImageJ (Schindelin et al., 2012). A classification model is created for automated image segmentation, based on selected training images and user-guided pixel classification, which is then applied to batches of selected images for segmentation and pixel counting (Arganda-Carreras et al., 2017) (presented in higher detail in Chapter III.1).

III.2.5. Results

III.2.5.1. Petrography and facies types

Based on thin section interpretations, and following the guidelines mentioned above, seven facies types were defined in this reservoir for the purpose of this study (Table III.2.1, Figure III.2.5) and are described in the following paragraphs. The dense, non-reservoir zone immediately underlying the UKM is characterized by mudstone facies with very low or null porosity (facies 1), which is not included in the reservoir facies classification scheme.

Table III.2.1. Facies/textural classes applied to petrographic interpretations.

Main texture	High interparticle micritic volume (or condensed)		Low interparticle micritic volume (or absent)
Rudstone-grainstone	5.1		5.2
Packstone-grainstone and Grainstone	4.1		4.2
Packstone	3.1	3.2	
Wackestone	2		

Biomicritic wackestone (facies 2): Micritic samples with echinoderm fragments and spicules, bivalves and foraminifera. Micritized orbitolinids are identified, preserving some intraparticle porosity. In some intervals, micritic peloids or ghost particles are identifiable. Minor visible macroporosity is mostly characterized by non-connected pores (vuggy, mouldic, fenestral) (Figure III.2.5a, b).

Biointraclastic micritic packstone (facies 3.1 and 3.2): Characterized by micritized intraclasts and peloids supported by a micritic matrix. Contains echinoderms, bivalves, foraminifera and micritized orbitolinids, sometimes preserving intraparticle porosity. Visible macroporosity is predominantly non-connected mouldic but minor interparticle macroporosity also occurs. A differentiation is made according to variations in allochems volume, which is relatively higher in facies 3.2 (Figure III.2.5d) when compared to facies 3.1 (Figure III.2.5c).

Biointraclastic packstone-grainstone with an interparticle micritic matrix (facies 4.1): Poorly to well sorted sand-grade fine to very coarse micritized intraclasts, recrystalized fragments of echinoderms, bivalves, gastropods and foraminifera. Micritized orbitolinids are identified with some preserved intraparticle macroporosity, although total macroporosity is mostly interparticle. Micritized particles show circumgranular cement rims (bladed or fibrous, sometimes difficult to identify). Characterized by the occurrence of variable volumes of a micritic phase with a packstone texture and variable volumes of peloids in between the allochems. Grainstones which are more condensed or more closely packed, with reduced interparticle macroporosity, are also included in this facies type (Figure III.2.5e).

Biointraclastic grainstone (facies 4.2): Fairly similar to facies 4.1, with the main difference being the absence of a micritic phase. Interparticle macroporosity remains mostly open, with a few exceptions, as will be discussed. Syntaxial cement overgrowths on echinoderm fragments are observed. Some grainstone intervals containing coated grains, including ooids, and occurring towards the top of the reservoir are also included in this facies type (Figure III.2.5f).

Biointraclastic rudstone-grainstone with a packstone-grainstone matrix (facies 5.1): Generally poorly to very poorly sorted and contain considerable volumes of micritized intraclasts and recrystalized skeletal grains which are larger than 2 mm in size (more than 5-10%). Skeletal grains include echinoderms, bivalves, gastropods and foraminifera. Rudstone-grainstones with rudist fragments are categorized in this facies type. Contains a micritic phase with packstone-grainstone texture in between the coarser particles. The majority of visible macroporosity is interparticle but intraparticle macroporosity is also identified. Syntaxial cement overgrowths are identified on echinoderm fragments (Figure III.2.5g).

Biointraclastic rudstone-grainstone (facies 5.2): Similar to facies 5.1 but interparticle space remains mostly open, with no micritized phase. Most of the macroporosity is interparticle, as well. Syntaxial cement overgrowths are identified on echinoderm fragments (Figure III.2.5h).

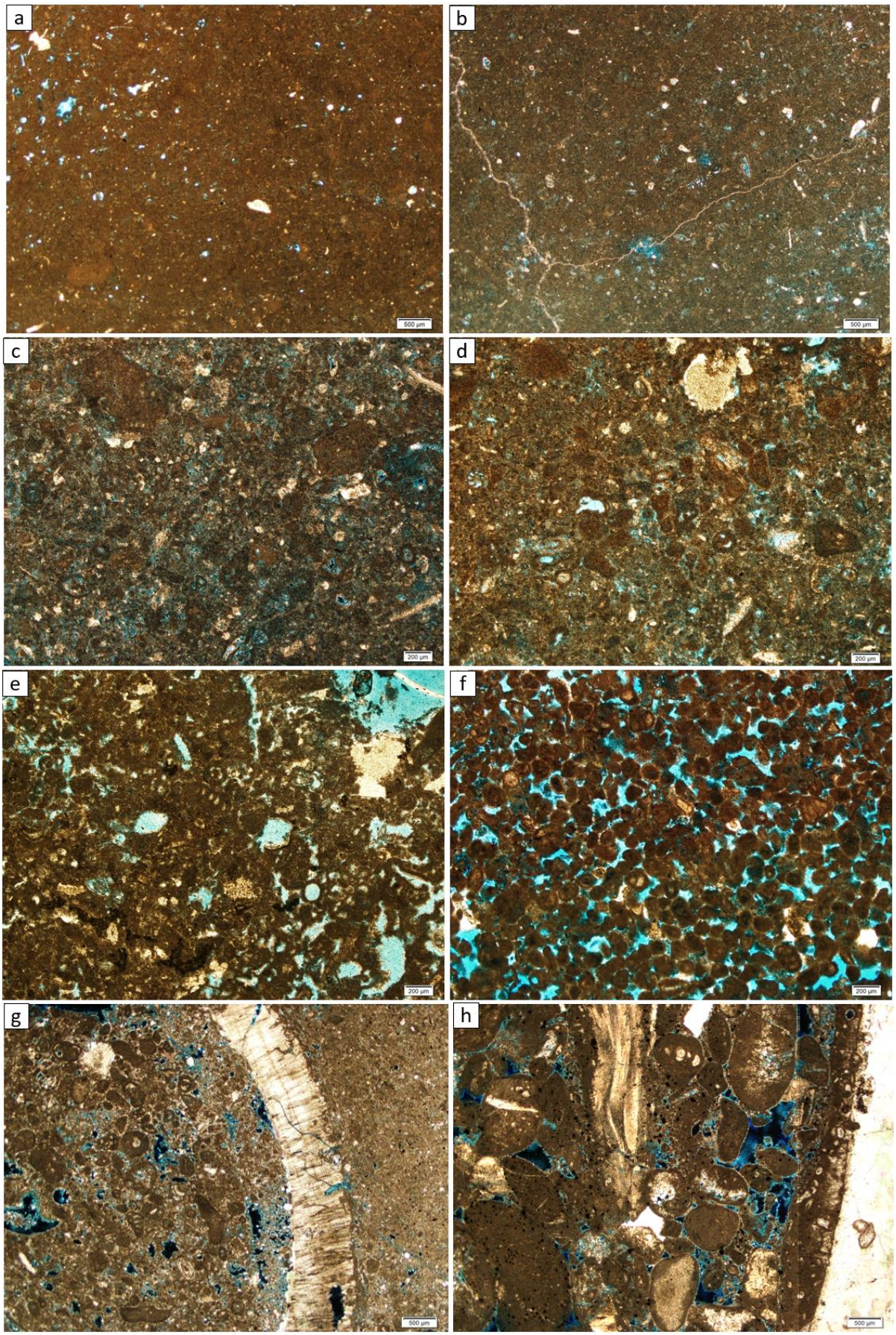
a
b
c
d
e
f
g
h

Figure III.2.5. Photomicrographs examples of different facies from reference well A. **a:** subzone 4, facies 2. Biomicritic wackestone. Fully micritic, with few scattered skeletal fragments, some identifiable micritized intraclasts and very low visible macroporosity (in blue); **b:** subzone 4, facies 2. Biomicritic wackestone with few scattered skeletal fragments, some identifiable micritized intraclasts and practically null macroporosity. Calcite-filled fractures occur; **c:** subzone 3U, facies 3.1. Biointraclastic micritic packstone. Poorly sorted micritized intraclasts and recrystalized skeletal fragments supported by a micritic matrix and practically null macroporosity; **d:** subzone 3U, facies 3.2. Intrabioclastic micritic packstone. Poorly sorted micritized intraclasts and recrystalized skeletal fragments supported by a micritic matrix, with very low visible macroporosity (in blue). An echinoderm fragment with syntaxial calcite cement is visible; **e:** subzone 3U, facies 4.1. biointraclastic packstone-grainstone with an interparticle micritic matrix. Micritized intraclasts, recrystalized skeletal grains, including echinoderm fragments with syntaxial cement and micritized foraminifera filled by calcite cement. Interparticle space is partially filled by a micritic phase with a packstone texture. Cementation of interparticle space is generally low. Low to moderate visible macroporosity, with some mouldic porosity occurring (in blue); **f:** subzone 2, facies 4.2. Well sorted intraclastic grainstone with micritic ooids, intraclasts and recrystalized skeletal grains. Moderate visible macroporosity (in blue) and very low to null interparticle cementation; **g:** subzone 2, facies 5.1. Intrabioclastic rudstone-grainstone with a grainstone-packstone matrix. Contains micritized intraclasts and skeletal grains, as well as recrystalized skeletal grains, some larger than 1 mm. Low visible macroporosity (in black); **h:** subzone 2, facies 5.2. Intrabioclastic rudstone-grainstone, poorly sorted with very coarse micritized intraclasts and recrystalized skeletal grains with a micritic film, some larger than 1 mm. Moderate interparticle macroporosity is visible (in black), with very low interparticle cementation.

III.2.5.2. Diagenesis

The particles in grainstones are lined with an early-stage calcite cement rim, which is generally fibrous, but sometimes difficult to distinguish between fibrous or bladed (Figure III.2.6). Apart from these relatively early-stage cement phases, interparticle cementation is considerably low or non-existent in most intervals (Figure III.2.6a, b, c, d), except at a few levels where relatively strong interparticle calcite cementation is observed, which occur close to subzone boundaries. Syntaxial cement overgrowths around echinoderm fragments are identified in different intervals of the upper half of the reservoir. In some wackestone layers, inequigranular, euhedral-subhedral, floating microrhombic dolomite crystals occur in the micritic matrix (Figure III.2.6e). The effects of compaction are expressed through different features, such as point-contact, long, concave-convex and sutured contacts between particles (Figure III.2.6). Grain fracturing and pressure dissolution along stylolites are also observed.

The micritization of allochems has resulted in the creation of a microporosity within these particles (e.g. Morad et al., 2016), through the formation of a framework of granular subhedral rounded to sub-rounded micrite crystals (Figure III.2.7) (described according to Kaczmarek et al., 2015). The interparticle micritic matrix, when present, adds to the microporous volume and to total porosity in packstones and some grainstone/rudstone-grainstone intervals.

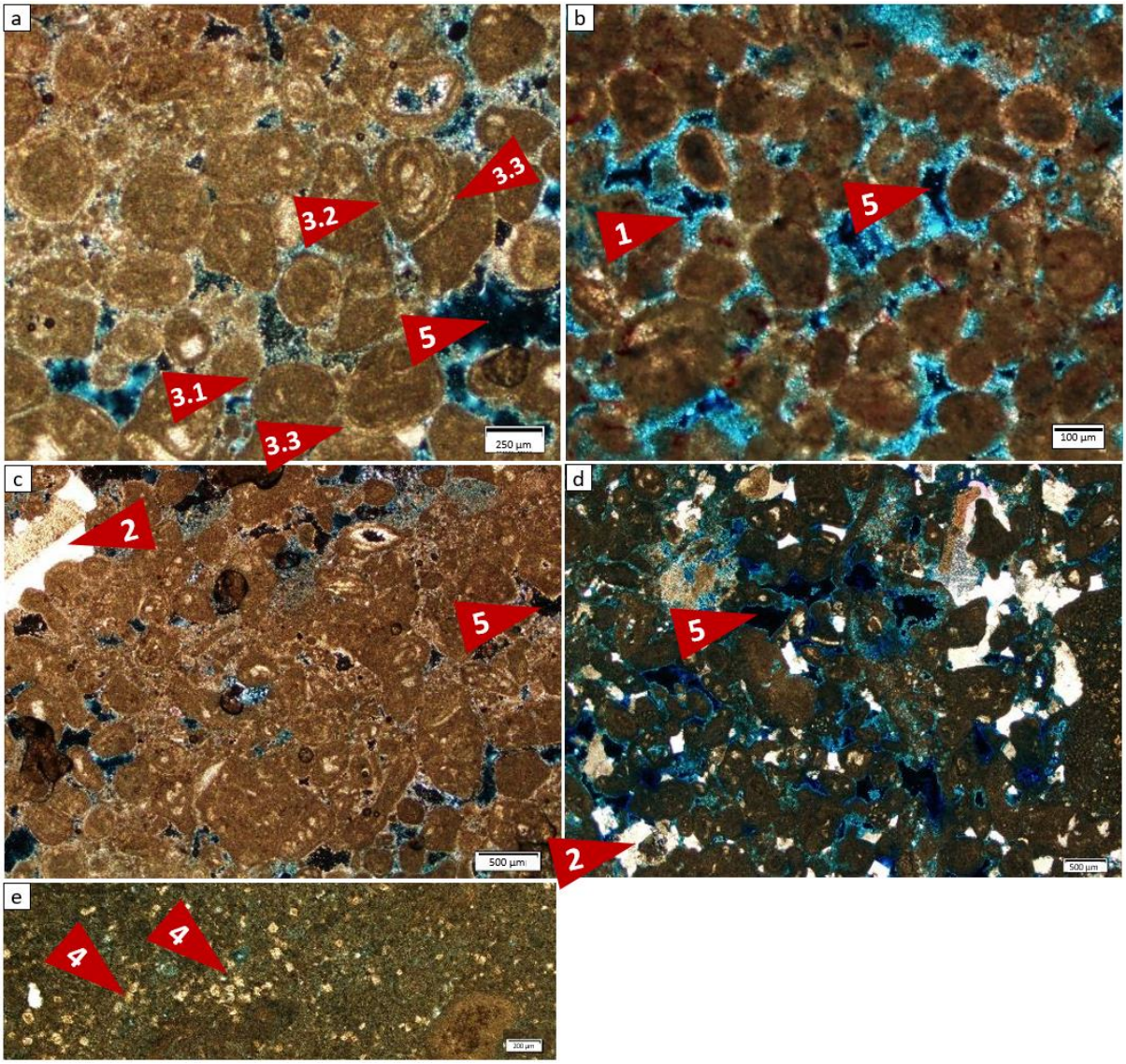

Figure III.2.6. Examples of diagenetic features. **a**: well sorted oointraclastic grainstone (facies 4.2); **b**: well sorted intraclastic grainstone with ooids (facies 4.2); **c**: biointraclastic grainstone (facies 4.2); **d**: biointraclastic grainstone (facies 4.2); **e**: micritic wackestone with dolomite rhombs (facies 2). 1: Clearly identifiable circumgranular rim cement phase (fibrous or bladed(?)); 2: Echinoderm fragments with syntaxial calcite cement overgrowths; 3.1: Point-contact; 3.2: Tangential contacts; 3.3: Concavo-convex contacts; 4: Inequigranular, euhedral-subhedral, floating microrhombic dolomite crystals in wackestone facies; 5: Interparticle space, mostly preserved as open macroporosity in grainstone facies.

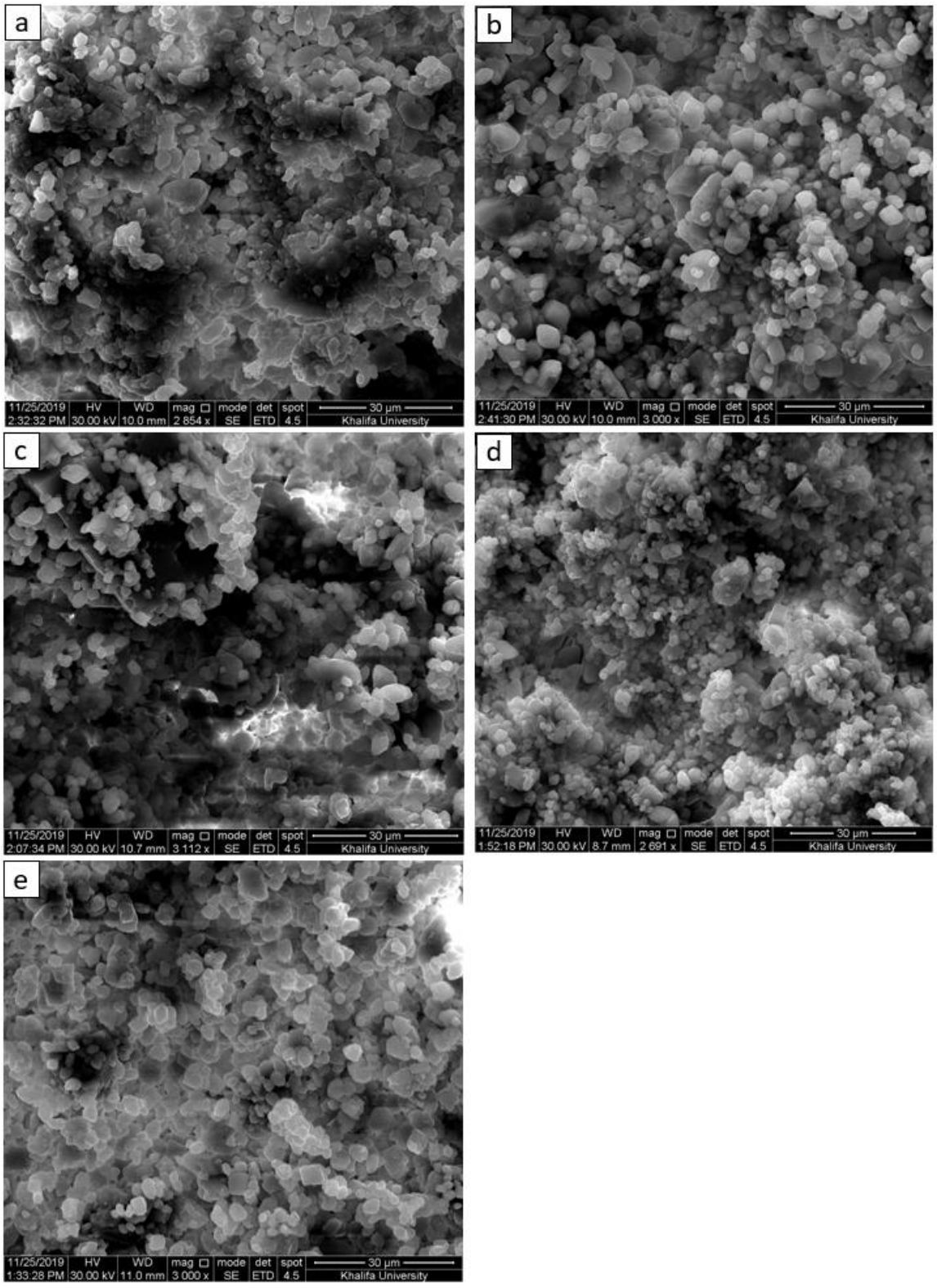

Figure III.2.7. SEM images of well A core chips. Microporous framework with rounded to sub-rounded micrite crystals defining a granular-subhedral texture. **a**: subzone 2; **b**: subzone 3U; **c**: subzone 3U; **d**: subzone 4; **e**: subzone 4.

III.2.5.3. Quantitative and semi-quantitative analysis

The results of a detailed semi-quantitative analysis show considerable variability in relative volumes of sample constituents throughout the analysed intervals. Reference well A has a higher sample density and is shown below to illustrate the vertical variability in relative volume of each sample component in the more heterogeneous upper half of the reservoir (Figure III.2.8).

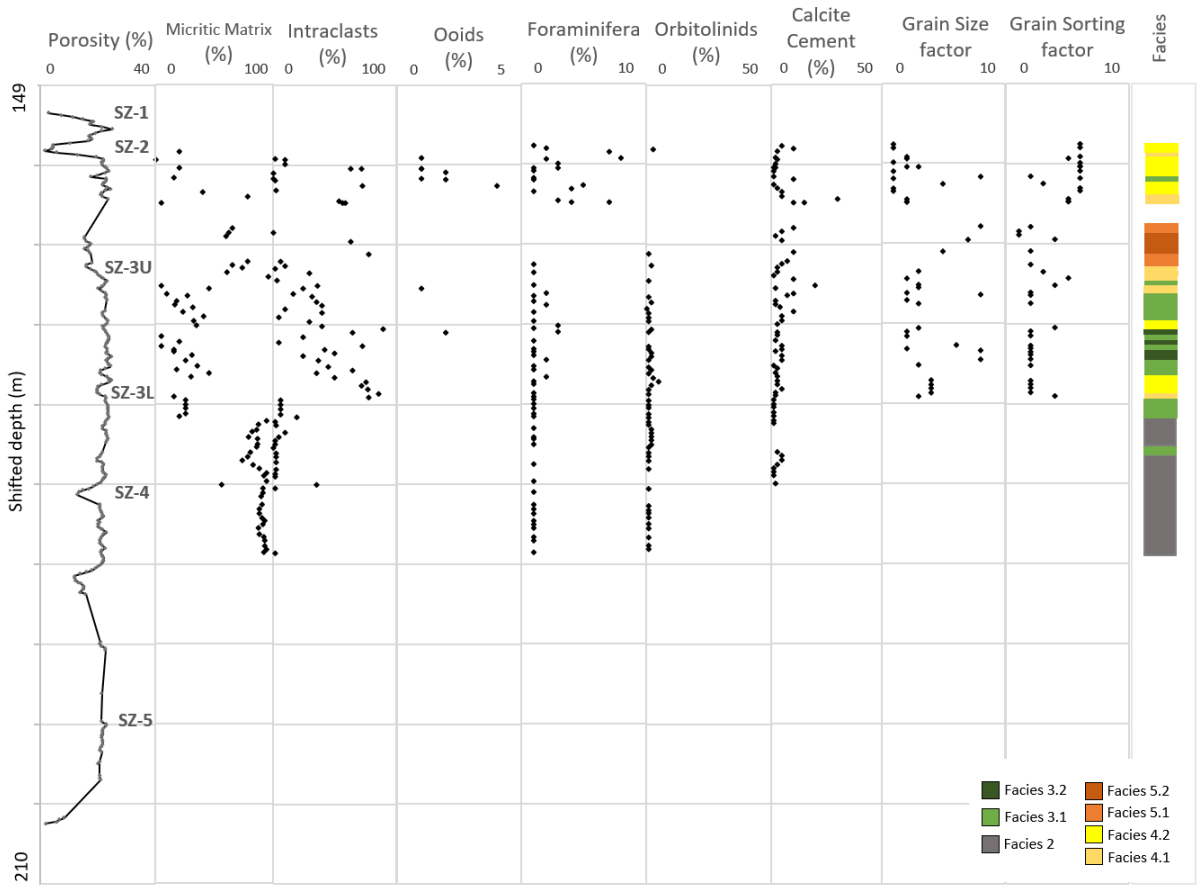

Figure III.2.8. Semi-quantitative analysis from reference well A. Total porosity available from conventional core analysis (CCA) is represented on the first column. Far-right column represents facies types (see Table III.2.1 and Figure III.2.5). Subzone tops are indicated on the first column, which are generally described in the following section. The extended results of this analysis for the four wells are available in Appendix III.2.A.

Macroporosity was measured using digital image analysis, through non-contiguous colour selection and guided machine learning and the results are here integrated (Figure III.2.8). These methodologies and the results are presented in detail in Chapter III.1. Calculated microporosity reaches values of more than 60 % of total porosity, reaching close to 100 % in micritic wackestones, where virtually no macroporosity is present. The results of this semi-quantitative analysis for all 4 wells are compiled and presented in composite panels (see Appendix III.2.A).

The strongest break in the succession is observed at around the transition from a wackestone-dominated interval to a packstone-grainstone interval (Figure III.2.8). A marked sharp decrease in the volume of micritic matrix and an increase in intraclasts volume occurs at this level. Although in low volumes, orbitolinids are regularly observed below the rudstone-grainstone interval, becoming virtually absent from this level onwards. Intraparticle cement is low overall, as previously mentioned, with peaks occurring below and above the rudstone-grainstone interval in well A (Figure III.2.8). Grain sorting generally increases towards the top of the reservoir, while grain size is generally lower above the rudstone-grainstone interval, showing some variability below (Figure III.2.8).

The potential relationship between the measured and estimated parameters are shown in the correlation matrix below (Table III.2.2). The correlation factor between permeability and total porosity for the full set of samples is very low or non-existing (factor of -0.02), while permeability and digitally measured interparticle macroporosity show a considerably higher correlation factor of 0.46. The grain sorting and facies type parameters show moderate to good direct correlation with permeability (factors of 0.42 and 0.52, respectively). The dominant microporosity percentage in this reservoir is reflected by the 0.90 correlation factor between this parameter and total measured porosity.

Table III.2.2. Correlation matrix of petrophysical and estimated petrographic parameters. Inter. Macrop. = interparticle macroporosity; Non-connected Macrop. = non-connected macroporosity; Micritie = microporous micritic matrix.

	Depth	Perm.	Total Porosity	Macro-porosity	Inter. Macrop.	Non-connected Macrop.	Micro-porosity	Facies	Grain Sorting	Grain Size	Micrite
Depth	1.00										
Perm.	-0.29	1.00									
Total Porosity	0.01	-0.02	1.00								
Macro-porosity	-0.12	**0.37**	0.00	1.00							
Inter. Macrop.	-0.12	**0.46**	0.06	**0.91**	1.00						
Non-connected Macrop.	-0.02	-0.04	-0.03	**0.53**	0.13	1.00					
Micro-porosity	0.06	-0.18	**0.90**	**-0.49**	**-0.35**	-0.26	1.00				
Facies	**-0.36**	**0.52**	-0.13	**0.42**	**0.43**	0.09	-0.30	1.00			
Grain Sorting	-0.10	**0.42**	-0.18	-0.09	-0.01	**-0.35**	-0.09	**0.33**	1.00		
Grain Size	-0.05	-0.18	0.13	0.27	0.22	**0.37**	-0.04	-0.19	**-0.67**	1.00	
Micrite	**0.37**	**-0.36**	-0.14	**-0.38**	**-0.41**	-0.16	0.03	**-0.62**	-0.05	-0.07	1.00

III.2.5.4. Reservoir zonation

As previously mentioned, the UKM is divided into subzones bounded by thin lower porosity layers, which are correlatable over large distances in Abu Dhabi (Figures III.2.8, III.2.9). The general characteristics for each subzone are presented, based on core observations, facies and variability in different parameters. Internal sedimentary features and patterns are also indicated, where present and identifiable. The subzones are described from bottom to the top of the reservoir.

Subzone 5: Fine-grained, grey-coloured wackestones with scattered skeletal grains and moderate volumes of orbitolinids, which increase towards the upper half. This interval is marked by the occurrence of discrete thinly laminated layers, sometimes developing stylolites. Bioturbated levels occur, with carbonate nodules most likely representing infilled burrows. The top of this subzone is picked based on the occurrence of a low porosity layer, with no clear lithological expression observed.

Subzone 4: Characterized by wackestone facies with scattered skeletal grains and orbitolinids. Discrete layers of increased influx of these elements occur. Discontinuity surfaces are visible towards the upper half (Figure III.2.10), normally preceding thin intervals showing some vuggy porosity. Stylolites, as well as signs of bioturbation, are identified throughout. An interval with stronger dolomitization occurs in this subzone.

Subzone 3L/3U: This interval is dominated by wackestone facies in the lower half (3L), with packstones and grainstones characterizing the upper half (3U). Discontinuity-bounded grainstone/packstone intervals of between approximately 1 and 3 ft (30 to 90 cm) are observed in 3U. These intervals are generally characterized by the occurrence of a relatively thin bottom interval with vuggy porosity and coarser particles, followed by sediments with a relatively more homogeneous appearance, defining fining-upwards trends.

Subzone 2: Characterized by grainstones, rudstone-grainstones and packstone (to grainstone) facies, with the occurrence of coarser skeletal grains and shell fragments, including rudists. Small-scale facies variability is observed in discontinuity-bounded intervals with thicknesses varying between 0.5 and 3 ft (15 to 90 cm). These intervals generally have a highly bioclastic basal layer, an overall fining-upwards trend and show moderate to high vuggy porosity (Figure III.2.11). This highly bioclastic zone terminates on a strongly cemented interval.

Subzone 1: Predominantly characterized by grainstone facies, with moderate volumes of skeletal grains and some intervals with vuggy porosity. Shows a generally fining-upwards trend.

The reservoir zone is followed by a grey limestone (mudstone facies), showing stylolites, wispy seams and thinly laminated layers. Orbitolinids and bioturbation (infilled burrows) are identified in this interval.

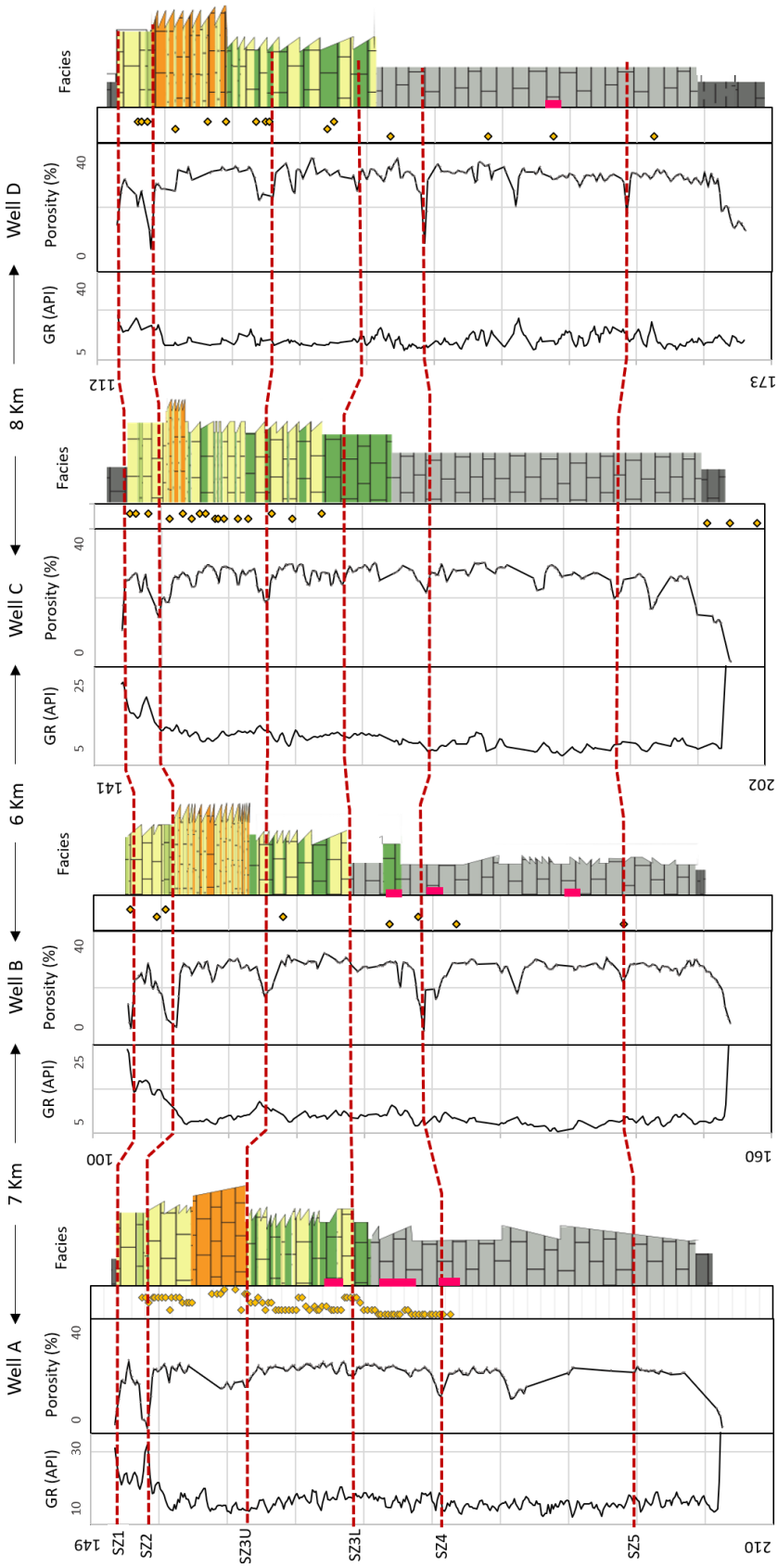

Figure III.2.9. Representation of the four analysed wells, including GR and core porosity logs, as well as facies interpretations based on core observations (dark grey: mudstone. Light grey: wackestone. Green: packstone. Yellow: grainstone. Orange: rudstone-grainstone. Pink: identified dolomitized zones). Vertical axis represents shifted depths in metres and all wells are plotted in an interval of approximately 60 m (200 ft). Subzone (SZ) tops are indicated. Thin section depths are represented on the third column for each well. Approximate distance between wells is indicated.

.

III.2.6. Discussion

III.2.6.1. Overall facies evolution

The facies succession of the UKM shows an overall trend that is well known and identical in all fields across Abu Dhabi, including the wells here analysed. The lower half of the UKM is predominantly characterized by micritic wackestones until the top of subzone 3L and has a very homogeneous appearance, defining sedimentation in relatively low-energy settings. The upper half of the reservoir has a more heterogeneous appearance, with a succession of packstone, grainstone and rudstone-grainstones intervals. Subzone 2 is characterized by an abundance of rudist fragments in poorly-sorted rudstone-grainstone facies 5.1 and 5.2, but moderately to well sorted oolitic-intraclastic grainstones are also identified in subzones 1 and 2. Such facies reflect deposition in higher energy environments of deposition. This overall facies succession is identical in the 4 analysed wells (Figure III.2.9), with clear differences only in smaller-scale variability, as will be discussed, and defines a shoaling upwards trend, reflecting deposition during the transgressive-regressive phases of a 3rd order sequence, as previously mentioned (e.g. Van Buchem et al, 2002, 2010; Davies et al., 2002; Strohmenger et al., 2006).

III.2.6.2. Discontinuities and small-scale facies variability linked to petrophysical properties

Stronger heterogeneity in the UKM becomes clearer at smaller observations scales. The analysis of core slabs reveals facies variability in discontinuity-bounded intervals, which becomes more prominent towards the top. Relatively thin layers with large vugs occur and considerable variability in petrophysical properties, including digitally measured macroporosity, is observed. The values for permeability and porosity are presented for the examples here discussed, as one of the main objectives of this study is to address the depositional controls on petrophysical heterogeneity. The wireline log data shows some variability trends in the more heterogeneous subzones, as well, and will also be addressed in this section. In subzone 4, apparent discontinuity surfaces are visible, normally followed by intervals showing signs of bioturbation (Figure III.2.10), as previously mentioned, but clear indications of facies cyclicity or depositional trends are not observed.

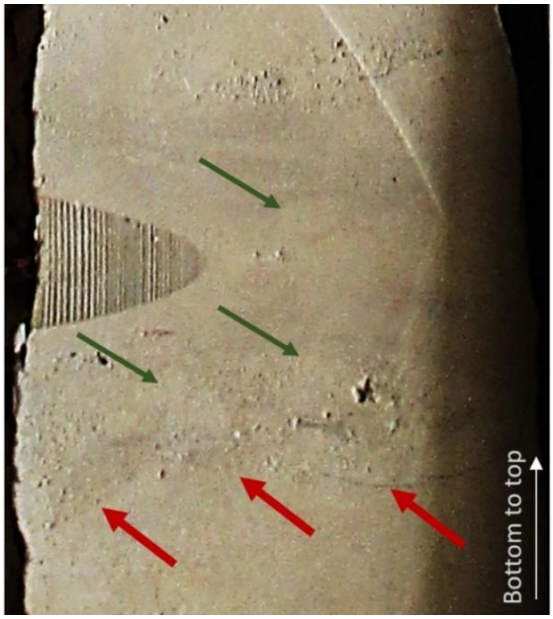

Figure III.2.10. Well A, subzone 4. Example of discontinuity surface (red arrows) and signs of burrowing with subsequent infilling (green arrows). Vuggy porosity is clearly visible.

Discontinuity-bounded intervals with an average thickness of 2.5 ft (0.76 m), varying between 1 ft (0.3 m) and 9 ft (2.7 m), are identified in subzone 3U. These cyclical intervals generally show higher vuggy porosity and coarser skeletal grains in intraclastic packstone-grainstone basal layers with variable thickness, sometimes showing bioturbation and coarser intraclasts. Above this basal layer, sediments have a more homogeneous appearance (with packstone to grainstone textures) and vuggy porosity becomes less clear on core (Figures III.2.11, III.2.12, III.2.13).

At the base of subzone 3U, a 7 ft (~2 m) interval shows a typical fining-upwards trend, gradually transitioning from grainstones with skeletal grains and intraclasts (facies 4.2) into packstones (facies 3.2) (Figure III.2.13). Intervals with similar characteristics are observed throughout this subzone, with varying thicknesses. In subzone 2, similar discontinuity-bounded fining-upwards intervals are also observed. Discontinuity surfaces are overlain by highly bioclastic (including rudist fragments) and vuggy layers (rudstone-grainstone facies 5.1 and 5.2) of variable thickness, which grade upwards into relatively finer sediments, with lower content in coarser shell fragments and lower visible vuggy porosity. Rudists are present in the form of shell fragments and no complete shells are identified (articulated or disarticulated), probably defining shell lag deposits (e.g. Kreisa, 1981; Mohseni and Al-Aasm, 2004) or what have been described as rudist-rich rudist channel lags (e.g. Van Buchem et al., 2002). Average thickness of these fining-upwards depositional bodies is 1.4 ft (43 cm), varying between 0.5 ft (15 cm) and 3 ft (90 cm), in similarity with a Late Cretaceous rudist-dominated carbonate outcrop case study described by Carannante et al. (2003), which reports an average thickness of 30 cm for depositional cycles containing accumulations of rudist shell fragments.

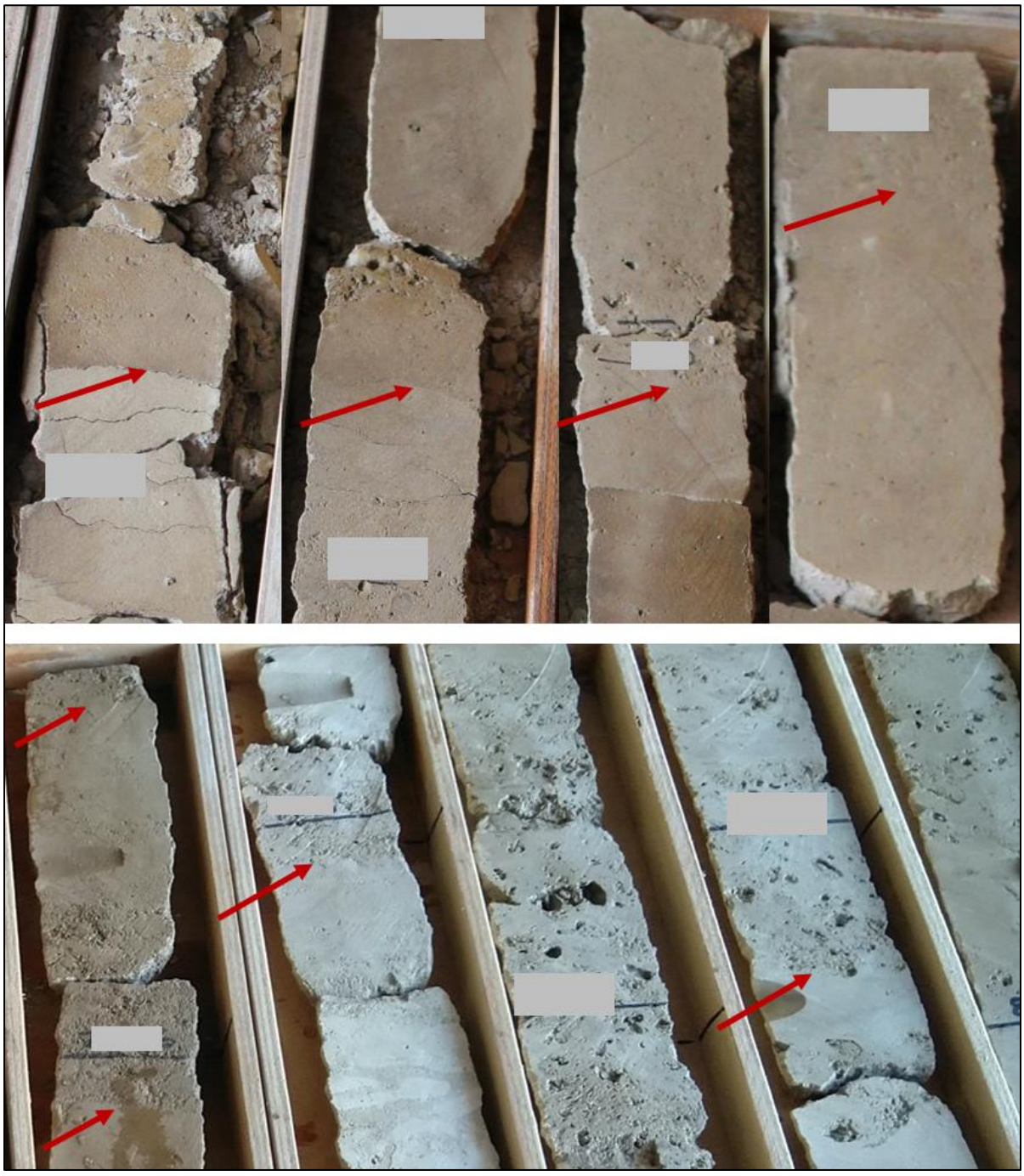

Figure III.2.11. Examples of discontinuity surfaces identified on core. **Top**: well A, top of subzone 3U (close to transition to subzone 2), showing packstone to grainstone facies, with discontinuity surfaces directly overlaid by relatively thin intervals containing moderate to high amount of large vugs. **Bottom**: well B, subzone 2. Interval containing packstone-grainstones, grainstones and rudstone-grainstones with rudist fragments. Discontinuity surfaces separate relatively finer facies below from coarser facies above, with abundant vuggy porosity and large skeletal fragments, including rudists. A darker-coloured interval of packstone-grainstones and grainstones occur towards the top.

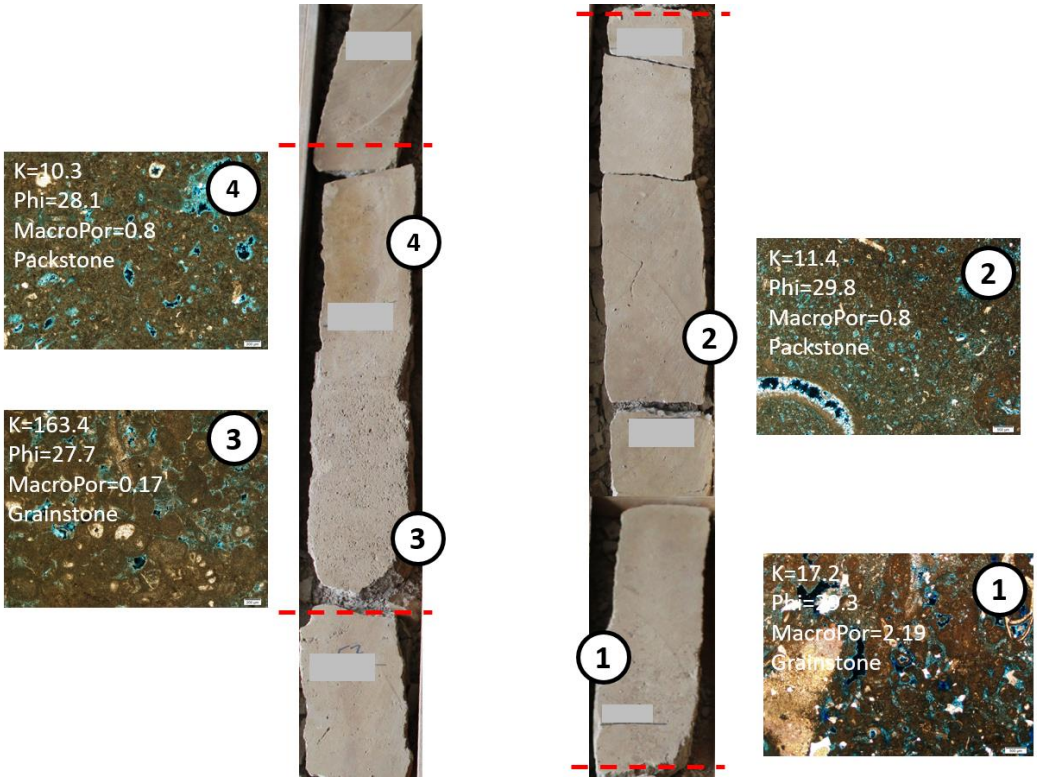

Figure III.2.12. Examples of two discontinuity-bounded intervals with thicknesses of approximately 1.4 and 2.2 ft (43 and 67 cm). Grey boxes overlaid on core are place at 1 ft (30 cm) intervals. Permeability (K) in mD, porosity (Phi) in % and macroporosity (MacroPor) in %, are indicated on each image, as well as the main texture.

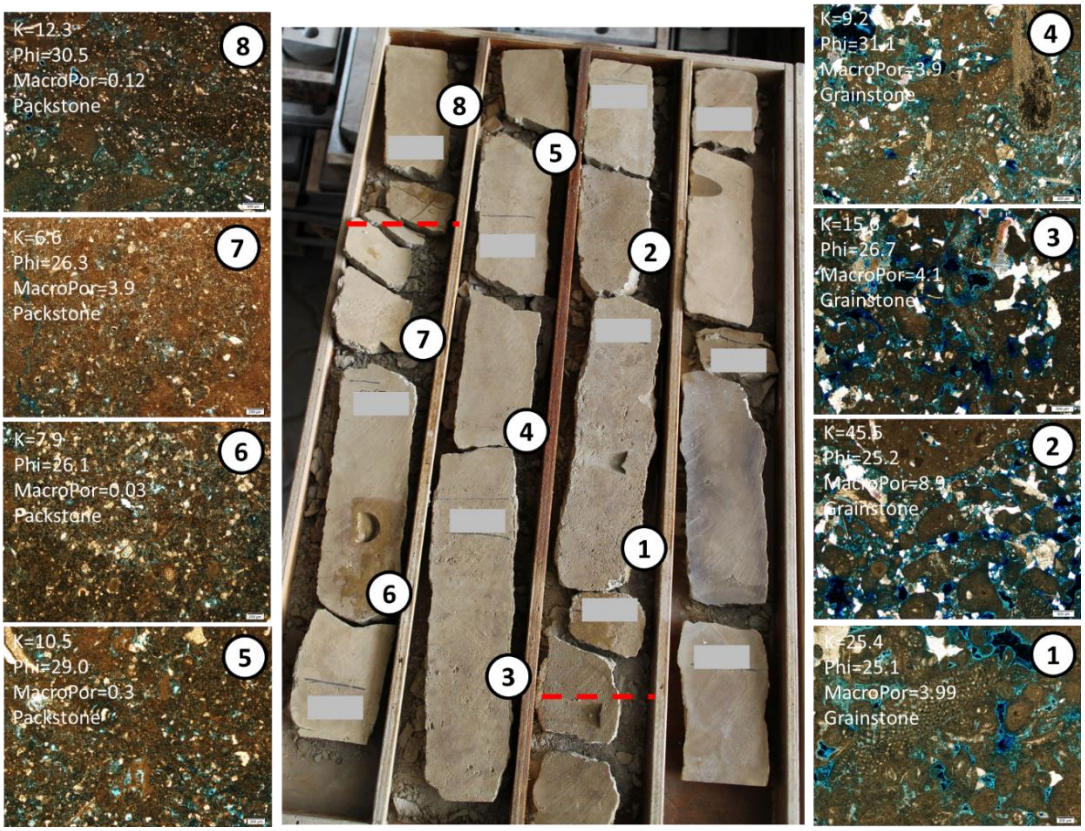

Figure III.2.13. Basal interval of subzone 3U, with a thickness of 7 ft (2 m). Dashed red lines mark discontinuities identified on core. Grey boxes overlaid on core are placed at 1 ft (30 cm) intervals. Main textures evolve from intraclastic grainstones (facies 4.2) into micritic, bioclastic packstones (facies 3.1). Permeability (K) in mD, porosity (Phi) in %, macroporosity (MacroPor) in % and main texture are indicated on each image.

Observations and interpretations on wireline logs and semi-quantitative data also reveal trends in the variability of different parameters in subzone 3U (Figure III.2.14). This represents an intermediate observation scale, between the small-scale variability identified on core discussed above and the larger scale facies trends characterizing the full reservoir succession (see Section III.2.6.1). The GR log is generally decreasing through subzone 3U, although smaller-scale trends are also identified, which are difficult to assign to depositional features. The base of this subzone shows higher estimated macroporosity (interparticle and moldic), while permeability shows two peaks and no clear trends. The estimated volume of intraclasts is generally decreasing upwards, in similarity to the GR trend, while the estimated volume of micritic matrix shows decreasing trends in two different intervals with an overall decreasing upward signature. These two intervals are separated by an intraclastic grainstone layer, corresponding to the second permeability peak. The estimated volume of interparticle cement shows an overall increasing-upward trend until the top of this subzone. The two permeability peaks in this subzone correspond to the occurrence of layers with grainstone facies type (facies 4.2), while the permeability variability in between these peaks is not significant (varies between 6 and 28 mD) and a clear correlation with eventual depositional factors is not clear.

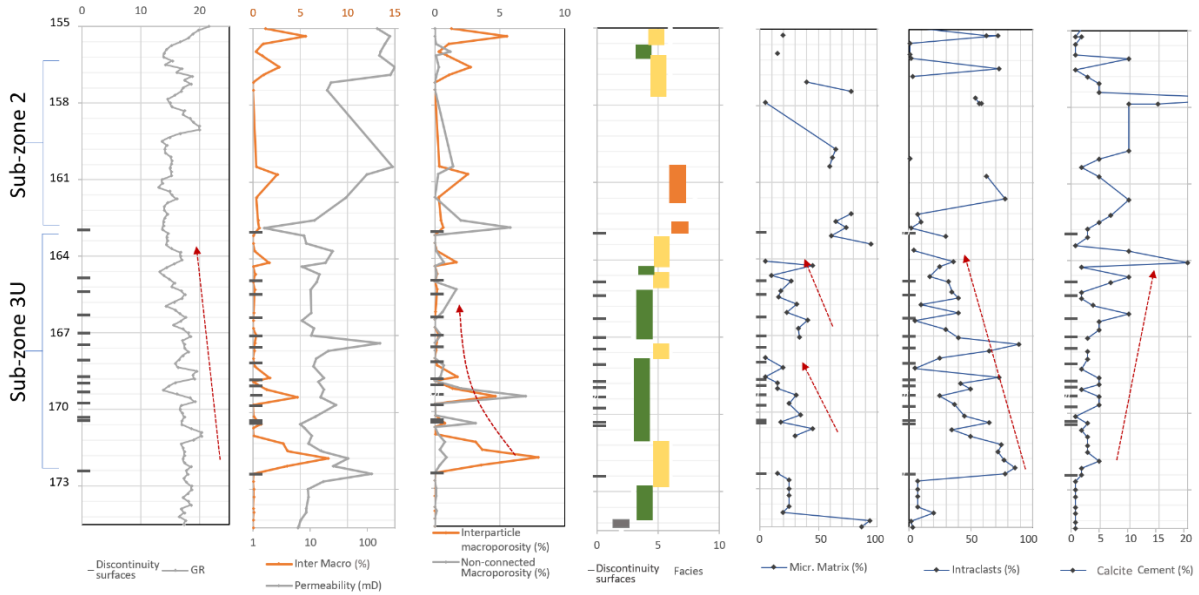

Figure III.2.14. Composite panel for subzone 3U and subzone 2 showing variability in GR, interparticle macroporosity, non-connected macroporosity, permeability, main depositional texture, estimated volumes of micritic matrix, intraclasts and calcite cement. Vertical axis represents shifted depth in metres. Visible trends are indicated by red arrows. Grey indicators on the depth axis indicate discontinuity surfaces identified on core. Facies colour code: grey = wackestone; green = packstone and packstone-grainstone; yellow = grainstone; orange = rudstone-grainstone.

III.2.6.3. Lateral correlations and paleoenvironment

This reservoir shows a 'layer-cake' geometry/zonation at a larger-scale, with regionally correlatable subzones bounded by thin clay-rich layers, as previously mentioned and as reported in several published papers (e.g. Harris et al., 1968; Alsharhan and Nairn, 1997; Davies et al., 2002; Ehrenberg et al., 2016, 2018). However, at a smaller scale, within each subzone, a direct correlation between discontinuity-bounded depositional packages in the four analysed wells is difficult to define, given the differences in small-scale facies variability/cyclicity discussed above (Figure III.2.9). This lateral heterogeneity has been previously reported for this field (e.g. Grötsch et al., 1998; Strohmenger et al., 2006) and other fields in Abu Dhabi (Alsharhan, 1990; El Wazir et al., 2015; Jeong et al., 2017; Ehrenberg et al., 2016, 2018), and is most likely controlled by factors such as complex depositional geometries resulting from variable palaeoenvironmental and depositional conditions, possibly affected by storm events (e.g. Pittet et al., 2002; Van Buchem et al., 2002; Ehrenberg et al., 2018). This small-scale variability has been recently analysed by Ehrenberg et al. (2018) in a nearby field, where a possible explanation envisages the deposition of coarse beds as occurring randomly, influenced by storm activity and not by high-frequency depositional cyclicity. These high-energy deposits have been interpreted to result from the transport of sediments originating in high to moderate energy shallower-water environments, driven by such storm-events and developing tempestites (Grötsch et al., 1998; Ehrenberg et al., 2018), also suggesting likely deposition in a slightly more basinward position, away from shoal crest settings (Grötsch et al., 1998).

III.2.6.3.1. Subzones 4 and 5

Subzones 4 and 5 are characterized by wackestones with skeletal grains and orbitolinids, and were deposited in a low energy, mid-ramp setting (below fair-weather wave base) (e.g. Van Buchem et al., 2002; Strohmenger et al., 2006). Lateral facies variations between the studied wells in these subzones seems to be very low, as they have the same generally homogeneous wackestone appearance, as is the case for different fields across Abu Dhabi also (e.g. Harris et al., 1968; El Wazir et al., 2015; Ehrenberg et al., 2018). With sedimentation occurring in lower-energy mid-ramp (to distal) setting, there is probably less pronounced lateral variability in

depositional geometries, and tabular or sheet-like bodies showing moderate to high lateral facies continuity are most likely developed.

III.2.6.3.2. Subzones 2 and 3U

The above-discussed small-scale depositional trends in subzones 3U and 2, as well as their variability between wells, are interpreted to result from the laterally variable hydrodynamic conditions typical of relatively high-energy, shallow-water settings, which are controlling sediment distribution and creating complex depositional geometries and geometric relationships between geobodies (e.g. Van Buchem et al., 2002; Ehrenberg et al., 2018), in moderate similarity to present day shallow water carbonate cases (e.g. Reeder and Rankey, 2008; Alsharhan and Kendall, 2010). Subzone 3L does not show such clear vertical facies variability. The interpreted lateral sediment distribution, as well as the variable depositional geometries, could have also been partially controlled by the geographical distribution of ooids shoals, rudist build-ups and the development of tidal channels observed in shallow-water depositional environments (e.g. Van Buchem et al., 2002; Reeder and Rankey, 2008; Alsharhan and Kendall, 2010). This will possibly lead to the development of lenticular or wedge-like geobodies.

The sediments of subzone 2 were deposited during the late regressive phase, in shallow platform settings, with the interpreted presence of higher-energy channel deposits, including rudist-rich channel lags, laterally transitioning into rudist biostromes where a finer micritic phase is preserved (e.g. Van Buchem et al., 2002), which would correspond to the packstone-grainstones and rudstone-grainstones of facies 4.1 and 5.1. The intervals with very coarse shell fragments, intraclasts and an absence of a finer micritic matrix (facies 4.2 and 5.2), are indicative of persistent higher energy levels. The coarser beds have also been interpreted to represent transported deposits originating from different points of the high-energy environment assisted by storm events, as mentioned above (e.g. Pittet et al., 2002; Van Buchem et al., 2002; Ehrenberg et al., 2018). Subsequent lower energy periods would promote settling and deposition of finer sediments that could infiltrate the coarser beds (e.g. Kreisa, 1981; Al-Awwad and Pomar, 2015), which could represent facies 4.1 and 5.1. Such observations offer further insights into the complex lateral variability in conditions of deposition, which are controlling facies heterogeneity.

The rudist content in facies 5.1 and 5.2 of subzone 2 is characterized by shell fragments and an absence of articulated or disarticulated rudists, suggesting moderate reworking over short to moderate transport distances, as reported in some rudist-rich outcrop studies (e.g. Carannante et al, 2003; Du et al., 2015). These studies report that beds containing rudist fragments are not laterally traceable, showing lenticular geometries with decimetric thicknesses and erosive bases, also possibly representing infilling channel-like structures controlled by hydrodynamics

and possibly storm events (e.g. Carannante et al, 2003; Ruberti et al., 2006). Such examples provide further insights into the depositional geometries, palaeoenvironmental conditions and sediment distribution in subzone 2 of the UKM, which might represent reworked particles transported over relatively short distances from different points of the high-energy environment and deposited in the form of lenticular or possibly wedge-like geobodies (Figure III.2.15).

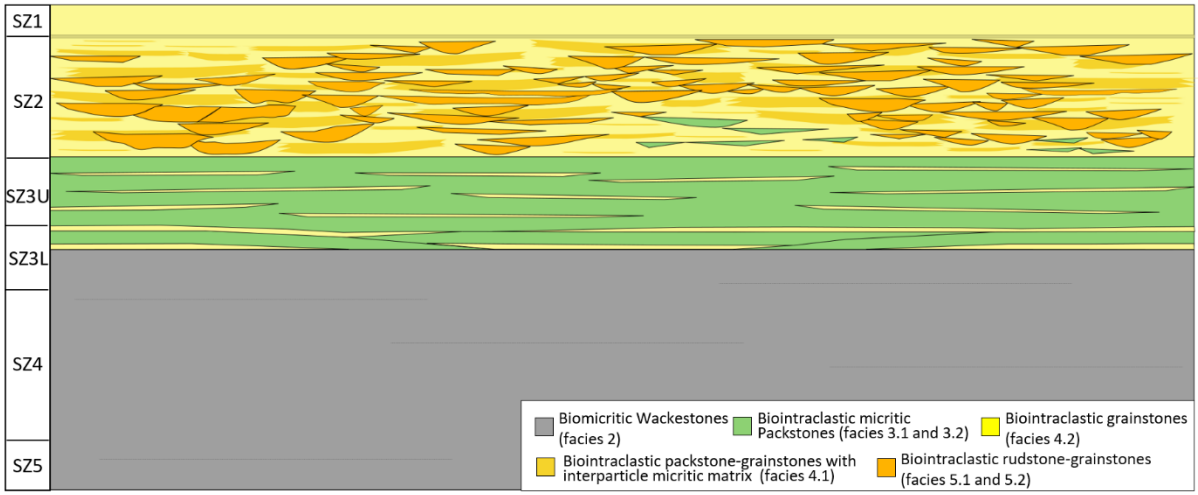

Figure III.2.15. Simplified conceptual model showing facies distribution and potential depositional geometries, with lenticular bodies, channel like structures and possibly wedge-like bodies developing in the younger subzones, characterized by the occurrence of higher-energy sediments. Vertical extension is approximately 180 ft (55 m). Horizontal distance is approximately 20 Km. At this scale of representation, some aspects are exaggerated. Based on interpretations of the studied wells and elements from published studies (e.g. Pittet et al., 2002; Van Buchem et al., 2002; Strohmenger et al., 2006; Ehrenberg et al., 2018).

III.2.6.3.3. Potential tectonic influence on sedimentation

Although sedimentation in the Barremian is considered to occur during a relatively quiet tectonic phase, as might be reflected in the large-scale, regional similarity in depositional facies succession across the Abu Dhabi region (e.g. Alsharhan, 1989; Davies et al., 2002; Peters et al., 2003; Al Kindi and Richard, 2014), there are still some indications for potential minor tectonic influence on deposition (e.g. Van Buchem et al., 2002).

The tectonic uplift of the Paleozoic-established Qatar Arch (see Figure III.2.1 for location) has been reported to be active during the late Hauterivian-early Barremian (e.g. Hassan et al., 1975, in Davies et al., 2002), and has considerable influence on sedimentation in the area, with depositional units generally thickening away from the arch (e.g. Alsharhan and Nairn, 1997). In the Northern Emirates of the U.A.E., Hauterivian deposits are reportedly characterized by mixed siliciclastic-carbonate turbidites with burrowed muddy sediments and repeating

unconformities, recording times of sediments slumping, which indicate deposition under the influence of minor tectonic pulses in these areas of the U.A.E. and in Oman (e.g. Alsharhan, 1989). Halokinetic activity also adds complexity to sedimentation in the region, starting from the Paleozoic until the Tertiary (Alsharhan, 1985, and references therein), having led to the creation of major structures containing oil accumulations in areas where salt deposits are thicker (see Figure III.2.1), in offshore Abu Dhabi and in Oman (e.g. Murris, 1980; Alsharhan, 1985; Loosveld, 1996; Peters et al., 2003; Stern and Johnson, 2010; Thomas et al., 2015; Richard et al, 2017; Faghih et al., 2019). During the Early Cretaceous, halokinesis is reportedly reduced, with strongly increased activity from Late Cretaceous onwards (e.g. Peters et al., 2003; Richard et al, 2017). However, indications of minor salt movement affecting deposition of the Kharaib Formation in offshore Abu Dhabi have been reported, as expressed by sediment thinning across the structures of some fields, interpreted to possibly occur in response to gentle topographic variations resulting from diapirism (e.g. Hassan et al., 1975, in Alsharhan and Kendal, 1991; Alsharhan, 1990).

Deposition of the UKM precedes the development of the Barremian-Aptian intrashelf Bab Basin (e.g. Murris, 1980; Van Buchem et al., 2002, 2010), which is located in a similar geographic position as the Oxfordian- Kimmeridgian Diyab and Cenomanian Shilaif intrashelf basins (e.g. Murris, 1980; Vahrenkamp et al., 2015b). This might be an indication of recurring structural activity occurring along the same underlying tectonic features or patterns at different points in time, influencing sedimentation through the creation of these localized depressions or intrashelf basins. The thickness map for the UKM and for the dense unit above (Hawar Member) preceding the development of the Bab Basin show a relative thinning along a northwest-southeast axis across Abu Dhabi (see figure 6 of Vahrenkamp et al., 2015b and figure 13 of Pierson et al., 2010), in a direction which is roughly parallel to the deep Najd fault system (e.g. Loosveld et al., 1996; Sharland et al., 2001; Pierson et al., 2010; Vahrenkamp et al., 2015b). This might suggest minor to moderate tectonic controls on sedimentation during this time, through the creation of a gentle seafloor topography (e.g. Van Buchem et al., 2002; Pierson et al., 2004, 2010; Davies et al., 2002). Differential sedimentation rates in the Abu Dhabi region would have most likely enhanced the development of this basin, as well (e.g. Alsharhan, 1989; Van Buchem et al., 2002; Vahrenkamp et al., 2015b). In this context, and supporting this view, Burchette and Wright (1992) indicate examples of intrashelf basins in passive margins with a tectonic origin, controlled by extensional fault movements or by structural activity along basement lineaments. These authors do also mention a subsequent control on the intrashelf basin development exerted by the dynamics of the carbonate platform growth.

III.2.6.4. Petrophysical properties variability

The variability in total porosity through the reservoir does not show a clear trend in each well individually, although there is an overall decrease in total porosity with increasing depth when considering the combined data of the four analysed wells (Figure III.2.16). Porosity is considerably lower near the top and bottom of the reservoir zone, in the transition zone from and into the non-porous dense layers below and above. Lower porosity intervals within the reservoir zone are related to the clay-rich boundaries of each subzone, with stronger dissolution and cementation occurring in the adjacent limestone layers (e.g. Oswald et al., 1995; Grötsch et al., 1998; Ehrenberg et al., 2016). Porosity in the reservoir zone, excluding these low porosity intervals, varies between approximately 23 and 32 %.

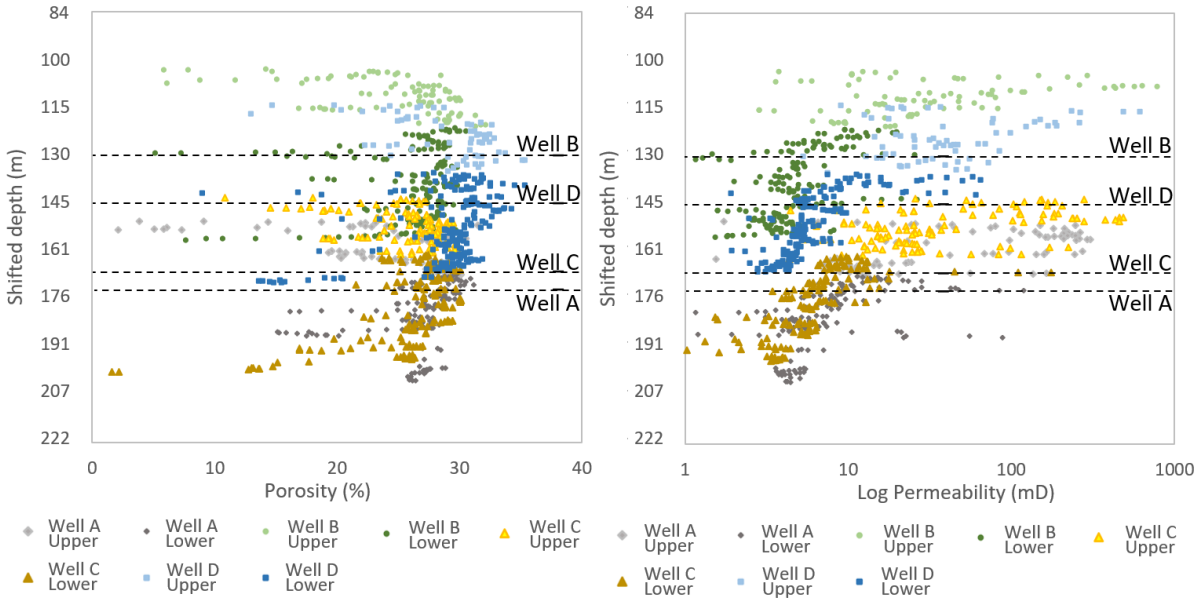

Figure III.2.16. **Left**: Total porosity vs depth; **right**: Permeability vs depth. Dashed lines represent average depth for each well. Vertical axis represents shifted depth in metres.

Well D shows relatively higher values for total porosity, although it is not the shallowest well (Figure III.2.16). This could be related to its northernmost geographic location and the relative position in the paleoenvironment setting or to minor variations in the effects of diagenesis. Well B was drilled higher in the crestal zone, although total porosity values are generally lower than in well D (Figure III.2.16). Well B is located near a major northwest-southeast fault zone/corridor, which might have some effect of rock property variations. Wells A and C are both deeper than the previously mentioned wells and both show slightly lower overall porosities, following the general trend of decreasing porosity with increasing depth, although values are similar.

Vertical permeability variations are much more pronounced than porosity variations (Figure III.2.16), reaching values above 100 mD in subzone 3 and higher in subzone 2 (above 300 and above 600 mD in some cases). There is a strong increase in permeability from the microporous, wackestone sediments in the lower reservoir interval (subzones 3L and 4), into the packstones, grainstones and rudstone-grainstones of the upper interval (subzones 1, 2 and 3U). This trend is similar in all four wells, as well as in other fields throughout the Abu Dhabi region (e.g. Alsharhan, 1990; El Wazir et al., 2015; Ehrenberg et al., 2016, 2018, 2020b). The younger subzones are characterized by a much more heterogeneous pore system, as mentioned previously (Figure III.2.17).

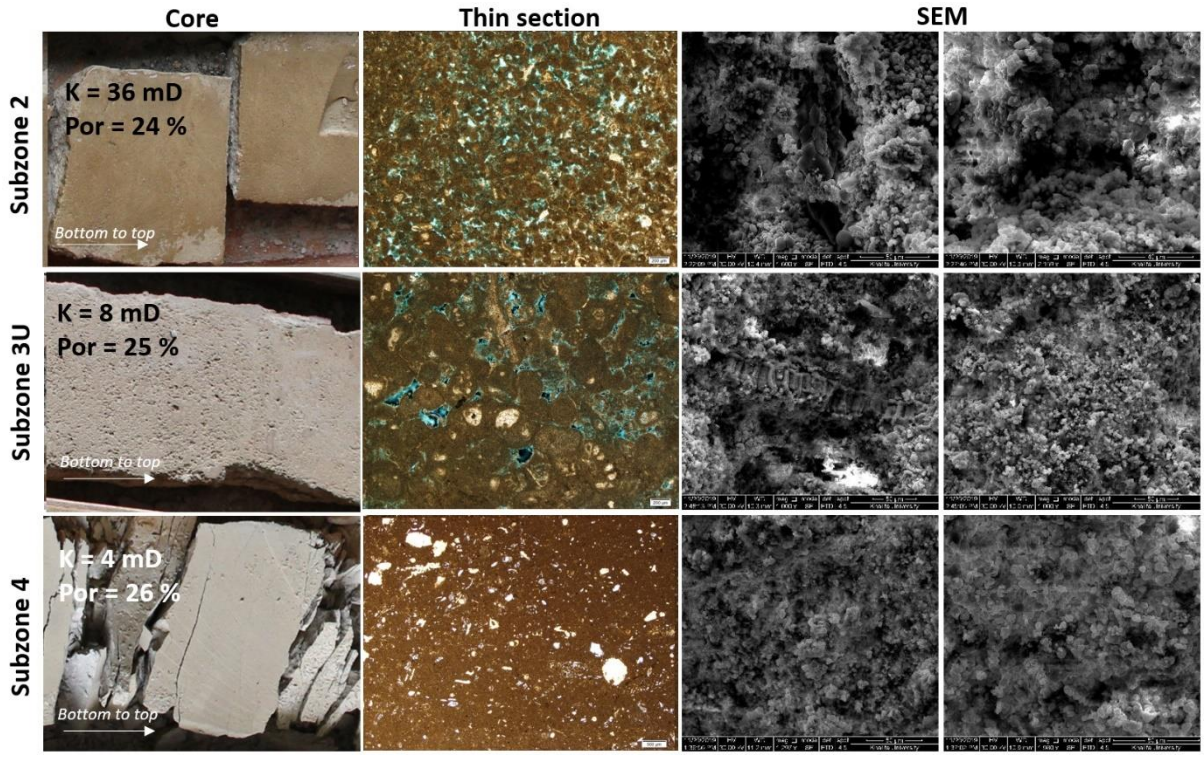

Figure III.2.17. Comparison between core, thin section and SEM photos of subzones 4, 3U and 2. Subzone 4 shows a homogeneous pore system, characterized almost in its entirety by microporosity (some vuggy porosity occurs). Total porosity is slightly higher than the examples shown for subzones 3U and 2, although permeability is lower. Subzones 3U and 2 show a more heterogeneous appearance, with higher interparticle macroporosity.

III.2.6.4.1. Porosity vs. permeability

The correlation between total porosity and permeability measured on core-plugs is weak in all wells (Table III.2.2). This is also illustrated by the data scatter on the porosity-permeability cross-plot (Figure III.2.18a). In order to acquire a better understanding of the controls on petrophysical properties variations, petrographic interpretations, such as facies classification and macroporosity measured through DIA were integrated. Samples were divided into three

major groups, with group 1 including grainstones with no micritic content and rudstone-grainstones (facies 4.2, 5.1 and 5.2), group 2 including packstone-grainstones with micritic content and packstones (facies 3.1, 3.2 and 4.1), and group 3 including wackestones (facies 2). The correlation between porosity and permeability is clearer for group 3 textures, as they are characterized by a homogeneous microporous network, and becomes progressively weaker for groups 1 and 2, due to the more heterogeneous nature of their dual-porosity network and the variable effects of diagenesis. A comparison between permeability and measured interparticle macroporosity results in a seemingly improved correlation (Table III.2.2, Figure III.2.18b).

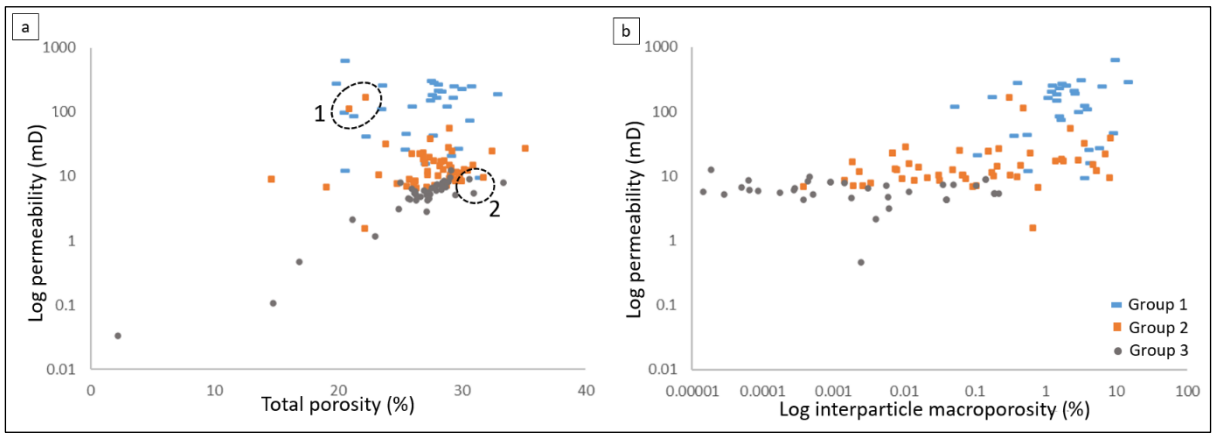

Figure III.2.18. **a**: Permeability vs. total porosity. **b**: Permeability vs interparticle macroporosity. Samples are divided in three major groups. Group 1: grainstones with no micrite and rudstone-grainstones; Group 2: packstone-grainstones and packstones; Group 3: wackestones.

Two samples from group 2 show increased permeability, plotting in the group 1 field (circle 1 in Figure III.2.18a). One is a bioclastic-micritic packstone with moderate moldic macroporosity probably connected through microporosity, approaching a point of textural inversion where moldic pores are open and lined with calcite cements. The other is a micritic, bioclastic packstone with peloids, coated grains and probable Porostromata. The referred features might be enhancing permeability, although the possible presence of additional aspects such as fractures in the measured plugs is unknown and should not be discarded. A group 1 sample plots within the group 3 samples field (dashed circle 2 in Figure III.2.18a). This sample represents a moderately compacted/condensed grainstone with high volume of syntaxial cement around echinoderm fragments. These features could have reduced permeability considerably, through the partial occlusion of original pore space and pore throats.

III.2.6.4.2. High permeability values vs. depositional rock properties

The occurrence of high permeability intervals is important to understand, as they behave as preferred fluid flow paths strongly affecting reservoir performance (e.g. Weber, 1986; Cunningham and Chaliha, 2002; Carvalho et al., 2011). In order to further investigate depositional and textural controls on permeability variation, a cut-off of 60 mD is applied to separate between high-permeability and low-permeability values, based on the analysis and interpretations of the available data. The resulting set of low-permeability samples, characterized by wackestones, packstones and packstone-grainstones, plots within class 3 of Lucia classification scheme (Lucia, 1983, 2007) (Figure III.2.19a, b), which represents mud-dominated, microporous textures. The high-permeability samples plot in class 2 (Figure III.2.19a, b) and are mainly characterized by grainstone textures (facies 4.2), which show higher measured interparticle macroporosity, although other facies are also represented (Figure III.2.19c). Similar results are reported for the same reservoir in a nearby field (Ehrenberg, 2019). In the Lucia classification scheme, which addresses the relationship between petrophysical properties and rock fabric, grainstones should plot in class 1 (Lucia, 1983, 2007; Jennings and Lucia, 2003). In this case, the intraparticle microporosity of the micritized particles affects the behaviour of grainstone samples, which are projected in class 2 instead of class 1, when plotted against total porosity (Lucia, 2007). In this classification scheme, microporosity is considered as non-connected vuggy porosity, as these pore types will contribute to total porosity but not to permeability (e.g. Lucia, 2007; Amel et al., 2015). The difficulty in modelling and predicting permeability in such heterogeneous carbonate systems is high and the complexity and pitfalls of applying such classification schemes are revealed these cases, as different schemes will have their own limitations and each case study might show specific differences which might require that specific methodologies and workflows are developed (e.g. Johnson et al., 2010; Bust et al., 2011; Rebelle and Lalanne, 2014).

As mentioned above, a number of high-permeability samples are characterized by different depositional facies and not all samples with grainstone facies 4.2 show high-permeability (Figure III.2.19c), which is related to variations in the depositional characteristic of the sediments (Figure III.2.19d) and diagenesis. Low permeabilities within facies 4.2 show poor to very poor grain sorting (Figure III.2.19d), while most high-k samples are moderately to well sorted with virtually no interparticle cementation and no micritic matrix (Figure III.2.20). A few high-permeability, poorly-sorted grainstones are associated with the presence of coarser particles (Figure III.2.19d). Depositional factors, including grain sorting and size are, therefore, considered as important parameters controlling permeability variations in the studied wells. The quantification of such petrographic parameters is important to integrate with textural interpretations, as this kind of data reveals valuable information regarding the controls on petrophysical properties variability. However, diagenesis will also have an important effect in the evolution of reservoir properties (see section 5.4.3) and the extent of these diagenetic effects

will dictate the relative contribution of depositional and diagenetic factors to petrophysical properties variability (e.g. Wardlaw, 1996; Ehrenberg et al., 2008; Swei and Tucker, 2012; Amel et al., 2015).

Mid-permeability values show no clear correlation with depositional textures (Figure III.2.19c). These intervals are generally characterized by packstones and packstone-grainstones with higher volumes of micritic matrix, as well as wackestone facies with interparticle macroporosity lower than 1 % and very close to 0 % (Figure III.2.18b). Permeability in these samples is low, as it is predominantly controlled by the microporosity network within the micritic framework.

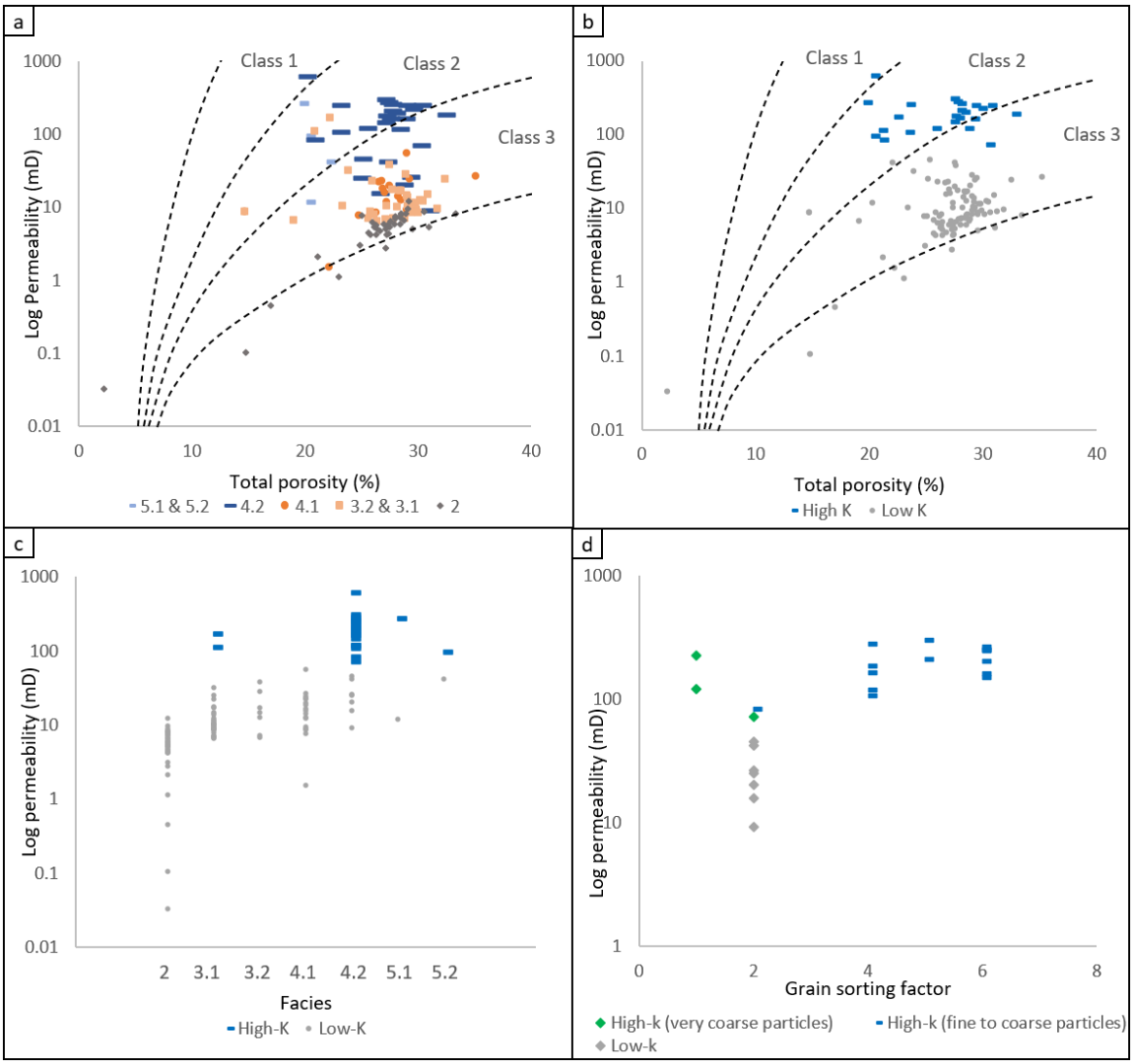

Figure III.2.19. **a:** Permeability vs total porosity; different colours represent different facies. Dashed curves represent class boundaries of Lucia (1983, 2007); **b:** Same data as plot (**a**), but separating low and high-permeability samples; **c:** Permeability plotted against facies types. Most high-k samples are represented by samples with facies 4.2 (grainstones with virtually no interparticle cementation); **d:** Permeability plotted against grain sorting factor for facies 4.2 only (higher grain sorting factor indicates better sorting). High-permeability, very coarse-grained samples are differentiated, in green.

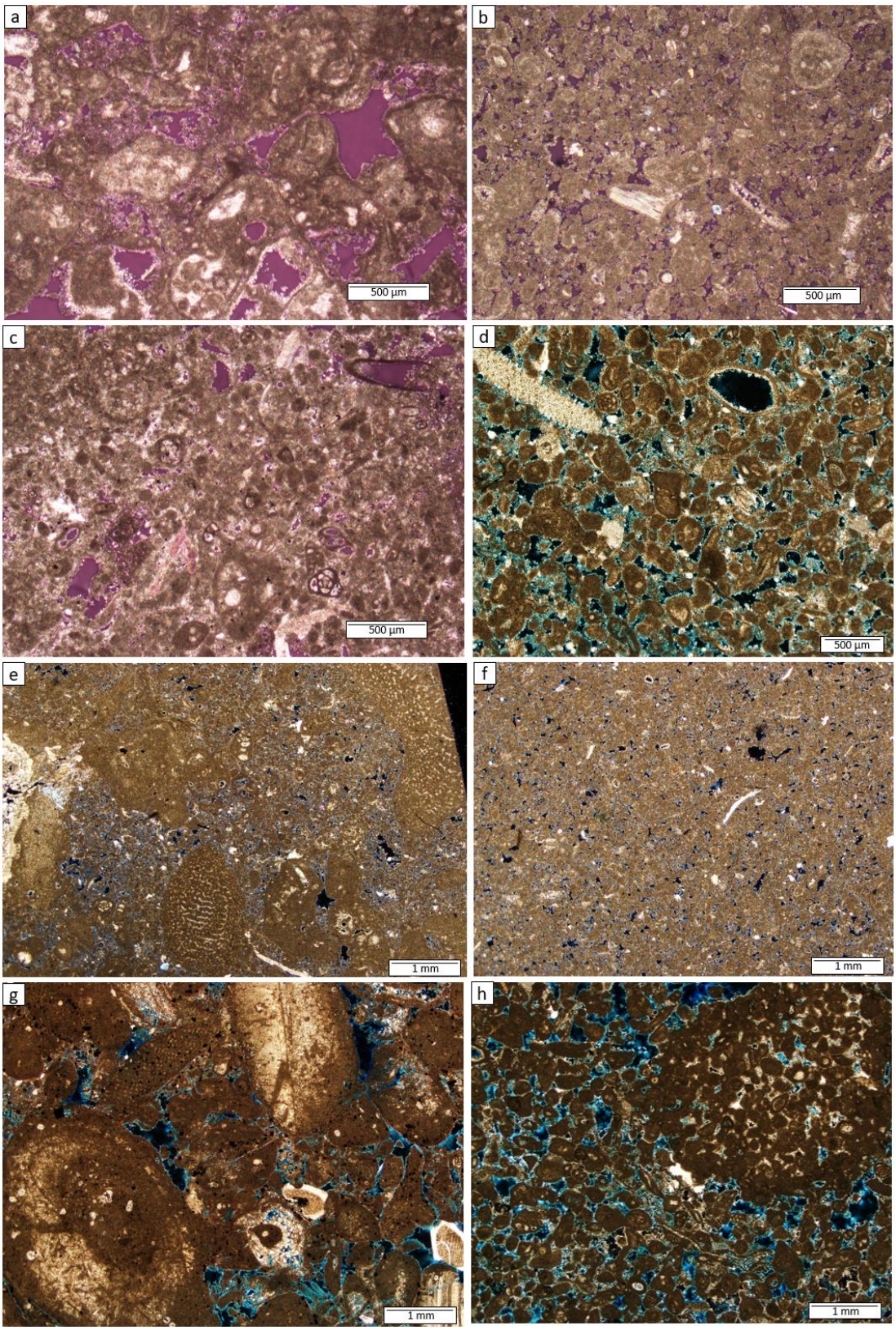

Figure III.2.20. Thin section examples for high-permeability samples. Total porosity is available from conventional core analysis and estimated macroporosity measured through DIA. **a**: CCA Permeability (K) = 281 mD, CCA total porosity (cpor) = 27 %, macroporosity (macro) = 13 %; **b**: K = 83 mD, cpor = 21 %, macro = 1.5 %; **c**: K = 120 mD, cpor = 26 %, macro = 3 %; **d**: K = 265 mD, cpor = 28 %, macro = 2 %; **e**: K = 71 mD, cpor = 30 %, macro = 2 %; **f**: K = 188 mD, cpor = 33 %, macro = 2.5 %; **g**: K = 96 mD, cpor = 20 %, macro = 3 %; **h**: K = 245 mD, cpor = 29 %, macro = 6 %.

III.2.6.4.3. Potential diagenetic controls on rock properties variations

The variability in porosity and permeability is a result of the combined effects of depositional and diagenetic controls (e.g. Oswald et al., 1995; Lucia, 2007; Swei and Tucker, 2012; Ehrenberg, 2019; Ehrenberg et al., 2020a). While the main control on the occurrence of high permeability intervals is considered to be depositional in the studied wells, as discussed above, diagenesis will also exert strong influence on the evolution of petrophysical properties, mainly through compaction, low cementation and micritization.

Compaction had an important effect in reducing original porosity to different extents, as expressed by the different types of contact between grains (Figure III.2.6), as well as features such as stylolites and the associated localized cementation, with partial occlusion of the pore-space (e.g. Harris et al., 1968; Paganoni et al., 2016; Ehrenberg, 2019). Throughout burial diagenesis, physical and chemical compaction has increasingly promoted the degradation of porosity, which generally decreases with depth in the region (e.g. Oswald et al., 1995; Ehrenberg et al., 2008; Ehrenberg et al., 2020a). This trend, of decreasing porosity with depth, is well known and reported for the Abu Dhabi regional dataset for this reservoir (Ehrenberg et al., 2020a), as well as in a larger dataset for Cretaceous reservoirs in the Arabian Platform (Ehrenberg et al., 2008). Although this trend is perceived in the studied data (Figure III.2.16), the depth difference between the shallowest and deepest sample is relatively low at close to 350 ft (approximately 107 m) and the facies variability, from packstones, grainstones and rudstone-grainstones in the upper half to wackestones in the lower half might be influencing this porosity variation trend. A larger dataset will, therefore, facilitate this observation.

Calcite cementation of interparticle macroporosity in grainstones and rudstone-grainstones is generally low to very low in the studied well intervals, with most of the macroporous space remaining open (Figures III.2.5, III.2.6, III.2.20), although in intervals close to subzone boundaries, the cement volume is increased. However, this weak cementation of the pore space will still have an effect on permeability variations, as the observed cement rims (Figure III.2.6) will partially occlude the original pore throats, probably deteriorating permeability (e.g. Lucia, 1983; Hollis et al., 2017). The impact of such diagenetic effects is difficult to objectively quantify, is most likely variable through different intervals of the reservoir, and will probably have some role in altering the correlation of permeability with porosity and depositional facies.

Micritization had an important role in controlling porosity evolution in this reservoir, having led to the creation of microporosity as the dominant fraction of total porosity (Figures III.2.12, III.2.13), as expressed by the difference between total CCA porosity and estimated macroporosity, with higher-permeability grainstone intervals also showing considerable volumes of microporosity within the micritized particles (e.g. Morad et al., 2016). The process of micritization is not fully understood in the UKM and has been described as originating from different processes (e.g. Morad et al., 2016), such as mineralogic stabilization and

recrystallization or cementation under the influence of marine pore waters during early diagenesis (Budd, 1989; Moshier, 1989), stabilization of depositional muds of low-Mg calcite during early diagenesis, prior to burial (Volery et al., 2010), burial precipitation of microrhombic calcite controlled by regional basinal fluid flow (Vahrenkamp et al., 2014), conversion of allochems into peloids and precipitation of micrite and microspar partly controlled by phases of stylolitization (Morad et al., 2016). Further studies, utilizing higher-resolution imaging would be required to characterize and better understand the heterogeneity and fluid flow within this microporous network.

In this case study, diagenesis had a strong role in the development of the present-day heterogeneous dual micro-macroporosity system but primary depositional parameters such as depositional facies, original interparticle macroporosity, grain sorting or volume of micritic matrix are the main controls on the stronger permeability variations (Figures III.2.19c, d, III.2.21), in moderate similarity to what has been reported for a nearby field (Ehrenberg, 2019). However, the average porosity values for this reservoir are different between these fields, as well as other fields in Abu Dhabi (Ehrenberg et al., 2020a).

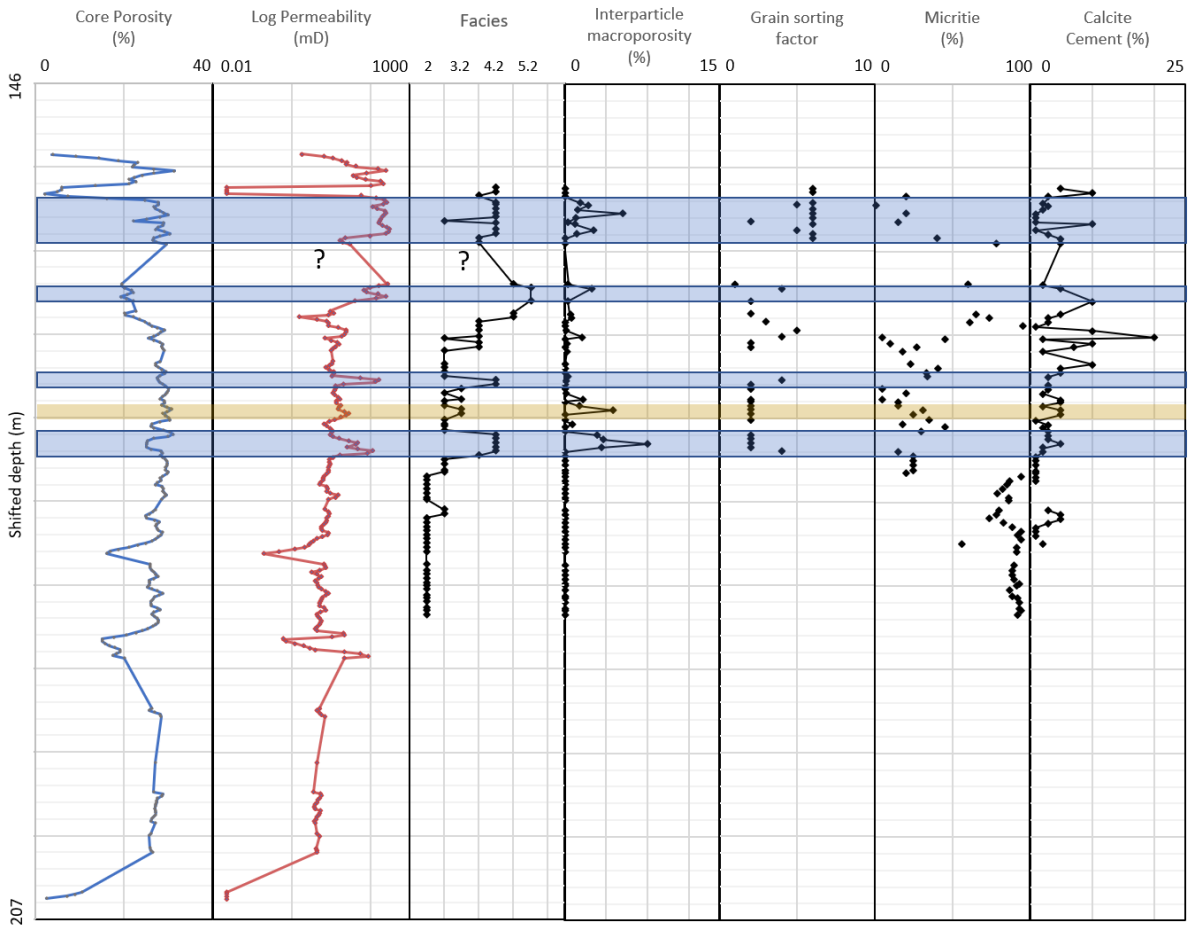

Figure III.2.21. Composite panel showing high permeability layers (blue shade) correlating with facies 4.2 (and also 5.2), and generally with overall higher interparticle macroporosity. Gold shaded area indicates sample with relatively high interparticle macroporosity and with a heterogeneous appearance, mostly showing a packstone (to grainstone) texture, but also areas with coarse particles and high interparticle porosity. Vertical axis represents shifted depth in metres.

III.2.6.4.4. Potential influence of oil emplacement on regional porosity variation

Differential diagenesis and the effects of oil emplacement have been described in past studies for different fields in Abu Dhabi, with most of them comparing between crest and flank positions to show higher porosity preservation in crestal areas after oil emplacement (e.g. Oswald et al., 1995; Grötsch et al., 1998; Melville et al., 2004; Cox et al., 2010; El Wazir et al., 2015; Paganoni et al., 2016; Ehrenberg et al., 2016; Morad et al., 2019). Differential diagenesis regionally across different fields will have most likely occurred, according to data reported in recent studies (e.g. Vahrenkamp et al., 2014; Barata et al., 2015; Ehrenberg et al., 2020a, 2020b), affecting the variability in petrophysical properties of this reservoir, with oil emplacement reported as one of the main controls on porosity variations (e.g. Ehrenberg et al., 2020a).

In the deeper Field 2, immediately to the north/northeast of the studied field, average porosity for the UKM is lower, possibly due to the reported moderate calcite cementation of macroporosity, given that correlation between porosity and depositional texture is relatively poor, while microporosity remains open (Ehrenberg, 2019; Ehrenberg, 2020a). In Field 3, located to the west-northwest of the studied field, across the Falaha syncline, deeper than Field 1 and shallower than Field 2, shows average porosity values similar to Field 1 (e.g. Ehrenberg, 2020a) and partial occlusion of macroporosity by calcite cementation (El Wazir et al., 2015), in closer similarity to the weaker cementation observed in Field 1. The offshore Field 5 to the north shows lower average porosity than Field 1, although they are at similar depths (e.g. Ehrenberg, 2020a), with higher volumes of calcite cement reported for this reservoir in Field 5 (e.g. Thorpe, 2014) (see Figure III.2.4 for field locations). The large-scale regional porosity variations are suggested to result mainly from differences in burial depth, while porosity variability at similar depths could result from these regional variations in the extent of pore space cementation (e.g. Ehrenberg et al., 2020a), which might occur as a consequence of the different timing for hydrocarbons emplacement on the different structures in Abu Dhabi, as will be discussed below. This increases the difficulty in predicting the spatial variability in petrophysical properties, as the extent of cementation is not easy to predict. However, the precipitation of calcite cement in macroporosity of the UKM in Field 1 is low in the studied wells and depositional texture shows a moderate correlation with permeability and macroporosity, as previously discussed (Table III.2.2, Figures III.2.19, III.2.21). The

correlation between depositional texture and total porosity is weak, due to the presence of a dominating microporous phase, demonstrating the importance of performing a quantitative analysis of macroporosity and the different pore types.

Cementation dynamics and differential diagenesis at field and regional scale in Abu Dhabi are, in part, influenced by the history of oil emplacement (e.g. Cox et al., 2010; Thorpe, 2014; Wood et al., 2014; Fullmer et al., 2014), which has most likely occurred at different times in different fields and structures (e.g. Alsharhan, 1989; Taher, 1996), and might have influenced the regional variability in petrophysical properties. An initial phase of migration, starting as early as the Santonian (Oswald et al., 1995), from the more mature southwestern area of the Falaha syncline would have charged the structurally higher nearby fields 1 and 3 (Alsharhan, 1989; see figure 20 of Taher, 1997). This would have reduced the rate of calcite cementation at an earlier stage, preserving higher porosities in these fields. Meanwhile, calcite cementation is ongoing in the other fields which would have remained mostly water-filled during these initial stages of oil migration and emplacement. With continued tilting of the strata to the north-northeast, related to the ophiolite loading and the Zagros collision, additional volumes of hydrocarbons, as well as burial brines, will have migrated from the increasingly deeper buried units in the east-northeast of the U.A.E. into the northeastern fields of Abu Dhabi (including fields 2 and 4), with fill-and-spill providing further secondary migration pathways and hydrocarbon charge to the adjacent fields towards the south/southwest, including Field 1 (Taher, 1997). This hydrocarbon migration model, as reported by Alsharhan (1989) and Taher (1997), might explain the lower porosities of fields 2, 4, and 5, in comparison to fields 1 and 3, due to the effects of hydrocarbon emplacement (occurring at different times in different fields) in retarding cementation (e.g. Cox et al., 2010; Thorpe, 2014; Wood et al., 2014). The later phase of relatively rapid East to West tectonically-driven regional flow of burial brines, as also proposed in different studies (e.g. Vahrenkamp et al., 2014; Barata et al., 2015; Paganoni et al., 2016; Morad et al., 2019), as well as of hydrocarbons and other associated fluids, will have further affected diagenesis during migration, through recrystallization or chemical dissolution promoted by these migrating source rock fluids (e.g. Worden and Heasley, 2000). However, these models for regional flow of burial brines and their effect on differential diagenesis are a working hypothesis that requires further studies and additional data for confirmation.

III.2.7. Impact of the results on field development and reservoir modelling

The controls on reservoir heterogeneity are not fully understood in most cases and, in addition, the process of upscaling well data in the development of reservoir models will lead to detailed geological information to be lost. Reservoir rock types are defined based on their dynamic behaviour, in integration with geological information. As such, the depositional facies and geometries, as well as their variability need to be well understood in order to achieve a rock type classification scheme which properly describes the reservoir behaviour while maintaining a good link to the geology and facies scheme (e.g. Gomes et al., 2008; Chandra et al., 2015). A quantitative, detailed understanding of depositional textures and pore types heterogeneity in this reservoir provides additional information that may contribute to the development of upscaled reservoir models with stronger geological meaning and bring improvements to field development plans.

The occurrence of high permeability intervals in macroporous grainstone and rudstone-grainstone will affect processes such as water injection and waterflooding used to increase oil production and oil recovery, as they will behave as preferred fluid flow paths, as previously mentioned. Early water breakthrough impacting reservoir sweep efficiency is observed in the Thamama Group reservoirs of different Abu Dhabi fields, including the offshore fields (e.g. Broomhall et al., 2008; Shekhar et al., 2017; Edwards et al., 2019), particularly affecting oil recovery efficiency in the lower half of the reservoir (SZ3L and SZ4), with volumes of bypassed hydrocarbon remaining in the micropores, which will not contributing to fluid flow and to production (Figure III.2.22) (e.g. Weber, 1986; Wardlaw, 1996; Cunningham and Chaliha, 2002; Dabbouk et al., 2002; Carvalho et al., 2011). Although the spatial continuity of high permeability bodies in SZ2 and SZ3U might be reduced or non-existing in some cases, as previously discussed, preferred flow paths will still connect through these bodies across rock volumes of relatively lower permeability facies 4.1 (biointraclastic packstone-grainstone, thus with some micrite), 3.1 and 3.2 (biointraclastic micritic packstones) in some places, also controlled by the effects of variability in wettability and capillary pressure in the heterogeneous pore network (e.g. Namba and Hiraoka, 1995; Chilingarian et al., 1992; Masalmeh, 2002; Masalmeh et al., 2003).

Given that the presence of high permeability intervals is mainly controlled by the depositional characteristics of the sedimentary succession of this reservoir in the studied wells, an integrated analysis of textural features linked to petrophysical parameters and semi-automated digital quantification of macroporosity within a stratigraphic framework will facilitate the understanding on reservoir heterogeneity, offering further insights into the predictability of lateral reservoir properties variations between wells.

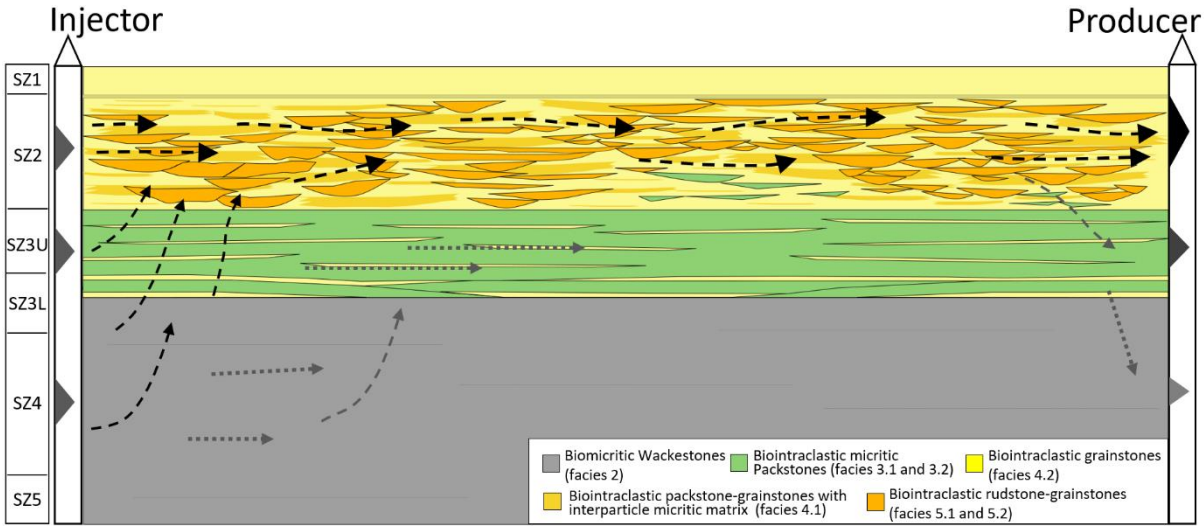

Figure III.2.22. Simplified, conceptual geological cross section of the UKM across the studied field, based on interpretations of the studied wells and elements from previous studies (e.g. Van Buchem et al., 2002; Strohmenger et al., 2006; Ehrenberg et al., 2018). Considering only one injector well and one producer well, dashed arrows are a simplified representation of preferred fluid flow paths through the more permeable upper half of the reservoir, after a certain time of continued injection and production (based on Cunningham and Chaliha, 2002; Carvalho et al., 2011).

III.2.8. Conclusions

The present study offers further insight into the factors controlling reservoir heterogeneity in the Barremian Upper Kharaib Member in Abu Dhabi through the analysis of core and thin sections from 4 selected wells of an onshore field, focusing on small-scale heterogeneity. New quantitative data on macroporosity and pore type distribution, generated in this study through digital image analysis, including guided machine learning, was integrated with petrographic and available petrophysical data in order to achieve these objectives. This kind of analysis provides invaluable information for a better understanding of the reservoir and its performance.

The Upper Kharaib Member shows well-known and well-described large scale vertical heterogeneity in depositional facies and permeability, but not so much in total porosity. The lower half is characterized by more homogeneous micritic wackestone intervals, while the upper half is defined by stronger variability between packstone, packstone-grainstone, grainstone and rudstone-grainstone facies, as well as by the occurrence of high permeability intervals, especially in subzones 2 and 3U. At a smaller scale, vertical heterogeneity is more complex to define in this upper half of the reservoir and the lateral variability in facies and reservoir properties in inter-well areas is a major issue regarding reservoir modelling efforts. Small-scale, discontinuity-bounded intervals are clearly identified in subzones 2 and 3U,

showing vertical variability trends in facies and to some extent in pore type distribution. These rhythmic successions vary from well to well, indicating complex depositional geometry patterns and limited lateral extension of geobodies.

The acquisition of quantitative data on pore types obtained through semi-automated digital image analysis provides valuable information on the occurrence of high permeability intervals, important for proper reservoir characterization and improved model construction to better understand reservoir performance. Permeability is significantly higher in virtually non-cemented, well-sorted grainstone facies with higher interparticle macroporosity, which will act as main fluid flow drivers. The dual micro- and macroporosity system characterizing this reservoir, where microporosity constitutes the larger fraction of total porosity (in the micritic matrix and in the micritized grains), will strongly affect reservoir performance and oil recovery efficiency.

Integrating digital image analysis results with semi-quantitative petrographic data and petrophysical data provides valuable insights into the factors controlling heterogeneity in rock properties. Macroporosity distribution directly relates to the occurrence of high permeability intervals and is closely related to variations in depositional facies, which is an indication that improved degrees of predictability might be obtained through this type of integrated analysis. Such detailed studies will help in the construction of reservoir models with improved geological meaning, enhancing inter-well predictability of rock properties and helping to improve field development plans.

Appendix III.2.A

Figure III.2.23. Composite panels for the four analysed wells, showing GR, porosity and permeability logs, as well as facies intepretations, digitally measured macroporosity and estimated relative volumes of sample constituents. Coloured boxes are used to provide reference levels for easier visualization. Tops of subzones (SZ) are indicated on the GR log. Vertical axis represents shifted depth in metres.

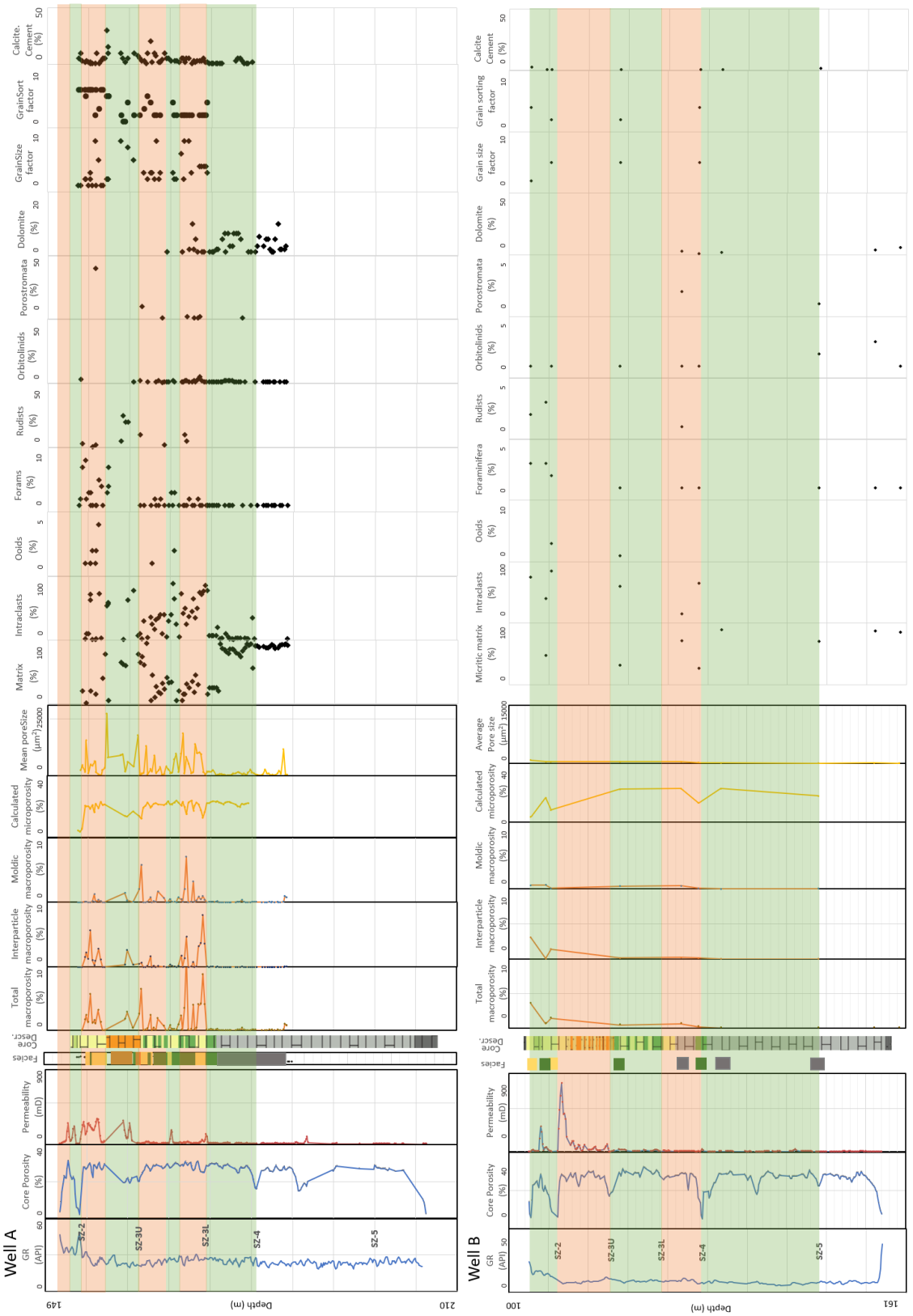

Figure III.2.23. (continued)

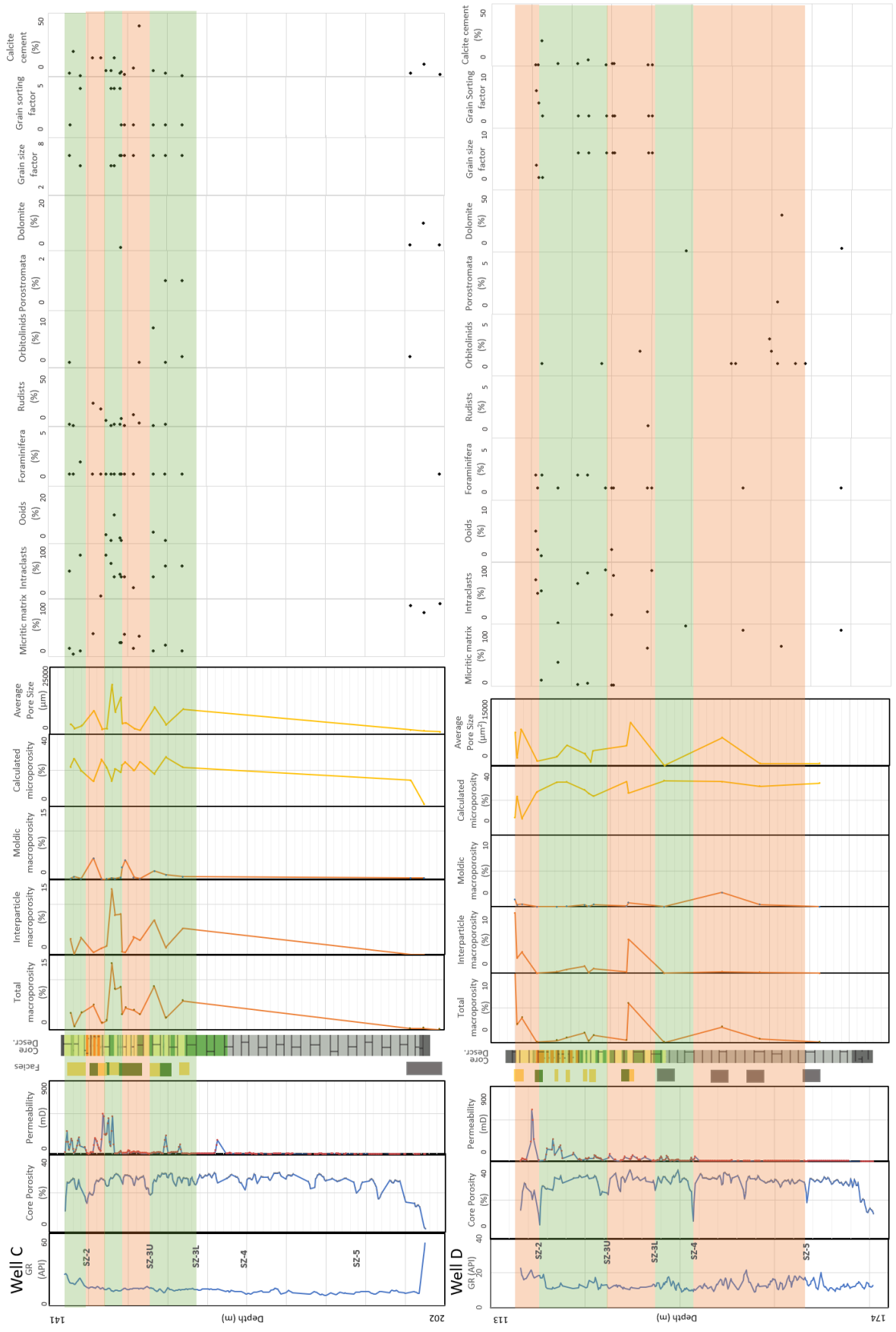

Chapter IV. The Santo António-Candeeiros Formation, Lusitanian Basin, Portugal

IV.1. Multi-scale outcrop analysis of depositional geometries - Comparison with the U.A.E. subsurface case

IV.1.1. Abstract

Outcrop observations offer valuable insights into depositional architecture as a primary control on facies and reservoir properties variability, being of crucial interest for subsurface cases, where observation points are limited to well locations. This approach was used, comparing the potential reservoir facies of Bathonian-Callovian carbonate succession outcrops of the Maciço Calcário Estremenho (MCE) region, central Lusitanian Basin, Portugal, with the Lower Cretaceous subsurface carbonate reservoir from Abu Dhabi (U.A.E.). The MCE succession is characterized by high-energy, inner-ramp facies and is exposed in recently-cut quarry fronts showing minimal weathering effects, allowing for detailed observations on depositional geometries. The U.A.E. case study is characterized by facies of mid to inner ramp, interpreted using core and thin section data from 4 wells.

Outcrop geometries vary from tabular, wedge-like, lensoids and coral build-ups, controlling facies distribution, which are generally defined as oobiointraclastic grainstones, biointraclastic grainstone-rudstones and coral/algal boundstones. Moderate similarities in depositional geometries with the U.A.E. case were identified, with the latter evolving from tabular, wedge-like and lenticular geobodies into rudist-rich intervals. There are differences in terms of facies, with the MCE case reflecting relatively higher-energy depositional conditions. A multi-scale outcrop analysis shows moderate continuity of larger-scale depositional packages over moderate distances, but considerable variability at smaller scales, driving the spatial variability in facies and, potentially, petrophysical properties over short distances, as is interpreted to occur in the Abu Dhabi case. The ultimate objective of such studies is to understand the spatial variability of facies, reduce the uncertainty of subsurface reservoir models and improve the predictability of reservoir properties in inter-well areas.

IV.1.2. Introduction

Carbonate sedimentary systems are characterized by complex depositional geometries, which develop under the influence of different environmental constraints and factors such as topography or hydrodynamics and, at a larger scale, the balance between carbonate

productivity and accommodation space (e.g. McNeill et al., 2004; Schlager, 2005; Pomar and Kendall, 2008; Reeder and Rankey, 2008; Palermo et al., 2010; Alsharhan and Kendall, 2010; Hönig and John, 2015; Sequero et al., 2019). The characterization of these depositional geometries is important in obtaining a better understanding of the depositional system controlling facies distribution (e.g. Mutti et al., 1996; Azerêdo, 1998; Asprion et al., 2008; Jung and Aigner, 2012; Van Tuyl et al., 2018; Petrovic, 2020), but the interpretation and prediction of variability of these features and reservoir properties in subsurface 3D volumes is difficult to attain due to the limited amount of data in inter-well space. This leads to considerable levels of uncertainty in carbonate modelling (e.g. Melville et al., 2004; Yose et al., 2006; Burchette, 2012).

Outcrop observation and analysis is important to improve subsurface geological modelling efforts, by providing valuable information on geometric relationship between depositional bodies at different observation scales, which are not achievable in the subsurface through seismic data, to further improve the understanding of variations in depositional features (e.g. Weber, 1986; Van Buchem et al., 2002; Strohmenger et al., 2006; Palermo et al., 2012; Fitch et al., 2015).

The main objective of this study is to identify and characterize the architecture of deposition of a shallow-water carbonate succession, through the analysis of recently cut quarry fronts at different locations of the Maciço Calcário Estremenho (MCE) in the Lusitanian Basin (LB). In addition, a comparison between the depositional facies and geometries of the studied outcrops and of the subsurface Barremian carbonate reservoir in Abu Dhabi, U.A.E. referred to as the Upper Kharaib Member (UKM), of the Kharaib Formation (following the terminology of Pittet et al., 2002; Van Buchem et al., 2002; 2010), was done to provide further insights into the depositional controls on reservoir heterogeneity. Freshly cut quarry fronts eliminate the factors related to extended outcrop exposure to weathering and offer better opportunities to observe and interpret depositional geometries more clearly. Defining the organizational geometries of a depositional succession will help to better characterize the 3D variability of facies and better understand the lateral and vertical variability of rock properties.

IV.1.3. Geological Background

IV.1.3.1. Lusitanian Basin

The LB extends in a north-south direction in eastern central Portugal (Figure IV.1.1), and is delimited to the east by the exposed Hercynian basement and to the west by the uplifted blocks of a horst-graben marginal system (e.g. Wilson et al., 1989; Pinheiro et al., 1996; Alves et al., 2002, 2003a). The LB developed in an extensional regime associated with the Atlantic opening, under the influence of a strong tectonic activity and different rifting phases, which controlled

sedimentation and structuration at different stages (e.g. Wilson, 1975; Mougenot et al., 1979; Boillot et al., 1979; Vanney and Mougenot, 1981; Wright and Wilson, 1984; Wilson et al., 1989; Hiscott et al., 1990; Rasmussen et al., 1998; Alves et al., 2002, 2003a, 2006; Kullberg et al., 2013).

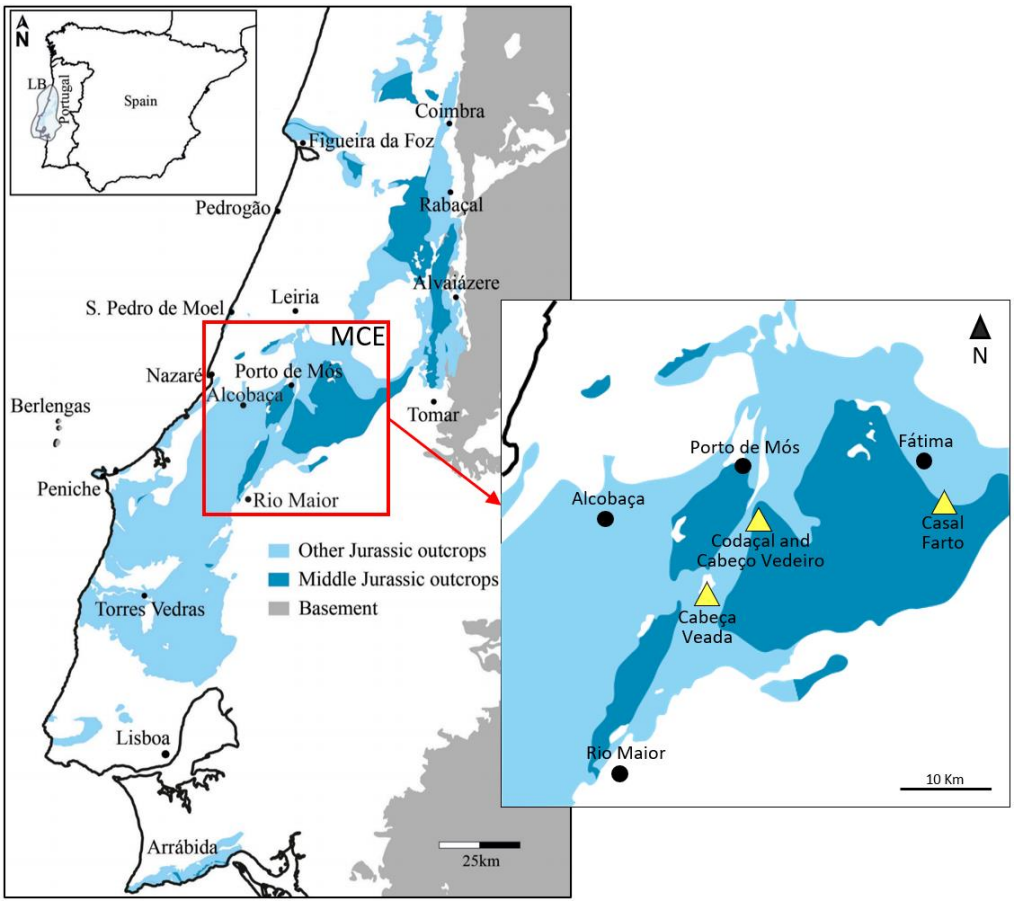

Figure IV.1.1. Simplified geological map of the Lusitanian Basin and the MCE (Azerêdo et al., 2020). Detail map indicated by the red square represents the Maciço Calcário Estremenho location (MCE in figure). Yellow triangles represent the locations of the analysed outcrops.

The Middle Jurassic sediments in the LB were deposited in between two major rifting phases occurring in the Sinemurian-Pliensbachian and the Oxfordian (Rasmussen et al., 1998; Alves et al., 2002, 2003a), at a time when a homoclinal carbonate ramp dipping towards the west/northwest was developing (Azerêdo, 1988, 1993, 1998, 2007; Duarte et al., 2001; Duarte, 2007; Silva et al., 2015). The subsequent continued tectonic activity led to the development and reactivation of faults, creating complex structural patterns in the region (e.g. Mougenot et al., 1979; Wilson et al., 1989; Rasmussen et al., 1998; Alves et al., 2002, 2003a; Kullberg et al., 2013). The associated halokinetic activity, increasing towards the Late Jurassic and Cretaceous, has created salt pillows and salt anticlines, which are more prominent in areas with

thicker salt deposits, along the present-day continental margins and offshore areas of the LB (e.g. Wilson et al., 1989; Rasmussen et al., 1998; Alves et al., 2002, 2003a; Walker et al., 2021). During the Cenozoic, fault reactivation, structural inversion and uplift occurred as a consequence of compressional phases (e.g. Wilson et al., 1989; Rasmussen et al., 1998; Uphoff, 2005; Alves et al., 2003a, 2006).

The Maciço Calcário Estremenho (MCE) refers to a limestone region across the hills of 'Serra de Aire' and 'Serra dos Candeeiros' onshore western Portugal, corresponding to the eastern part of the LB. The outcrops of the MCE are represented mainly by Middle Jurassic shallow-water limestones and dolostones, generally characterized by inner ramp, high-energy barrier-island and lower energy lagoonal facies, and peritidal protected, back-barrier facies.

IV.1.3.1.1. Stratigraphic context

The Middle Jurassic in the LB developed within a major 1st order transgressive-regressive (T-R) cycle beginning in the Late Triassic and ending in the Middle Jurassic (Callovian) (e.g. Wilson et al., 1989; Soares et al., 1993; Azerêdo et al., 2003, 2014). The Lower and Middle Jurassic are further defined by five 2nd order facies cycles, the youngest one corresponding to the time of deposition of the early Bathonian (except for its lowermost interval) to Callovian units including those targeted in this work (Azerêdo et al., 2014). This 2nd order T-R cycle is defined by a transgressive phase characterized by increasingly aggradational patterns and minor progradation (Azerêdo, 1998; Azerêdo et al., 2014), which ends with a clear though brief retrogradational episode in the early Callovian, transitioning into a regressive phase during the Callovian, which culminates the Middle Jurassic-Upper Jurassic discontinuity (Azerêdo et al., 2014).

The beginning of the Lower Jurassic in the LB is marked by evaporitic and dolomitic sedimentation in the Hettangian-Sinemurian. This succession is preceded by detrital continental and fluvial deposits in the Late Triassic and followed by the gradual development of open marine conditions, with sedimentation of hemipelagic deposits in the Sinemurian-Toarcian (e.g., Duarte et al., 2001, 2010; Duarte, 2007). During the Middle Jurassic, while deeper-water facies dominate the western/northwestern region of the basin, shallow water facies progressively dominate the eastern/southeastern areas of the LB during the Bathonian, with inner ramp and protected lagoonal sediments, reflecting a shallowing upwards depositional sequence characterized by an overall westward progradation of the system (e.g. Azerêdo, 1988, 1993, 1998, 2007; Soares et al., 1993; Azerêdo et al., 2003). The late Bajocian is characterized by marly limestones intercalated with dolomitized oo-bioclastic intervals and dolomites of the Chão das Pias Formation towards the top. The transition into the Bathonian marks the occurrence of high energy inner ramp and barrier island oo-bioclastic limestones, represented in the Codaçal and Pé da Pedreira members of the Santo António-Candeeiros

Formation, with progradation and aggradation of the depositional system, reflecting a shallowing upwards sequence and a cyclicity between sand barrier and protected lagoonal sediments. The Santo António-Candeeiros Formation dominantly characterizes the western areas of the MCE and transitions laterally through interfingering with the protected lagoonal limestones of the Serra de Aire Formation, more developed towards the east (e.g. Azerêdo, 1993, 1998, 2007). The shallow-water carbonates of the younger Callovian Moleanos Member of the Santo António-Candeeiros Formation were deposited in similar depositional conditions, with an initial retrogradational interval followed by mostly continued progradation of the system, ending on a discontinuity palaeosurface (e.g. Azerêdo, 1993, 1998, 2002, 2007). The Oxfordian Cabaços Formation overlies this disconformity and is generally typified by sediments varying regionally from lacustrine and restricted lagoon limestones and marls to lignites and locally sandstones (e.g. Wilson, 1979; Azerêdo, 1998; Azerêdo et al., 2002). The lithostratigraphy of the Middle Jurassic is summarized in the figure below (Figure IV.1.2).

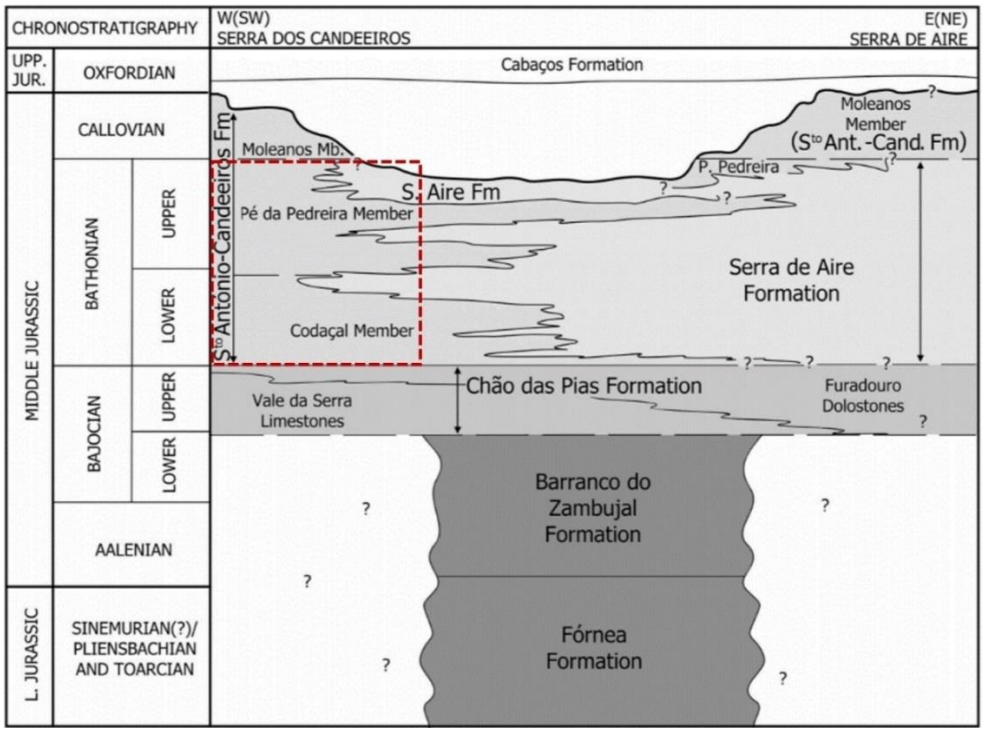

Figure IV.1.2. Lithostratigraphy of the Middle Jurassic in the MCE, LB (Azerêdo, 2007, in Azerêdo et al., 2020). Red box indicates the studied interval.

IV.1.4. Materials and methods

The Codaçal Member of the Santo António-Candeeiros Formation was analysed along recent quarry fronts at Cabeço Vedeiro and Codaçal, while the Pé da Pedreira Member of the same formation was observed in quarry fronts at the Cabeça Veada location (Figure IV.1.1).

Observations were done along quarry fronts with a height of approximately between 35 and 40 m and different lengths at the Codaçal and Cabeço Vedeiro locations. At Cabeça Veada, the observed quarry fronts had estimated heights of between 10 and 12 m. An additional location was analysed at Casal Farto (Figure IV.1.1), in proximity to an area where the Pé da Pedreira Member contacts through a tectonic fault with the younger Moleanos Member (Callovian), as previously mentioned (Azerêdo, 2007; Carvalho and Lisboa, 2018). Discontinuity surfaces, bed thickness variations, sedimentary patterns and internal features were identified at these locations. Macrofacies variability was addressed in intervals where such heterogeneities are clear. Although a petrographic analysis of material from the MCE was not done in this study, elements from previous studies were taken into consideration.

Geometric features were analysed and interpreted at different scales; from the centimetre-metre scale, to the decametre scale, with the assistance of photographic material. These outcrop observations of structures and geometries of the analysed units provide information on the depositional succession and palaeoenvironmental conditions. This kind of information is not obtainable in subsurface case studies such as the Upper Kharaib Member (UKM) in Abu Dhabi. These outcrop and subsurface case studies will be compared, in an attempt to define guidelines for interpretations of the UKM reservoir, where data is limited to well locations. The UKM data and interpretations are based on 4 cored wells and 142 thin sections. These thin sections were analysed and described taking into account elements of the classification schemes by Dunham (1962) and Folk (1959, 1962), applying modifying terms when required (e.g Lokier and Junaibi, 2016). Facies types were grouped into major groups to create a simplified scheme for the present study.

IV.1.5. Case studies review

IV.1.5.1. The Santo António-Candeeiros Formation

The depositional facies and depositional settings characterizing this stratigraphic interval in this area were well defined in previous studies (e.g. Azerêdo, 1993, 1998, 2007; Azerêdo et al., 2015, 2020). This formation is subdivided into three members, generally described in the following paragraphs.

The early Bathonian Codaçal Member thickness varies between 50 and 80 m and is generally characterized by biointraclastic limestones (Figure IV.1.3a) and oobiointraclastic limestones (Figure IV.1.3b), with dolomitized levels. These facies intercalate and interfinger with intervals of coral and algal biostromes. Oobiosparite grainstones-rudstones with intraclasts, peloids and oncoids and well sorted oolitic grainstones (Figure IV.1.3c) are identified (Azerêdo, 2007).

The Bathonian Pé da Pedreira Member carbonate deposits are more than 150 meters thick and characterized by grainstones and rudstones containing ooids, peloids, skeletal grains and

intraclasts (Figure IV.1.3d). Frequent coarse-grained bioclastic intervals reaching up to 3 m occur, representing biostromes or tempestites (Azerêdo, 2007).

The Moleanos Member is generally 150 m thick, reaching thicknesses of 200 m in places. This member contains rudstones, grainstones and packstones with ooid, skeletal grains, oncolites, lithoclasts content, which intercalate with fossiliferous intervals described as coral and algal biostromes. The sediments in this member are generally poorly sorted and coarsening upwards. The lowermost 30 m are represented by intercalations of oolitic layers and coarse-grained, poorly-sorted bioclastic layers (Figure IV.1.3e, f), followed by 40 m of micritic carbonates with peloids, skeletal grains and scattered oncoids (Azerêdo, 2007).

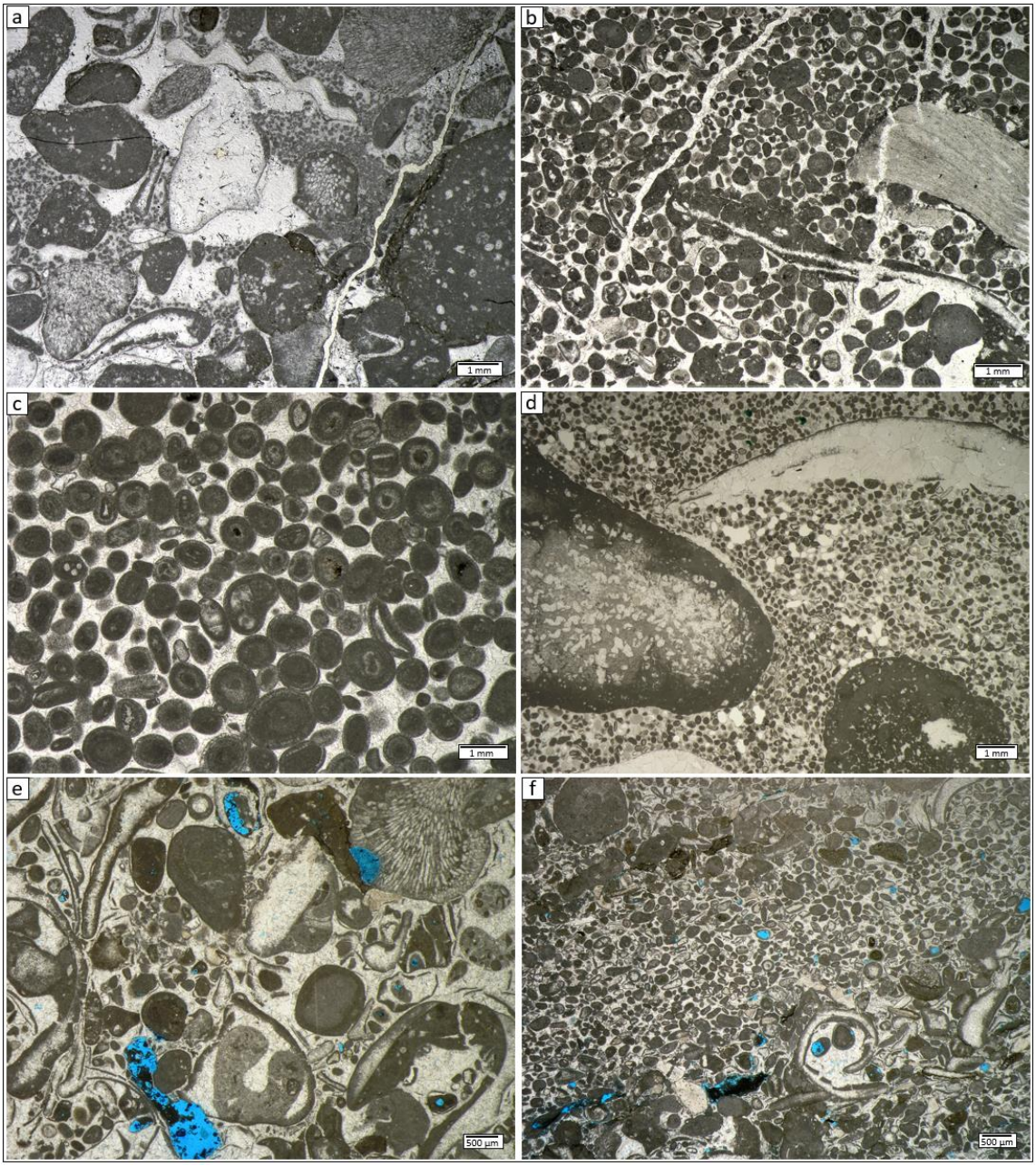

Figure IV.1.3. **a**: Very poorly sorted biointraclastic grainstone. Interparticle space is calcite cemented but a finer peloidal phase exhibiting a geopetal infiltration fabric is also identified; stylolite with residual seam and roughly orthogonal microfractures are also evidenced (Codaçal Member); **b**: moderately sorted cemented biointraclastic grainstone with ooids (Codaçal Member); **c**: well sorted cemented oolitic grainstone (Codaçal Member); **d**: peloidal intraclastic grainstone with coarser coated grains (large coral and aggregate grain, both with oncoidal coatings) and skeletal grains (large recrystallized bivalve shell whose form is preserved through peripheral micritization). Interparticle space is calcite-cemented (Pé da Pedreira Member); **e**: poorly sorted, mostly coarse-medium grained biointraclastic grainstone with Porostromata (Moleanos Member); **f**: bimodal biointraclastic grainstone showing clearly differentiated coarser (oncoids, larger intraclasts and skeletal grains) and finer (ooids, smaller intraclasts) grained layers; gastropods, bivalves and echinoid fragments are visible (Moleanos Member). In (e) and (f) thin-section are impregnated with blue dye.

IV.1.5.1.1. Depositional architecture and regional facies variations

The depositional architecture developed throughout the Bathonian is characterized by overall aggradational patterns, with minor progradation of stacked barrier sandbodies towards the west-northwest in response to the dynamic variability in relative sea-level and in accommodation space. This interplay between stacking patterns is reflected in the depositional geometries which range from the more regularly occurring tabular or sheet-like bodies to wedges, lensoid bodies, isolated biostrome mounds and layers occasionally showing micro-clinoforms (Azerêdo, 1998; Azerêdo et al., 2020). The early Callovian is marked by a brief phase of retrogradation before a return to progradational patterns (Azerêdo, 1998; Azerêdo et al., 2020 and Figure 24 within).

The high-energy facies defining the sandbodies generally transition laterally and/or vertically into open marine deposits towards the west and into back-barrier lagoonal facies towards the east, corresponding to the lagoonal limestones of the Serra de Aire Formation cropping out in the MCE region (Azerêdo, 1998; Azerêdo, 2007). Sediment deposition and distribution throughout this time is interpreted to have been affected by waves, shore-parallel currents and, to a lesser extent, by storm activity under a micro-tidal regime (Azerêdo, 1998).

Towards the east of the MCE, in outcrops of the Casal Farto area, upper Bathonian to Callovian shallow-water deposits of the Pé da Pedreira and Moleanos members are exposed. At this stage, features depicting ramp drowning and retrogradational trends are identified (Azerêdo, 1998; Azerêdo et al., 2020). The main facies observed at quarries of this location are characterized by grainstones containing moderate to high oolitic content (Manuppella et al., 1985; Azerêdo, 2007; Carvalho and Lisboa, 2018). In this Fátima - Casal Farto region, the sediments of the Pé da Pedreira Member, corresponding to the Fátima oolitic limestones in Manuppella et al. (1998), as defined in Azerêdo (2007), are exposed along a corridor with an approximate southeast-northwest direction (Manuppella et al., 1998). This member contacts tectonically with the younger Moleanos Member (of Callovian age) in the Casal Farto area (Azerêdo, 2007; Carvalho and Lisboa, 2018), which is characterized by oolitic-bioclastic-lithoclastic

packstones, grainstones and rudstones with interbedded algal/coral biostromes and bioturbated pelmicritic limestones (Azerêdo, 2007; Azerêdo et al., 2020). This member is also exposed along an approximately southeast to northwest corridor in the Fátima - Casal Farto region, approximately parallel to the exposure of the Pé da Pedreira Member in this area (Manuppella et al., 1998).

There is considerable lateral bed thickness and facies variability in the Casal Farto region across relatively short distances within this stratigraphic interval (Carvalho and Lisboa, 2018). In the surrounding areas, towards the west and east of Casal Farto, the basal and middle parts of the Serra de Aire Formation are exposed (Azerêdo, 2007; Azerêdo et al., 2015; Carvalho and Lisboa, 2018). Increasingly younger sediments are exposed to the north of Casal Farto, going through the Callovian Moleanos Member and into the Oxfordian Cabaços Formation (Manuppella et al., 1998).

In addition to the vertical transitions between facies, the complex depositional architecture and geometries developed in this region lead to considerable lateral facies variability through gradation and interfingering at different scales (Azerêdo, 1998; Azerêdo et al., 2020).

IV.1.5.1.2. Reservoir facies potential

The Middle Jurassic units of the MCE outcrops have been addressed from a petroleum systems perspective in published studies and are considered to show potential as hydrocarbon reservoir units (e.g. Azerêdo and Inês, 2011; Azerêdo, 2015; Ferreira et al., 2016; Azerêdo and Duarte, 2017; Azerêdo et al., 2020). The Bathonian-Callovian shallow-water facies of the Santo-António Candeeiros Formation show variable reservoir quality in sandbodies, biostromes and dolomitic limestones, with considerable heterogeneity in petrophysical properties resulting from variations in facies characteristics and in diagenetic features. Mouldic, intraparticle and vuggy porosity are identified in sandbody facies and estimated to be generally lower than 5 % but in some cases reaching up to around 20 %. Microporosity has also developed in oncoids and coated grains in some sandbody facies. Growth-framework, intraskeletal and vuggy porosity has been identified in biostromal facies, while dolomitic limestones mainly show intercrystalline porosity, sometimes with development of mouldic and vuggy porosity, and have variable estimated porosities of between 6 and 20 % (Azerêdo et al., 2020). Petrophysical laboratory measurements through helium injection on a few samples show an average porosity of close to 3 %, slightly higher in biostromes (between approximately 3 and 6 %) than in sandbodies (between approximately 1 and 4 %), and virtually null permeability, except for one sample showing 160 mD, most likely as a result of diagenetic and mechanical modification (Ferreira et al., 2016). These facies, with potential reservoir properties, generally evolve vertically and/or laterally into mid to outer ramp facies to the west and micritic lagoonal sediments towards the east, as mentioned above, which might act as baffles to fluid flow,

potentially leading to the creation of stratigraphic traps, besides the complex diagenesis that may impose further heterogeneities and diagenetic traps (Azerêdo et al., 2020).

IV.1.5.2. The Upper Kharaib Member, Rub Al Khali Basin (U.A.E.)

The Barremian UKM of the Kharaib Formation was deposited in the Rub Al Khali Basin, in the east-southeast of the Arabian Peninsula (see Chapter III, Figures III.1.1, III.2.1) (e.g. Powers et al., 1966; Murris, 1980; Soliman and Al Shamlan, 1982; Alsharhan and Nairn, 1997) and represents the most important hydrocarbon reservoir in Abu Dhabi, U.A.E. (e.g. Harris et al., 1968; Lijmbach et al., 1992; Taher, 1996; Alsharhan and Nairn, 1997).

This Formation is part of the Lower Cretaceous Thamama Group (see Chapter III), which is characterized by an overall 'layer cake' stratigraphy with reservoir zones interlayered with argillaceous limestones deposited in a widespread carbonate platform (e.g. Harris et al., 1968; Murris, 1980; Azer and Toland, 1993; Alsharhan and Nairn, 1997; Davies et al., 2002; Van Buchem et al., 2002). The UKM has a thickness of around 55 m in the crest of the analysed field and is divided into 6 regionally correlatable subzones (see Chapter III), which are bounded by thin non-sealing layers showing decreased porosities and a slight increase in alumina content, which is proportional to clay content (e.g. Ehrenberg et al., 2016, 2018). These layers can be followed over large distances across the different Abu Dhabi fields (e.g. Harris et al., 1968; Alsharhan, 1990, 1993; Van Buchem et al., 2002; Strohmenger et al., 2006; El Wazir et al., 2015; Ehrenberg, 2016). The boundaries of these subzones have been reported to correspond to the tops of parasequence sets (Strohmenger et al., 2006). This subzone classification scheme is widely used in the operating companies in Abu Dhabi and will be the terminology adapted here, for practical reasons.

The UKM is defined by a shallowing-upward trend, gradually developing from low-energy, relatively deeper-water facies into higher-energy, shallow-water inner ramp or shoal facies (e.g. Schlumberger, 1981; Alsharhan, 1990; Azer and Toland, 1993; Alsharhan and Nairn, 1997; Van Buchem et al., 2002; Strohmenger et al., 2006). The lower half of this reservoir is dominated by microporous skeletal/bioclastic wackestones with orbitolinids, echinoderm fragments, bivalves, and with few bioturbation horizons (burrowing), deposited during the transgressive phase of a 3rd order cycle, while the upper half is generally characterized by intercalations of packstones with skeletal grains and peloids, biointraclastic grainstones (some of them containing ooids and other coated grains) and biointraclastic rudstone-grainstones with rudist fragments, characterizing subzones 1, 2 and 3U, as well as part of subzone 3L, and deposited during a regressive phase (see Chapter III and Figure IV.1.4) (e.g. Harris et al., 1968; Alsharhan, 1993; Grötsch et al., 1998; Van Buchem et al., 2002; Strohmenger et al., 2006; El Wazir et al., 2015; Ehrenberg, 2016).

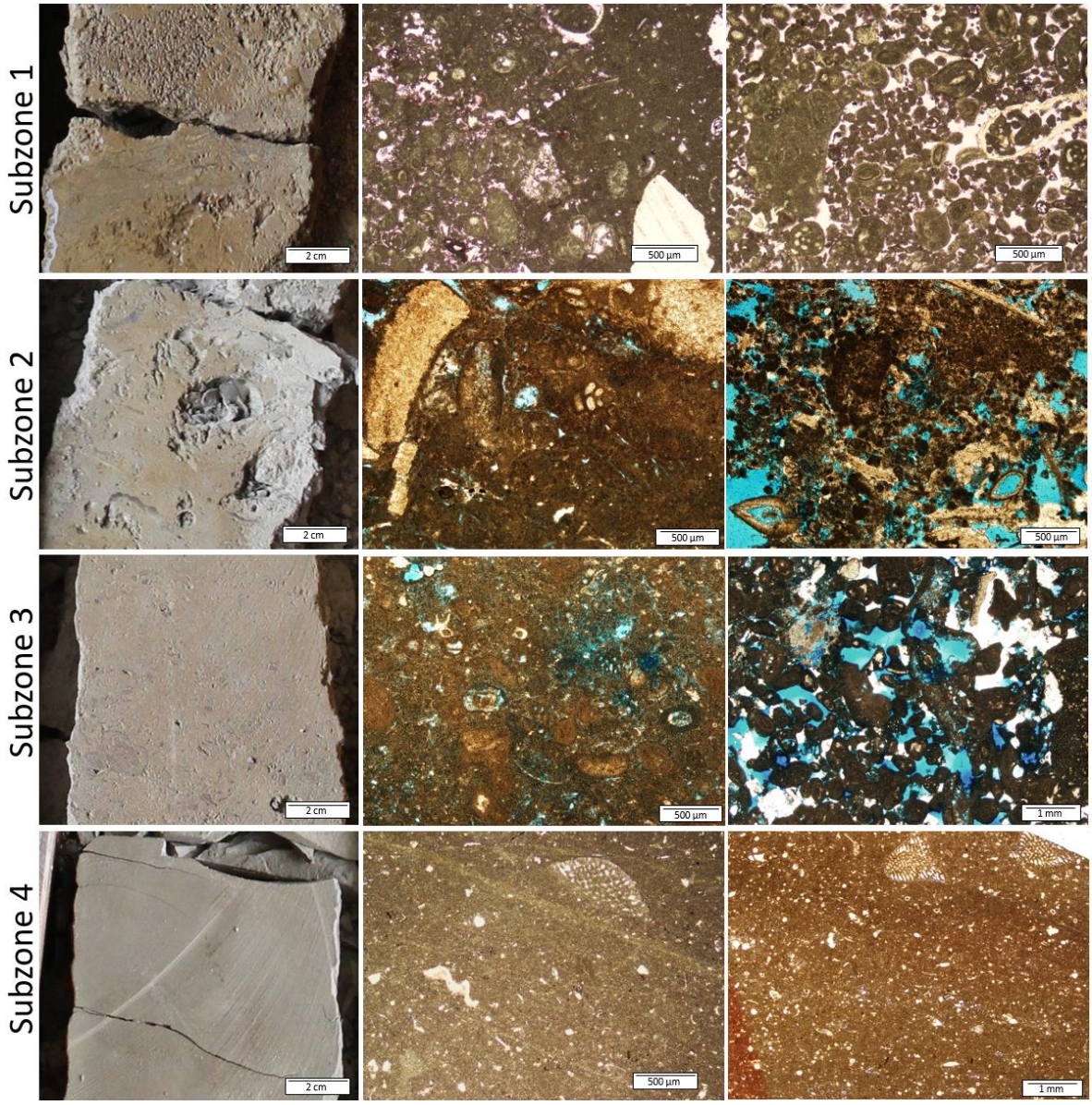

Figure IV.1.4. Examples of typical macro and microfacies of the UKM. Subzone 4: biomicritic wackestone with orbitolinids and other skeletal grains; subzone 3: biointraclastic micritic packstones and biointraclastic grainstones with micritized intraclasts and skeletal grains including echinoderm fragments; subzone 2: biointraclastic rudstone-grainstones containing rudists and a micritic phase with a packstone-grainstone texture, and biointraclastic grainstones; subzone 1: biointraclastic packstone to grainstones and oobiointraclastic grainstones.

Subzones 2 and 3U are characterized by the occurrence of high-permeability layers and by clear small-scale vertical facies heterogeneity, which is variable and poorly correlatable between wells (e.g. Grötsch et al., 1998; Strohmenger et al., 2006; Ehrenberg et al., 2018; see also Chapter III). This small-scale vertical facies variability and the differences in the succession between wells are a possible response to palaeoenvironmental conditions and factors, such as varying hydrodynamic conditions within high-energy environments, controlling sediment distribution and creating complex geometries and geometric relationships

between geobodies (e.g. Grötsch et al., 1998; Van Buchem et al., 2002; El Wazir et al., 2015; Ehrenberg et al., 2018;). However, the controls on this facies variability in this reservoir are not fully understood. A dual macro and microporosity system characterizes this reservoir, where microporosity is dominant. While the intervals defined by wackestone facies show a mostly homogeneous microporous network, the remaining facies are defined by a more heterogeneous network, with interparticle macroporosity, as well as intraparticle microporosity within the micritized particles and microporosity within the micritic matrix, where present (e.g. Budd, 1989; Moshier, 1989; Oswald et al., 1995; Vahrenkamp et al., 2014; Morad et al., 2016; Ehrenberg, 2019). Total porosity reaches up to around 30 % and shows no clear vertical variation trends, while permeability shows significantly higher values in the regressive phase sediments, reaching values of more than 100 mD, with peaks in the range of 400 and 800 mD at some locations.

IV.1.6. Outcrop observations

IV.1.6.1. Depositional facies

Based on macroscopic observations, oolitic-bioclastic-intraclastic grainstones are the main facies observed on the exposed quarry fronts, but bio-lithoclastic grainstone/rudstones and coral-rich boundstones also occur. Texture variations are observed across different layers (Figure IV.1.5a, b, c) and, in some cases, within certain layers, especially when cross-bedding or cross-lamination is observed (Figure IV.1.5d). These variations are often recognized even at microscale. Intervals of grainstone-rudstone facies are identified containing oncoids, skeletal grains and lithoclasts, sometimes showing sharp vertical transitions into bio-intraclastic grainstone intervals (Figure IV.1.5c). Towards the top of the Codaçal Member section observed, coral-rich intervals, with coral biostromes and boundstone facies are observed with large corals and coral fragments. The corals, which show different levels of preservation, and coral-rich bodies are generally encased by sediments characterized by bio-intraclastic grainstones and grainstone-rudstone facies (Figure IV.1.5e, f). The Pé da Pedreira Member at the analysed Cabeça Veada outcrops are characterized by more massive, thicker intervals of grainstone to rudstone facies containing ooids, skeletal grains and intraclasts (Figure IV.1.5b), with the occurrence of interbedded tempestite intervals containing boulder to sand-sized grains (Figure IV.1.5a). At Casal Farto, this member shows dominant facies characterized by oolitic-bioclastic-intraclastic grainstones, although towards the bottom of the succession in the observed quarry fronts, dark-coloured thin (centimetric) laminated layers are observed interbedded with bioclastic limestones intervals (Figure IV.1.6a to d). These layers show signs of strong compaction, as expressed by the presence of pressure-solution seams and by the horizontal elongation of burrows infilled by younger light-coloured carbonate sediments (Figure IV.1.6d).

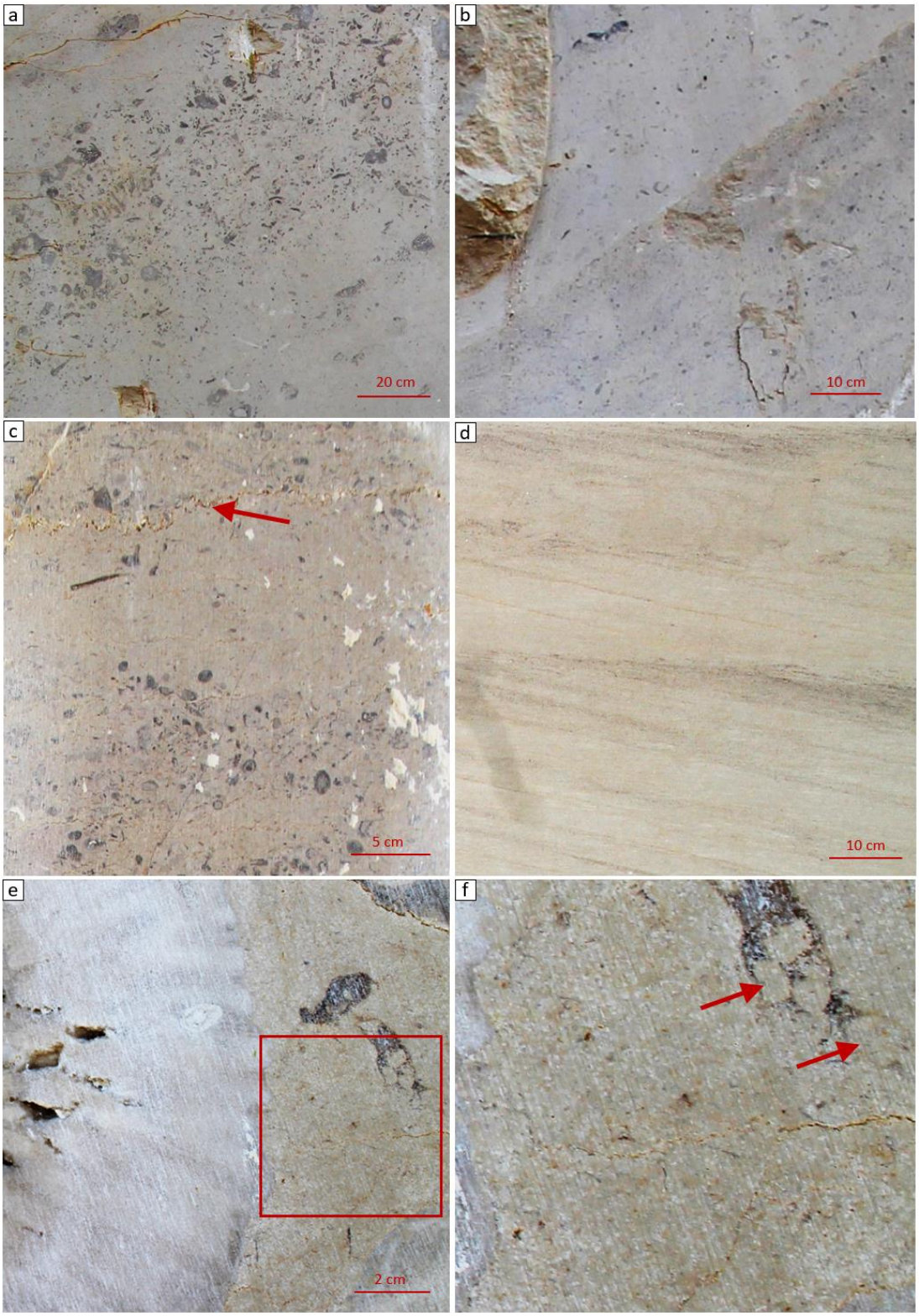

Figure IV.1.5. Macroscopic view of the different depositional facies observed on outcrop. **a**: Tempestite interval with boulder to sand-sized grains; **b**: Oolitic-bioclastic-intraclastic grainstone to rudstone facies. The two grainstone bodies contact through a sharp, erosional surface; **c**: Oncolitic-bioclastic-lithoclastic grainstone-rudstone and interbedded bio-intraclastic grainstone layer. The top of the grainstone layer is marked by a stylolitic surface (arrow); **d**: Oolitic-bioclastic-intraclastic grainstones with cross-bedding; **e** and **f**: Details of coral-algal boundstones laterally transitioning into bio-intraclastic grainstones and grainstone-rudstone bodies. Preserved coral (**e**) and coarse intraclasts (arrows in **f**) are observed. Image (**f**) is a zoom-in of the red box area within image (**e**).

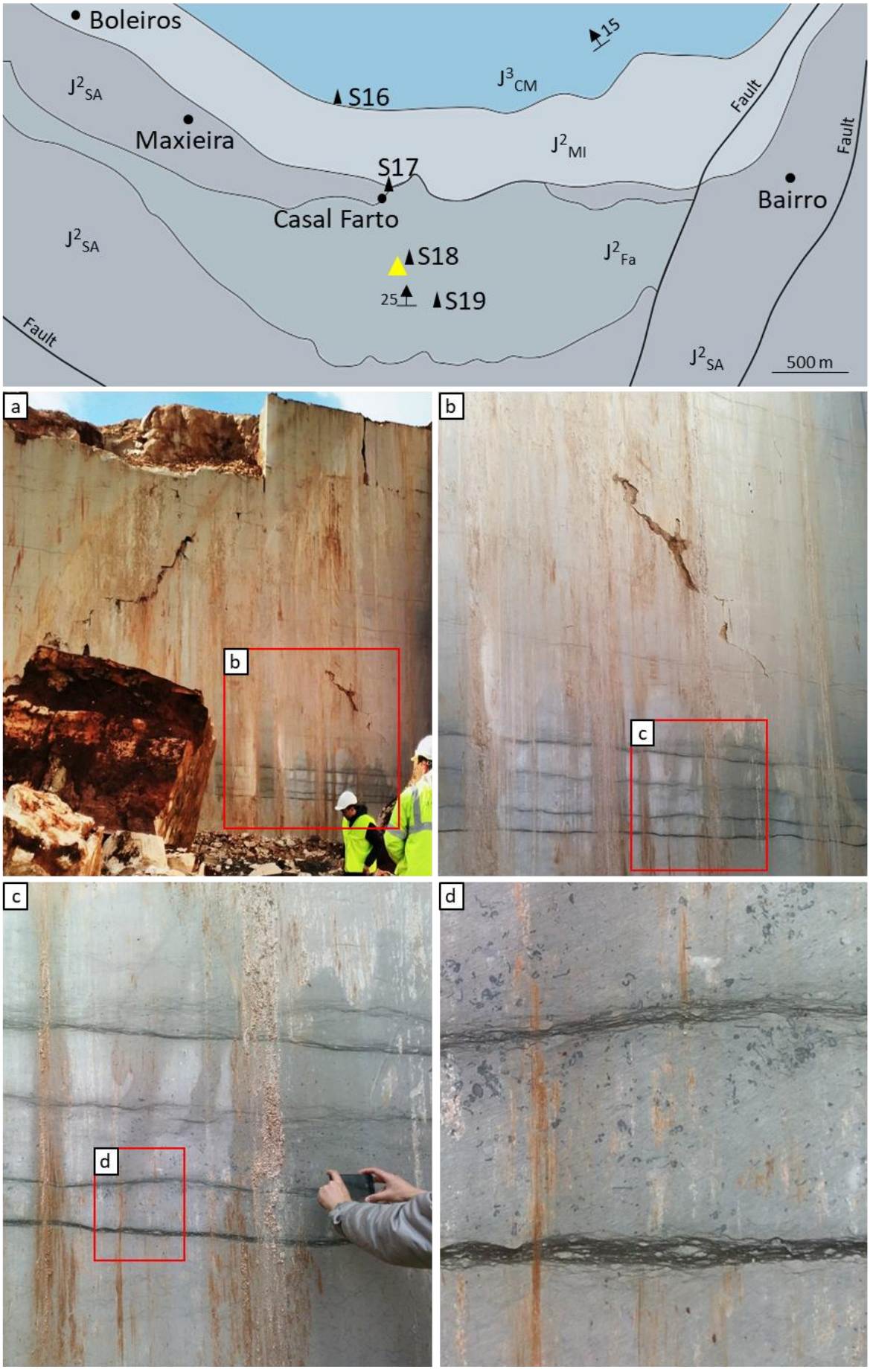
Boleiros
15
J^2_{SA}
S16
J^3_{CM}
Fault
Maxieira
J^2_{MI}
Fault
S17
Bairro
Casal Farto
J^2_{SA}
S18
J^2_{Fa}
25
S19
Fault
J^2_{SA}
500 m
a
b
b
c
c
d
d

Figure IV.1.6. **Top**: Simplified geological map of the Casal Farto region. Overall layer dipping direction and angle are indicated (based on Manuppella et al., 1998) with yellow triangle showing location of quarry front represented in photos **a**, **b**, **c** and **d**. S16 to S19 represent drilled wells. J^3_{CM} : *Camadas de Cabaços e Montejunto*, Oxfordian to Kimmeridgian; J^2_{MI} : Moleanos limestones (Moleanos Member, Santo António-Candeeiros Formation), Callovian; J^2_{Fa} : Fátima oolitic limestones (Pé da Pedreira Member, Santo António-Candeeiros Formation), Bathonian; J^2_{SA} : Serra de Aire micritic limestones (Serra de Aire Formation), Bathonian (Manuppella et al., 1998). The dark-coloured thin laminated layers are here exposed (**a**, **b**, **c** and **d**).

IV.1.6.2. Depositional geometries and architecture

The analysed quarry fronts at the Codaçal location have an estimated height of between 36 and 40 m. The succession is generally characterized by an evolution from intervals of geobodies with tabular, sheet or wedge-like geometries, with thickness variations observed on outcrop, into an interval characterized by the presence of coral/algal build-ups. The bottom interval, of approximate 12 m thickness, is defined by packages with close-to-parallel bedding surfaces (Figure IV.1.7a), showing thickness variations at a larger decametre scale. The 11 m above are characterized by the occurrence of packages with clear internal sedimentary structures. At a smaller centimetric/decimetric scale, these tabular beds show clear cross-bedding/lamination (2-10 cm) (Figure IV.1.7b), which increase in size laterally into sigmoidal geometries with varying heights of between 70 cm and 2 m, with a north/northwest strike direction. The overlying 6 m contains depositional packages with lenticular bodies pinching-out over distances of between 10 and 25 m and the top interval of 7 m is characterized by the development of coral/algal build-ups with no clear internal structures/arrangements, transitioning laterally into apparent stratified bioclastic and coral-rich grainstones (Figure IV.1.7c).

At the Cabeça Veada location, large scale tabular beds with parallel to sub-parallel bedding surfaces are observed (Figure IV.1.8a). Some of these beds show cross-bedding while others have a more massive appearance. Strong discontinuities are clearly visible and can be followed along the quarry fronts. This section is characterized by the occurrence of coarse-grained beds (rudstones) with varying thicknesses of between 1.5 and 3 m.

At Casal Farto, the succession evolves vertically through an interval containing tabular or wedge-like bodies of oolitic-bioclastic grainstones and into an interval of apparently retrograding/prograding grainstone bodies close to the top of the exposed quarry fronts (Figure IV.1.8b; see discussion also). The dark laminated layers mentioned above are exposed at approximately 17 to 20 m below the top of the quarry front in the basal interval of the observed fronts.

Figure IV.1.7. Photos of quarry front at Codaçal (Codaçal Member). **a:** Basal interval of the observed quarry front, with parallel bedding surfaces and tabular-like geobodies; **b**: Heterogeneity driven by small-scale geometric variations defined by cross-bedding sedimentary structures; **c:** Topmost outcropping interval, with coral/algal build-ups within the red dashed polygons, surrounded by grainstone and grainstone-rudstone facies. A marked discontinuity is indicated by the red arrow.

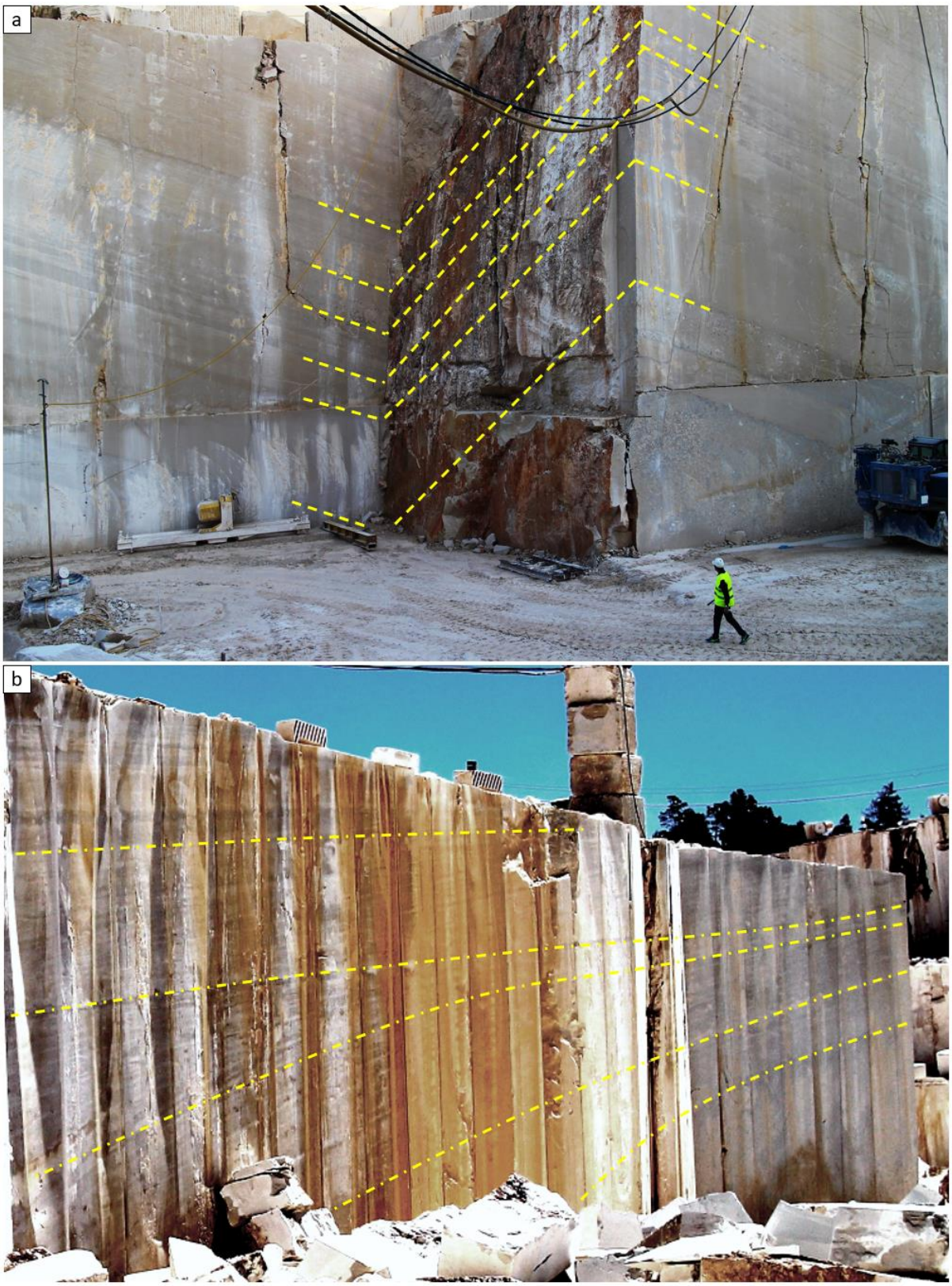

Figure IV.1.8. **a**: Parallel bedding planes and apparent tabular geometries at Cabeça Veada (Pé da Pedreira Member); **b**: Prograding/retrograding grainstone bodies at Casal Farto (Pé da Pedreira Member). The height of this front is estimated to be approximately 20 m. Additional detailed interpretations on this quarry front are shown in section IV.1.7.2.1.

IV.1.7. Discussion

The observations reported above expose the complex depositional architecture and strong heterogeneity of carbonate ramp systems. The full extent of the geometric relationships at different scales is discussed in this section. Larger-scale packages are correlatable over moderate distances, but smaller-scale sedimentary structures drive facies variability over shorter distances. The interpretations on this outcrop case study, and specifically the quarry fronts at Codaçal, will be compared to the subsurface case study from the U.A.E., in terms of similarities and contrasting points.

IV.1.7.1. Depositional facies and settings

In general terms, the oobiointraclastic grainstone and rudstone facies reflect deposition in high-energy depositional settings and are seen to represent shoreface deposits with cross-bedding and biostrome development in the Codaçal Member (at Codaçal and Cabeço Vedeiro) and shoreface deposits with tempestites and high-energy storm deposits in the Pé da Pedreira Member (at Cabeça Veada; see also Azerêdo, 2007; Azerêdo et al., 2020). Moderate spatial facies heterogeneity controlled by the depositional architecture is observed, as will be discussed later.

Further to the east, the Pé da Pedreira Member at Casal Farto shows its typical oobiointraclastic grainstone to rudstone high-energy facies and is characterized by the occurrence of strong progradational-retrogradational patterns higher in the succession. However, in the basal interval of the analysed quarry fronts, dark laminated layers (possibly rich in organic matter) are observed, as mentioned above. Organic-rich, marly thin layers, seams and lenses have also been reported in a lower Bathonian Serra de Aire Formation interval at the Galinha quarry, east of Casal Farto (Azerêdo et al., 2015). Although different in age and depositional setting to the Casal Farto potentially organic-rich layers, they are an example of the localized occurrence of organic-rich deposits in localized intervals interspersed within the higher-energy facies successions in the LB at that time, as they have only been recognized at the Galinha quarry. In addition, previous studies have reported the presence of scattered migrated organic matter and bitumen in the high-energy facies of the Bathonian-Callovian in the MCE (Santos, 2017; Azerêdo et al., 2020) and Torres Vedras regions (Gonçalves et al., 2014; Brito et al., 2017), resulting from the flow of hydrocarbons or organic-rich fluids through fractures and through the rock volume. The exposed succession at Casal Farto is interpreted to be of late Bathonian-Callovian age, according to information from nearby wells S17, S18 and S19, located 80 to 420 m away from the observed quarry front (see Figure IV.1.6 for locations), which drilled through 40 to 60 m of Bathonian-aged sediments, as defined by the biostratigraphic data (Manuppella et al., 1985). The topmost interval of the S17 well, close to the northern limit of the analysed quarry, is most likely Callovian in age, as is the upper part of the S16 well, located

further towards the north (Manuppella et al., 1985), an age assignment supported by more recent studies (Azerêdo et al., 2020). During this time, drowning of the carbonate ramp occurred, with development of retrogradational patterns, as previously mentioned (Azerêdo, 1998; Azerêdo et al., 2020). This could provide further indications of deposition occurring in relatively deeper water, lower-energy conditions and possible slight sediment starvation locally, possibly promoting the moderate preservation of some organic matter. It could, therefore, be possible that the dark-coloured laminated layers exposed at the Casal Farto quarries contain some content in organic matter, although laboratory testing would be required to confirm this. This succession, exposed in the Casal Farto quarry fronts, shows moderate similarities with an intra-shelf basin succession of late Albian to Turonian age in Abu Dhabi, U.A.E. (Shilaif Formation), which shows basinal sediments of interbedded laminated organic-rich mudstones and mudstones-wackestones with pelagic fauna transitioning laterally and vertically, near the intra-shelf basin margins, into the prograding shallow-water platform-edge sediments of the Mishrif Formation (see figures 5 and 6 of Vahrenkamp et al., 2015a).

IV.1.7.2. Depositional architecture

IV.1.7.2.1. Large-scale geometries

As mentioned above, the architecture of deposition generally shows an evolution from tabular geobodies and cross-bedded layers, into an interval characterized by coral/algal build-ups, as observed at Codaçal (Figure IV.1.9). Depositional packages show large-scale thickness variations, which might result from the combination of depositional and erosional processes, as suggested by the regular and irregular discontinuity surfaces identified throughout the succession, showing signs of intraformational erosion and reworking (Figures IV.1.10, IV.1.11).

Cross-bedded intervals are interpreted to reflect the effects of minor progradation of grainstone bodies with an approximate north/northwest direction, or mobile shoreface bars, within a predominantly aggradational system. These progradational patterns become absent towards the top of the exposed front, where aggradational patterns are dominant and depositional geometries become more complex, with pinching-out bodies and lateral interfingering between different depositional facies. The topmost interval is characterized by coral/algal biostromes and grainstone lenses with subtle lamination/stratification parallel to the bedding planes, where geometric arrangements are influenced by the overall geometries of the bioclastic/coral build-ups. Lateral facies variations occur across very short distances within this interval (Figure IV.1.7c).

Figure IV.1.9. Vertical succession and overall geometries of the Codaçal Member. Generally tabular geometries in the lower half (bedding planes represented by blue lines) and biostromes and coral/algal build-ups towards the top (red polygons). Vertical height of the quarry front is an estimated 35 to 40 m.

Figure IV.1.10. Examples of discontinuities observed on outcrop at Codaçal (red arrows), with indications of erosion/reworking in some.

Depositional geometries of the younger Pé da Pedreira Member analysed on quarry fronts at Cabeça Veada, to the south/southwest of the Codaçal location, do not show the type of small-scale variability seen at Codaçal. An aggradational depositional pattern is dominant, with geobodies showing an overall tabular appearance (Figure IV.1.8a). Bedding planes are parallel to sub-parallel and only minor indications for large-scale thickness variations are observed (Figures IV.1.8a, IV.1.11c). Significant variations will likely occur at a scale larger than the extent of the exposed quarry fronts and are, therefore, not appraisable. Although the full lateral extent of these geobodies is not observed, some of them are interpreted to probably represent wedge-like geometries, given the observed minor thickness variations.

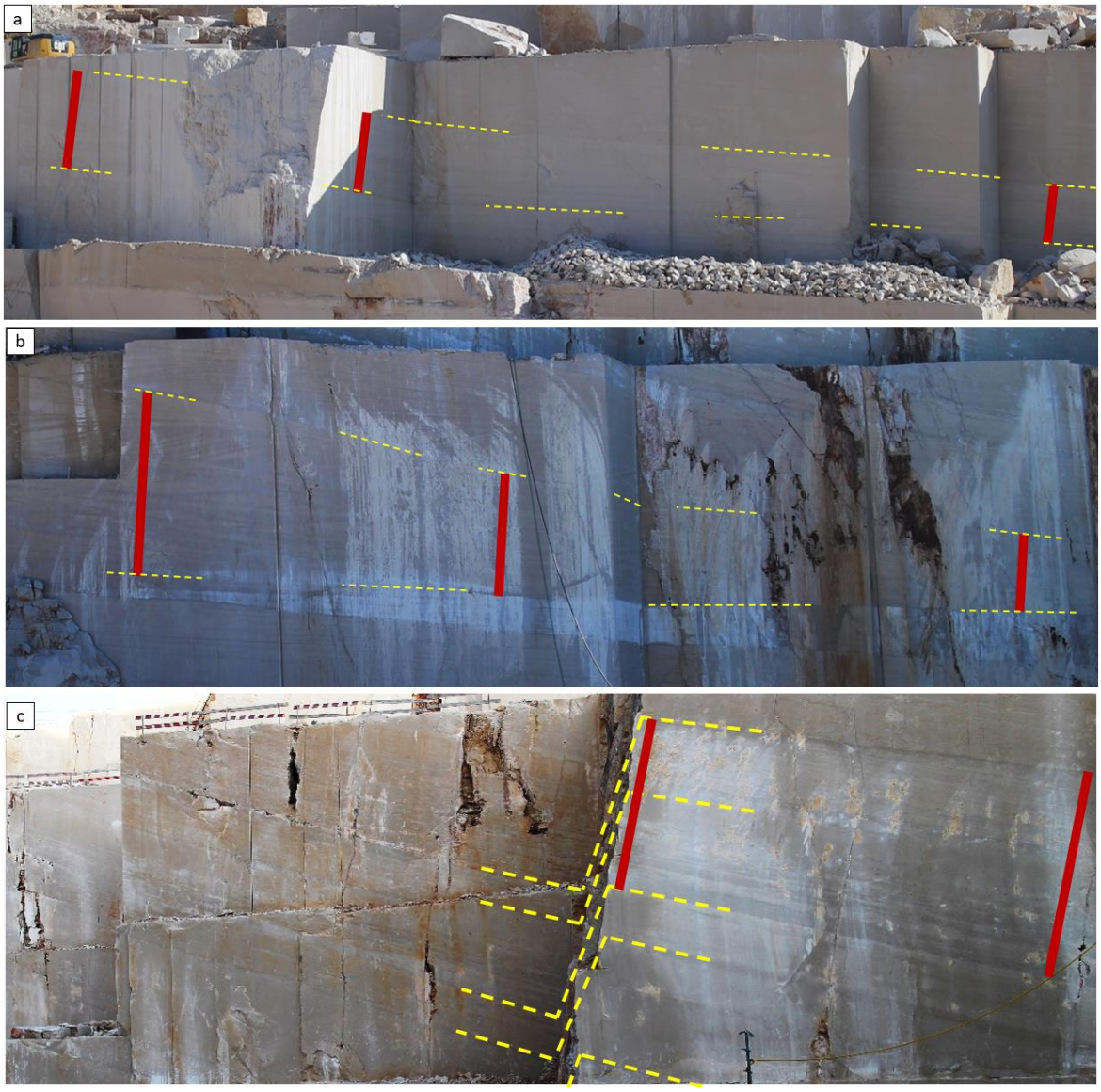

Figure IV.1.11. Photos of quarry fronts at Codaçal (**a** and **b**) and at Cabeça Veada (c). Red bars represent the thickness at different points; **a**: Thickness changes from 11 m (left red bar) to 6 m (right red bar) along a transect of approximately 100 m; **b**: Thickness changes from 3 (right red bar) to 8 m (left red bar) along an interval of approximately 40 m; **c**: Estimated 3 m (left red bar) to 4 m (right red bar)

thickness change along an approximately 9 m transect. Dashed yellow lines indicate the surfaces followed along the quarry front.

The Pé da Pedreira Member succession exposed at the analysed Casal Farto quarry fronts shows a vertical evolution from tabular or wedge-like oobioclastic grainstone bodies into an interval of clinoform-like geobodies towards the top. Geometric configurations such as the downlap and onlap of surfaces, as well as discontinuity surfaces with truncation of underlying beds are here observed (Figures IV.1.12, IV.1.13). This evolution is interpreted to reflect a gradual transition into an interval reflecting stronger progradation with periods of retrogradation. Within the topmost interval, progradation seems to become weaker, and a stronger expression of aggradational patterns are observed. Large-scale lateral thickness variations are observed within these successions, with an example package almost doubling its thickness along a 100 m sector, from an estimated 6 m to 11 m, in the basal outcrop interval at Codaçal (Figure IV.1.11a). One other example in this outcrop shows a thickness change from an estimated 3 m to 8 m along an approximately 40 m sector (Figure IV.1.11b). In the Pé da Pedreira Member at Cabeça Veada, thickness variations are not as clear, in part due to the laterally limited exposure of the succession on outcrop, as mentioned above, but there are some indications of moderate variability. As an example, an estimated thickness variation of 3 to 4 m along a 10 m transect is observed for a depositional package on one of the observed quarry fronts (Figure IV.1.11c).

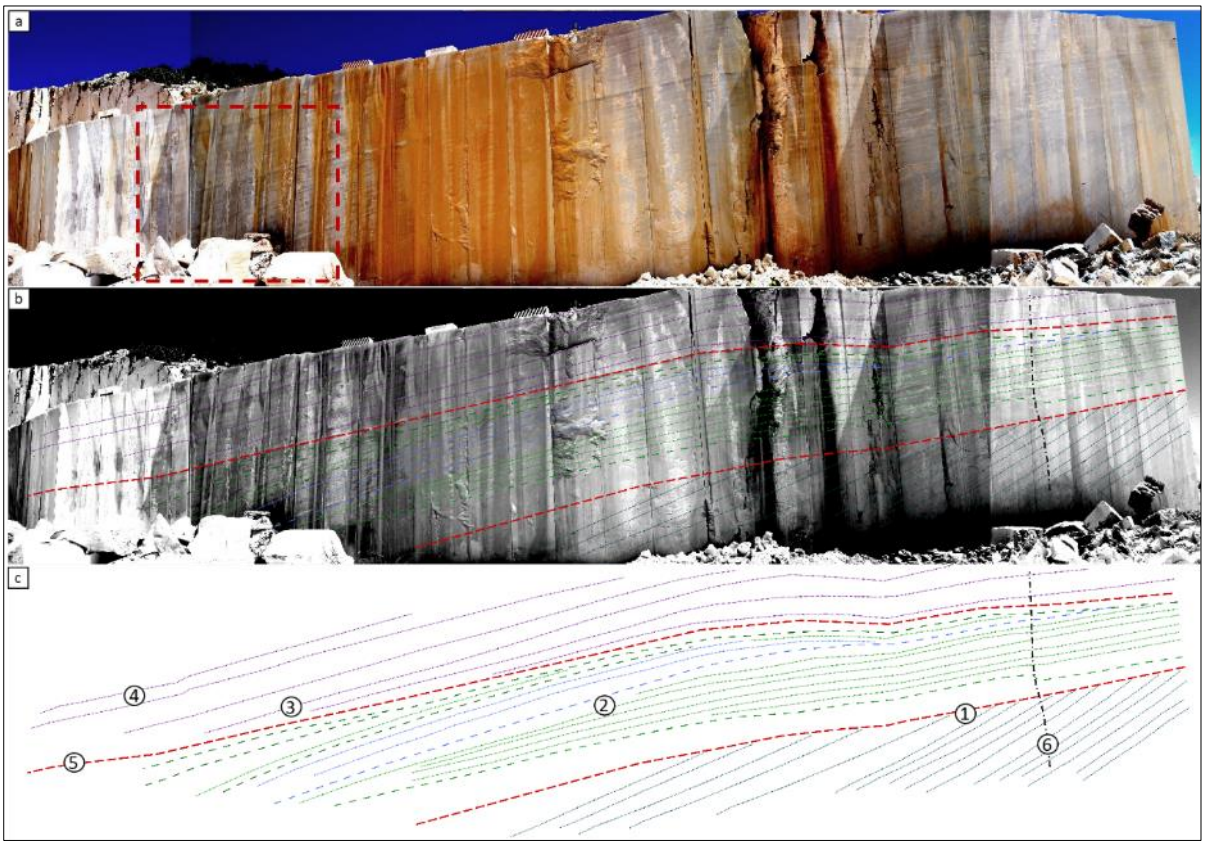

Figure IV.1.12. **a**: Top interval of the exposed quarry fronts at Casal Farto (Pé da Pedreira Member) showing overall apparent progradational patterns. The height of this front is approximately 20 m. Details in dashed red square are shown in Figure IV.1.13; **b**: Photo of quarry front with interpretations of main surfaces; **c**: Surfaces interpretations only. 1: Discontinuity surface, erosion and truncation of underlying units. 2: apparent truncation. 3: apparent downlap. 4: stronger aggradation, with minor progradation 5: burrowed surface 6: probable fault.

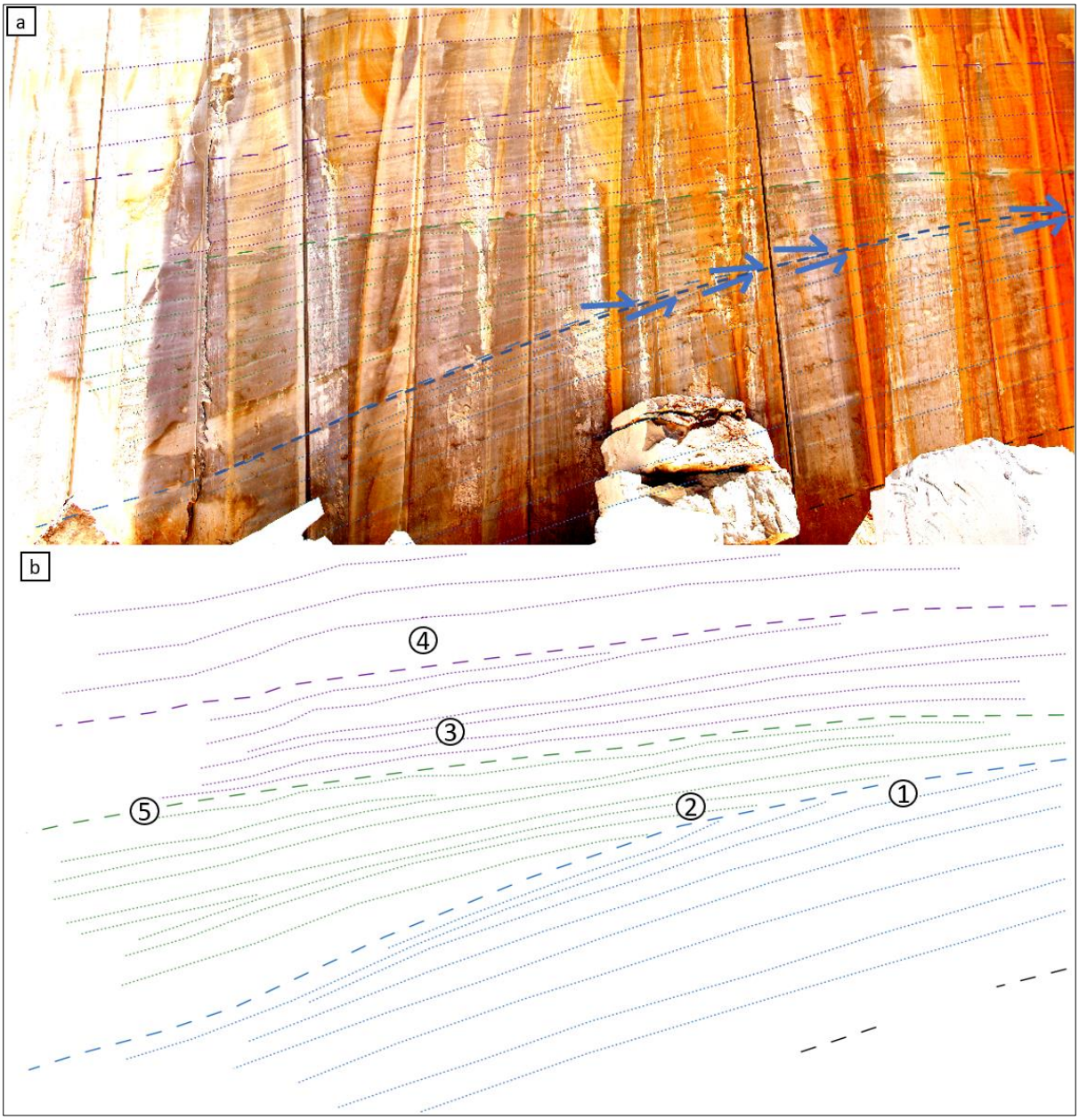

Figure IV.1.13. Zoom-in of quarry front indicated in Figure IV.1.12a by dashed red square. Scale is indicated on legend of Figure IV.1.12. **a**: Quarry front with surface interpretations; **b**: Surface interpretations only. 1: discontinuity surface showing truncation of underlying units. 2: onlap of surfaces onto discontinuity surface. 3: stronger aggradation, with minor progradation. 4: stronger aggradation. 5: burrowed surface (surface 5 in Figure IV.1.12).

IV.1.7.2.2. Small-scale geometries

As mentioned previously, rock property heterogeneity and geometric variability can be perceived differently at varied observation scales. At a smaller centimetric to decimetric scale, heterogeneity becomes more apparent (Figure IV.1.7). Such multi-scale variability is typical in carbonates and has been previously mentioned and discussed for the Peniche and Abu Dhabi case studies (Chapters II and III). The freshly cut quarry walls at the MCE allow for clear observations on depositional geometries and lateral facies transitions, due to the minimal effects of weathering. Clear vertical variability between massive, coarse-grained packages and relatively finer cross-bedded layers is observed (Figure IV.1.10a). These depositional packages are characterized by intraclastic-bioclastic grainstones, showing apparent spatial variability in grain size, based on macroscopic outcrop observations.

Variability at a centimetric scale is clear in the interval with tabular beds characterized by thinly cross-bedded and cross-laminated structures, locally interbedded with planar laminated structures. These set of sedimentary structures indicate hydrodynamic activity with prevailing moderate to high energy wave-dominated processes, with interference of stronger uni-directional currents (e.g. Azerêdo, 1998; Azerêdo et al., 2020). These packages are thickening in an apparent north/northwest direction, with the small-scale cross-bedding gradually changing laterally into thicker cross-bedded structures, resembling sigmoidal bodies, which might be a reflection of lateral variations in accommodation space (Figure IV.1.14). The overlying interval is characterized by the occurrence of coarser-grained lenticular bodies with decimetric thickness, pinching-out over moderate distances within a background of relatively finer-grained sediments (Figure IV.1.15a).

To some extent, the top interval of this quarry front shows depositional geometries of higher complexity, as, in addition to the hydrodynamic conditions controlling sediment distribution, one must take into account the biogenic factors related to reef growth dynamics (e.g. Pomar and Kendal, 2008; Van Tuyl et al., 2018). Coral/algal build-ups containing in-situ corals transition laterally, through interfingering, into grainstones and grainstone-rudstones with coral fragments arranged in decimetric intercalations (Figure IV.1.15b). Facies variability is relatively high and occurs over short distances (decimetres to a few meters). The grainstone and grainstone-rudstone layers show apparent lamination, and a shape and geometry that is influenced by the overall geometry of the coral/algal build-ups.

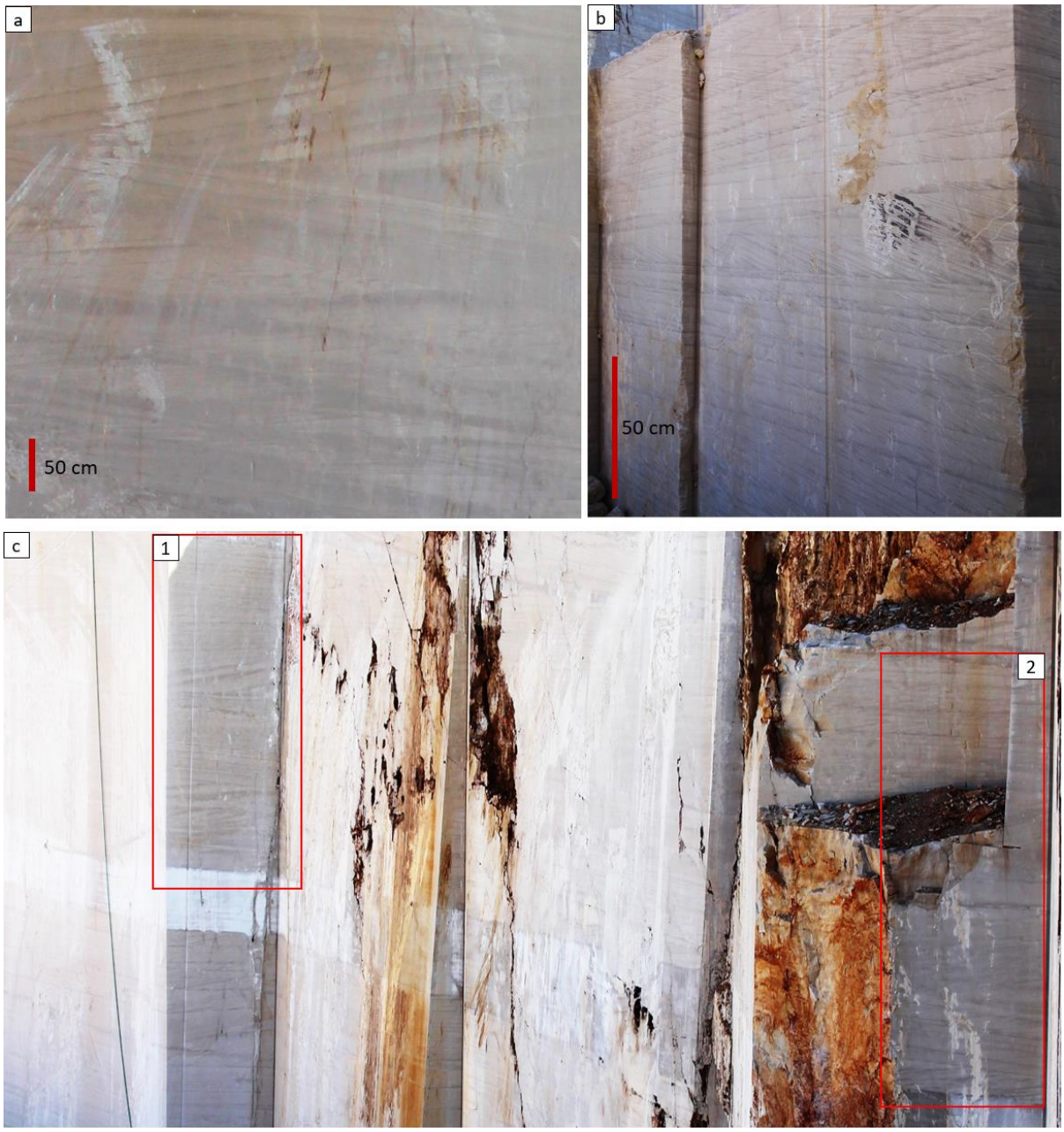

Figure IV.1.14. Lateral variation in geometric characteristics of cross-bedded packages within interval reflecting relatively stronger progradation. **a**: Thicker packages with apparent sigmoidal bodies; **b**: Coeval cross-bedded interval where sigmoidal geometries are not clear; **c**: Quarry front showing sigmoidal bodies (1) and small-scale cross-bedding (2) overlying the white-coloured reference layer. Distance between (1) and (2) is approximately 20-25 m.

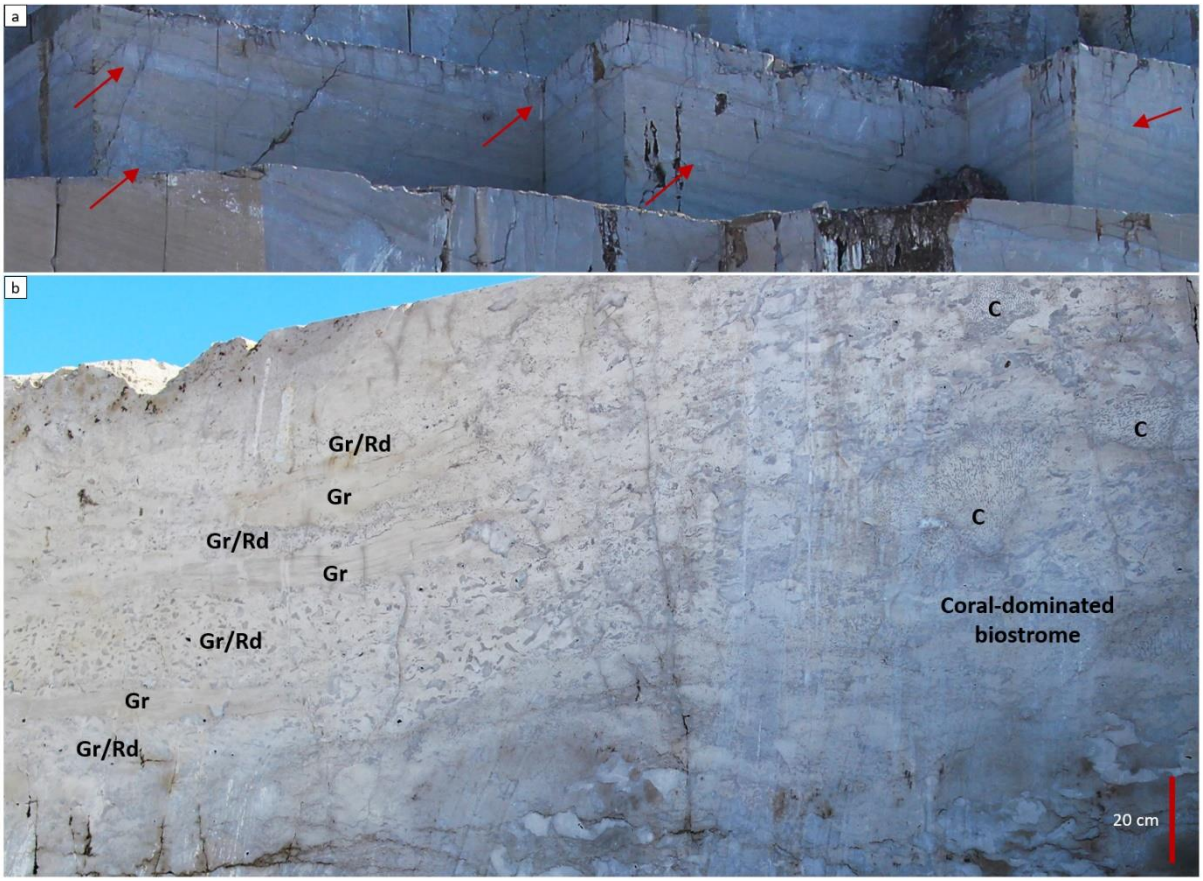

Figure IV.1.15. **a**: Outcrop interval generally showing grainstone facies, with decimetric, coarser-grained lenticular grainstone bodies with skeletal grains, pinching-out over relatively short distances (light-coloured bodies indicated by red arrows). Height of quarry face is between 5-7 m. **b**: Overlying coral-dominated biostrome with in-situ corals (c), transitioning laterally into decimetric intercalations of grainstones (Gr), and grainstone-rudstones with coral fragments (Gr/Rd).

The bedding surfaces, discontinuity surfaces and major geometric arrangements of the quarry fronts at Codaçal can be followed along the continuous front of between approximately 25 and 30 m in length, where clear lateral variability in geometric arrangements and package thickness are identified (Figure IV.1.16). While the major bedding surfaces can be laterally correlated along the exposed quarry fronts over moderate distances, the lateral extent of internal sedimentary structures is strongly limited, further illustrating the complexity in lateral subsurface correlation of depositional packages utilizing discrete data points at well locations.

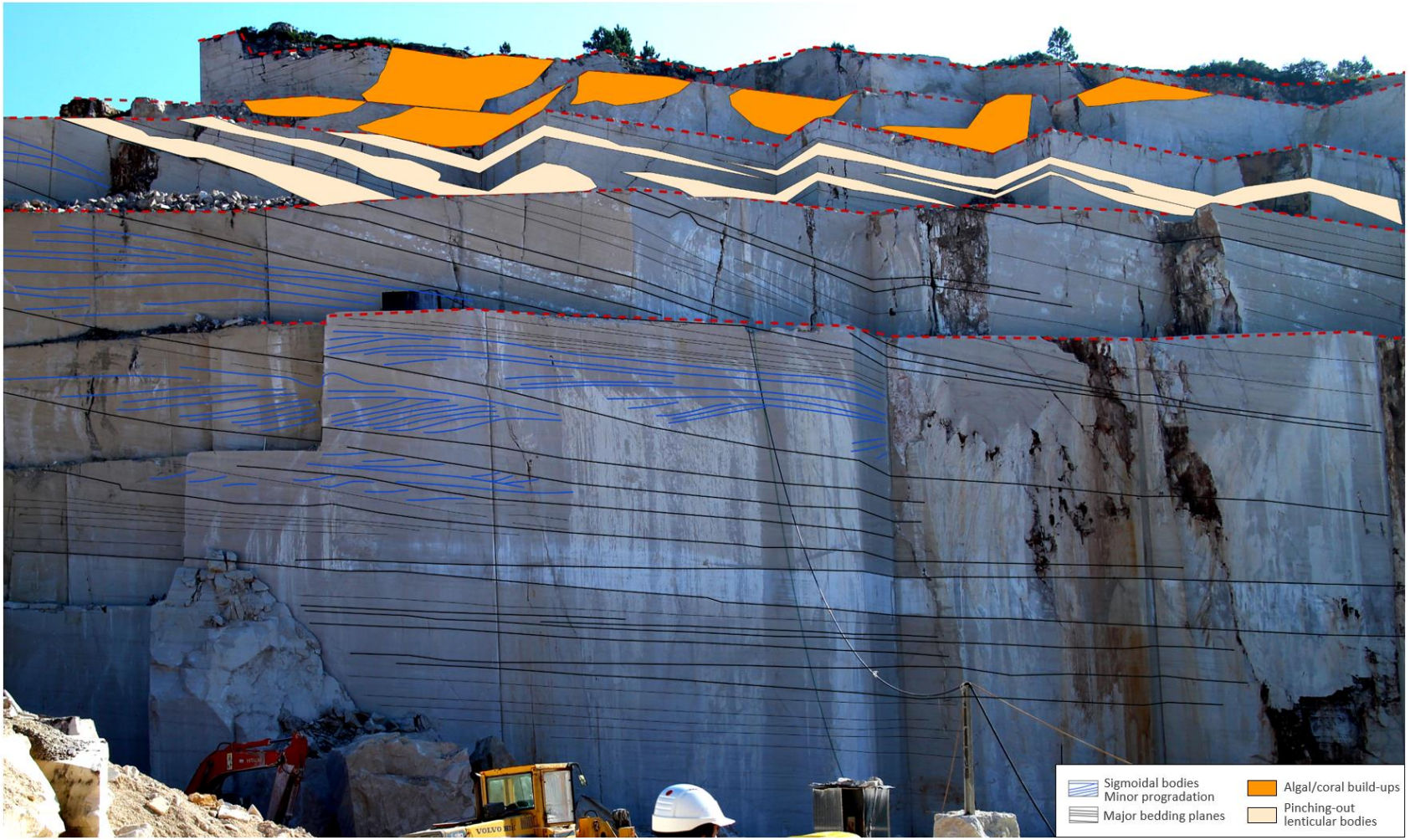

Figure IV.1.16. Interpretation of outcrop features, major bedding surfaces and depositional geometries at Codaçal (Codaçal Member). Horizontal field of view is approximately 60 m. Vertical hight of quarry front is between an estimated 36 and 40 m.

IV.1.7.3. Depositional controls on reservoir architecture and heterogeneity

The reservoir architecture and sediment distribution are influenced by varied depositional controls. Variations in accommodation space driven by the combined effects of relative sea-level fluctuations and tectonic controls, biological activity or variable hydrodynamic conditions lead to the development of complex geometric relationships (e.g. McNeill et al., 2004; Schlager, 2005; Pomar and Kendall, 2008; Reeder and Rankey, 2008; Alsharhan and Kendall, 2010). In the basal interval of the analysed quarry front at Codaçal (Codaçal Member), sediment influx was most likely keeping up with relative sea-level rise, resulting in the prevailing aggradational stacking pattern and geobodies with apparent tabular geometries. The vertical transition into the apparent progradational patterns, cross-bedding and sigmoidal bodies mentioned above, which might also represent mobile shoreface bars (Azerêdo, 1998), is interpreted to reflect a decrease in accommodation space accompanied by higher sediment influx rates in relation to the rate of relative sea-level increase (e.g. Flügel, 2004; Schlager, 2005; Pomar and Kendall, 2008). Cross-bedding structures tend to disappear towards the top of this quarry front, which shows stronger aggradation, in an interpreted response to an increase in accommodation space and sediment influx keeping-up with relative sea-level variations, leading to the tabular and lenticular geometries observed. The geometries and sediment distribution in this interval are interpreted to be controlled by hydrodynamics and moderate to high energy currents, which would have led to deposition of lenticular bodies pinching-out over short distances. The geometries of the overlying interval are mainly controlled by the growth dynamics of the coral/algal build-ups, but will also be influenced by the effects of current activity transporting sediments in areas between these build-ups, leading to the intercalations of grainstone layers with grainstone-rudstone layers containing abundant coral fragments.

The observed complex geometric arrangements and depositional architecture are the main controls on lateral facies variability over short distances, which, depending on the diagenetic history also, could result in considerable petrophysical heterogeneity.

IV.1.7.4. MCE outcrop vs. Abu Dhabi subsurface

While the two case studies here addressed show important differences, there are also a few limited similarities between them and the contrasting/comparable points of interest will be discussed in this section. Outcrop observations provide valuable insights into facies heterogeneity controlled by the architecture of deposition that allow the establishment of some parallelisms with the subsurface.

As previously mentioned, subsurface reservoir studies are based on well data, providing limited control points, as opposed to outcrop study cases, which allow for laterally continuous observations (e.g. Weber, 1986; Van Buchem et al., 2002; Strohmenger et al., 2006; Palermo et al., 2012; Fitch et al., 2015). This leads to the increased difficulty and higher uncertainty in predicting lateral variations in depositional geometries and reservoir properties between well locations (e.g. Mellvile et al., 2004; Yose et al., 2006; Lucia, 2007; Burchette, 2012). This issue can be illustrated by creating 3 pseudo-wells intersecting the studied quarry front at Codaçal (Figure IV.1.17).

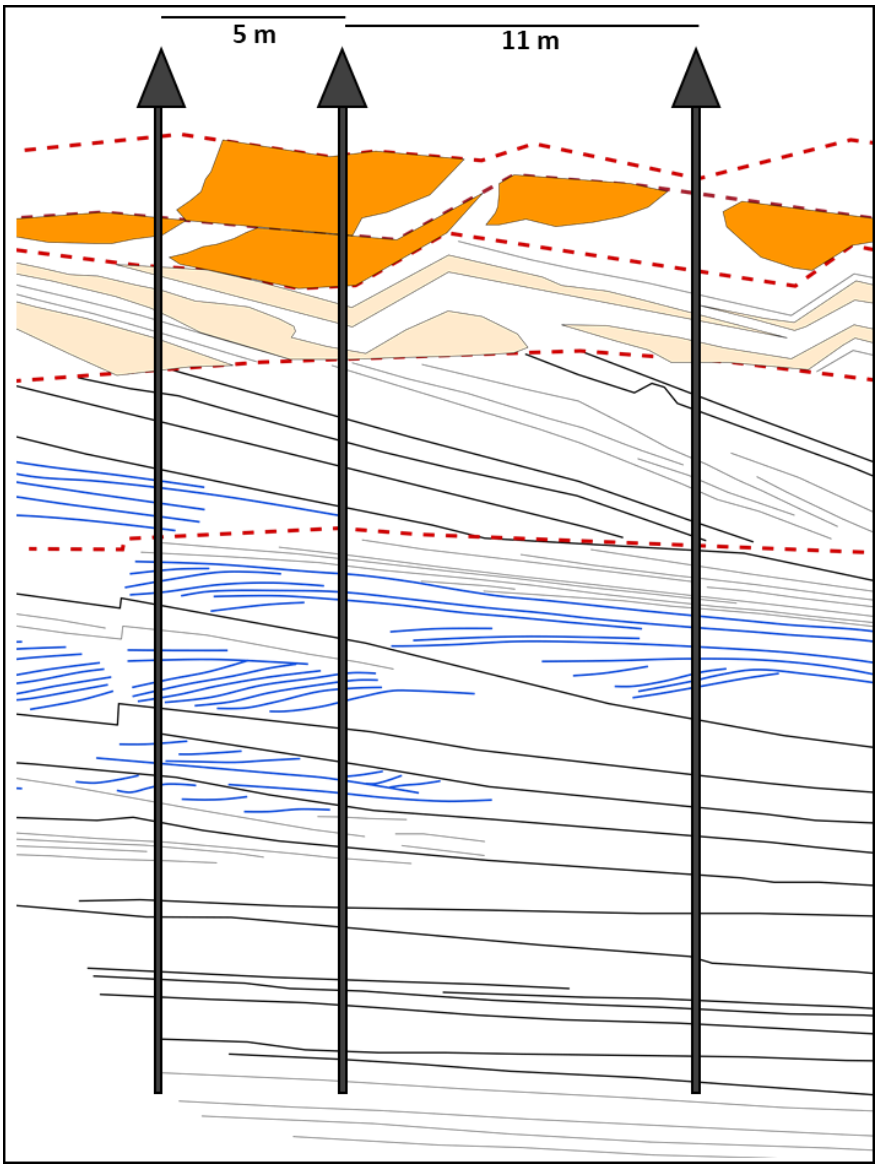

Figure IV.1.17. Major sedimentary structures along the analysed quarry front at the Codaçal location. Three pseudo-wells were created intersecting the section. The coral build-ups are only intercepted by two wells and the thickness of coeval layers is varying between wells (see Figure IV.1.16 for colour code). Dashed red lines represent breaks in this schematic representation of the succession in between each quarry face, due to the angle of visualization (see Figure IV.1.16).

If no inter-well data is available, the connectivity and lateral continuity of geobodies between wells become a major uncertainty, given the observed strong heterogeneity over short distances. Lateral correlations and interpreting lateral variability between wells can lead to a number of different equiprobable models and moderate to high uncertainty. This exercise illustrates how the facies succession in each well is different, as a consequence of the reservoir architecture. Only two pseudo-wells would have drilled through algal/coral build-ups, which would also show different thicknesses for each well. In the lower intervals, coeval layers will show different thicknesses and bedding surfaces might show different dipping angles from well to well. The outcrop case study here addressed is compared to the subsurface case study of the UKM, in the U.A.E., in an attempt to provide further insight into the controls on heterogeneity in the subsurface. This formation is part of the Lower Cretaceous Thamama Group, which is described as having an overall layer-cake stratigraphy, with correlatable zones/subzones over large distances across the different fields in Abu Dhabi (e.g. Van Buchem et al., 2002; El Wazir et al., 2015; Ehrenberg, 2016). However, the UKM shows small-scale vertical facies trends which vary between wells, in similarity to what is observed in the MCE Codaçal case. This outcrop (Figures IV.1.16, IV.1.17) will be compared to the interval between the base of the UKM and the top of the rudist-rich subzone 2, with emphasis given to the intervals of subzones 2 and 3 (see Chapter III).

IV.1.7.4.1. Facies succession

The basal part, and most of the lower half of the UKM (subzones 5, 4 and basal 3L) are generally characterized by wackestone facies with scattered orbitolinids (Figure IV.1.4) and a few dolomitized intervals. Discontinuity surfaces are visible towards the top of subzone 4, normally followed by slightly vuggy thin layers. Stylolites are identified and signs of bioturbation are visible throughout this interval. This type of relatively low-energy facies is not exposed in the analysed Middle Jurassic MCE quarry fronts (though it occurs in the same region, less widely than the higher energy facies), and are more typically represented towards the western/northwestern areas of the LB (e.g. Azerêdo, 1988, 1993, 1998).

Subzone 3U of the UKM is generally characterized by packstone facies, intercalating with grainstone intervals, and evolves upwards into the packstone, grainstone and rudstone-grainstone layers with rudist fragments of Subzone 2 (Figure IV.1.4; see also Chapter III). Some grainstone and rudstone-grainstone intervals show a micritic phase with packstone-grainstone texture partially occupying the interparticle space, while intervals of oolitic-intraclastic grainstones occur towards the top of this reservoir. The analysed intervals of the Santo António-Candeeiros Formation are generally characterized by grainstone and rudstone facies with intraclasts, peloids, skeletal grains, oncoids and ooids, with spar cements occluding the original pore space and an overall absence of a finer micritic phase (Figure IV.1.3).

Grainstone facies are not as dominant in the UKM as in the Codaçal and Pé da Pedreira members, although some intervals show significant similarities (Figure IV.1.18; Table IV.1.1).

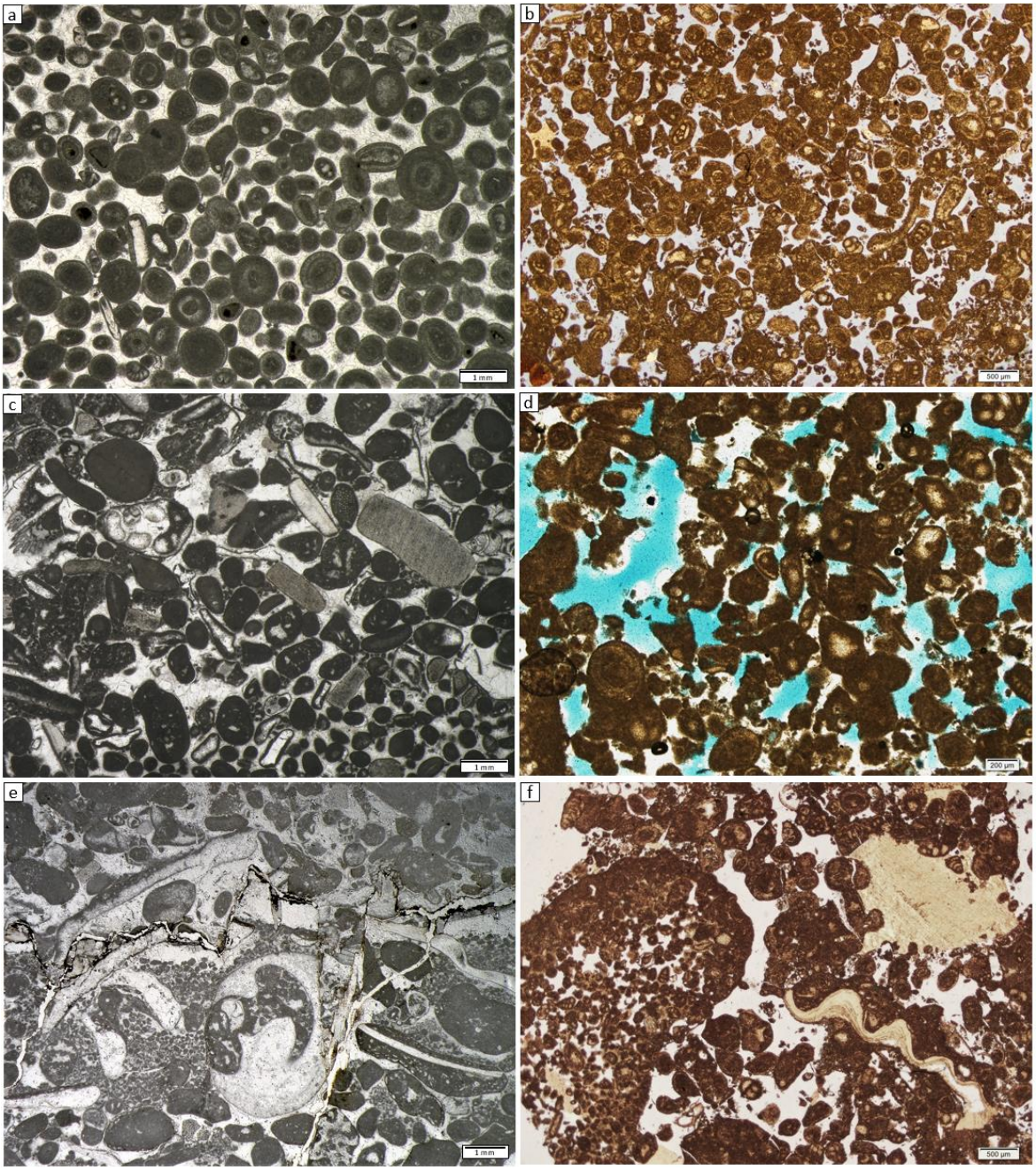

Figure IV.1.18. **a**: Well sorted cemented oolitic grainstone (MCE, Codaçal Member); **b**: Well sorted oobiointraclastic grainstone (Abu Dhabi, UKM, subzone 2); **c**: Moderately sorted cemented biointraclastic grainstone showing clear alternation between coarser- and finer-grained layers (cross lamination), bioclast-intraclast dominated and ooid dominated, respectively (MCE, Codaçal Member); **d**: Moderately sorted intraclastic grainstone with a few ooids (UKM, subzone 2); **e**: Very poorly sorted biointraclastic grainstone. Interparticle space is calcite cemented but a finer peloidal phase exhibiting a geopetal infiltration fabric is also identified; prominent stylolite with residual seam and roughly orthogonal microfractures are also evidenced (MCE, Codaçal Member); **f**: Very poorly sorted intrabioclastic grainstone with ooids, including large aggregate grains (left side of picture), with skeletal grains and coarser lithoclasts composed by skeletal grains, peloids and intraclasts (UKM, subzone 2).

The Codaçal Member interval containing coral/algal build-ups transitioning laterally into grainstone lenses facies could be comparable to the rudist-rich UKM intervals in subzone 2, as these organisms normally develop in reef structures. However, this UKM case study might represent sediments transported over short distances (e.g. Grötsch et al., 1998; Van Buchem et al., 2002; Ehrenberg et al., 2018). The UKM subzones 2 and 3 show small-scale vertical facies variations and discontinuity-bounded intervals generally showing fining-upwards trends, with moderate vuggy porosity at the base. These intervals are poorly correlatable between wells, exposing the difficulty in predicting lateral facies variability.

Table IV.1.1. Main facies types observed in the studied successions of the Santo António-Candeeiros Formation (MCE) and UKM (Abu Dhabi). The MCE facies types correspond to the lithofacies defined in Azerêdo (1998) and Azerêdo et al. (2020). The UKM facies types are defined as a simplification of the facies scheme developed by Strohmenger et al. (2006).

	Facies types	**Main features**
MCE, Portugal Facies identified on outcrops	Oolitic and bio/intraclastic cross-bedded grainstones (LF1)	Ooids, intraclasts, skeletal grains. Well to moderately sorted. Low to high angle cross lamination. Calcite-cemented.
	Oncolitic/bioclastic/lithoclastic rudstones, grainstones and packstones (LF2)	Oncoids, litho/intraclasts, skeletal grains. Poorly to moderately sorted. May contain a finer peloidal sediment exhibiting an infiltration fabric, often geopetal. Calcite-cemented.
	Coral/algal boundstones (biostromes) (LF3)	Framestones and bafflestones with *in situ* corals and abundant coral fragments, as well as red algae and many other skeletal grains. Peloidal-intraclastic packstone often occurs as internal sediment.
UKM, U.A.E. Simplified facies types	Biointraclastic rudstone-grainstone	Intraclasts, skeletal grains. Includes intervals with rudist fragments, other bivalves and skeletal grains. Generally poorly to very poorly sorted. Includes facies where a relatively finer packstone-grainstone matrix occurs.
	Biointraclastic grainstones and packstone-grainstones	Intraclasts, skeletal grains, peloids. Poorly to well sorted. Coated grains, including ooids, occur in some better sorted grainstones. Includes facies where a relatively finer packstone-grainstone matrix occurs.
	Biointraclastic packstone	Intraclasts, skeletal grains, peloids, with a micritic matrix.
	Biomicritic wackestone	Micritic matrix with scattered skeletal grains, including micritized orbitolinids.

IV.1.7.4.2. Depositional environment

The wackestone intervals of the UKM (subzone 5, 4 and part of 3L) were deposited in deeper, lower-energy waters in a distal to mid-ramp setting (e.g. Van Buchem et al., 2002; Strohmenger et al., 2006). The UKM depositional system gradually evolves into inner ramp, shallower water and high-energy environments. The well-sorted oolitic-intraclastic grainstones towards the top of the reservoir zone mark deposition in higher-energy settings, close to shoal or shoal-crest setting, in upper ramp (e.g. Van Buchem et al., 2002; Strohmenger et al., 2006). The small-scale heterogeneity and facies trends of subzones 3U and 2 of the UKM might be a reflection of moderate to strong hydrodynamic activity influencing sediment deposition and distribution, as previously mentioned (e.g. Grötsch et al., 1998; Van Buchem et al., 2002; Ehrenberg et al., 2018). To some extent, there are some similarities with the depositional settings of the Santo António-Candeeiros Formation at the MCE, defined as inner ramp, shoreface and upper shoreface setting with high-energy grainstone and rudstone facies (e.g. Azerêdo, 1998, 2007). However, the weaker expression of grainstone facies in the UKM and the relatively stronger presence of a micritic phase, compared to the Codaçal and Pé da Pedreira members, indicates relatively higher energies of deposition in the depositional environment of the latter. In addition, the Codaçal Member is characterized by intervals with relatively higher volumes of ooids and oolitic grainstones (Figures IV.1.18a, IV.1.19). The intraclastic grainstones occurring at Codaçal contain very well-rounded particles with relatively higher sphericity (Figure IV.1.18c), when compared to similar intraclastic grainstones of the UKM, which generally show moderately to well-rounded intraclasts with low to moderate sphericity (Figure IV.1.18d).

Figure IV.1.19. Macroscopic view of an oolitic limestone/grainstone with low-angle ripple laminae at Codaçal, MCE.

IV.1.7.4.3. Depositional architecture

Subzone 4 of the UKM is most likely characterized by less pronounced lateral geometric variations, with deposition of tabular or sheet-like bodies showing moderate to high lateral facies continuity, dominated by wackestones. Heterogeneity is higher in subzones 3L and 3U, as previously mentioned, increasing towards the top, which shows relatively thin (around 30 to 90 cm) fining upwards discontinuity-bounded packages. The facies succession is different from well to well, as previously mentioned, which leads to the interpretation that the lateral extension and continuity of these bodies is relatively weak between wells and at the field scale. There are no clear indications of progradational patterns in the observed cores, although clinoforms have been identified in subzone 3 on outcrops of this formation in the Northern Emirate of Ras Al Khaima, U.A.E. (Strohmenger et al., 2006). However, it should be taken into account that this outcrop is at a distance of around approximately 350 Km from the studied field, and would have been located close to the platform margin and edge of the Tethys ocean (e.g. Murris, 1980). The possibility that the discontinuity surfaces observed on cores represent the boundaries of low-angle prograding wedges or lensoids should not be dismissed, nevertheless. These fining-upwards packstone/grainstone intervals of the UKM subzone 3 are interpreted to have been deposited in relatively high-energy environments under the influence of moderate hydrodynamic activity and possible storm activity controlling sediment distribution (e.g. Grötsch et al., 1998; Pittet et al., 2002; Van Buchem et al., 2002; Ehrenberg et al., 2018), leading to deposition of wedge-like or lenticular bodies (e.g. Van Buchem et al., 2002). The Codaçal outcrop at MCE, on the other hand, shows intervals with clear strong small-scale cross-bedding patterns, suggesting well-developed progradational patterns, as previously discussed (Figures IV.1.5d, IV.1.7b, IV.1.14).

In the subsurface UKM case, the rudist-rich bodies of subzone 2 identified on cores are characterized by the presence of shell fragments, with no articulated or disarticulated rudist shells. They are interpreted to represent deposition of reworked particles transported over relatively short distances from different points of the high-energy environment (e.g. Grötsch et al., 1998; Van Buchem et al., 2002; Ehrenberg et al., 2018), in similarity to reports from rudist-rich outcrop studies (e.g. Carannante et al., 2003; Du et al., 2015), and are intercalating with biointraclastic grainstone intervals. These sediments would, therefore, probably be deposited in the form of lenticular bodies, as opposed to in-situ rudist reefs/build-ups. These rudist-rich bodies are thinner (between 15 and 90 cm) than the coral/algal build-ups observed on the Codaçal outcrop, which transition laterally into grainstone intervals over short distances (Figure IV.1.15b). The interpreted degree of lateral facies variability in subzone 2 of the UKM might not be as strong as that observed on the MCE outcrop (Figure IV.1.20), but there might be considerable heterogeneity on a relatively larger scale, given the mentioned variability of the facies succession between the analysed wells. While the analysed quarry fronts show significant lateral heterogeneity observed over centimetric/decametric distances, the large

distances between the studied wells of the UKM subsurface case (between 6 and 8 Km) prevents detailed interpretations on the lateral continuity and connectivity of geobodies at a smaller scale. Closely positioned wells and/or data from long horizontal wells would provide further valuable insight on this small-scale lateral facies variability and reservoir architecture.

Although both cases are considered to show important differences, as discussed above, comparable physical controls related to hydrodynamics and current activity are interpreted to have an important influence on sediment distribution in both. The lateral extent of geobodies and lateral thickness variability within the UKM is most likely defined by this activity, leading to erosional truncations or depositional pinch-outs, similar to what is partially observed, regarding thickness variations in some intervals of the MCE Codaçal outcrop.

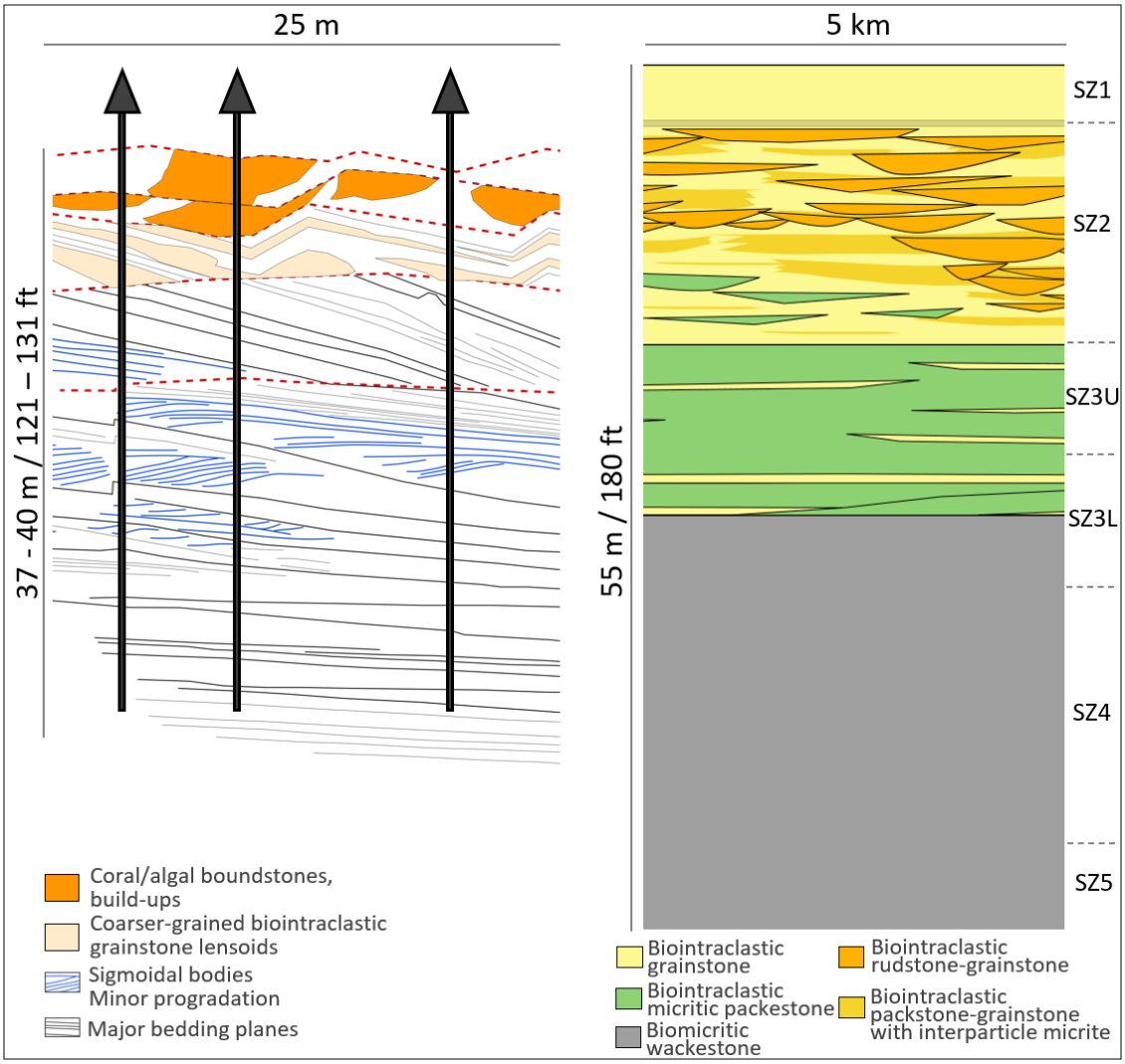

Figure IV.1.20. Comparison between the MCE outcrop section (left) and the conceptual model representing the UKM reservoir unit (right; Chapter III.2). Although the successions show some similarities at a larger scale, with a general evolution from tabular geobodies, through intervals of potential progradation, with lenticular bodies, and into sections characterized by the presence of reef-building organisms, a detailed analysis shows some significant differences. **Left**: Codaçal Member at

Codaçal. Depositional facies are generally characterized by oolitic and bio-intraclastic grainstones, with coarser-grained biointraclastic grainstones (lenses/lenticular bodies) and coral/algal boundstones and build-ups towards the top. **Right**: UKM reservoir unit at the studied field in Abu Dhabi. Interpretations indicate probable tabular geometries in subzone 4, lenticular bodies or wedges within subzone 3 and subzone 2, with variations between packstone-grainstone-rudstone facies.

IV.1.7.5. Relevance of outcrop analogues for reservoir modelling

The uncertainty associated with lateral variability in facies and in reservoir properties has great impact on field development plans and, ultimately, in hydrocarbon recovery efficiency. An improved understanding of the reservoir architecture as the main primary control on depositional facies variability will help to reduce this uncertainty (e.g. Mutti et al., 1996; Asprion et al., 2008; Jung and Aigner, 2012; Petrovic and Aigner, 2017; Van Tuyl et al., 2018; Azerêdo et al., 2020). This can be achieved through the analysis of outcrop analogues, which provide continuous observation points in a way that is not achievable in the subsurface (e.g. Weber, 1986; Van Buchem et al., 2002; Strohmenger et al., 2006; Palermo et al., 2012; Adam et al., 2018). Although seismic data covers the inter-well areas, its resolution will not capture details at smaller scales, preventing the proper description of depositional geometries and reservoir architecture (e.g. Mellvile et al., 2004; Yose et al., 2006; Alnazghah et al., 2013).

In the studied field in Abu Dhabi, the depositional controls are interpreted to be the main drivers for petrophysical heterogeneity (Chapter III.2), which means that stronger predictability of rock properties variability might be obtained with an improved understanding of the depositional architecture and facies distribution. This variability in depositional facies and petrophysical properties, namely capillary pressure and relative permeabilities, will control fluid flow in the reservoir, which is also influenced by the effects of variable wettability within its heterogeneous pore system (e.g. Namba and Hiraoka, 1995; Chilingarian et al., 1992; Masalmeh, 2002; Masalmeh et al., 2003; Gomes et al., 2008), having great impact on reservoir performance (e.g. Weber, 1986; Namba and Hiraoka, 1995; Wardlaw, 1996; Cunningham and Chaliha, 2002; Dabbouk et al., 2002; Carvalho et al., 2011). The analysed outcrop case study illustrates the strong depositional heterogeneities typical of carbonate systems and shows how depositional facies and, potentially, petrophysical properties can vary over relatively short distances, strongly influencing fluid flow through the usually complex pore network. A detailed understanding of reservoir architecture at different scales will provide additional information contributing to the development of more reliable reservoir models based on sound geological concepts.

IV.1.8. Conclusions

The freshly cut quarry fronts at the MCE offer an excellent opportunity to study depositional geometries at different observation scales, offering valuable insights into the controls on the facies heterogeneity and depositional architecture of carbonate reservoirs. Moderate continuity of depositional packages is observed on the analysed MCE outcrops at a larger scale, over considerable distances (dozens to hundreds of meters), but strong spatial variability over short distances, at centimetre to meter scale, also occurs, driven by the presence of progradational patterns, pinching-out geometries and reef build-ups. These observations are comparable to the Abu Dhabi subsurface case study, where there is strong continuity of large-scale depositional packages inside and across fields, but moderate to strong small-scale heterogeneity is considered to occur, based on the interpretations of core data. While the successions of both the outcrop and the subsurface case studies show some general similarities regarding depositional geometries, considerable differences exist in terms of the interpreted depositional settings, with the MCE facies reflecting relatively higher-energy palaeoenvironments. In spite of the existing differences, depositional factors such as hydrodynamics, current activity and palaeotopography are seen as some of the main controls on sediment distribution and on the development of geometric features in both cases, which in turn will define facies variability. This dynamic behaviour of carbonate systems and the complex nature of carbonate rocks reveal the importance in pursuing an improved understanding of the controls on small-scale variability in depositional geometries as fundamental elements to help improve reservoir models and the predictability of spatial facies variations and, potentially, of reservoir properties.

Chapter V. Conclusions and final remarks

Carbonate successions deposited in high-energy settings are known to show strong spatial facies heterogeneity. This variability is driven by primary depositional controls such as biogenic factors, hydrodynamics or topography, as defined by the palaeoenvironment and depositional system itself, and is further influenced by diagenetic factors throughout burial and periods of uplift. The primary depositional factors will have a strong influence on sediment distribution and will determine the physical properties of the carbonate particles, such as size and sorting, which are important parameters defining reservoir quality and reservoir heterogeneity. The present study addresses these controls on heterogeneity, through the analysis of Lower and Middle Jurassic outcrop case studies in Portugal, as well as a subsurface reservoir in Abu Dhabi. A Toarcian-Aalenian(?) outcrop section along 4 km of the western to southern Peniche Peninsula margins was analysed, as well as Bathonian-Callovian outcrops in quarry fronts of different heights at three locations of the MCE. A total of 312 thin sections were analysed from the Peniche outcrops, two offshore wells near Peniche and 4 onshore wells in Abu Dhabi.

In each of the previous chapters, the conclusions individually addressing the respective discussed topic are presented. In this section, the overall main results of interest and concluding remarks are summarized and presented for the different case studies. The future work perspectives are also presented in this final chapter.

V.1. The Cabo Carvoeiro Formation case study

The upper CC5 Member of this Formation in Peniche represents a distinct sedimentary succession in the context of the LB. In a succession that is seemingly homogeneous in terms of depositional facies, generally characterized by oo-intraclastic grainstones with quartz, interpreted in this study to have been deposited in infralittoral prograding wedges, the applied subfacies classification scheme helped reveal the spatial facies heterogeneity and the variability in relative volume of rock constituents and grain sorting. This detailed analysis allowed for the interpretation and identification of facies cycles resulting from the combined effects of relative sea level changes and tectonics associated with the uplift of the Berlengas basement block. Three new subdivisions for the CC5 Member are proposed for this 160 m grainstone interval, resulting in a total of five subdivisions for this Member. This grainstone succession shows good potential hydrocarbon reservoir properties. However, its original petrophysical properties have been altered by diagenesis, namely porosity-occluding calcite cementation. Tectonics and strong structural activity create a variety of potential structural traps, but there is also strong potential for the development of stratigraphic traps, considering the lateral facies variability observed between the Peniche outcrops and the 17C-1 and 20B-1 wells north and south of

Peniche. This lateral variability was driven by the overall architecture of deposition, which shows thickness variations, truncation and pinching-out features. The hypothetical development of sedimentary successions deposited in analogous settings to the Peniche case study, with similar depositional facies, and in association with such potential trapping mechanisms would present good opportunities for hydrocarbon exploration activities in the Lusitanian and Peniche basins.

V.2. The Kharaib Formation case study

In the prolific hydrocarbon-producing Rub Al Khali Basin, in Abu Dhabi, its largest producing reservoir (Upper Kharaib Member) is well studied and densely drilled in various onshore and offshore fields. However, uncertainty still exists regarding lateral variability in depositional facies and reservoir properties, which will ultimately influence field development decision on well placement and selection of perforation intervals, for example. The large-scale vertical facies succession of the studied reservoir zone is well known, with the more homogeneous lower half dominated by wackestone facies and the heterogeneous upper half characterized by packstone, grainstone and rudstone-grainstone facies. At a smaller scale, discontinuity-bounded, generally fining-upwards intervals are identified. This observed small-scale facies variability is different from well to well and lateral correlation is not straight forward, indicating a complex depositional architecture, and the most likely development of lenticular or wedge-like bodies, deposited under the influence of variable hydrodynamics or storm activity.

This reservoir shows moderate to strong variability in permeability, which is not directly correlatable with total porosity. This porous network is characterized by a heterogeneous dual macro and microporosity system, with micritization leading to the development of considerable volumes of microporosity, including in the micritized carbonate particles of grainstone intervals. The quantification of different pore types through digital image analysis and guided machine learning, in integration with petrographic data, has provided invaluable insights into the controls on reservoir heterogeneity. The high-permeability layers are directly related to the occurrence of non-cemented, well-sorted grainstone facies with higher macroporosity, with relatively low or non-existing calcite cementation in the analysed wells. Such observations indicate a certain degree of predictability in permeability variations might be obtained through this type of integrated analysis, and through the establishment of a detailed stratigraphic framework. This is important, as high-permeability layers behave as preferred fluid flow pathways, strongly affecting the reservoir performance and hydrocarbon recovery efficiency.

V.3. The Santo António-Candeeiros Formation case study

The analysis of freshly-cut quarry fronts at the MCE offered valuable information on the controls of depositional architecture on lateral facies variability within the high-energy inner ramp and barrier island environments characterizing the Middle Jurassic Santo António-Candeeiros Formation at a level of detail that is not possible in outcrops affected by weathering. Multi-scale outcrop observations offered further insight into this variability and provided some comparable points of interest between this case and the Abu Dhabi subsurface case study. Moderate to strong lateral continuity is observed at a larger scale, but strong geometric heterogeneity occurs at smaller centimetre/metre scales in the MCE outcrops. Cross-bedding, pinching-out of wedge-like bodies, lenticular geometries and coral/algal build-ups are the main architectural features controlling lateral facies variability at centimetre to meter scales. Pseudo-wells placed along an analysed quarry front show how a direct lateral correlation between wells would be difficult to achieve in these settings without the additional observations from outcrop analysis. Such uncertainties are some of the main issues in subsurface reservoir modelling, where data is limited to well locations, as previously mentioned.

A comparison between the MCE outcrop analysed at Codaçal and the Abu Dhabi subsurface reservoir shows that, while this outcrop is not a direct analogue for the reservoir, the vertical successions show moderate similarities in terms of the depositional architecture. The outcrop observations support the interpretations on the Abu Dhabi subsurface case study, where there is strong continuity of large-scale depositional packages within a field and also throughout the region between fields, but moderate to strong small-scale heterogeneity is observed, leading to reduced or non-existing lateral continuity between wells in a given field.

V.4. Final remarks and future work perspectives

The analysed outcrops offered valuable, detailed information on lateral facies variability and depositional geometries to an extent which is not achievable in the subsurface, where data is limited to well locations. In the three addressed case studies, variability in depositional geometries is observed at different scales, with strong to moderate continuity at larger decametre to kilometre scale, but considerably stronger variability at smaller centimetre/metre scales. The analysis of this small-scale variability, through the application of fit-for-purpose facies classification schemes in integration with quantitative methodologies, revealed important information regarding carbonate heterogeneity issues, such as the effects of parameters such as grain sorting, grain size and pore type distribution on petrophysical variability in the subsurface case study. The interpretations on reservoir architecture and on the depositional controls on heterogeneity in the studied field in Abu Dhabi might be useful to increase the predictability of reservoir properties between wells. A better understanding of such issues is indispensable for improved reservoir characterization studies, as well as exploration

and field development plans. The added data and interpretations might contribute to the development of more reliable conceptual models, with increased geological meaning. However, with reservoir properties varying within the thin layers of grainstones and grainstone-rudstones of the UKM (15 to 90 cm), some of the small-scale heterogeneity might be lost in reservoir models through the process of upscaling, depending on the cell size of the models. It is fundamental that the acquired detailed understanding is provided to the modellers, with the objective of developing the best approaches to maintain the relevant level of detail in the modelling process.

In addition to the main topics related to heterogeneity in carbonate rocks and, specifically, to hydrocarbon reservoirs, this thesis offers relevant information contributing to the advancement of the sedimentologic and stratigraphic knowledge of the Jurassic in the LB.

Taking into consideration the quality of the case studies addressed, various lines of interest could be proposed for future studies. Only a few are proposed here, in what relates to the main topics addressed in this thesis.

Regarding the Cabo Carvoeiro Formation case study, a detailed analysis of diagenesis and the relative timing of fracture-filling cement phases could be a point of interest for future work. Fractures are one of the main factors reducing the efficiency of hydrocarbon trapping mechanisms and it would be of interest to define the timing of cementation within these fractures, as well as in interparticle pore space, in relation to the timing of hydrocarbon migration. The application of techniques such as fluid inclusion analysis or stable isotope analysis would help to further understand this issue and establish the role of fractures in hydrocarbon migration. The application of stable isotope analysis could also be used to attempt to define the age of the younger deposits in this exposed succession, as uncertainty remains regarding the Toarcian-Aalenian transition.

As for the Santo António-Candeeiros Formation studied on the MCE quarry outcrops, considering the regular advance in rock extraction from these locations, it would be useful to return to the same quarry front at different timings, in order to acquire an improved, increasingly detailed 3D understanding of the depositional geometries and reservoir architecture. Though microfacies of the studied unit are known on a regional basis, site-specific thin section acquisition and petrographic analysis done in parallel with macroscopic outcrop observations would add useful detailed information regarding the variability in facies and depositional textures across different geobodies in this hypothetical 3D volume. In addition, the correlation of outcrop and nearby borehole data, where available, would be of high interest and would greatly contribute to the advancement of such projects.

The Abu Dhabi case study was based on 4 widely-spaced wells. The quantitative methodologies used on this study could be applied to additional wells at different locations and

more closely-spaced within the studied field. In subsequent stages, wells from different fields could be added, in order to pursue an improved, integrated regional overview of the factors controlling heterogeneity. The machine learning methodologies to quantify macroporosity can be easily applied to additional thin section datasets, from the same studied field or from other nearby fields, as to improve the understanding of regional trends. Diagenesis is an important factor to consider and could be further analysed in these additional fields through stable isotope analysis, in order to pursue an improved understanding of the relative timing of diagenetic stages in different fields. The ultimate goal of such studies, as has been previously mentioned, is to improve the understanding on carbonate reservoir heterogeneity and to improve reservoir modelling efforts in carbonate systems, specifically to better characterize the lateral and vertical variability in facies and petrophysical properties through the use of reservoir models with increasingly accurate geological and rock properties information.

Chapter VI. References

Adam, A., Rudy, S., Abdulghani, W., Abdlmutalib, A., Hariri, M. and Abdulraheem, A. (2018). Reservoir heterogeneity and quality of Khuff carbonates in outcrops of central Saudi Arabia. *Marine and Petroleum Geology*, 89 (3), 721-751.

Agard, P., Omrani, J., Jolivet, L., Whitechurch, H., Vrielynck, B., Spakman, W., Monié, P., Meyer, B. and Wortel, R. (2011). Zagros orogeny: a subduction dominated process. *Geological Magazine*, 148 (5-6), 692-725.

Al Khalifa, H., Glover, P.W.J. and Lorinczi, P. (2020). Permeability Prediction and Diagenesis in Tight Carbonates Using Machine Learning Techniques. *Marine and Petroleum Geology*, 112.

Al Kindi, M. and Richard, P.D. (2014). The main structural styles of the hydrocarbon reservoirs in Oman. *Geological Society, London, Special Publications*, 392, 409-445.

Al Suwaidi, A., Taher, A.K., Alsharhan, A.S. and Salah, M.G. (2000). Stratigraphy and geochemistry of upper Jurassic Diyab Formation, Abu Dhabi, U.A.E. In: Alsharhan, A.S. and Scott, R. W. (Eds.), *Middle East Models of Jurassic/Cretaceous Systems*. SEPM Special Publication, 69, pp. 249-271.

Al-Awwad, S.F. and Pomar, L. (2015). Origin of the rudstone-floatstone beds in the Upper Jurassic Arab-D reservoir, Khurais Complex, Suadi Arabia. Marine and Petroleum Geology, 67, 743-768.

Alnazghah, M.H., Bádenas, B., Pomar, L., Aurell, M. and Morsilli, M. (2013). Facies heterogeneity at interwell-scale in a carbonate ramp, Upper Jurassic, NE Spain. *Marine and Petroleum Geology*, 44, 140-163.

Alsharhan, A.S. (1985). Depositional Environment, Reservoir Units Evolution, and Hydrocarbon Habitat of Shuaiba Formation, Lower Cretaceous, Abu Dhabi, United Arab Emirates. AAPG Bulletin, 69 (6), 899-912.

Alsharhan, A.S. (1989). Petroleum geology of the United Arab Emirates. *Journal of Petroleum Geology*, 12 (3), 253-288.

Alsharhan, A.S. (1990). Geology and reservoir characteristics of Lower Cretaceous Kharaib Formation in Zakum Field, Abu Dhabi, United Arab Emirates. *Geological Society, London, Special Publications*, 50, 299-316.

Alsharhan, A.S. (1991). Sedimentological interpretation of the Albian Nahr Umr Formation in the United Arab Emirates. *Sedimentary Geology*, 73 (3-4), 317-327.

Alsharhan, A.S. (1993). Asab Field-United Arab Emirates, Rub Al Khali Basin, Abu Dhabi. In: Foster, N.H. and Beaumont, E.A. (Eds.), *Structural VIII: AAPG Treatise of Petroleum Geology, Atlas of Oil and Gas Fields*, pp. 69-97

Alsharhan, A.S. (1995). Facies variation, diagenesis and exploration potential of the Cretaceous rudist-bearing carbonates of the Arabian Gulf. *AAPG Bulletin*, 79, 531-550.

Alsharhan, A.S. (2014). Petroleum systems in the Middle East. *Geological Society, London, Special Publications*, 392, 361-408.

Alsharhan, A.S. and Kendall C.G.St.C. (1991). Cretaceous chronostratigraphy, unconformities and eustatic sealevel changes in the sediments of Abu Dhabi, United Arab Emirates. *Cretaceous Research*, 12 (4), 379-401.

Alsharhan, A.S. and Kendall, C.G.St.C. (2010). Introduction to Quaternary carbonate and evaporite sedimentary facies and their ancient analogues. In Kendall, C. G. St. C., & Alsharhan, A. S. (Eds.). *Quaternary carbonate and evaporite sedimentary facies and their ancient analogues*. International Association of Sedimentologists, Special Publication, 43. Wiley-Blackwell, pp. 1-9.

Alsharhan, A.S. and Nairn, A.E.M. (1997). *Sedimentary Basins and Petroleum Geology of the Middle East*. Elsevier, Amsterdam, 942 pp.

Alsharhan, A.S. and Scott, R.W. (2000). Hydrocarbon potential of Mesozoic carbonate platform basin systems, UAE. In: A.S. Alsharhan and R.W. Scott (Eds.), *Middle East Models of Jurassic/Cretaceous carbonate Systems*. Special Publication, 69, SEPM (Society for Sedimentary Geology), U.S.A., 329-351.

Alves, T.M., Gawthorpe, R.L., Hunt, D.H. and Monteiro, J.H. (2002). Jurassic tectono-sedimentary evolution of the northern Lusitanian basin (offshore Portugal). *Marine Petroleum Geology*, 19, 727-754.

Alves, T.M., Gawthorpe, R.L., Hunt, D.W. and Monteiro, J.H. (2003a). Cenozoic tectono-sedimentary evolution of the Western Iberian Margin. *Marine Geology,* 195, 75-108.

Alves, T.M., Gawthorpe, R.L., Hunt, D.W. and Monteiro, J.H., (2003b). Post-Jurassic tectono-sedimentary evolution of the northern Lusitanian Basin (western Iberian margin). *Basin Research*, 15, 227-249.

Alves, T.M., Moita, C., Sandnes, F., Cunha, T., Monteiro, J.H. and Pinheiro, L.M. (2006). Mesozoic-Cenozoic evolution of North Atlantic continental slope basins: The Peniche Basin, western Iberian margin. *AAPG Bulletin*, 90 (1), 31-61.

Amel, H., Jafarian, A., Husinec, A., Koeshidayatullah, A. and Swennen, R. (2015). Microfacies, depositional environment and diagenetic evolution controls on the reservoir quality of the Permian Upper Dalan Formation, Kish Gas Field, Zagros Basin. *Marine and Petroleum Geology*, 67, 57-71.

Andrade, B. (2006). Los braquiópodos del tránsito Jurásico Inferior-Jurásico Medio de la Cuenca Lusitánica (Portugal). [The braquiopods from the Lower Jurassic-Middle Jurassic transition of the Lusitanian Basin (Portugal)]. *Coloquios de Paleontología,* 56, pp. 5-194.

Anselmetti, F.S., Luthi, S. and Eberli, G.P. (1998). Quantitative characterization of carbonate pore systems by digital image analysis. *AAPG Bulletin,* 82, 1815-1836.

Arganda-Carreras, I., Kaynig, V., Rueden, C., Eliceiri, K., Schindelin, J., Cardona, A. and Seung, H. (2017). Trainable Weka Segmentation: A machine learning tool for microscopy pixel classification. *Bioinformatics* (Oxford, England), 33 (15), 2424-2426.

Asprion, U., Westphal, H., Nieman, M. and Pomar, L. (2008). Extrapolation of depositional geometries of the Menorcan Miocene carbonate ramp with ground-penetrating radar. *Facies,* 55 (1), 37-46.

Azer, S.R. and Toland, C. (1993). Sea level changes in the Aptian and Barremian (Upper Thamama) of offshore Abu Dhabi, UAE. *Proceedings of the Society of Petroleum Engineers Middle East Oil Technology Conference,* Bahrain, April 1993. SPE-25610, 141-154.

Azerêdo, A.C. (1988). Calcareous debris-flow as evidence for a distally steepened carbonate ramp in West-Central Portugal. *Comunicações dos Serviços Geológicos de Portugal, Lisboa,* 74, 56-67.

Azerêdo, A.C. (1993). *Jurássico Médio do Maciço Calcário Estremenho* (*Bacia Lusitânica): análise de fácies, micropaleontologia, paleogeografia*. Tese de Doutoramento (não publicada), Departamento de Geologia, Faculdade de Ciências, Universidade de Lisboa, 366 pp.+36 ests. (2 vols.).

Azerêdo, A.C. (1998). Geometry and facies dynamics of Middle Jurassic carbonate ramp sandbodies, West-Central Portugal. In: Wright V.P. and Burchette, T. (Eds.): Carbonate Ramps. *Geological Society of London*, Special Publications, 149, 281-314.

Azerêdo, A.C. (1999). Etudes micropaléontologiques dans les séries carbonatées du Jurassique moyen du Basin Lusitanien (Portugal). *Comunicações do Instituto Geológico e Mineiro,* 86: 59-84.

Azerêdo, A.C. (2007). Formalização da litostratigrafia do Jurássico Inferior e Médio do Maciço Calcário Estremenho (Bacia Lusitânica). *Comunicações Geológicas,* 94, 29-51.

Azerêdo, A.C. (2015). Análise de reservatórios carbonatados em afloramento (Bacia Lusitânica) e outros aspectos aplicados à exploração petrolífera. In: Livro-guia, Módulo "Trabalho de campo na Bacia Lusitânica", Curso de Formação Avançada em Geo-Engenharia de Reservatórios Carbonatados. FCUL/Galp/Petrobras, 64 pp.

Azerêdo, A.C. and Duarte, L.V. (2017). Stratigraphy, sedimentary patterns and reservoir features of Jurassic carbonate successions from the Lusitanian Basin. *Ciências da Terra/Earth Sciences Journal,* 19 (1), 13-33.

Azerêdo, A.C. and Inês, N. (2011). Main diagenetic, porosity and reservoir features of limestone and dolomitic sandbodies from the Middle Jurassic of the Lusitanian Basin, Portugal. *Geophysical Research Abstracts, 13,* EGU2011-3556.

Azerêdo, A.C., Duarte, L. V., Henriques, M. H. and Manuppella, G. (2003). Da dinâmica continental no Triásico aos Mares do Jurássico Inferior e Médio. Cadernos de Geologia de Portugal. *Instituto Geológico e Mineiro,* Lisboa, 43 pp., 7 ests.

Azerêdo, A.C., Duarte, L. V. and Silva, R. L. (2014). Configuração sequencial em Ciclos (2a ordem) de Fácies Transgressivas-Regressivas do Jurássico Inferior e Médio da Bacia Lusitânica (Portugal). *Comunicações Geológicas, 101,* Fascículo Especial I, 383-386.

Azerêdo, A.C., Inês, N. and Bizarro, P. (2020). Carbonate reservoir outcrop analogues with a glance at pore-scale (Middle Jurassic, Lusitanian Basin, Portugal). *Marine and Petroleum Geology*, 20, 815-851.

Azerêdo, A.C., Wright, V.P., Mendonça-Filho, J.G., Cabral, M.C. and Duarte, L.V. (2015). Deciphering the history of hydrologic and climatic changes on carbonate lowstand surfaces: calcrete and organic-matter/evaporite facies association on a palimpsest Middle Jurassic landscape from Portugal. *Sedimentary Geology*, 323, 66-91.

Azerêdo, A.C., Wright, V.P. and Ramalho, M.M. (2002). The Middle-Late Jurassic forced regression and disconformity in central Portugal: eustatic, tectonic and climatic effects on a carbonate ramp system. *Sedimentology*, 49(6), 1339-1370.

Azzam, I.N. and Taher, A.K. (1995). Sequence Stratigraphy and Source Rock Potential of the Aptian (Bab Member). In *East Onshore Abu Dhabi: A Model Approach to Oil Exploration*. 9th SPE Middle East Oil Show, Bahrain, pp.305-317. SPE-29802.

Barata, J., Duarte, L.V. and Azerêdo, A.C. (2021). Facies types and depositional cyclicity of a Toarcian-Aalenian(?) carbonate-siliciclastic mixed succession (Cabo Carvoeiro Formation) in the Lusitanian Basin, Portugal. *Journal of Iberian Geology*.

Barata, J., Vahrenkamp, V., Van Laer, P. J., Swart, P. and Murray, S. (2015). A regional analysis of clumped isotope geochemistry to define the timing of creation of micro-porosity in a Lower Cretaceous giant reservoir. *Abu Dhabi International Petroleum Exhibition and Conference*, Abu Dhabi. Society of Petroleum Engineers, SPE-177922.

Barbosa, B., Soares, A.F., Rocha, R.B., Manupella, G. and Henriques, M.H. (1988). Carta geológica de Portugal, na escala 1/50000. Notícia explicativa da folha 19-A (Cantanhede). *Serviços Geológicos Portugal*, Lisboa.

Bazalgette, L. and Salem, H. (2018). Mesozoic and Cenozoic structural evolution of North Oman: New insights from high-quality 3D seismic from the Lekhwair area. *Journal of Structural Geology*, 111, 1-13.

Beydoun Z.R. (1991). Arabian Plate Hydrocarbon Geology and Potential-A Plate Tectonic Approach. *AAPG Studies in Geology*, 33, AAPG, Tulsa.

Biddle, K.T. and Wielchowsky, C.C. (1994). Hydrocarbon traps. In: Magoon, L.B., Dow, W.G., (Eds.): The Petroleum System - From Source to Traps. *AAPG Memoir*, 60, 219-235.

Billings, M.P. (1946). Structural geology (second printing). Prentice-Hall, New York.

Blanc, E.J.P., Allen, M.B., Inger, S. and Hassani, H. (2003). Structural styles in the Zagros Simple Folded Zone, Iran. *Journal of the Geological Society, London*, 160, 401-412.

Boillot, G., Malod, J.A. and Mougenot, D. (1979). Evolution géologique de la marge ouest-ibérique. *Ciências da Terra*, 5, Universidade Nova de Lisboa, Lisboa, 215-222.

Borgomano, J., Masse, J.P. and Al Maskiry, S. (2002). The lower Aptian Shuaiba carbonate outcrops in Jebel Akhdar, northern Oman: Impact on static modeling for Shuaiba petroleum reservoirs. *AAPG Bulletin*, 86 (9),1513-1529.

Bourillot, R.L., Vennin, E., Rouchy, J., Durlet, C., Rommevaux, V., Kolodka, C. and Knap, F. (2010). Structure and evolution of a Messinian mixed carbonate-siliciclastic platform: the role of evaporites (Sorbas Basin, South-east Spain). *Sedimentology*, 57, 477-512.

Braithwaite, C.J.R., (1973). Settling behaviour related to sieve analysis of skeletal sands. *Sedimentology*, 20, 251-262.

Breiman, L. (2001). Random Forests. *Machine Learning*, 45, 5-32.

Brett, C.E. (1999). Chapter 6, Middle Ordovician Trenton Group of New York, USA. In Hess, H., Ausich, W. I., Brett, C. E., and Simms, M. J. (Eds.), *Fossil crinoids*. Cambridge University Press, Cambridge, United Kingdom, pp. 63-67.

Brito, M., Rodrigues, R., Baptista, R., Duarte, L.V., Azerêdo, A.C. and Jones, C.M., 2017. Geochemical characterization of oils and their correlation with Jurassic source rocks from the Lusitanian Basin (Portugal). *Marine and Petroleum Geology*, 85, 151-176.

Broomhall, R.W., Fullmer, S., Deshpande, A., Kaufman, J., Edwards, E. and Al Henshiri, Y. (2008). Water movement controls in an Early Cretaceous reservoir: An integrated analysis from a large offshore field, Abu Dhabi, United Arab Emirates. In *Proceedings from GEO 2008 Conference*, 3-5 March, 2008, Bahrain. Abstract 115435.

Buckman, J., Bankole, S., Zihms, S., Lewis, H., Couples, G. and Corbett, P. (2017). Quantifying Porosity through Automated Image Collection and Batch Image Processing: Case Study of Three Carbonates and an Aragonite Cemented Sandstone. *Geosciences*, 7 (70).

Budd, D. (1989). Micro-rhombic calcite and microporosity in limestones: a geochemical study of the lower cretaceous Thamama Group, U.A.E. In: *Middle East, Nature and Origin of Microrhombic Calcite and Associated Microporosity*. Carbonate Strata, Sedimentary Geology, 63, pp. 293-311.

Burchette, T.P. (1993). Mishrif Formation (Cenomanian-Turonian), southern Arabian Gulf: carbonate platform growth along a cratonic basin margin. In: Simo, J.A., Scott, R.W. and Masse, J-P (eds.), *Cretaceous Carbonate Platforms*. AAPG Memoir, 56, 185-199.

Burchette, T. (2012). Carbonate rocks and petroleum reservoirs: a geological perspective from the industry. *Geological Society, London, Special Publications*, 370, 17-37.

Burchette, T.P. (2019). Are carbonate reservoirs 'difficult'?. *GEOExPro*, 16 (5).

Burchette, T. and Wright, V.P. (1992). Carbonate ramp depositional systems. *Sedimentary Geology*, 79, 3-57.

Bust, V.K., Oletu, J.U. and Worthington, P.F. (2011). The challenges for carbonate petrophysics in petroleum resource estimation. *SPE Reservoir Evaluation & Engineering*, 14 (1), 25-34. SPE-142819.

Camarate França, J., Zbyszewski, G. and Moitinho de Almeida, F. (1960). Carta Geológica de Portugal na escala de 1/50000. Notícia explicativa da folha 26-C Peniche.

Carannante, G., Ruberti, D. and Simone, L. (2003). Sedimentological and taphonomic characterization of low energy rudist-dominated Senonian carbonate shelves (Southern

Apennines, Italy): a North African perspective. In: Gili, E., Negra, M.H. and Skelton, P.W. (Eds.) *North African Cretaceous Rudist and Coral Formations and their Contributions to Carbonate Platform Development*. NATO ASI Series, Kluwer, Dordrecht, 189-201.

Cardoso, F., Teixeira, B., Pimentel, N., Pena dos Reis, R., Cortesão, A. and Reis, M. (2014). Evaluation of the thermal maturation of Jurassic potential source rocks in the Western Iberian Margin, based on modelling of Lusitanian Basin's wells and Peniche Basin's pseudo-wells. *Comunicações Geológicas*, LNEG, 101, 397-400.

Carvalho, J.M.F. and Lisboa, J.V. (2018). Ornamental stone potential areas for land use planning: a case study in a limestone massif from Portugal. *Environmental Earth Sciences,* 77 (5), 206 pp.

Carvalho, A.L.B., Dias, A.C. and Ribeiro, M.T. (2011). Oil Recovery Enhancement for Thamama B Lower in an Onshore Abu Dhabi Field. *Reservoir Characterisation and Simulation Conference and Exhibition*, Abu Dhabi. Society of Petroleum Engineers. SPE-148268.

Catuneanu, O. (2006). *Principles of Sequence Stratigraphy*. Elsevier, Amsterdam.

Catuneanu, O. (2019). Scale in sequence stratigraphy. *Marine and Petroleum Geology*, 106, 128-159.

Chandra, V., Barnett, A., Corbett, P., Geiger, S., Wright, P., Steele, R. and Milroy, P. (2015). Effective integration of reservoir rock-typing and simulation using near-wellbore upscaling. *Marine and Petroleum Geology*, 67, 307-326.

Chandra, V., Tallec, G. and Vahernkamp, V. (2019). Improved Reservoir Characterization Through Rapid Visualization and Analysis of Multiscale Image Data Using A Digital Core Analysis Ecosystem. *Abu Dhabi International Petroleum Exhibition and Conference*, Abu Dhabi. Society of Petroleum Engineers, SPE-197628.

Chiarella, D., Longhitano, S. and Tropeano, M. (2017). Types of mixing and heterogeneities in siliciclastic-carbonate sediments. *Marine and Petroleum Geology,* 88, 617-627.

Chilingarian, G. V., Torabzadeh, J., Rieke, H. H., Metghalchi, M. and Mazzullo, S. J. (1992). Interrelationships Among Surface Area, Permeability, Porosity, Pore Size, and Residual Water Saturation. *Developments in Petroleum Science,* 30, 379-397.

Choquette, P.W. and Pray, L.C. (1970). Geological nomenclature and classification of porosity in sedimentary cabonates. *American Association of Petroleum Geologists Bulletin*, 54 (2), 207-250.

Cohen, K.M., Finney, S.C., Gibbard, P.L. and Fan, J.-X. (2013; updated). The ICS International Chronostratigraphic Chart. *Episodes,* 36, 199-204.

Coimbra, R. and Duarte, L. V. (2020). The distinctive character of lumpy limestones (Early Jurassic, Lusitanian Basin, W Portugal). *Geological Journal,* 55 (1), 1003-1022.

Cox, P., Wood, R., Dickson, J., Al Rougha, H., Shebl, H. and Corbett, P. (2010). Dynamics of cementation in response to oil charge: Evidence from a Cretaceous carbonate field, UAE. *Sedimentary Geology,* 228 (3-4), 246-254.

Cunha, P.P. and Pena dos Reis, R. (1995). Cretaceous sedimentary and tectonic evolution of the northern sector of the Lusitanian Basin. *Cretaceous Research*, 16, 155-170.

Cunningham, A. and Chaliha, P. (2002). Field Testing and Study of Horizontal Water Injectors in Increasing Ultimate Recovery from a Reservoir in Thamama Formation in a Peripheral Water Injection Scheme in a Giant Carbonate Reservoir, United Arab Emirates. *Abu Dhabi International Petroleum Exhibition and Conference*, Abu Dhabi. Society of Petroleum Engineers. SPE-78480.

Dabbouk, C., Liaqat, A., Williams, G. and Beattie, G. (2002). Waterflood in Vuggy Layer of a Middle East Reservoir - Displacement Physics Understood. *Abu Dhabi International Petroleum Exhibition and Conference*, Abu Dhabi. Society of Petroleum Engineers, SPE-78530.

Davies, R.B, Casey, D.M., Horbury, A.D., Sharland, P.R. and Simmons, M.D. (2002). Early to mid-Cretaceous mixed carbonate-clastic shelfal systems: examples, issues and models from the Arabian Plate. *Geoarabia,* 7 (3), 541-598.

Davison, I. and Barreto, P. (2020). Deformation and sedimentation processes, and hydrocarbon accumulations on upturned salt diapir flanks in the Lusitanian Basin, Portugal. *Petroleum Geoscience*, 27 (1), petgeo2019-138.

De Graciansky, P.C., Jacquin, T. and Hesselbo, S.P. (1998). The Ligurian cycle: an overview of the Lower Jurassic 2nd-order transgressive/regressive facies cycles in Western Europe. In De Graciansky, P. C., Hardenbol, J., Jacquin, T. and Vail, P. R. (Eds.) *Mesozoic and Cenozoic Sequence Stratigraphy of European Basins*. SEPM Special Publication, 60, 467-479.

De Loriol, P. (1891). Description de la faune jurassique du Portugal: embranchement des échinodermes. *Commission des travaux géologiques du Portugal*, Lisboa, 179 pp., 29 pl.

De Matos, J.E. and Hulstrand, R.F. (1995). Regional characteristics and depositional sequences of the Oxfordian and Kimmeridgian, Abu Dhabi. In, M.I. Al-Husseini (Ed.), *Middle East Petroleum Geosciences*, GEO'94. Gulf PetroLink, Bahrain, 1, 346-356.

Di Stefano, P., Galácz, A., Mallarino, G., Mindszenty, A. and Vörös, A. (2002). Birth and early evolution of a Jurassic escarpment: Monte Kumeta, Western Sicily. *Facies*, 46, 47-50.

Din, S., Dernaika, M., Hosani, I., Hannon, L., Skjæveland, S. and Kalam, M. (2010). Whole Core Versus Plugs: Integrating Log and Core Data to Decrease Uncertainty in Petrophysical Interpretation and STOIP Calculations. *Abu Dhabi International Petroleum Exhibition and Conference*. Society of Petroleum Engineers, SPE-137679.

Dinis, J.L., Rey, J., Cunha, P.P., Callapez, P. and Rena dos Reis, R. (2008). Stratigraphy and allogenic controls of the western Portugal Cretaceous: an updated synthesis. *Cretaceous Research*, 29 (5-6), 772-780.

Dobrin, M.B. (1977). Seismic Exploration for Stratigraphic Traps. In: Payton, C.E. (Ed.): Seismic Stratigraphy — Applications to Hydrocarbon Exploration. *AAPG Memoir*, 26, 329-351.

Dolan, J.F. (1989). Eustatic and Tectonic Controls on Deposition of Hybrid Siliciclastic/Carbonate Basinal Cycles: Discussion with Examples. *AAPG Bulletin*, 73, 1233-1246.

Doyle, L.J. and Roberts, H.H. (1988). *Carbonate-Clastic Transitions*. Developments in Sedimentology, 42, Elsevier, 304 pp.

Du, Y., Zhang, J., Zheng, S., Xin, J., Chen, J. and Li, Y. (2015). The rudist buildup depositional model, reservoir architecture and development strategy of the cretaceous Sarvak formation of Southwest Iran. Petroleum, 1 (1), 16-26.

Duarte, L.V. (1995). O Toarciano da Bacia Lusitaniana. Estratigrafia e evolução sedimentogenética. PhD Thesis (unpublished), Geosciences Center, Departamento de Ciências da Terra, Universidade de Coimbra. 349 pp.

Duarte, L.V. (1997). Facies analysis and sequential evolution of the Toarcian-Lower Aalenian series in the Lusitanian Basin (Portugal). *Comunicações do Instituto Geológico e Mineiro*, 83, 65-94.

Duarte, L.V. (2007). Lithostratigraphy, sequence stratigraphy and depositional setting of the Pliensbachian and Toarcian series in the Lusitanian Basin (Portugal). *Ciências da Terra*, 16, 17-23.

Duarte, L.V. and Soares, A. F. (2002). Litostratigrafia das séries margo-calcárias do Jurássico Inferior da Bacia Lusitânica (Portugal). *Comunicações do Instituto Geológico e Mineiro*, 89, 135-154.

Duarte, L.V., Comas-Rengifo, M.J., Silva, R.L., Paredes, R. and Goy, A. (2014). Carbon isotope stratigraphy and ammonite biochronostratigraphy across the Sinemurian-Pliensbachian boundary in the western Iberian margin. *Bulletin of Geosciences*, 89 (4), 719-736.

Duarte, L.V., Krauter, M. and Soares, A.F. (2001). Bioconstructions à spongiaires siliceux dans le Lias terminal du Bassin lusitanien (Portugal): stratigraphie, sédimentologie et signification paléogéographique. *Bulletin de la Société Géologique de France, Paris*, 172, 637-646.

Duarte, L.V., Mattioli, E., Rocha, R.B. and Silva, R.L. (2017). The Lower Jurassic at Peniche (Lusitanian Basin): recent advances in Stratigraphy and Sedimentary Geology. *Earth Sciences Journal*, 19 (1), 35-51.

Duarte, L.V., Perilli, N., Dino, R., Rodrigues, R. and Paredes, R. (2004). Lower to Middle Toarcian from the Coimbra region (Lusitanian Basin, Portugal): Sequence stratigraphy, calcareous nannofossils and stable-isotope evolution. *Rivista Italiana di Paleontologia e Stratigrafia, Milano*, 100, 115-127.

Duarte, L.V., Silva, R.L., Felix, F., Comas-Rengifo, M.J., da Rocha, R.B., Mattioli, E., Paredes, R., Mendoça Filho, J.G. and Cabral, M.C. (2017). The Jurassic of the Peniche Peninsula (Portugal): scientific, education and science popularization relevance. *Revista de la Sociedad Geológica de España*, 30, 55-70.

Duarte, L.V., Silva, R.L. and Mendonça Filho, J.G. (2013). Variação do COT e Pirólise Rock-Eval do Jurássico Inferior da região de S. Pedro de Moel (Portugal). Potencial de geração de hidrocarbonetos. In: Duarte, L.V., Silva, R.L. and Azerêdo, A.C. (Eds.): Fácies carbonatadas ricas em matéria orgânica do Jurássico da Bacia Lusitânica. Novos contributos paleontológicos, sedimentológicos e geoquímicos. *Comunicações Geológicas*, 100, volume especial I, pp. 107-111.

Duarte, L.V., Silva, RL., Mendoça Filho, J.G., Poças Ribeiro, N. and Chagas, R.B.A. (2012). High-resolution stratigraphy, palynofacies and source rock potential of the Água de Madeiros Formation (Lower Jurassic), Lusitanian Basin, Portugal. *Journal of Petroleum Geology*, 35 (2), 105-126.

Duarte, L.V., Silva, R.L., Oliveira, L.C.V., Comas-Rengifo, M.J. and Silva, F. (2010). Organic-rich facies in the Sinemurian and Pliensbachian of the Lusitanian Basin, Portugal: Total Organic Carbon distribution and relation to transgressive-regressive facies cycles. *Geologica Acta*, 8 (3), 325-340.

Duarte, L.V. (Coord.), Wright, V.P., Fernandez-Lopez, S., Elmi, S., Krauter, M., Azerêdo, A.C., Henriques, M.H., Rodrigues, R. and Perilli, N. (2004). Early Jurassic carbonate evolution in the Lusitanian Basin: facies, sequence stratigraphy and cyclicity. In: Duarte, L.V. and Henriques, M.H. (Eds.): Carboniferous and Jurassic Carbonate Platforms of Iberia. *23rd IAS Meet. Sedimentology*, Coimbra, Field Trip Guide Book Vol. I, 45-71.

Dunham, R.J. (1962). Classification of Carbonate Rocks according to Depositional Texture. *American Association of Petroleum Geologists*, 1, 108-121.

Ebdon, C.C., Frase, A.J., Higgins, A.C., Mitchener, B.C. and Strank, A.R.E. (1990). The Dinantian stratigraphy of the East Midlands: a seismostratigraphic approach. *Journal of the Geological Society*, 147, 519-536.

Edwards, E., Gomes, J. and Shekhar, R. (2019). Identifying Geological Flow Drivers of an Early Cretaceous Reservoir Regionally Over Abu Dhabi: Implications for Field Development. *Abu Dhabi International Petroleum Exhibition and Conference*, Abu Dhabi. Society of Petroleum Engineers, SPE-197834.

Ehrenberg, S.N. (2006). Porosity destruction in carbonate platforms. *Journal of Petroleum Geology*, 29 (1), 41-52.

Ehrenberg, S.N. (2019). Petrophysical heterogeneity in a lower cretaceous limestone reservoir, onshore Abu Dhabi, United Arab Emirates. *AAPG Bulletin*, 103, 527-546.

Ehrenberg, S.N., Aqrawi, A.A.M. and Nadeau, P.H. (2008). An overview of reservoir quality in producing Cretaceous strata of the Middle East. *Petroleum Geosciences*, 14, 307-318.

Ehrenberg, S.N., Lokier, S.W., Yaxin, L. and Chen, R. (2018). Depositional cycles in a lower cretaceous limestone reservoir, onshore Abu Dhabi, U.A.E. *Journal of Sedimentary Research*. 88, 753-776.

Ehrenberg, S.N., Morad, S., Yaxin, L. and Chen, R. (2016). Stylolites and porosity in a Lower Cretaceous limestone reservoir, onshore Abu Dhabi. *Journal of Sedimentary Research,* 86, 1228-1247.

Ehrenberg, S.N., Nadeau, P.H. and Aqrawi, A. (2007). A Regional Comparison of Khuff and Arab Reservoir Potential Throughout the Middle East. *AAPG Bulletin*, 91 (3), 275-286.

Ehrenberg, S.N., Zhang, J. and Gomes, J.S. (2020a). Regional porosity variation in Thamama-B reservoirs of Abu Dhabi. *Marine and Petroleum Geology,* 114.

Ehrenberg, S.N., Zhang, J. and Gomes, J.S. (2020b). Regional variation of permeability in Thamama-B reservoirs of Abu Dhabi. *Marine and Petroleum Geology,* 116.

Ehrlich, R., Kennedy, S.K., Crabtree, S.J and Cannon, R.L. (1984). Petrographic image analysis, I. Analysis of reservoir pore complexes. *Journal of Sedimentary Research*, 54 (4), 1365-1378.

El Wazir, Z., Al-Madani, N., Omobude, O.A. and Alhoot, A.R. (2015). Facies, deposition and diagenesis characteristics of the Upper Kharaib Member (late Barremian), onshore Abu Dhabi, UAE. *Abu Dhabi International Petroleum Exhibition and Conference,* Abu Dhabi. Society of Petroleum Engineers, SPE-177859.

Ellouz-Zimmermann, N., Lallemant, S.J., Castilla, R., Mouchot, N., Leturmy, P., Battani, A., Buret, C., Cherel, L., Desaubliaux, G., Deville, E., Ferrand, J., Lügcke, A., Mahieux, G., Mascle, G., Mühr, P., Pierson-Wickmann, A.C., Robion, P., Schmitz, J., Danish, M., Hasany, S., Shahzad, A. and Tabreez, A. (2007). Offshore Frontal Part of the Makran Accretionary Prism: The Chamak Survey (Pakistan). In: O. Lacombe, J. Lavé, F. Roure, J. Vergés (Eds.), *Thrust Belts and Foreland Basins: From Fold Kinematics to Hydrocarbon Systems*. Springer-Verlag, Berlin, pp. 351-366.

Eltom, H., Kubur, A., Abdulraziq, A., Babalola, L., Makkawi, M., Abdullatif, O. and Bokhari, A. (2019). Three-dimensional outcrop reservoir analog model: A case study of the Upper Khuff Formation oolitic carbonates, central Saudi Arabia. *Journal of Petroleum Science and Engineering*, 150, 115-127.

ENMC/UPEP (1976a). Well report, 17C-1.

ENMC/UPEP (1976b). Well report, 20B-1.

ENMC/UPEP (1981). Well report, Cp-1.

ENMC/UPEP (2016). Exploration: Promising portugal. *GeoExpro, Geoscience and Technology Explained*, 13 (2), 20-23.

ENMC/UPEP (2018). Petroleum Systems. http://www.enmc.pt/en-GB/activities/exploration-and-production-of-petroleum-resources/oil-research-in-portugal/petroleum-systems/. Accessed on 14/04/2018.

Faghih, A., Ezati-Asl, M., Mukherjee, S. and Soleimany, B. (2019). Characterizing halokinesis and timing of salt movement in the Abu Musa salt diapir, Persian Gulf, offshore Iran. *Marine and Petroleum Geology,* 105, 338-352.

FastRandomForest Weka package. https://code.google.com/archive/p/fast-random-forest/

Fernández-Salas, L.M., Dabrio, C.J., Goy, J.L., Díaz del Río, V., Zazo, C., Lobo, F.J., Sanz, J.L. and Lario, J. (2009). Land-sea correlation between late Holocene coastal and infralittoral deposits in the SE iberian peninsula (western Mediterranean). *Geomorphology*, 104 (1-2), 4-11.

Ferreira, J., Azerêdo, A.C., Bizarro, P., Ribeiro, T. and Sousa, A. (2016). The importance of outcrop reservoir characterization in oil-industry facies modelling workflows - a case study from the Middle Jurassic of the Maciço Calcário Estremenho, Portugal. *Abu Dhabi International Petroleum Exhibition and Conference*, Abu Dhabi. Society of Petroleum Engineers, SPE-183305.

Ferreira, E., Mateus, A. Azerêdo, A.C., Duarte, L.V., Mendonça-Filho, J. and Tassinari, C.C.G. (2020). Tracing bottom-water redox conditions during deposition of Lower and Upper Jurassic organic-rich sedimentary rocks in the Lusitanian Basin (Portugal): Insights from inorganic geochemistry. *Marine and Petroleum Geology*, 117.

Fitch P., Lovell, M.A., Davies, S.J., Pritchard, T. and Harvey, P.K. (2015). An integrated and quantitative approach to petrophysical heterogeneity. *Marine and Petroleum Geology*, 63, 82-96.

Flood, P. and Orme, G.R. (1988). Mixed siliciclastic/carbonate sediments of the northern Great Barrier Reef Province, Australia. In Doyle, L. J., and Roberts. H. H. (eds.), *Carbonate - Clastic Transitions*. Developments in sedimentology, 42, pp. 175-205.

Flügel, E. (2004). Microfacies of carbonate rocks: analysis, interpretation and application. Springer, Berlin, 976 pp.

Folk, R.L. (1959). Practical petrographic classification of limestones. *AAPG Bulletin*, 43 (1), 1-38.

Folk, R.L. (1962). Spectral subdivision of limestone types. In: Ham, W.E. (Ed.): Classification of carbonate rocks. *AAPG Memoir*, 1, 62-84.

Folk, R.L. (1966). A review of grain-size parameters. *Sedimentology*, 6 (2), 73-93.

Fullmer, S.M., Guidry, S.A., Gournay, J., Bowlin, E., Ottinger, G., Al Neyadi, A., Gupta, G., Gao, B. and Edwards, E. (2014). Microporosity: characterization, distribution, and influence on oil recovery. *Conference Proceedings, International Petroleum Technology Conference*. Society of Petroleum Engineers, SPE- 171940.

Garcia, A., Armelenti, G., Reis, R., Pimentel, N. and Rocha, L. (2010). Diagenetic Processes and Porosity Evolution Controls in Upper Jurassic Siliciclastic deposits of the Lusitanian Basin (Portugal). *II Central and North Atlantic Conjugate Margins Conference*, Lisbon, vol. III, pp. 121-124.

Garcia-Hernandez, A., Miska, S., Yu, M., Takach, N. and Zettner, C. (2007). Determination of Cuttings Lag in Horizontal and Deviated Wells. *Proceedings of SPE Annual Technical Conference and Exhibition,* Anaheim, California, November. SPE-109630.

Garland, J., Neilson, J., Laubach, S.E. and Whidden, K.J. (2012). Advances in carbonate exploration and reservoir analysis, *Geological Society, London, Special Publications*, 370 (1), 1-15.

Ghiasi-Freez, J., Soleimanpour, I., Kadkhodaie-Ilkhchi, A., Ziaii, M., Sedighi, M. and Hatampour, A. (2012). Semi-automated porosity identification from thin section images using image analysis and intelligent discriminant classifiers. *Computers & Geosciences*, 45, 36-45.

Glennie, K.W. (2010). Structural and stratigraphic evolution of Abu Dhabi in the context of Arabia. *Arabian Journal of Geosciences,* 3, 331-349.

Gomes, J.N. (1981). Evolução e perspectiva da prospecção de petróleo em Portugal. *Geonovas*, 1 (1), 25-42.

Gomes, J.S. and Alves, F.B. (2013). *The universe of the oil and gas industry: From exploration to refining*. Partex Oil and Gas, 738 pp.

Gomes, J.S., Ribeiro, M.T., Strohmenger, C.J., Naghban, S. and Kalam, M.Z. (2008). Carbonate reservoir rock typing - The link between geology and SCAL. *Abu Dhabi International Petroleum Exhibition and Conference*, Abu Dhabi. Society of Petroleum Engineers, SPE-118284.

Gonçalves, P.A., Mendonça Filho, J.G., Silva, F.S. and Flores, D. (2014). Solid bitumen occurrences in the Arruda sub-basin (Lusitanian Basin, Portugal): petrographic features. *International Journal of Coal Geology*, 131, 239-249.

Gonçalves, P.A., Silva, T.F., Mendonça Filho, J.G. and Flores, D. (2015). Palynofacies and source rock potential of Jurassic sequences on the Arruda sub-basin (Lusitanian Basin, Portugal). *Marine and Petroleum Geology*, 59, 575-592.

Google (2020). Google Maps location for Peniche, Portugal. Retrieved on May 13, 2020, from https://goo.gl/maps/jNPJnqoHfC3Z1bWs8.

Google (2020a). Central/Southern Europe, North Africa and Middle East satellite image. https://www.google.com/maps/@40.3872517,13.2920028,4968822m/data=!3m1!1e3. Last accessed on March 17, 2021.

Google (2020b). Satellite image of western central Portugal. https://www.google.com/maps/@39.3214143,-9.137952,157706m/data=!3m1!1e3. Last accessed on March 17, 2021.

Google (2020c). Satellite image of eastern/southeastern Arabian Peninsula. https://www.google.com/maps/@24.4095205,53.7409163,371274m/data=!3m1!1e3. Last accessed on March 17, 2021.

Grammer, G., Harris, P. and Eberli, G. (2004). Integration of outcrop and modern analogs in reservoir modelling. *AAPG Memoir*, 80.

Grötsch, J., Al-Jelani, O. and Al-Mehairi, Y. (1998). Integrated reservoir characterisation of a giant Lower Cretaceous oil field, Abu Dhabi, U.A.E. *Abu Dhabi International Petroleum Exhibition and Conference*, Abu Dhabi. Society of Petroleum Engineers, SPE-49454.

Grove, C. and Jerram, D.A. (2011). jPOR: An ImageJ macro to quantify total optical porosity from blue-stained thin sections. *Computers & Geosciences*, 37, 1850-1859.

Guéry, F. (1984). Evolution sédimentaire et dynamique du bassin marginal-ouest portugais au Jurassique (province d'Estramadura, secteur de Caldas da Rainha - Montejunto). These Univ. Claude Bernard, Lyon, 477 pp.

Guéry, F., Montenat, C. and Vachard, D. (1986). Evolution tectono-sedimentaire du bassin portugais au Mesozoique suivant la transversale de Peniche (Estremadure). *Bull. Cent. Rech. Explor. Prod. Elf-Aquitaine*, 10, 83-94.

Hall, M., Frank, E., Holmes, G., Pfahringer, B., Reutemann, P. and Witten, I.H. (2009). The weka data mining software: an update. *ACM SIGKDD Explor. Newslett.,* 11, 10-18.

Haq, B. U. (2018). Jurassic Sea-Level Variations: A Reappraisal. *GSA Today,* 28, 4-10.

Hardenbol, J., Thierry, J., Farley, M.B., Jacquin, T., de Graciansky, P. and Vail, P.R. (1998). Mesozoic and Cenozoic Sequence Chronostratigraphic Framework of European Basins. In De Graciansky, P., Hardenbol, J., Jacquin, T. and Vail, P.R. (eds.), *Mesozoic and Cenozoic Sequence Stratigraphy of European Basins*. SEPM Special Publication, 60.

Harris, T.J., Hay, J.T.C. and Twombley, B.N. (1968). Contrasting limestone reservoirs in the Murban field, Abu Dhabi. *Society of Petroleum Engineers of the American Institute of Mining, Metallurgical, and Petroleum Engineers*, 39.

Hassan, T.H., Mudd, G.C. and Twombel, B.W. (1975). The stratigraphy and sedimentation of the Thamama Group (lower Cretaceous) of Abu Dhabi. *9th Arab Petroleum Congress*, 107, B-3, Dubai.

Hastie, T., Tibshirani, R. and Friedman, J. (2008). *The Elements of Statistical Learning* (2nd ed.). Springer.

Hernández-Molina, F.J., Fernández-Salas, L.M., Lobo, F., Somoza, L., Diaz-del-Rio, V. and Alveirinho Dias, J.M. (2000). The infralittoral prograding wedge: a new large-scale progradational sedimentary body in shallow marine environments. *Geo-Marine letters*, 20, 109-117.

Hess, H., Ausich, W.I., Brett, C.E. and Simms, M.J. (1999). *Fossil Crinoids*. Cambridge University Press, Cambridge.

Hill, G. (1989). Distal alluvial fan sediments from the Upper Jurassic of Portugal: controls on their cyclicity and channel formation. *Journal of the Geological Society*, 146 (3), 539-555.

Hiscott, R.N., Wilson, R.C., Gradstein, F.M., Pujalte, V., Garcia-Mondéjar, J., Boudreau, R.R. and Wishart, H.A. (1990). Comparative stratigraphy and subsidence history of Mesozoic rift basins of North Atlantic. *AAPG Bulletin,* 74 (1), 60-76.

Hollis, C., Lawrence, D.A., Periere, M.D. and Al Darmaki, F. (2017). Controls on porosity preservation within a Jurassic oolitic reservoir complex, U.A.E. *Marine and Petroleum Geology*, 88, 888-906.

Hollis, C., Vahrenkamp, V., Tull, S., Mookerjee, A., Taberner, C. and Huang, Y. (2010). Pore system characterisation in heterogeneous carbonates: An alternative approach to widely-used rock-typing methodologies. *Marine and Petroleum geology*, 27 (4), 772-793.

Hönig, M.R. and John, C.M. (2015). Sedimentological and isotopic heterogeneities within a Jurassic carbonate ramp (UAE) and implications for reservoirs in the Middle East. *Marine and Petroleum Geology,* 68, 240-257.

Inês, N., Bizarro, P. and Ribeiro, T. (2015). Integrated Carbonate Reservoir Characterization and Modelling with Depositional and Diagenetic Trends. *SPE Reservoir Characterisation and Simulation Conference and Exhibition*, Abu Dhabi. Society of Petroleum Engineers. SPE-175673.

Jach, R. (2005). Storm-dominated deposition of the Lower Jurassic crinoidal limestone in the Krížna Unit, Western Tatra Mountains, Poland. *Facies*, 50, 561-572.

Jacquin, T. and De Graciansky, P.C. (1998). Major transgressive/regressive cycles: the stratigraphic signature of European basin development. In De Graciansky, P.C., Hardenbol, J., Jacquin, T. and Vail, P.R. (Eds.), *Mesozoic and Cenozoic Sequence Stratigraphy of European Basins*. SEPM Special Publication, 60, pp.15-30.

James, R.A. (1995). Application of petrographic image analysis to the characterization of fluid-flow pathways in a highly-cemented reservoir: Kane Field, Pennsylvania, U.S.A. *Journal of Petroleum Science and Engineering,* 13 (3-4), 141-154.

Jenkyns, H.C. (1971). Speculations on the genesis of crinoidal limestones in the Tethyan Jurassic. *Geol Rundsch,* 60, 471-488.

Jennings, J.W.Jr. and Lucia, F.J. (2003). Predicting permeability from well logs in carbonates with a link to geology for interwell permeability mapping. *SPE Reservoir Evaluation & Engineering*, 6 (4), 215-225. SPE-84942.

Jeong, J., Al-Ali, A.A., Jung, H., Abdelrahman, A., Dhafra, A., Shebl, H.T., Kang, J., Bonin, A., Perriere, M.D. and Foote, A. (2017). Controls on Reservoir Quality and Reservoir Architecture of Early Cretaceous carbonates in an Abu Dhabi Onshore Field Lekhwair, Kharaib and Lower Shuaiba Formations. *Abu Dhabi International Petroleum Exhibition and Conference*, Abu Dhabi. Society of Petroleum Engineers, SPE-188420.

Johnson, K., Barnett, A. and Wright, V.P. (2010). An evaluation of existing carbonate pore system classifications and rock-typing approaches. *AAPG Annual Convention and Exhibition*, New Orleans, LA, 11-14 April.

Johnson, C.A., Hauge, T., Al-Menhali, S., Bin Sumaidaa, S., Sabin, B. and West, B. (2005). Structural styles and tectonic evolution of onshore and offshore Abu Dhabi, UAE. *International Petroleum Technology Conference*, Doha, Qatar. IPTC-10646.

Jung, A. and Aigner, T. (2012). Carbonate geobodies: hierarchical classification and database - a new workflow for 3D reservoir modelling. *Journal of Petroleum Geology*, 35, 49-65.

Kaczmarek, S.E., Fullmer, S.E. and Hasiuk, F.J. (2015). A Universal Classification Scheme For the Microcrystals That Host Limestone Microporosity. *Journal of Sedimentary Research*, 85 (10), 1197-1212.

Krajewski, M., Olchowy, P. and Salamon, M.A. (2019). Late Jurassic (Kimmeridgian) sea lilies (Crinoidea) from central Poland (Łódz´ Depression). *Annales de Paleontologie*, 105, 63-73.

Kreisa, R.D. (1981). Storm-Generated Sedimentary Structures in Subtidal Marine with Examples from the Middle and Upper Ordovician of Southwestern Virginia. *Journal of Sedimentary Research*, 51 (3), 823-848.

Kullberg, J.C., Mouterde, R. and Rocha, R. (1997). Reinterpretation de l'Histoire Stratigraphique et Tectonique de la Structure de Serra de El-Rei (Portugal). *Cahiers Université Catholique de Lyon*, 10, 191-208.

Kullberg, J.C., Olóriz, F., Marques, B., Caetano, P.S. and Rocha, R.B. (2001). Flat-pebble conglomerates: a local marker for Early Jurassic seismicity related to syn-rift tectonics in the Sesimbra area (Lusitanian Basin, Portugal). *Sedimentary Geology*, 139, 49-70.

Kullberg, J.C., Rocha, R.B., Soares, A.F., Rey, J., Terrinha, P., Azerêdo, A.C., Callapez, P., Duarte, L.V., Kullberg, M.C., Martins, L., Miranda, J.R., Alves, C., Mata, J., Madeira, J., Mateus, O. and Moreira, M. (2013). A Bacia Lusitaniana: Estratigrafia, Paleogeografia e Tectónica. In Dias R., Araújo, A., Terrinha, P. and Kullberg, J.C. (Eds.), *Geologia de Portugal no contexto da Ibéria. Vol. II - Geologia Meso-cenozóica de Portugal*. Livr. Escolar Editora, pp. 195-347.

Leinfelder, R.R. (1993). A sequence stratigraphic approach to the Upper Jurassic mixed carbonate siliciclastic succession of the central Lusitanian Basin, Portugal. *Profil*, 5, 119-140.

Leinfelder, R.R. and Wilson, R. (1998). Third-order sequences in an Upper Jurassic rift-related second-order sequence, Central Lusitanian Basin, Portugal. In: DE Graciansky, P.C., Hardenbol, J., Jaquin, T. and Vail, P.R. (Eds.), *Mesozoic and Cenozoic Sequence Stratigraphy of European Basins*.

Lijmbach, G., Toxopeus, J., Rodenburg, T. and Hermans, L. (1992). Geochemical study of Crude Oils and Source Rocks in Onshore Abu Dhabi. *Proceedings Abu Dhabi Petroleum Conference*, Abu Dhabi. Society of Petroleum Engineers, pp. 395-422. SPE-24513.

LNEG (2020). GeoPortal da energia e geologia. Accessed on December 02, 2020. https://geoportal.lneg.pt/pt/.

Lobo, F.J., Fernández-Salas, L.M., Hernández-Molina, F.J., González, R., Dias, J.M.A., del Río, V.D. and Somoza, L. (2005). Holocene highstand deposits in the Gulf of Cadiz, SW Iberian Peninsula: A high-resolution record of hierarchical environmental changes. *Marine Geology*, 219 (2-3), 109-131.

Lokier, S. and Junaibi, M. (2016). The petrographic description of carbonate facies: Are we all speaking the same language?. *Sedimentology*, 63 (7), 1843-1885.

Longiaru, S. (1987). Visual comparators for estimating the degree of sorting from plane and thin section. *Journal of Sedimentary Research*, 57 (4), 791-794.

Loosveld, R., Bell, A. and Terken, J.J.M. (1996). The tectonic evolution of interior Oman. *GeoArabia*, 1, 28-51.

Lucia, F.J. (1983). Petrophysical Parameters Estimated from Visual Descriptions of Carbonate Rocks: A Field Classification of Carbonate Pore Space. *Journal of Petroleum Technology*, 35, 629-637.

Lucia, F.J. (2007). *Carbonate Reservoir Characterization: An Integrated Approach*. Second edition. Berlin, Germany, Springer-Verlag.

Lucia, F.J., Kerans, C. and Jennings, J.W. (2003). Carbonate Reservoir Characterization. *Journal of Petroleum Technology*, 55 (6), 70-72.

Maher, J.D. (1964). The composite interpretive method of logging drill cuttings. *Oklahoma Geological Survey Guidebook* XIV, 48 pp.

Manuppella, G. and Azerêdo, A.C. (1996). Contribuição para o conhecimento da geologia de Sesimbra. *Comunicações do Instituto Geológico e Mineiro,* 82, 37-50.

Manuppella, G., Antunes, M.T., Pais, J., Ramalho, M.M., and Rey, J. (1999). Notícia Explicativa da Folha 30-A, Lourinhã. *Instituto Geológico e Mineiro,* 83, Lisboa.

Manuppella, G., Barbosa, B., Machado, S. and Carvalho, J. (1998). Folha 27-A Vila Nova de Ourém. In: Carta Geológica de Portugal à escala 1:50000, 2a ed. *Instituto Geológico e Mineiro*, Lisboa.

Manuppella, G., Moreira, J.C.B., Costa, J.R.G. and Crispim, J.A. (1985). Calcários e dolomitos do Maciço Calcário Estremenho. *Estudos Notas e Trabalhos, S.F.M.,* 27, 3-48.

Masalmeh, S.K. (2002). The Effect of Wettability on Saturation Functions and Impact on Carbonate Reservoirs in the Middle East. *Abu Dhabi International Petroleum Exhibition and Conference*, Abu Dhabi. Society of Petroleum Engineers, SPE-78515.

Masalmeh, S.K., Jing, X., Vark, W., Christiansen, S., Van der Weerd, H. and Van Dorp, J. (2003). Impact of SCAL (special core analysis) on carbonate reservoirs: How capillary forces can affect field performance predictions. *Petrophysics*, 45, 403-413.

Matenco, L. and Haq, B. (2020). Multi-scale depositional successions in tectonic settings. *Earth Science Reviews,* 200, 102991.

McNeill, D.F., Cunningham, K.J., Guertin, L.A. and Anselmetti, F.S. (2004). Depositional Themes of Mixed Carbonate-siliciclastics in the South Florida Neogene: Application to Ancient Deposits. In Grammer, G.M., Harris, P.M. and Eberli, G.P. (Eds.), *Integration of Outcrop and Modern Analogs in Reservoir Modeling*. AAPG Memoir, 80, pp. 23-43.

Melville, P., Al Jeelani, O., Al Menhali, S. and Grötsch, J. (2004). Three-dimensional seismic analysis in the characterization of a giant carbonate field, onshore Abu Dhabi, United Arab Emirates. In: Eberli, G.P., Massaferro, J.L. and Sarg, R.F. (Eds.), *Seismic Imaging of Carbonate Reservoirs and Systems*, AAPG Memoir, 81, 123-148.

Metwalli, M.H. and Khouri, N.B. (2016). The Petroleum Geology of The Cretaceous Formations in Abu Dhabi, United Arab Emirates. *International Journal of Ground Sediment & Water*, 4.

Mohseni, H. and Al-Aasm, I.S. (2004). Tempestite deposits on a storm-influenced carbonate ramp: An example from the Pabdeh Formation (Paleogene), Zagros Basin, SW, Iran. *Journal of Petroleum Geology*, 27 (2), 163-178.

Montenat, C., Guery, F., James, M. and Berthou, Y.P. (1988). Mesozoic evolution of the Lusitanian Basin: comparison with the adjacent margin. In: Boillot, G., Winterer, E.L. et al. (*Coords.): Proceedings of the Ocean Drilling Program, Scientific Results*, 103, 757-775.

Moore, C.H., and Druckman, Y. (1981). Burial diagenesis and porosity evolution, Upper Jurassic Smackover, Arkansas and Louisiana. *AAPG Bulletin*, 65, 597-628.

Morad, S., Al Suwaidi, M., Mansurbeg, H., Morad, D., Ceriani, A., Paganoni, M. and Al-Aasm, I. (2019). Diagenesis of a limestone reservoir (Lower Cretaceous), Abu Dhabi, United Arab Emirates: comparison between the anticline crest and flanks. *Sedimentary Geology,* 380, 127-142.

Morad, D., Paganoni, M., Al Harthi, A., Morad, S., Ceriani, A., Mansurbeg, H., Al Suwaidi, A., Al-Aasm, I.S. and Ehrenberg, S.N. (2016). Origin and evolution of microporosity in packstones and grainstones in a Lower Cretaceous carbonate reservoir, United Arab Emirates. In Armitage, P.J., Butcher, A.R., Churchill, J.M., Csoma, A.E., Hollis, C., Lander, R.H., Omma, J.E. and Worden, R.H. (Eds.), *Reservoir quality of clastic and carbonate rocks: analysis, modelling and prediction*. Geological Society, London Special Publication, 435 pp.

Moshier, S. (1989). Development of microporosity in a micritic limestone reservoir, Lower Cretaceous. In: Middle East, Nature and Origin of Microrhombic Calcite and Associated Microporosity in Carbonate Strata. *Sedimentary Geology*, 63, 217-240.

Mougenot, D., Monteiro, J.H., Dupeuble, P.A. and Malod, J.A. (1979). La marge continentale sud-portugaise: évolution structurale et sédimentaire. *Ciências da Terra*, Universidade Nova de Lisboa, Lisboa, 5, 223-246.

Mount, J. (1984). Mixing of siliciclastic and carbonate sediments in shallow shelf environments. *Geology*, 12, 432-435.

Mouterde, R., Rocha, R.B., Ruget, C. and Tintant, H., 1979. Facies, biostratigraphie et paleogeographic du Jurassique portugais. *Ciências da Terra*, 5, 29-52.

Murris, R.J. (1980). Middle East: Stratigraphic Evolution and Oil Habitat. *AAPG Bulletin*, 64, 597-618.

Mutti, M., Eberli, G., Bernoulli, D. and Vecsei, A. (1996). Depositional Geometries and Facies Associations in an Upper Cretaceous Prograding Carbonate Platform Margin (Orfento Supersequence, Maiella, Italy). *Journal of Sedimentary Research*, 66 (4), 749-765.

Nabawy, B. (2014). Estimating porosity and permeability using Digital Image Analysis (DIA) technique for highly porous sandstones. *Arabian Journal of Geosciences*, 7, 10.

Nader, F.H. (2017), *Multi-scale quantitative diagenesis and impacts on heterogeneity of carbonate reservoir rocks*. Springer, 146 pp.

Nader, F.H., De Boever, E., Gasparrini, M., Liberati, M., Dumont, C., Ceriani, A., Morad, S., Lerat, O. and Doligez, B. (2013). Quantification of diagenesis impact on reservoir properties of the Jurassic Arab D and C members (offshore, U.A.E.). *Geofluids*, 13, 204-220.

Naganawa, S., Suzuki, M., Ikeda, K., Inada, N. and Sato, R. (2018). Modeling of Cuttings Lag Distribution in Directional Drilling to Evaluate Depth Resolution of Mud Logging. *IADC/SPE Drilling Conference and Exhibition, Fort Worth, Texas, USA.* SPE-189615.

Namba, T. and Hiraoka, T. (1995). Capillary Force Barriers in a Carbonate Reservoir Under Waterflooding. *Middle East Oil Show*, Bahrain. Society of Petroleum Engineers. SPE-29773.

Nanjo, T. and Tanaka, S. (2019). Carbonate Lithology Identification with Machine Learning. *Abu Dhabi International Petroleum Exhibition & Conference*, Abu Dhabi. Society of Petroleum Engineers, SPE-197255.

Nazari, M. H., Tavakoli, V., Rahimpour-Bonab, H. and Sharifi-Yazdi, M. (2019). Investigation of factors influencing geological heterogeneity in tight gas carbonates, Permian reservoir of the Persian Gulf. *Journal of Petroleum Science and Engineering*, 183.

Nazemi, M., Tavakoli, V., Rahimpour-Bonab, H., Hosseini, M. and Sharifi-Yazdi, M. (2018). The effect of carbonate reservoir heterogeneity on Archie's exponents (a and m), an example from Kangan and Dalan gas formations in the central Persian Gulf. *Journal of Natural Gas Science and Engineering*, 59, 297-308.

Oliveira, L.C., Rodrigues, R., Duarte, L.V. and Lemos, V.B. (2006). Avaliação do potencial gerador de petróleo e interpretação paleoambiental com base em biomarcadores e isótopos estáveis de carbono da secção Pliensbaquiano - Toarciano inferior (Jurássico Inferior) da região de Peniche (Bacia Lusitânica, Portugal). *Boletim de Geociências da Petrobras*, 14, 207-234.

Oswald, E.J., Mueller, H.W.III, Goff, D.F., Al-Habshi, H. and Al-Matroushi, S. (1995). Controls on porosity evolution in Thamama Group carbonate reservoirs in Abu Dhabi, United Arab Emirates. *Middle East Oil Show*, Bahrain. Society of Petroleum Engineers, SPE-029797.

Paganoni, M., Harthi, A., Morad, D., Morad, S., Ceriani, A., Mansurbeg, H., Al Suwaidi, A., Al-Aasm, I., Ehrenberg, S. and Sirat, M. (2016). Impact of stylolitization on diagenesis of a Lower Cretaceous carbonate reservoir from a giant oilfield, Abu Dhabi, United Arab Emirates. *Sedimentary Geology*, 335.

Pal, A., Garia, S., Ravi, K. and Nair, A. (2019). Porosity Estimation by Digital Image Analysis. *ONGC Bulletin*, 53 (2), 59-72.

Palain, C. (1976). Une série détritique terrigène. Les «Grès de Silves»: Trias et Lias inférieur du Portugal. *Memórias dos Serviços Geológicos de Portugal*, Nova Série, 25, Lisboa, 377 pp.

Palermo, D., Aigner, T., Nardon, S. and Blendinger, W. (2010). Three-dimensional facies modeling of carbonate sand bodies: Outcrop analog study in an epicontinental basin (Triassic, southwest Germany). *AAPG Bulletin,* 94 (4), 475-512.

Palermo, D., Aigner, T., Seyfang, B. and Nardon, S. (2012). Reservoir properties and petrophysical modelling of carbonate sand bodies: Outcrop analogue study in an epicontinental basin (Triassic, Germany). *Geological Society of London Special Publications,* 370 (1), 111-138.

Parker, A. and Bruce, W.S. (1994). *Quantitative Diagenesis: Resent developments and applications to reservoir geology*. Kluwer Academic Press, Dordrecht, Netherland, 288 pp.

Peters, J.M., Filbrandt, J.B., Grotzinger, J.P., Newall, M.J., Shuster, M.W. and Al-Siyabi, H. (2003). Surface-piercing salt domes of interior North Oman, and their significance for the Ara carbonate 'stringer' hydrocarbon play. *Geoarabia,* 8 (2), 2312-270.

Peters, T. and Mercolli. I. (1997). Formation and evolution of the Masirah Ophiolite (Sultanate of Oman). *Ofioliti,* 22, 15-34.

Petrovic, A. (2020). Spatial heterogeneities in a bioclastic shoal outcrop reservoir analogue: Architectural, cyclical and diagenetic controls on lateral pore distribution. Marine and *Petroleum Geology*, 113, 104098.

Petrovic, A., Aigner, T. (2017). Are shoals reservoirs discrete bodies? A coquina shoal outcrop analogue from the Mid Triassic Upper Muschelkalk, SW-Germany. *Journal of Petroleum Geology*, 40, 249-275.

Pierson, B., Eberli, G., Al Mehsin, K., Al-Menhali, S., Warrlich, G., Droste, H., Maurer, F., Whitworth, J. and Drysdale, D. (2010). Seismic stratigraphy and depositional history of the Upper Shu'aiba (Late Aptian) in the UAE and Oman. In Frans S.P. van Buchem, Moujahed I. Al-Husseini, Florian Maurer, Henk J. Droste (Eds.), *Barremian - Aptian Stratigraphy and Hydrocarbon Habitat of the Eastern Arabian Plate* (*vol. 2).* Geoarabia Special Publication, 4, pp. 411-444.

Pierson, B.J., Rosell, R.M., Al-Zaabi, N.O. and Abdulsattar, M.M. (2004). Tectonic control over Shu'aiba Formation depositional facies. 6th Middle East Geosciences Conference, GEO 2004. *GeoArabia, Abstract,* 9 (1), 116.

Pilkey, O.H., Bush, D.M. and Rodriguez, R.W. (1988). Carbonate-Terrigenous Sedimentation on the North Puerto Rico Shelf. In Doyle, L. J., and Roberts, H. H. (eds.), *Carbonate-Clastic Transitions*. Developments in Sedimentology, 42, Elsevier, pp. 231-250.

Pimentel, N. and Pena dos Reis, R., 2016. Petroleum Systems of the West Iberian Margin: A Review of the Lusitanian Basin and the Deep Offshore Peniche Basin. *Journal of Petroleum Geology*, 39 (3), 305-326.

Pinheiro, L.M., Wilson, R.C.L., Reis, R.P., Whitmarsh, R.B. and Ribeiro, A. (1996). The western Iberia margin: a geophysical and geological overview. In Whitmarsh, R.B., Sawyer, D. S., Klaus, A. and Masson, D. G. (Eds.), *Proceedings of the Ocean Drilling Program Scientific Results*, 149, 3-23.

Pittet, B., Van Buchem, F., Hillgaertner, H., Grötsch, J. and Droste, H. (2002). Ecological succession, palaeonvironmental change, and depositional sequences of Barremian-Aptian shallow-water carbonates in northern Oman. *Sedimentology*, 49, 555-581.

Pittman, E.D. (1971). Microporosity in carbonate rocks. *AAPG Bulletin*, 55, 1873-1881.

Poças Ribeiro, N., Mendonça Filho, J.G., Duarte, L.V., Silva, R.L., Mendonça, J.O. and Silva, T.F. (2013). Palynofacies and organic geochemistry of the Sinemurian carbonate deposits in the western Lusitanian Basin (Portugal): Coimbra and Água de Madeiros formations. *International Journal of Coal Geology*, 111, 37-52.

Pomar, L. and Kendall, C.G.S.C. (2008). Architecture of Carbonate Platforms: A Response to Hydrodynamics and Evolving Ecology. In: Lukasik, J. and Simo, J.A. (Eds), *Controls on Carbonate Platform and Reef Development*. SEPM Special Publications, 89, 187-216.

Pomar, L. and Tropeano, M. (2001). The Calcarenite di Gravina formation in Matera (southern Italy): New insights for coarse-grained, large-scale, cross-bedded bodies encased in offshore deposits. *AAPG Bulletin*, 85 (4), 661-689.

Pomar, L., Aurell, M., Badenas, B., Morsilli, M. and Al-Awwad, S.F. (2015). Depositional model for a prograding oolitic wedge, Upper Jurassic, Iberian basin. *Marine and Petroleum Geology*, 67, 556-582.

Pomar, L., Molina, J.M., Ruiz-Ortiz, P.A. and Vera, J.A. (2019). Storms in the deep: Tempestite- and beach-like deposits in pelagic sequences (Jurassic, Subbetic, South of Spain). *Marine and Petroleum Geology*, 107, 365-381.

Posamentier, H.W. and Allen, G.P. (1993). Variability of the sequence stratigraphic model: effects of local basin factors. *Sedimentary Geology*, 86 (1-2), 91-109.

Powers, R., Ramirez, L., Redmond, C. and Elberg, E. (1966). Geology of the Arabian Peninsula. *Geological survey professional paper*, 560, 1-147.

Rasmussen, E.S., Lomholt, S., Andersen, C. and Vejbael, O.V. (1998). Aspects of the structural evolution of the Lusitanian basin in Portugal and the shelf and slope area offshore Portugal: *Tectonophysics*, 300, 199-225.

Read, J.F. (1982). Carbonate platforms of passive (extensional) continental margins: types, characteristics and evolution. *Tectonophysics*, 81, 195-212.

Rebelle, M. and Lalanne, B. (2014). Rock-typing In Carbonates: A Critical Review of Clustering Methods. *Abu Dhabi International Petroleum Exhibition and Conference*, Abu Dhabi. Society of Petroleum Engineers. SPE-171759.

Reeder, S.L. and Rankey, E.C. (2008). Interactions between tidal flows and ooid shoals, Northern Bahamas. *Journal of Sedimentary Research*, 78, 97-117.

Reijmer, J., Palmieri, P., Groen, R. and Floquet, M. (2015). Calciturbidites and calcidebrites: Sea-level variations or tectonic processes?. *Sedimentary geology*, 317, 53-70.

Rey, J., Dinis, J.L., Callapez, P. and Cunha, P.P. (2006). *Da rotura continental à margem passiva. Composição e evolução do Cretácico de Portugal*. Cadernos de Geologia de Portugal, INETI, Lisboa, 75 pp.

Richard, P., Zampetti, V., Volery, C., Gesbert, S., Krayenbuehl, T., Spaak, M., Murzin, S., Neves, F. and Hosani, S.A. (2017). Abu Dhabi Structural Evolution and Its Implications for Exploration. *Abu Dhabi International Petroleum Exhibition and Conference*, Abu Dhabi. Society of Petroleum Engineers. SPE-188973.

Roberts, H.H. and Murray, S.P. (1988). Gulfs of the northern Red Sea: depositional settings of abrupt siliciclastic-carbonate transitions. In Doyle, L.J. and Roberts. H.H. (Eds.), *Carbonate - Clastic Transitions*. Developments in sedimentology, 42, Elsevier, pp. 99-142.

Rocha, R.B. and Soares, A.F. (1984). Algumas reflexões sobre a sedimentação jurássica na orla meso-cenozóica ocidental de Portugal. *Mem. Notícias*, 97, 133-142.

Rocha, R.B., Mattioli, E., Duarte, L.V., Pittet, B., Mouterde, R., Cabral, M. C., Comas-Rengifo, M., Gómez, J.J., Goy, A., Hesselbo, S., Jenkyns, H., Littler, K., Mailliot, S., Luiz, C., Oliveira, L.C., Maria Luisa, O., Perilli, N., Pinto, S. and Suan, G. (2016). Base of the Toarcian Stage of the Lower Jurassic defined by the Global Boundary Stratotype Section and Point (GSSP) at the Peniche Section (Portugal). *Episodes*, 39, 460-481.

Roehl, P.O. and Choquette, P.W. (1985). *Carbonate Petroleum Reservoirs*. Springer, New York.

Ruberti, D., Toscano, F., Carannante, G. and Simone, L. (2006). Rudist lithosomes related to current pathways in Upper Cretaceous temperate-type, inner shelves: a case study from the Cilento area, southern Italy. *Geological Society, London, Special Publications*, 255 (1), 179-195.

Ruget-Perrot, C. (1961). Etudes stratigraphiques sur le Dogger et le Malm inférieur du Portugal au Nord du Tage. *Memórias dos Serviços Geológicos de Portugal*, 7, 197.

Santos, M. (2017). Mecanismos de descoloração dos calcários "azuis" do Maciço Calcário Estremenho. Tese de mestrado (MSc thesis) em Geologia Económica (Prospeção Mineral). Departamento de Geologia da Faculdade de Ciências da Universidade de Lisboa.

Schenk, C.J., Tennyson, M.E., Klett, T.R., Finn, T.M., Mercier, T.J., Gaswirth, S.B., Marra, K.R., Le, P.A., Hawkins, S.J., Leathers-Miller, H.M. and Paxton, S.T. (2016). Assessment of undiscovered oil and gas resources of the Lusitanian Basin Province, Portugal. *U.S. Geological Survey Fact Sheet*, 2016-3086, 2 pp.

Schindelin, J., Arganda-Carreras, I., Frise, E., Kaynig, V., Longair, M., Pietzsch, S., Preibisch, S., Rueden, C., Saalfeld, S., Schmid, B., Tinevez, J., White, D.J., Hartenstein, V., Eliceiri, K., Tomancak, P. and Cardona, A. (2012). Fiji: an open-source platform for biological-image analysis. *Nat Methods*, 9, 676-682.

Schlager, W. (2005). *Carbonate Sedimentology and Sequence Stratigraphy*. SEPM Concepts in Sedimentology and Paleontology, 8.

Schlumberger (1981). *Well Evaluation Conference, United Arab Emirates/Qatar*. Coordinated by D. J. Pinnington, Schlumberger Middle East, 271 pp.

Schmoker, J.W. (1984). Empirical relation between carbonate porosity and thermal maturity: an approach to regional porosity prediction. *AAPG Bulletin*, 68, 1697-1703.

Scholle, P.A. and Ulmer-Scholle, D.S. (2003). *A Color Guide to the Petrography of Carbonate Rocks: Grains, textures, porosity, diagenesis*. AAPG Memoir, 77.

Schowalter, T. (1979). Mechanics of Secondary Hydrocarbon Migration and Entrapment. *AAPG Bulletin*, 63 (5), 723-760.

Searle, M.P. (1988). Structure of the Musandam culmination (Sultanate of Oman and United Arab Emirates) and the Straits of Hormuz syntaxis. *Journal of the Geological Society, London,* 145, 831-845.

Searle, M.P., Cherry, A.G., Ali, M. and Cooper, J.W. (2014). Tectonics of the Musandam Peninsula and northern Oman Mountains: From ophiolite obduction to continental collision. *Geoarabia Manama,* 19, 135-174.

Sêco, S.L.R., Duarte, L.V., Pereira, A.J.S.C. and Silva, R.L. (2018). Field gamma-ray patterns and stratigraphic reinterpretation of offshore well-log data from Lower Jurassic organic-rich units of the Lusitanian Basin (Portugal). *Marine and Petroleum Geology*, 98, 860-872.

Sêco, S.L.R., Silva, R.L., Watson, N., Duarte, L.V., Pereira, A.J.S.C. and Wach, G. (2019). Application of petrophysical methods to estimate total organic carbon in Lower Jurassic source rocks from the offshore Lusitanian Basin (Portugal). *Journal of Petroleum Science and Engineering*, 180, 1058-1068.

Sequero, C., Aurell, M. and Bádenas, B. (2019). Sedimentary evolution of a shallow carbonate ramp (Kimmeridgian, NE Spain): Unravelling controlling factors for facies heterogeneities at reservoir scale. *Marine and Petroleum Geology,* 109, 145-174.

Serag El Din, S., Dernaika, M.R., Al Hosani, I., Hannon, L., Skjaeveland, S.M. and Kalam, M.Z. (2010). Whole Core Versus Plugs: Integrating Log and Core Data to Decrease Uncertainty in Petrophysical Interpretation and STOIP Calculations. *Abu Dhabi International Petroleum Exhibition and Conference*, Abu Dhabi. Society of Petroleum Engineers. SPE-137679.

Sharland, P.R., Archer, R., Casey, D.M., Davies, R.B., Hall, S.H., Heward, A.P., Horbury, A.D. Simmons, M.D. (2001). Arabian Plate Sequence Stratigraphy. *GeoArabia Special Publication 2*, Gulf PetroLink, Bahrain, 371.

Shekhar, R., Al Naqbi, A., Obeta, C., Ottinger, G., Herrmann, R., Obara, T., Almazrouei, S. J., Al Maqrami, Z., Al Neyadi, A., Edwards, E., Li, D., Al Shehhi, B. H. and Fazal, A. (2017). Implementation of High Resolution Diagenetic Features into the Static and Dynamic Reservoir Models of a Giant Offshore Oil Field, Abu Dhabi. *Abu Dhabi International Petroleum Exhibition and Conference,* Abu Dhabi. Society of Petroleum Engineers. SPE-188872.

Silva, F., Duarte, L.V., Oliveira, L.C.V., Comas-Rengifo, M.J. and Rodrigues, R. (2010). Contribution to the knowledge of petroleum generative potential of Late Sinemurian-Pliensbachian of the Lusitanian Basin, northern sector (portugal). In: Pena dos Reis, R. and Pimentel, N. (Eds.), *II Central and North Atlantic Conjugate Margins Conference Extended Abstracts*. Portugal, Lisbon, 256-260.

Silva, F., Duarte, L.V., Oliveira, L.C.V., Rodrigues, R. and Comas-Rengifo, M.J. (2007). Caracterização do Carbono Orgânico Total e pirólise Rock-Eval no intervalo Sinemuriano superior-Pliensbaquiano do sector norte da Bacia Lusitânica (Portugal). In: Gomes, E.P. and Alencoão, A.M., (Coords.): Actas do VI Congresso Ibérico de Geoquímica. Vila Real, 564-567.

Silva, R.L. and Duarte, L.V. (2015). Organic matter production and preservation in the Lusitanian Basin (Portugal) and Pliensbachian climatic hot snaps. *Global and Planetary Change*, 131, 24-34.

Silva, R.L., Duarte, L.V. and Comas-Rengifo, M.J. (2015). Facies and carbon isotope chemostratigraphy of Lower Jurassic carbonate deposits, Lusitanian Basin (Portugal): implications and limitations to the application in sequence stratigraphic studies. In Ramkumar, M. (Ed.), *Chemostratigraphy: Concepts, Techniques, and Applications*. Elsevier, pp. 341-371.

Silva, R.L., Duarte, L.V., Comas-Rengifo, M.J., Mendonça Filho, J.G. and Azerêdo, A.C. (2011). Update of the carbon and oxygen isotopic records of the Early-Late Pliensbachian (Early Jurassic, ~187 Ma): Insights from the organic-rich hemipelagic series of the Lusitanian Basin (Portugal). *Chemical Geology*, 283, 177-184.

Silva, R.L, Mendonça Filho, J.G., Azerêdo, A.C. and Duarte, L.V. (2014). Palynofacies and TOC analysis of marine and non-marine sediments across the Middle-Upper Jurassic boundary in the central-northern Lusitanian Basin (Portugal). *Facies*, 60, 255-276.

Silva, R.L., Mendonça Filho, J.G., Da Silva, F.S., Duarte, L.V., Silva, T.F., Ferreira, R. and Azerêdo, A.C. (2012). Can biogeochemistry aid in the palaeoenvironmental/early diagenesis reconstruction of the ~187 Ma (Pliensbachian) organic-rich hemipelagic series of the Lusitanian Basin (Portugal)? *Bulletin of Geosciences*, 87, 373-382.

Soares, A.F., Kullberg, J.C., Marques, J.F., Rocha, R.B. and Callapez, P.M. (2012). Tectono-sedimentary model for the evolution of the Silves Group (Triassic, Lusitanian basin, Portugal). *Bulletin de la Société Géologique de France*, 183 (3), 203-216.

Soares, A.F., Rocha, R.B., Elmi, S., Henriques, M.H., Mouterde, R., Alméras, Y., Ruget, C., Marques, J., Duarte, L., Carapito, M.C. and Kullberg, J.C. (1993). Le sous-bassin nord lusitanien (Portugal) du Trias au Jurassique moyen: histoire d´un "rift avorté". *Comptes rendus de l'Académie des sciences Paris*, 317, série II, 1659-1666.

Soliman, F.A. and Al Shamlan, A. (1982). Review on the Geology of the Cretaceous Sediments of the Rub' al-Khali, Saudi Arabia. *Cretaceous research*, 3, 187-194.

Spalletti, L., Franzese, J., Matheos, S. and Schwarz, E. (2000). Sequence stratigraphy of a tidally dominated carbonate-siliciclastic ramp; the Tithonian-Early Berriasian of the Southern Neuquen Basin, Argentina. *Journal of the Geological Society*, 157, 433-446.

Spigolon, A.L.D., Bueno, G.V., PENA dos Reis, R., Pimentel, N.L. and Matos, V. (2010). The Upper Jurassic Petroleum System: evidence of secondary migration in carbonate fractures

of Cabaços Formation, Lusitanian Basin (Portugal). *II Central and North Atlantic Conjugate Margins Conference*, Lisbon, vol. III, 274-278.

Stern. R.J. and Johnson, P. (2010). Continental lithosphere of the Arabian Plate: A geologic, petrologic, and geophysical synthesis. *Earth-Science Reviews,* 101, 29-67.

Stewart, S.A. (2016). Structural geology of the Rub' Al-Khali Basin, Saudi Arabia. *Tectonics,* 35 (10), 2417-2438.

Strohmenger, C.J., Weber, L.J., Ghani, A., Al-Mehsin, K., Al-Jeelani, O., Al-Mansoori, A., Al-Dayyani, T., Vaughan, L., Khan, S.A. and Mitchell, J.C. (2006). High-resolution sequence stratigraphy and reservoir characterization of Upper Thamama (Lower Cretaceous) Reservoirs of a giant Abu Dhabi oil field, United Arab Emirates. In P.M. Harris and L.J. Weber (Eds.), *Giant Hydrocarbon Reservoirs of the World: From Rocks to Reservoir Characterization and Modeling*. American Association of Petroleum Geologists Memoir 88, pp. 139-171.

Swei, G.H. and Tucker, M.E. (2012). Impact of diagenesis on reservoir quality in ramp carbonates: Gialo Formation (Middle Eocene), Sirt Basin, Libya. *Journal of Petroleum Geology*, 35 (1), 25-48.

Taher, A. (1996). Delineation of organic richness and thermal history of the Lower Cretaceous Thamama Group, East Abu Dhabi: a modeling approach for oil exploration. *GeoArabia Bulletin,* 2 (1), 65-88.

Tavakoli, V. (2020). *Carbonate Reservoir Heterogeneity: Overcoming the Challenges*. Springer International Publishing, 108 pp.

Teixeira, B.A., Pimentel, N. and Pena dos Reis, R. (2012). Regional variations in Source Rock maturation in the Lusitanian Basin (Portugal) - the role of rift events, subsidence, sedimentation rate, uplift and erosion. *Abstracts III Atlantic Conjugate Margins Conference*, 91-92.

Thomas, R.J., Ellison, E.A., Goodenough, K.M., Roberts, N.M.W. and Allen, P.A. (2015). Salt domes of the UAE and Oman: Probing eastern Arabia. *Precambrian Research*, 256, 1-16.

Thorpe, D.T. (2014). *Controls on reservoir quality in Early Cretaceous carbonate oil fields and implications for basin modelling* (Doctoral dissertation). Retrieved from http://hdl.handle.net/1842/18014.

Tovey, N. and Wang, J. (1997). An automatic image acquisition and analysis for a scanning electron microscope. *Scanning Microscopy*, 11, 211-227

Tucker, M.E. (2003). Mixed Clastic-Carbonate Cycles and Sequences: Quaternary of Egypt and Carboniferous of England. *Geologia Croatica,* 56, 19-37.

Tucker, M.E. and Wright, V.P. (1990). *Carbonate Sedimentology*. Blackwell, Oxford, pp 482.

Uphoff, T.L. (2005). Subsalt (pre-Jurassic) exploration play in the northern Lusitanian basin of Portugal. *AAPG Bulletin*, 89 (6), 699-714.

Uphoff, T.L., Stemler, D.P. and McWhorter, R.J. (2010). Jurassic reef exploration play in the southern Lusitanian Basin, Portugal. *II Central and North Atlantic Conjugate Margins Conference*, Lisbon, III, 284-288.

Vahrenkamp, V., Barata, J., Van Laer, P.J., Swart, P. and Murray, S. (2014). Micro rhombic calcite of a giant Barremian (Thamama B) reservoir onshore Abu Dhabi - Clumped isotope analyses fix temperature, water composition and timing of burial diagenesis. *Abu Dhabi International Petroleum Exhibition and Conference*, Abu Dhabi. Society of Petroleum Engineers, SPE-172033.

Vahrenkamp, V., Franco, B.J., Popa, D., Barata, J., Grelaud, C., Razin, P., Grosheny, D. and Bulot, L. (2015a). Development and Infill of the Late Albian to Turonian Shilaif Intrashelf Basin at the Eastern Margin of the Giant Mesozoic Arabian Carbonate Platform: Basin Architecture and Time Stratigraphy. *International Petroleum Technology Conference*, 18488, 6-9 December, Doha, Qatar.

Vahrenkamp, V., Van Laer, P., Franco, B., Celentano, M.A., Grelaud, C. and Grazin, P. (2015b). Late Jurassic to Cretaceous Source Rock Prone Intra-Shelf Basins of the Eastern Arabian Plate - Interplay between Tectonism, Global Anoxic Events and Carbonate Platform Dynamics. *International Petroleum Technology Conference*, Doha, Qatar. IPTC-18470.

Val, J., Bádenas, B. and Aurell, M. (2018). Sedimentary architecture of a prograding oolitic-siliciclastic wedge: Response to changes in wave-base oscillation (Kimmeridgian, Iberian Basin). *Marine and Petroleum Geology*, 96, 113-127.

Van Buchem F.S.P., Al-Husseini, M.I., Maurer, F., Droste, H.J. and Yose, L.A. (2010). Sequence-stratigraphic synthesis of the Barremian-Aptian of the eastern Arabian Plate and implications for the petroleum habitat. In Van Buchem, F.S.P., Al-Husseini, M.I., Maurer, F., Droste, H.J. (Eds.), *Barremian - Aptian stratigraphy and hydrocarbon habitat of the eastern Arabian Plate*. GeoArabia Special Publication 4, Gulf PetroLink, Bahrain, 1, pp. 9-48

Van Buchem, F.S.P., Pittet, B., Hillgärtner, H., Grötsch, J., Al Mansouri, A., Billing, I.M., Droste, H.J. and Oterdoom, W.H. (2002). High resolution sequence stratigraphic architecture of Barremian/Aptian carbonate systems in northern Oman and the United Arab Emirates (Kharaib and Shu'aiba formations). *GeoArabia*, 7 (3), 461-500.

van Laer, P., Nederlof, P., Ahsan, S.A. and Al Katheeri, F. (2012). Northern Rub Al Khali Upper Jurassic - Lower Cretaceous Petroleum System. Proceedings of EAGE Fourth Arabian Plate Geology Workshop, *Late Jurassic/Early Cretaceous Evaporite-Carbonate-Siliciclastic Systems of the Arabian Plate*, 9-12 December, Abu Dhabi, United Arab Emirates.

Van Siclen, D.C. (1958). Depositional topography—examples and theory. *AAPG Bulletin*, 42 (8), 1897-1913.

Van Tuyl, J., Alves, T.M. and Cherns, L. (2018). Geometric and depositional responses of carbonate build-ups to Miocene sea level and regional tectonics offshore northwest Australia. *Marine and Petroleum Geology*, 94, 144-165.

Vanney, J.R. and Mougenot, D. (1981). La plate-forme continentale du Portugal et des provinces adjacentes: analyse géomorphologique. *Memórias dos Serviços Geológicos de Portugal*, 28, 145 pp.

Volery, C., Davaud, E., Foubert, A. and Caline, B. (2010). Lacustrine microporous micrites of the Madrid Basin (Late Miocene, Spain) as analogues for shallow marine carbonates of the Mishrif reservoir Formation (Cenomanian to Early Turonian, Middle East). *Facies*, 56, 385-397.

Walker, O.A., Alves, T.M., Hesselbo, S.P., Pharaoh, T., Nuzzo, M. and Mattos, N.H. (2021). Significance of Upper Triassic to Lower Jurassic salt in the identification of palaeo-seaways in the North Atlantic. *Marine and Petroleum Geology*, 123, 104705.

Wardlaw, N.C. (1996). Factors affecting oil recovery from carbonate reservoirs and prediction of recovery. *Developments in Petroleum Science*, 44 (2), 867-903.

Weber, K.J. (1986). How heterogeneity affects oil recovery. In L. W. Lake, and H. B. J. Carroll, (Eds.), *Reservoir Characterization*. Orlando, FL, Academy Press, pp. 487-544.

Wei, C., Tian, C., Zheng, J., Cai, K., Du, D. Song, B., and Hu, Y. (2015). Heterogeneity Characteristics of Carbonate Reservoirs: A Case Study using Whole Core Data. *Reservoir Characterisation and Simulation Conference and Exhibition, Abu Dhabi*. SPE-175670.

Whittle, G. and Alsharhan, A.S. (1996). Diagenetic history and source rock potential of the Upper Jurassic Diyab Formation, offshore Abu Dhabi, United Arab Emirates. *Carbonates and Evaporites,* 11 (2), 145-154.

Wilson, J.L. (1967). Cyclic and reciprocal sedimentation in Virgilian strata of southern New Mexico. *Geologic Society of America Bulletin*, 78, 805-818.

Wilson, R.C.L. (1975). Atlantic opening and Mesozoic continental margin basins of Iberia. *Earth and Planetary Science Letters*, 25, 33-43.

Wilson, R.C.L. (1979). A reconnaissance study of Upper Jurassic sediments of the Lusitanian basin. *Ciências da Terra* (*Universidade Nova Lisboa)*, Lisboa, 5, 53-84.

Wilson, R.C.L., Hiscott, R.N., Willis, M.G. and Gradstein, F.M. (1989). The Lusitanian Basin of West Central Portugal: Mesozoic and Tertiary Tectonic, Stratigraphic, and Subsidence History. In Tankard, A. J. and Balkwill, H. (Eds.), *Extensional tectonics and stratigraphy of the North Atlantic margins*. AAPG Memoir, 46, pp. 341-361.

Wood, R., Thorpe, D., Wilkinson, M. and Barata, J. (2014). Dynamics of Calcite Cementation in Response to Oil Charge Carbonate Reservoir Retain Longest Cementation History. *AAPG Annual Convention and Exhibition*, Houston, Texas, USA, April 6-9, 2014.

Worden, R.H. and Heasley, E.C. (2000). Effects of petroleum emplacement on cementation in carbonate reservoirs. *Bulletin de la Société Géologique de France*, 171 (6), 607-620.

Wright, V.P. and Wilson, R.C.L. (1984). A carbonate submarine-fan sequence from the Jurassic of Portugal. *Journal of Sedimentary Research,* 54 (2), 394-412.

Yose, L.A., Ruf, A.S., Strohmenger, C.J, Schuelke, J.S, Gombos, A., Al-Hosani, I., Al-Maskary, S., Bloch, G., Al-Mehairi, Y. and Johnson, I.G. (2006). Threedimensional characterization of a heterogeneous carbonate reservoir, Lower Cretaceous, Abu Dhabi (United Arab Emirates). In Harris, P.M and Weber, L.J. (Eds.), *Giant hydrocarbon reservoirs of the world: From rocks to reservoir characterization and modeling*. AAPG Memoir, 88, 173-212.

Zeller, M., Verwer, K., Eberli, G. P., Massaferro, J. L., Schwarz, E. and Spalletti, L. (2015). Depositional controls on mixed carbonate-siliciclastic cycles and sequences on gently inclined shelf profiles. *Sedimentology,* 62, 2009-2037.